

**THE EFFECT OF ADHESION ON THE CONTACT OF AN
ELASTICA WITH A RIGID SURFACE**

by
Amy J. Dalrymple

Thesis submitted to the faculty of the
Virginia Polytechnic Institute and State University
in partial fulfillment of the requirements for the degree of

Master of Science
In
Civil Engineering

APPROVED BY:

Dr. Raymond H. Plaut, Chairman

Dr. David A. Dillard

Dr. Siegfried M. Holzer

December 8, 1999
Blacksburg, Virginia 24061

Keywords: Work of Adhesion, Surface Energy, Elastica, JKR Analysis, DMT Analysis

THE EFFECT OF ADHESION ON THE CONTACT OF A N ELASTICA WITH A RIGID SURFACE

by

Amy J. Dalrymple

R. H. Plaut, Chairman

Civil Engineering

(ABSTRACT)

The understanding of topics such as friction, wear, lubrication, and adhesive bonds is dependent on the ability to measure surface and interfacial energies. The surface energies of liquids may be measured accurately using a variety of techniques; however, surface energies of solids are much more difficult to accurately measure. In an attempt to develop a method that can be used to measure surface and interfacial energies of solids, this thesis proposes the use of a elastica. The elastica acts as an extremely flexible beam and provides a structure that will permit measurable deformation of the solid by relatively small surface attractions. The ends of the elastica are lifted, bent, and clamped vertically at an equal height and specified distance apart. They are then moved downward, allowing the strip to make contact with a flat, rigid, horizontal surface.

Two adhesion models are investigated. First, a JKR-type analysis, which examines the effect of adhesion forces that exist within the area of contact between the elastica and the rigid surface, is considered. Various values for the work of adhesion are examined. A DMT-type analysis, which assumes that the adhesion forces act in the region just outside of the contact area, is also considered. Results are obtained for linear and constant forces. Various values for the maximum DMT force and the vertical separation between the elastica and the rigid substrate at which the adhesion forces terminate are examined. Results from the two types of analyses are compared.

Acknowledgements

I would like to take this opportunity to thank Dr. Raymond Plaut for acting as my advisor and for providing his guidance throughout my research and writing efforts. His assistance was greatly appreciated. I would also like to thank Dr. Siegfried Holzer and Dr. David Dillard for serving as my committee members.

Additionally, I would like to thank Dr. Ken Hannsger of the Mathematics Department at Virginia Tech for sharing his knowledge of Mathematica and providing his assistance in the development of the Mathematica programs used to obtain the results for this thesis. Furthermore, I would like to extend my gratitude to the National Science Foundation for providing the financial support for my research through Grant CMS-9713949. I would also like to thank the Via Foundation for its generosity in the form of a Via Fellowship which has funded my graduate education.

I would like to thank the people who have continually supplied me with their love and support throughout my life. Thank you, Mom, Dad, and Kristy for your endless supply of love, support, advice, and understanding. I appreciate it more than you can imagine. Finally I would like to thank John Ryan and Jolyn Senne for their friendship and their encouragement.

Table of Contents

LIST OF FIGURES	VII
LIST OF TABLES	XVII
CHAPTER 1. INTRODUCTION	1
CHAPTER 2. LITERATURE REVIEW.....	5
2.1 INTRODUCTION	5
2.2 SURFACE AND INTERFACIAL ENERGIES OF SOLIDS	5
2.2.1 Analytical Research.....	6
2.2.2 Experimental Research.....	9
2.3 ELASTICA THEORY.....	13
2.3.1 Basic Elastica Theory.....	14
2.3.2 Applications of the Elastica Theory	17
2.4 CONCLUSIONS	21
CHAPTER 3. FORMULATION OF ANALYTICAL METHODS	22
3.1 INTRODUCTION.....	22
3.2 JKR-TYPE ANALYSIS	26
3.2.1 Description of Adhesion Forces	26
3.2.2 Minimization of Energy.....	27
3.2.3 Cases Examined.....	28
3.3 DMT-TYPE ANALYSIS	31
3.3.1 Description of Adhesion Forces	32
3.3.2 Linear DMT Force.....	32
3.3.3 Dugdale DMT Force.....	33
3.4 NO CONTACT, POINT CONTACT, AND LINE CONTACT SITUATIONS	34

Table of Contents, Continued

CHAPTER 4. RESULTS FROM THE JKR-TYPE ANALYSIS	36
4.1 INTRODUCTION	36
4.2 RESULTS FOR THE $C=0.4$ CASE (NO SELF-WEIGHT INCLUDED)	40
4.3 RESULTS FOR THE $C=0.8$ CASE (NO SELF-WEIGHT INCLUDED)	53
4.4 RESULTS FOR THE $C=0.4$ CASE (SELF-WEIGHT INCLUDED).....	61
CHAPTER 5. RESULTS FROM THE DMT-TYPE ANALYSIS.....	68
5.1 INTRODUCTION	68
5.2 RESULTS FOR THE LINEAR DMT-TYPE FORCE.....	74
5.2.1 Results for $c=0.4$ and $\eta=0$ (Line Contact Only).....	74
5.2.2 Results for $c=0.4$ and $\eta=2$ (Line Contact Only).....	83
5.2.3 Results for $c=0.4$ and $\eta=-2$ (Line Contact Only).....	89
5.2.4 Results for $c=0.8$ and $\eta=0$ (Line Contact Only).....	96
5.2.5 Results for $c=0.8$ and $\eta=2$ (Line Contact Only).....	105
5.2.6 Results for $c=0.8$ and $\eta=-2$ (Line Contact Only).....	114
5.3 RESULTS FOR THE DUGDALE DMT-TYPE FORCE	120
5.3.1 Results for $c=0.4$ and $\eta=0$ (Line Contact Only).....	121
5.3.2 Results for $c=0.4$ and $\eta=2$ (Line Contact Only).....	128
5.3.3 Results for $c=0.4$ and $\eta=-2$ (Line Contact Only).....	134
5.4 RESULTS FOR THE NO CONTACT AND POINT CONTACT CASES	141
CHAPTER 6. COMPARISON OF EXPERIMENTAL, FINITE ELEMENT, AND ANALYTICAL RESULTS.....	149
6.1 INTRODUCTION	149
6.2 COMPARISON OF ANALYTICAL AND EXPERIMENTAL RESULTS.....	151

Table of Contents, Continued

6.3 COMPARISON OF THE FINITE ELEMENT AND ANALYTICAL RESULTS ...	167
CHAPTER 7: CONCLUSIONS AND RECOMMENDATIONS FOR FUTURE RESEARCH	173
7.1 INTRODUCTION	173
7.2 JKR-TYPE ANALYSIS	173
7.3 DMT-TYPE ANALYSIS	175
7.3.1 Linear Force DMT-Type Analysis	175
7.3.2 Dugdale Force DMT-Type Analysis	176
7.3.3 Comparison on the Linear Force and Dugdale Force DMT-Type Analyses..	177
7.4 COMPARISON OF THE JKR- AND DMT-TYPE ANALYSIS RESULTS.....	180
7.5 RECOMMENDATIONS FOR FUTURE RESEARCH	184
REFERENCES.....	186
APPENDIX A	190
APPENDIX B	198
APPENDIX C	203
VITA.....	206

List of Figures

Figure	Page
3.1	Geometry of an Elastica in Contact With a Rigid Surface..... 24
3.2	Orientation and Location of Variables and Forces for an Elastica Experiencing Line Contact..... 24
3.3a	Location of Moment m_b 27
3.3b	Stress Distribution at the point of lift-off due to adhesion forces..... 27
3.4a	Shape of Elastica Before Contact When $c=0.4$ 29
3.4b	Typical Shape of Elastica With Line Contact When $c=0.4$ 29
3.5a	Shape of Elastica Before Contact When $c=0.9$ 30
3.5b	Typical Shape of Elastica With Line Contact When $c=0.8$ 30
3.6	Linear Force Applied in DMT-Type Analysis..... 33
3.7	Dugdale Force Applied in DMT-Type Analysis..... 34
4.1	Total Energy vs. Contact Length for $c=0.4$, $q=13$, and $\Delta\gamma=0.32$ 39
4.2	Total Energy vs. Contact Length for $c=0.8$, $q=-23.5$, and $\Delta\gamma=0.32$ 39
4.3	Contact Length vs. Vertical Force for $c=0.4$ 46
4.4	Contact Length vs. Vertical Deflection for $c=0.4$ 46
4.5	Vertical Deflection vs. Vertical Force for $c=0.4$ 47
4.6	Vertical Deflection vs. Vertical Force for $c=0.4$ (Locations of Points A-M: Table 4.1) 47
4.7	Vertical Force Experienced by the Elastica When it is Pushed Onto or Pulled Off the Rigid Surface. Vertical Deflection is Controlled..... 48
4.8	Vertical Force Experienced by the Elastica When it is Pushed Onto or Pulled Off the Rigid Surface. Vertical Deflection is Controlled. Curve with Adhesion Extends to $\delta<0$ 48
4.9	Vertical Force Experienced by the Elastica When it is Pushed Onto or Pulled Off the Rigid Surface. Vertical Force is Controlled 49

List of Figures, Continued

Figure	Page
4.10 Vertical Force Experienced by the Elastica When it is Pushed Onto or Pulled Off the Rigid Surface. Vertical Deflection is Controlled. Curve with Adhesion Extends to $\delta < 0$	49
4.11 Effect of Adhesion on the Contact Length for $c=0.4$, $\delta=0.150$	50
4.12 Shape of the Elastica at the Pull-Off and No Contact Stages for $c=0.4$	50
4.13 Moment (m_b) vs. Vertical Force for Varying Values of Work of Adhesion ($c=0.4$).....	51
4.14 Work of Adhesion vs. Moment (m_b) for $c=0.4$ and $q=20$	51
4.15 Contact Length vs. Work of Adhesion for $c=0.4$	52
4.16 Vertical Displacement vs. the Work of Adhesion for $c=0.4$	52
4.17 Contact Length vs. Vertical Force for $c=0.8$	54
4.18 Contact Length vs. Vertical Deflection for $c=0.8$	54
4.19 Vertical Displacement vs. Vertical Force for $c=0.8$	55
4.20 Vertical Displacement vs. Vertical Force for $c=0.8$ (Locations of Points A-M: Table 4.2).....	55
4.21 Effect of Adhesion on the Contact Length for $c=0.8$, $\delta=0.050$	56
4.22 Moment (m_b) vs. Vertical Force for $c=0.8$	56
4.23 Work of Adhesion vs. Moment (m_b) for $c=0.8$ and $q=2.5$	57
4.24 Contact Length vs. Work of Adhesion for $c=0.8$	57
4.25 Vertical Displacement vs. the Work of Adhesion $c=0.8$	58
4.26 Contact Length vs. Vertical Force for $c=0.4$ and $\Delta\gamma=0$	64
4.27 Contact Length vs. Vertical Displacement for $c=0.4$ and $\Delta\gamma=0$	64
4.28 Vertical Displacement vs. Vertical Force for $c=0.4$ and $\Delta\gamma=0$	65
4.29 Contact Length vs. Vertical Force for $c=0.4$ and $\Delta\gamma=0.64$	65

List of Figures, Continued

Figure	Page
4.30 Contact Length vs. Vertical Displacement for $c=0.4$ and $\Delta\gamma=0.64$	66
4.31 Vertical Displacement vs. Vertical Force for $c=0.4$ and $\Delta\gamma=0.64$	66
4.32 Contact Length vs. Vertical Force for $c=0.4$ and $\eta=2$	67
5.1a Linear Force vs. y for DMT-Type Analysis	70
5.1b Typical Corresponding Adhesion Force vs. x Plot for Linear Force DMT- Type Analysis	70
5.1c Typical y vs. x Plot From $x=0$ to $x=d$ for Linear Force DMT-Type Analysis	70
5.2 Contact Length vs. Vertical Force for $c=0.4$, $\eta=0$, and $\alpha=0.001$	76
5.3 Contact Length vs. Vertical Displacement for $c=0.4$, $\eta=0$, and $\alpha=0.001$	77
5.4 Vertical Displacement vs. Vertical Force for $c=0.4$, $\eta=0$, and $\alpha=0.001$	77
5.5 Moment (m_d) vs. Vertical Force for $c=0.4$, $\eta=0$, and $\alpha=0.001$	78
5.6 Moment (m_d) vs. Vertical Displacement for $c=0.4$, $\eta=0$, and $\alpha=0.001$	78
5.7 Contact Length vs. Vertical Force for $c=0.4$, $\eta=0$, and $\alpha=0.0001$	80
5.8 Contact Length vs. Vertical Displacement for $c=0.4$, $\eta=0$, and $\alpha=0.0001$...	81
5.9 Vertical Displacement vs. Vertical Force for $c=0.4$, $\eta=0$, and $\alpha=0.0001$	81
5.10 Moment (m_d) vs. Vertical Force for $c=0.4$, $\eta=0$, and $\alpha=0.0001$	82
5.11 Moment (m_d) vs. Vertical Displacement for $c=0.4$, $\eta=0$, and $\alpha=0.0001$	82
5.12 Contact Length vs. Vertical Force for $c=0.4$, $\eta=2$, and $\alpha=0.001$	84
5.13 Contact Length vs. Vertical Displacement for $c=0.4$, $\eta=2$, and $\alpha=0.001$	85
5.14 Vertical Displacement vs. Vertical Force for $c=0.4$, $\eta=2$, and $\alpha=0.001$	85
5.15 Moment (m_d) vs. Vertical Force for $c=0.4$, $\eta=2$, and $\alpha=0.001$	86
5.16 Moment (m_d) vs. Vertical Displacement for $c=0.4$, $\eta=2$, and $\alpha=0.001$	86

List of Figures, Continued

Figure	Page
5.17 Contact Length vs. Vertical Force for $c=0.4$, $\eta=2$, and $\alpha=0.0001$	87
5.18 Contact Length vs. Vertical Displacement for $c=0.4$, $\eta=2$, and $\alpha=0.0001$...	87
5.19 Vertical Displacement vs. Vertical Force for $c=0.4$, $\eta=2$, and $\alpha=0.0001$	88
5.20 Moment (m_d) vs. Vertical Force for $c=0.4$, $\eta=2$, and $\alpha=0.0001$	88
5.21 Moment (m_d) vs. Vertical Displacement for $c=0.4$, $\eta=2$, and $\alpha=0.0001$	89
5.22 Contact Length vs. Vertical Force for $c=0.4$, $\eta=-2$, and $\alpha=0.001$	90
5.23 Contact Length vs. Vertical Displacement for $c=0.4$, $\eta=-2$, and $\alpha=0.001$...	91
5.24 Vertical Displacement vs. Vertical Force for $c=0.4$, $\eta=-2$, and $\alpha=0.001$	91
5.25 Moment (m_d) vs. Vertical Force for $c=0.4$, $\eta=-2$, and $\alpha=0.001$	92
5.26 Moment (m_d) vs. Vertical Displacement for $c=0.4$, $\eta=-2$, and $\alpha=0.001$	92
5.27 Contact Length vs. Vertical Force for $c=0.4$, $\eta=-2$, and $\alpha=0.0001$	93
5.28 Contact Length vs. Vertical Displacement for $c=0.4$, $\eta=-2$, and $\alpha=0.0001$.	93
5.29 Vertical Displacement vs. Vertical Force for $c=0.4$, $\eta=-2$, and $\alpha=0.0001$...	94
5.30 Moment (m_d) vs. Vertical Force for $c=0.4$, $\eta=-2$, and $\alpha=0.0001$	94
5.31 Moment (m_d) vs. Vertical Displacement for $c=0.4$, $\eta=-2$, and $\alpha=0.0001$	95
5.32 Contact Length vs. Vertical Force for $c=0.8$, $\alpha=0.001$, and $f_0=1000$	96
5.33 Contact Length vs. Vertical Force for $c=0.8$, $\eta=0$, and $\alpha=0.001$	99
5.34 Contact Length vs. Vertical Displacement for $c=0.8$, $\eta=0$, and $\alpha=0.001$	99
5.35 Vertical Displacement vs. Vertical Force for $c=0.8$, $\eta=0$, and $\alpha=0.001$	100
5.36 Moment (m_d) vs. Vertical Force for $c=0.8$, $\eta=0$, and $\alpha=0.001$	100
5.37 Moment (m_d) vs. Vertical Displacement for $c=0.8$, $\eta=0$, and $\alpha=0.001$	101
5.38 Contact Length vs. Vertical Force for $c=0.8$, $\eta=0$, and $\alpha=0.0001$	103
5.39 Contact Length vs. Vertical Displacement for $c=0.8$, $\eta=0$, and $\alpha=0.0001$...	103

List of Figures, Continued

Figure	Page
5.40	Vertical Displacement vs. Vertical Force for $c=0.8$, $\eta=0$, and $\alpha=0.0001$ 104
5.41	Moment (m_d) vs. Vertical Force for $c=0.8$, $\eta=0$, and $\alpha=0.0001$ 104
5.42	Moment (m_d) vs. Vertical Displacement for $c=0.8$, $\eta=0$, and $\alpha=0.0001$ 105
5.43	Contact Length vs. Vertical Force for $c=0.8$, $\eta=2$, and $\alpha=0.001$ 107
5.44	Contact Length vs. Vertical Displacement for $c=0.8$, $\eta=2$, and $\alpha=0.001$ 108
5.45	Vertical Displacement vs. Vertical Force for $c=0.8$, $\eta=2$, and $\alpha=0.001$ 108
5.46	Moment (m_d) vs. Vertical Force for $c=0.8$, $\eta=2$, and $\alpha=0.001$ 109
5.47	Moment (m_d) vs. Vertical Displacement for $c=0.8$, $\eta=2$, and $\alpha=0.001$ 109
5.48	Contact Length vs. Vertical Force for $c=0.8$, $\eta=2$, and $\alpha=0.0001$ 111
5.49	Contact Length vs. Vertical Displacement for $c=0.8$, $\eta=2$, and $\alpha=0.0001$... 112
5.50	Vertical Displacement vs. Vertical Force for $c=0.8$, $\eta=2$, and $\alpha=0.0001$ 112
5.51	Moment (m_d) vs. Vertical Force for $c=0.8$, $\eta=2$, and $\alpha=0.0001$ 113
5.52	Moment (m_d) vs. Vertical Displacement for $c=0.8$, $\eta=2$, and $\alpha=0.0001$ 113
5.53	Contact Length vs. Vertical Force for $c=0.8$, $\eta=-2$, and $\alpha=0.001$ 115
5.54	Contact Length vs. Vertical Displacement for $c=0.8$, $\eta=-2$, and $\alpha=0.001$... 116
5.55	Vertical Displacement vs. Vertical Force for $c=0.8$, $\eta=-2$, and $\alpha=0.001$ 116
5.56	Moment (m_d) vs. Vertical Force for $c=0.8$, $\eta=-2$, and $\alpha=0.001$ 117
5.57	Moment (m_d) vs. Vertical Displacement for $c=0.8$, $\eta=-2$, and $\alpha=0.001$ 117
5.58	Contact Length vs. Vertical Force for $c=0.8$, $\eta=-2$, and $\alpha=0.0001$ 118
5.59	Contact Length vs. Vertical Displacement for $c=0.8$, $\eta=-2$, and $\alpha=0.0001$. 118
5.60	Vertical Displacement vs. Vertical Force for $c=0.8$, $\eta=-2$, and $\alpha=0.0001$... 119
5.61	Moment (m_d) vs. Vertical Force for $c=0.8$, $\eta=-2$, and $\alpha=0.0001$ 119
5.62	Moment (m_d) vs. Vertical Displacement for $c=0.8$, $\eta=-2$, and $\alpha=0.0001$ 120

List of Figures, Continued

Figure	Page
5.63 Contact Length vs. Vertical Force for $c=0.4$, $\eta=0$, and $\alpha=0.001$ (Dugdale).....	123
5.64 Contact Length vs. Vertical Displacement for $c=0.4$, $\eta=0$, and $\alpha=0.001$ (Dugdale).....	123
5.65 Vertical Displacement vs. Vertical Force for $c=0.4$, $\eta=0$, and $\alpha=0.001$ (Dugdale).....	124
5.66 Moment (m_d) vs. Vertical Force for $c=0.4$, $\eta=0$, and $\alpha=0.001$ (Dugdale).....	124
5.67 Moment (m_d) vs. Vertical Displacement for $c=0.4$, $\eta=0$, and $\alpha=0.001$ (Dugdale).....	125
5.68 Contact Length vs. Vertical Force for $c=0.4$, $\eta=0$, and $\alpha=0.0001$ (Dugdale).....	125
5.69 Contact Length vs. Vertical Displacement for $c=0.4$, $\eta=0$, and $\alpha=0.0001$ (Dugdale).....	126
5.70 Vertical Displacement vs. Vertical Force for $c=0.4$, $\eta=0$, and $\alpha=0.0001$ (Dugdale).....	126
5.71 Moment (m_d) vs. Vertical Force for $c=0.4$, $\eta=0$, and $\alpha=0.0001$ (Dugdale).....	127
5.72 Moment (m_d) vs. Vertical Displacement for $c=0.4$, $\eta=0$, and $\alpha=0.0001$ (Dugdale).....	127
5.73 Contact Length vs. Vertical Force for $c=0.4$, $\eta=2$, and $\alpha=0.001$ (Dugdale).....	129

List of Figures, Continued

Figure	Page
5.74 Contact Length vs. Vertical Displacement for $c=0.4$, $\eta=2$, and $\alpha=0.001$ (Dugdale).....	130
5.75 Vertical Displacement vs. Vertical Force for $c=0.4$, $\eta=2$, and $\alpha=0.001$ (Dugdale).....	130
5.76 Moment (m_d) vs. Vertical Force for $c=0.4$, $\eta=2$, and $\alpha=0.001$ (Dugdale).....	131
5.77 Moment (m_d) vs. Vertical Displacement for $c=0.4$, $\eta=2$, and $\alpha=0.001$ (Dugdale).....	131
5.78 Contact Length vs. Vertical Force for $c=0.4$, $\eta=2$, and $\alpha=0.0001$ (Dugdale).....	132
5.79 Contact Length vs. Vertical Displacement for $c=0.4$, $\eta=2$, and $\alpha=0.0001$ (Dugdale).....	132
5.80 Vertical Displacement vs. Vertical Force for $c=0.4$, $\eta=2$, and $\alpha=0.0001$ (Dugdale).....	133
5.81 Moment (m_d) vs. Vertical Force for $c=0.4$, $\eta=2$, and $\alpha=0.0001$ (Dugdale).....	133
5.82 Moment (m_d) vs. Vertical Displacement for $c=0.4$, $\eta=2$, and $\alpha=0.0001$ (Dugdale).....	134
5.83 Contact Length vs. Vertical Force for $c=0.4$, $\eta=-2$, and $\alpha=0.001$ (Dugdale).....	136
5.84 Contact Length vs. Vertical Displacement for $c=0.4$, $\eta=-2$, and $\alpha=0.001$ (Dugdale).....	136
5.85 Vertical Displacement vs. Vertical Force for $c=0.4$, $\eta=-2$, and $\alpha=0.001$ (Dugdale).....	137

List of Figures, Continued

Figure	Page
5.86 Moment (m_d) vs. Vertical Force for $c=0.4$, $\eta=-2$, and $\alpha=0.001$ (Dugdale).....	137
5.87 Moment (m_d) vs. Vertical Displacement for $c=0.4$, $\eta=-2$, and $\alpha=0.001$ (Dugdale).....	138
5.88 Contact Length vs. Vertical Force for $c=0.4$, $\eta=-2$, and $\alpha=0.0001$ (Dugdale).....	138
5.89 Contact Length vs. Vertical Displacement for $c=0.4$, $\eta=-2$, and $\alpha=0.0001$ (Dugdale).....	139
5.90 Vertical Displacement vs. Vertical Force for $c=0.4$, $\eta=-2$, and $\alpha=0.0001$ (Dugdale).....	139
5.91 Moment (m_d) vs. Vertical Force for $c=0.4$, $\eta=-2$, and $\alpha=0.0001$ (Dugdale).....	140
5.92 Moment (m_d) vs. Vertical Displacement for $c=0.4$, $\eta=-2$, and $\alpha=0.0001$ (Dugdale).....	140
5.93 Typical Vertical Displacement vs. Vertical Force Plot for DMT-Type Analysis.....	144
5.94 Vertical Force Experienced by the Elastica When it is Pushed Onto or Pulled Off the Rigid Surface. Vertical Displacement is Controlled.	144
5.95 Vertical Displacement Experienced by the Elastica When it is Pushed Onto or Pulled Off the Rigid Surface. Vertical Force is Controlled.	145
6.1 Set-up Used for Experimental Tests (Courtesy of Jia Qi)	150
6.2 Contact Length vs. Vertical Force for $c=0.4$ (Test 1)	153
6.3 Contact Length vs. Vertical Force for $c=0.2509$ (Test 2)	156
6.4 Contact Length vs. Vertical Force for $c=0.3515$ (Test 3)	157

List of Figures, Continued

Figure	Page
6.5 Contact Length vs. Vertical Force for $c=0.5348$ (Test 4)	159
6.6 Contact Length vs. Vertical Displacement for $c=0.5348$ (Test 4)	159
6.7 Contact Length vs. Vertical Force for $c=0.4305$ (Test 5, Day 1)	162
6.8 Contact Length vs. Vertical Displacement for $c=0.4305$ (Test 5, Day 1).....	162
6.9 Contact Length vs. Vertical Force for $c=0.4305$ (Test 5, Day 2)	163
6.10 Contact Length vs. Vertical Displacement for $c=0.4305$ (Test 5, Day 2).....	163
6.11 Contact Length vs. Vertical Force for $c=0.4305$ (Test 5, Day 3)	164
6.12 Contact Length vs. Vertical Displacement for $c=0.4305$ (Test 5, Day 3).....	164
6.13 Contact Length vs. Vertical Force for $c=0.5348$, $\eta=-0.91$ (Test 4)	166
6.14 Contact Length vs. Vertical Displacement for $c=0.5348$, $\eta=-0.91$ (Test 4) .	166
6.15 Vertical Displacement vs. Vertical Force for $c=0.5348$, $\eta=-0.91$ (Test 4)...	167
6.16 Contact Length vs. Vertical Force for $c=0.4$ (FEA 1)	170
6.17 Contact Length vs. Vertical Force for $c=0.6$ (FEA 2)	171
6.18 Contact Length vs. Vertical Force for $c=0.8$ (FEA 3)	172
7.1 Contact Length vs. Vertical Force for $c=0.4$ and $\eta=0$ (Linear Force DMT- Type Analysis)	178
7.2 Contact Length vs. Vertical Displacement for $c=0.4$ and $\eta=0$ (Linear Force DMT-Type Analysis).....	179
7.3 Contact Length vs. Vertical Force for $c=0.4$ and $\eta=0$ (Linear and Dugdale Force DMT-Type Analysis).....	179
7.4 Contact Length vs. Vertical Displacement for $c=0.4$ and $\eta=0$ (Linear and Dugdale Force DMT-Type Analysis)	180
7.5 Vertical Force vs. Work of Adhesion for the Transition Point Between Point Contact and Line Contact when $c=0.4$ and $\eta=0$	183

List of Figures, Continued

Figure	Page
7.6 Vertical Force vs. Work of Adhesion for the Transition Point Between Point Contact and Line Contact when $c=0.8$ and $\eta=0$	183
7.7 Pull-Off Force vs. Work of Adhesion for $c=0.4$ and $\eta=0$	184

List of Tables

Table	Page
3.1	Nondimensionalized Quantities 23
4.1	Values Corresponding to Points A-M in Figure 4.6 44
4.2	Values Corresponding to Points A-M in Figure 4.20 60
5.1	Values Used for the Linear DMT Force When $c=0.4$ 68
5.2	Values Used for the Linear DMT Force When $c=0.8$ 69
5.3	Values Used for the Dugdale DMT Force 73
5.4	Values for d , θ , and m_d When $c=0.4$, $\eta=0$, and $b=0$ 75
5.5	Values Corresponding to the Transition Point Between Line Contact ($b>0$) and Point Contact ($b=0$) for $c=0.4$ and $\eta=0$ 75
5.6	Values Corresponding to the Transition Point Between Line Contact ($b>0$) and Point Contact ($b=0$) for $c=0.4$ and $\eta=2$ 83
5.7	Values Corresponding to the Transition Point Between Line Contact ($b>0$) and Point Contact ($b=0$) for $c=0.4$ and $\eta=-2$ 90
5.8	Values for d , θ , and m_d When $c=0.4$ and $\eta=0$ 97
5.9	Values Corresponding to the Transition Point Between Line Contact ($b>0$) and Point Contact ($b=0$) for $c=0.8$ and $\eta=0$ 98
5.10	Values Corresponding to the Transition Point Between Line Contact ($b>0$) and Point Contact ($b=0$) for $c=0.8$ and $\eta=2$ 107
5.11	Values Corresponding to the Transition Point Between Line Contact ($b>0$) and Point Contact ($b=0$) for $c=0.8$ and $\eta=-2$ 115
5.12	Values Corresponding to the Transition Point Between Line Contact ($b>0$) and Point Contact ($b=0$) for $c=0.4$ and $\eta=0$ (Dugdale Force)..... 121
5.13	Values Corresponding to the Transition Point Between Line Contact ($b>0$) and Point Contact ($b=0$) for $c=0.4$ and $\eta=2$ (Dugdale Force)..... 128

List of Tables, Continued

Table	Page
5.14 Values Corresponding to the Transition Point Between Line Contact ($b > 0$) and Point Contact ($b = 0$) for $c = 0.4$ and $\eta = -2$ (Dugdale Force)	135
5.15 Values Corresponding to the Transition Point B Between Point Contact and No Contact for the Linear Force DMT-Type Analysis When $c = 0.4$	146
5.16 Values Corresponding to the Transition Point B Between Point Contact and No Contact for the Linear Force DMT-Type Analysis When $c = 0.8$	147
5.17 Values Corresponding to the Transition Point B Between Point Contact and No Contact for the Dugdale Force DMT-Type Analysis When $c = 0.4$	148
6.1 Test Specimen Data for Test 1	153
6.2 Test Specimen Data for Test 2	155
6.3 Test Specimen Data for Test 3	156
6.4 Test Specimen Data for Test 4	158
6.5 Test Specimen Data for Test 5	161
6.6 Experimental Values for b , q , and δ	161
6.7 Test Specimen Data for FEA 1	170
6.8 Test Specimen Data for FEA 2	171
6.9 Test Specimen Data for FEA 3	172

Chapter 1. Introduction

The measurement of surface and interfacial energies is of significant interest in the scientific and technical communities. A broader knowledge of these energies and their effects on material systems may lead to advancements in the understanding of areas such as friction, wear, lubrication, basic material behavior, adhesive bonds, and material durability. Additionally, industries involving bonding, coating, cleaning, and painting would all benefit from a greater understanding of surface energies and adhesion. Although reliable methods for measuring surface energies of liquids have been developed, determination of interfacial energies of solids has been more difficult.

Surface energies of liquids may be measured accurately using a variety of techniques including capillary rise experiments, the maximum bubble pressure method, and bubble or droplet shape techniques. However, accurate surface energy measurements for solids are much more difficult to obtain. Often, solids possess material stiffnesses that are large enough to prevent surface tensions from altering the shape of the solid. In an attempt to measure the surface energies of solids, yet avoid the limitations presented by the material stiffness, several techniques have been developed. Previously, estimates of surface energies for solids were made using the melted state of the material of interest and evaluating its behavior in the liquid form. To do so, one must assume that the energies of the liquid and solid are similar - an assumption which, upon further investigation, has been proven to be inaccurate in many cases. A second method of measurement uses the cleavage of brittle materials to estimate surface energies. Again, this method has limited applicability and cannot be used to measure surface energies of most practical materials. In addition to the techniques discussed above, various others involving limited technology have been reviewed (Adamson, 1967).

Recently, more sophisticated methods of surface energy estimation and measurement have been developed. In 1971, Johnson, Kendall, and Roberts published “Surface Energy and the Contact of Elastic Solids” which developed a mathematical model and experimental technique for the measurement of surface energies of solids. In their model, now referred to as the “JKR technique”, Johnson et al. (1971) examine two similar, solid, homogeneous spheres with frictionless surfaces. A normal force is applied to the spheres, bringing them into contact with one another. A flat, circular contact region between the spheres develops as additional force is applied. Adhesive forces are present within this contact region and are ignored outside of the region. Equilibrium conditions are then determined by minimizing the total energy of the system. The work of adhesion can be calculated using the values obtained from the analysis for the contact radius, the applied load, and the known material properties of the spheres. Similar to the other methods developed for measuring surface energies of solids, limitations also exist in the JKR model. To perform a JKR-type analysis, one of the materials of interest is typically an elastomer (a highly flexible material). If neither of the materials being considered is an elastomer, an elastomeric lens must be coated with one of the materials in order to perform the analysis. Although some success has been achieved with this method, not all materials can be deposited on the lens (Mangipudi, 1996).

In an attempt to develop a method that can be used to measure surface and interfacial energies of solids for a broader range of material types, the use of a flexible structure has been proposed. For the present research funded by the National Science Foundation, an elastica, acting as an extremely flexible beam, was chosen for use in our analytical model. The elastica is assumed to be thin, uniform, smooth, inextensible, and flexible in bending. Additionally, the elastica provides a structure that will permit measurable deformation of the solid by relatively small surface attractions. The ends of the elastica are lifted, bent, and clamped vertically at an equal height and specified distance apart. They are then moved downward, allowing the strip to make contact with a flat, rigid, horizontal surface. Additional downward force is then applied to the elastica, causing it to

flatten. When the effects of surface and interfacial energies are included in the analysis, the forces of attraction between the elastica and the rigid surface modify the elastica's shape and cause an elongation of the contact length. The advantages of using an elastica to measure surface and interfacial energies include the simplicity of the governing equations and the applicability of the method to a variety of materials.

Using the analytical model discussed above, two analyses are performed. First, a JKR-type analysis is considered. This analysis examines the effects of adhesion forces that exist only within the area of contact between the elastica and the rigid surface.

Separation distances between the fixed ends of the elastica equal to 0.4 and 0.8 times the length of the elastica are considered. Various values for the work of adhesion, $\Delta\gamma$, are used to determine the extent of the effect of adhesion.

The second analysis technique used to investigate the effect of surface and interfacial energies is based on a DMT-type theory. Named after the analysis method performed by Derjaguin, Muller, and Toporov (Derjaguin et al., 1975), the DMT method assumes that the attractive forces between materials occur in a small region just outside the contact area. For our analysis, we chose to examine two cases. First, a linear force is investigated (i.e. the force is a linear function of the vertical separation distance), with a maximum force of f_0 occurring at the point of separation of the elastica from the rigid surface and terminating when a specified vertical separation distance is reached. Second, a constant force g_0 , which occurs at the point of separation and acts until the vertical separation distance between the elastica and the surface reaches a specified value, is studied. Values for both f_0 and g_0 are varied, as are the values for the areas outside of the contact area over which the adhesion forces act.

Upon conclusion of the analysis, the results from the various models are compared and the effects of the adhesion forces are examined. Additionally, the analytical results are compared with available experimental results. The data is then discussed, conclusions

are drawn, and the need for future research is addressed. The ultimate goal of our efforts is to produce an alternative and possibly more precise method of determining surface energies of solids, using the methods and results obtained through this research.

The outline for the subsequent chapters is as follows. A review of previous research on the topics of a bent elastica and the surface energies of solids is presented in the following chapter (Chapter 2). Following the literature review, Chapter 3 gives the formulation of the analytical methods used for the present research. This chapter describes the JKR- and DMT-type analyses, respectively, that are utilized throughout this thesis. Chapters 4 and 5 present the results obtained through the JKR- and DMT-type analyses respectively and propose explanations for these results. In Chapter 6, a comparison is made between the results obtained analytically and those obtained by others through experiments and a finite element analysis. Finally, Chapter 7 will summarize the results and conclusions obtained from the present research and list suggestions for future research.

Chapter 2. Literature Review

2.1 INTRODUCTION

In order to develop a method that can be used to measure surface and interfacial energies of solids, the use of a flexible structure, or an elastica, has been proposed. Research has been conducted on both the measurement of surface and interfacial energies of solids and on structural applications for an elastica; however, the two have never coincided. The following are examples of how each of the subjects have been examined individually.

2.2 SURFACE AND INTERFACIAL ENERGIES OF SOLIDS

The classical solution of the problem of two spheres brought into contact with one another was originally proposed by Hertz in 1881. Hertz ignored the presence of both friction and adhesion and computed the contact area and stress distribution for a compressive load. More recently, two significant, distinctly different methods of analysis have been developed which have included the effects of adhesion. The first method, known as the JKR method and developed by Johnson et al. (1971), examines the effects of adhesion within the contact area. The method predicts that two adhering solids that are brought into contact will have an infinite tensile stress and a sharp discontinuity at the edge of the contact zone. Additionally, the JKR method predicts a contact area greater than that predicted by Hertz (Horn et al., 1987). The second method, known as the DMT method and developed by Derjaguin et al. (1975), suggests that the attractive forces between two solids exist just outside of the contact zone where the surfaces are a small distance apart. The DMT method assumes that the deformed shapes of the surfaces are Hertzian and, like JKR, a contact area greater than that predicted by Hertz is expected (Horn et al., 1987). A more extensive review of the work accomplished by Johnson et al. and Derjaguin et al. is included in the subsequent sections.

The following authors have addressed, either analytically or experimentally, issues such as the measurement of surface and interfacial energies and the effect of adhesion on the contact radius. Many of the authors have chosen to compare their results to those obtained by the Hertz theory and the JKR and DMT methods.

2.2.1 Analytical Research

In their paper, Johnson et al. (1971) investigate surface forces and their effect on the contact equilibrium between two lightly loaded elastic solids. The theory developed by Johnson et al. (called the JKR theory) suggests that adhesion forces are present only within the contact region between the two solid bodies. Additionally, the theory states that under zero load, the two elastic spheres are in contact and have a finite contact radius, a , due to the adhesion forces. To determine the contact equilibrium between the elastic spheres, the total energy of the system, U_T , is computed. The total energy consists of three components: the elastic energy, U_E , the mechanical energy, U_M , and the surface energy, U_S . The equilibrium condition is then found by adding the three components of U_T and minimizing the total energy of the system ($dU_T / da = 0$).

The JKR theory diverges from Hertz's theory not only in its consideration of adhesion forces, but also in its inclusion of tensile stresses within the contact region. According to the JKR theory, stresses between the surfaces are tensile at the edge of the contact region and are compressive only in the center of this region. This condition then requires the sphere to meet the interface at a right angle. Johnson et al. computed values for the contact radius and deflection by minimizing the total energy of the system. These results were compared to those values obtained by applying Hertz's theory. The JKR theory produced values for both the contact radius and the negative load needed to separate the two spheres that were greater than those predicted by Hertz (Hertz theory actually predicts that the spheres will separate when the load has been removed, or $P=0$). Johnson et al. also verified their findings with a short series of tests using gelatin and rubber

spheres. Agreement was good between the analytical results and the experimental results for these low modulus solids.

Shanahan (1997) developed a variant on the JKR test in which a spherical membrane under slight internal pressure is brought into contact with a flat, rigid surface. By using a hollow membrane, as opposed to a solid sphere, a larger contact area developed between the sphere and flat surface (when the same conditions such as material, radius, and applied force are observed). This contact area, which was approximately 10 times larger, allowed for easier measurement and reduced potential errors. For instance, in the JKR method, the adhesion energy is proportional to the cube of the contact area. Therefore, a small error in the measurement of the contact area results in a magnified error in the value for the adhesion energy. In contrast, in the method developed by Shanahan, the energy of adhesion is proportional to the square of the contact area, consequently reducing the magnitude of any propagated error in the calculation of the adhesion energy.

In addition to a larger contact area, Shanahan's balloon test yielded other results that differed from those predicted by JKR. First, the analysis conducted by Shanahan produced a value for the separation force 33% larger than that predicted by JKR. Also, once a material was chosen, the sphere used in the JKR test had inherent bulk and surface properties. However, with the balloon test, only surface properties were determined by the material type. The mechanical properties can be modified by changing the initial internal pressure of the spherical membrane. It must be noted, however, that the pressure in the sphere must remain small for the test to be advantageous.

Despite its advantages, the balloon test does present a few small problems. Initially, there may be difficulty in manufacturing the required spheres. Also, there may be difficulty in clamping the spheres during testing; however, this could be remedied by using two identical, flat plates on opposite sides of the sphere to provide stabilization.

Derjaguin et al. (1975) proposed an alternative analytical method to that derived by Johnson, Kendall, and Roberts. This method, known as the DMT theory, also predicted the deformed shapes, contact areas, and pull-off forces of a spherical ball in contact with a hard surface. In their analysis, several assumptions were made. First, only the elastic interaction of the ball and rigid surface was considered. Second, the modulus of elasticity of the surface was considered to be much greater than that of the ball. However, the modulus of elasticity of the ball should not be so small that the attractive forces present would not be able to change the form of the ball outside of the contact zone. The adhesion forces considered in this analysis act outside of the contact area in a ring-shaped zone. Additionally, the width of this ring-shaped zone in the radial direction decreases as the flattening of the ball occurs. Similar to the Hertz theory, only a compressive force was present within the contact zone, producing a contact area between the ball and the surface which resembled, in general appearance, that predicted by Hertz. Therefore, Derjaguin et al. predicted no discontinuities at the boundaries of the contact area.

After a detailed mathematical analysis, a series of equations that predicted values for the contact area, adhesion forces, and adhesion forces was developed. Derjaguin et al. concluded that the presence of van der Waal's forces led to an increase in the contact area (as compared to the Hertz theory). Additionally, Derjaguin et al. discovered that the force required to separate the surfaces is equal to the sticking force calculated for a sphere experiencing point contact and lacking contact deformation. No experimental work was conducted to verify the conclusions obtained by Derjaguin et al. (1975).

Muller et al. (1982) published an additional paper examining the force of sticking of an elastic sphere to a solid surface. Two methods were developed to calculate this pull-off force. The first method, the thermodynamic approach, required the calculation of the first derivative of the total energy of the adhesion interaction. This approach was later proven to be incorrect (Pashley, 1984). The second method, a force approach, involved a summation of the adhesive forces outside of the contact area between the sphere and the

rigid solid. Both methods produced values for the maximum adhesion force approximately equal to the force calculated for a sphere experiencing point contact and lacking contact deformation, as was predicted in Derjaguin et al. (1971). Additionally, the values obtained for the pull-off force were deemed valid whether the sphere was being brought into contact with the rigid surface or was being pulled away from the surface after deformation had occurred.

In an attempt to form a link between the DMT and JKR theories, Maugis (1992) developed a general theory using the previously mentioned methods as limiting cases. To do so, Maugis chose to use the Dugdale model for adhesion. The Dugdale model specifies that a constant constraining stress acts around the contact area in an annulus. The Dugdale zone can be simulated in actual testing by the presence of a liquid meniscus at the edge of the contact zone. As stated previously, the JKR and DMT theories were used as limiting cases for the general theory developed by Maugis. The JKR theory is valid only for short-range interactions and/or soft metals. In contrast, the DMT theory is applicable for long range interactions and/or hard materials.

Using the general theory, the limiting cases, and a liquid meniscus at the edge of the contact area, the change in profile of two crossed cylinders under zero load was examined as the size of the meniscus was altered (Maugis, 1992). Under dry air conditions, the cylinders experienced a sharp discontinuity at the edge of the contact zone, therefore resembling a JKR profile. When a water meniscus was present, the profile of the cylinders acted in accordance with the general theory developed by Maugis. Finally, when a large meniscus was present, the cylinders acted according to the DMT method.

2.2.2 Experimental Research

Experiments involving surface and interfacial energies of solids often concentrate on the measurement of adhesion forces and the examination of the deformed shapes of the solids in contact. Additionally, these experiments are often compared to results predicted

analytically by the DMT and JKR methods, which account for adhesion forces, and to those predicted by the Hertz theory, which ignores adhesion.

Using two sheets of mica and affixing them to cylindrical glass lenses, Horn et al. (1987) performed tests to measure surface forces as a function of separation between two solids. The test specimens were prepared by gluing the two sheets of mica to cylindrical glass lenses using the epoxy adhesive Epon 1004. Before assembling the specimen, the side of the mica that makes contact with the epoxy was coated with a reflective silver film that would act as an optical interferometer. This silver film then allowed the authors to take measurements of the separation distance between the layers of film. The thickness of the silver film and of the mica layers was subtracted from the initial measurement to obtain the separation distance between the outer faces of the mica. Load measurements were obtained through the use of a double-cantilever spring attached to one of the glass lenses. The glass cylinders were then oriented with their axes at right angles to so that their geometry resembled that of a sphere on a flat surface. Once assembled, the testing apparatus was filled with either a concentrated solution of KCL or an inert atmosphere, such as N₂. When the apparatus contained the KCL solution, a short range, repulsive interaction between the cylinders was experienced. The results obtained from this test were then compared to results predicted by the Hertz theory. When the apparatus contained the N₂ gas, only van der Waals forces were present, allowing the results to be compared to JKR theory.

Results obtained by Horn et al. were mixed. For the test involving nonadhesive contact, good agreement with the Hertz theory was recognized. The contact radius (a) increased with the application of load (P) according to the equation $P=Ka^3/R$ (where K is a constant and R is the radius of the sphere being brought into contact with a flat surface). When adhesion between the surfaces was present, the agreement between the predicted and actual outcomes was not as favorable. During testing, a plastic deformation of the epoxy layer occurred due to the presence of tensile stresses that exceeded the tensile capacity of

the epoxy. Therefore, the perfectly elastic system required to test the JKR theory fully could not be attained with the mica-epoxy-glass composite. Despite the plastic deformation of the system during testing, several conclusions were drawn from the tests where adhesion forces were present. First, at a given load, the contact radius is greater when adhesion forces are present and, under zero load conditions, a finite contact area exists. Secondly, an abrupt separation from a finite contact radius occurs as the adhering solids are pulled apart. The contact radius obtained at pull-off agreed with the value predicted by JKR.

Tabor (1977) chose to examine the effects of roughness and material ductility on the adhesion of solids. Before considering the effects of roughness on solids in contact, Tabor first analyzed two theoretical approaches for predicting adhesion forces, deformed shapes, and contact areas. First, the theory proposed by Derjaguin et al. (DMT theory) was examined. Tabor argued that by assuming a Hertzian shape for the deformed rubber ball, Derjaguin et al. ignored the deformation due to the attractive forces close to the edge of, but outside, the Hertzian circle. The author then argued that a theory that integrated the concepts of surface forces with the principles of contact mechanics was necessary. This second theory, which was developed by Johnson et al., stated that all important attractive forces were found within the immediate contact area. When there is no external load, a compression region formed in the center of the contact zone while tension existed in the outer regions. Additionally, a sharp discontinuity formed at the edge of the contact zone.

Using the contact mechanics approach as a guide, several experiments were conducted. First, an optically smooth rubber hemisphere and a hard, flat surface of Perspex were brought into contact. When the Perspex surface remained smooth, the values for the pull-off force and the contact radius agreed with the prediction made by contact mechanics. However, when the surface was roughened, the adhesion diminished as the roughness was increased. The main factor affecting the decrease in adhesion was the existence of a

few high asperities that exerted a large elastic force when penetrating the surface of the rubber hemisphere. Therefore, the adhesion between the two surfaces was decreased due to the presence of higher asperities that attempted to separate the surfaces and detracted from the adhesion forces between the lower asperities and the hemisphere.

An additional series of experiments was conducted to determine the adhesion of clean solids. Materials such as metals and other hard solids (diamond, sapphire, and TiC) were carefully cleaned in a high vacuum. Crossed cylinders, similar to those used by Horn et al. (1987), were used to conduct the experiments. Adhesion between cleaned ductile metals was high; however, regardless of the degree of cleaning, the adhesion of the hard solids remained low. Tabor explained this discrepancy in the following manner: “the lack of strong adhesion is a result of the fact that for hard elastic solids the extensibility of an adhered junction before it fails in tension is very small.” Therefore, when surfaces of solids come within atomic contact, the “graininess” of the material becomes relevant and atom-atom interactions become a vital factor. Additionally, the ductility of the material and its ability to deform elastically contribute to the extent to which the adhesion forces act.

Subsequent to his 1977 experiments, Tabor paired with Pashley (Pashley and Tabor, 1981) to perform additional experiments involving the contact of cleaned metal surfaces. Testing involved the contact of a 1 μ m radius tungsten tip with a single nickel crystal. The nickel and tungsten specimens were cleaned thoroughly until no traces of contamination were present on an Auger spectrum. The two surfaces were brought into contact and the applied load and contact resistance were recorded. The contact resistance, measured using a four-terminal ac resistance measuring system, could then be used to calculate the contact area.

Results were obtained for both clean metal surfaces and lightly oxidized surfaces. For cleaned metals under higher loads, a steady rise in adhesion with the application of

additional load was observed. This indicates that adhesion was dependent on the load and that plastic deformation of the specimens had occurred. At the higher loads, the results were in good agreement with earlier work by Tabor and Pethica (1979). For lower loads, adhesion was independent of the load and was affected solely by the surface forces. Additionally, a significant amount of scatter was experienced among data points at these low loads. Pashley and Tabor determined that varying amounts of contamination in the contact area resulted in a large scatter of the results, particularly at low loads. Additional results obtained through tests involving cleaned metals included the recognition that the adhesion measurements obtained from a contaminated contact were lower than those obtained from cleaner surfaces, the contact area had a finite value at zero load, and a ductile separation of the contacts occurred.

Next, testing was performed on a lightly oxidized nickel surface in contact with a clean tungsten tip. The values obtained for contact resistance varied considerably from area to area over the surface of the crystal, implying uneven surface oxidation had occurred. Despite variable data for the contact resistance, adhesion forces were consistently found to be 2 to 3 times less than those obtained under cleaned surface conditions.

Finally, for tests concerning both the cleaned metal and lightly oxidized surfaces, the loading-unloading curve was found to be highly irreversible. Through further study of the experimental results, it was concluded that the surface energies themselves were significantly larger than the bulk hardness of the nickel crystal and therefore were able to initiate plastic deformation of the crystal.

2.3 ELASTICA THEORY

Even though Euler derived the solution of the elastica in 1744, the elastica theory continues to be regenerated in a variety of new applications. Authors and researchers have used and modified Euler's original equations to solve problems involving the laying of pipelines in the ocean, peeling of adhesives, improving pole-vaulting techniques

(Griner, 1984), and predicting the largest axial compressive force a piece of paper passing through a copier can withstand before it will jam the machine (Vaillett et al., 1983). The following is a summary of only a portion of the work done which has used the elastica theory developed by Euler. Some of the authors who will be discussed in the following paragraphs have chosen to apply previously developed elastica equations to new applications, while the remaining authors have chosen to develop new methods of determining solutions for elastica problems.

2.3.1 Basic Elastica Theory

Timoshenko and Gere (1961), using a slender, vertical rod that was fixed at the base and free at the upper end, discussed large deflections of buckled bars. By considering a large vertical load, P , which was much greater than the critical buckling load, a large deflection in the bar was produced. The exact curvature of this deflected rod was given by $d\theta/ds$ when the distance, s , was measured from the origin, located at the free end of the bar. The curvature of the bar was then multiplied by the flexural rigidity (EI) to obtain the exact differential equation of the deflection curve. The shape of the elastic curve, when found using this exact differential equation, is called the elastica. Additionally, when the equation of the deflection curve is differentiated with respect to s , the following equation is obtained:

$$EI \frac{d^2\theta}{ds^2} = -P \sin \theta \quad (2.1)$$

The differential equation of the deflection curve resembles the form of the differential equation for the oscillations of a pendulum (Stoker, 1950).

After integrating the above equation and applying the appropriate end conditions, Timoshenko and Gere obtained equations for the total length of the rod and expressions for the x and y coordinates at the free end of the deformed rod. Additionally, coordinates of intermediate points along the deflection curve can be found using elliptic integrals.

The equations presented by Timoshenko and Gere were based on the assumption that the slender rod was fixed at one end while allowed to remain free at the other. The results, however, may also be used for a bar that is hinged at both ends. A series of curves, representing possible forms of equilibrium of the rod, can be derived for the slender fixed-free rod by substituting different values for the angle of the deflected tip into the equations given by Timoshenko and Gere. These curves can then be combined to obtain a variety of shapes for the hinged rod. Values for the forces necessary to produce the bending in the hinged rod can be found by combining the pertinent results from the analysis of the slender fixed-free rod.

Plaut et al. (1998) discussed various equilibrium shapes of an elastica in contact with a rigid surface. The strip was assumed to be elastic and inextensible and the bending moment was assumed to be proportional to the curvature. The weight of the strip and the friction between the strip and the rigid surface were neglected. Additionally, the rigid surface was assumed to be flat and horizontal. The ends of the elastica were lifted, bent, and clamped vertically at an equal height and specified distance apart. Therefore, when no contact occurred between the bent elastic and the rigid surface, the shape of the elastica was symmetric.

The analysis began by examining the elastica before any contact had occurred. All variables represented nondimensionalized quantities. The length of the elastica was defined as 2, the separation distance between the ends was $2c$, the arc length was s , the angle of the tangent with the horizontal was θ , and the horizontal and vertical coordinates were x and y , respectively. A constant horizontal force, p , was present along with a variable bending moment, m . The governing elastica equations were as follows:

$$\begin{aligned} \frac{dx}{ds} &= \cos \theta & \frac{dy}{ds} &= \sin \theta \\ \frac{d\theta}{ds} &= m & \frac{dm}{ds} &= -p \sin \theta \end{aligned} \quad (2.2 - 2.5)$$

A shooting method was utilized to determine values for p and m . To use this method, initial values of p and $m(0)$ were guessed; then the elastica equations were numerically integrated until $s=1$. Once the reactions p and $m(0)$ had been calculated, equilibrium shapes were determined using equations derived for the x and y values.

The symmetric case with point contact was examined next. Equations (2.2 – 2.4) remained the same; however, equation (2.5) was transformed to

$$dm/ds = -p \sin \theta + q \cos \theta \quad (2.6)$$

where q was half the nondimensionalized applied vertical force. Results for the reactions at separation distances of $c = 0, 0.2, 0.4, 0.6,$ and 0.8 were then determined. Additionally, the vertical deflection was determined by solving for y (1) and subtracting this value from the initial height determined by the no contact case.

Also included in this analysis were results for the symmetric elastica with line contact, a symmetric elastica with a buckled region, a symmetric elastica with two loops, and various asymmetric elastica equilibrium shapes. Reactions were found for the separation distances $c = 0, 0.2, 0.4, 0.6,$ and 0.8 for each of the cases listed above. These additional elastica configurations developed as the elastica was pushed further against the rigid surface (for instance, when greater deflections occurred). Asymmetric configurations occurred when the elastica was no longer stable as a symmetric structure and therefore shifted to the left or right. Practical applications for such investigations relate to the denting of vehicles, ships, and submarines (Kitching et al., 1975), the deformations of tires (Mack et al., 1983), the testing of pressure on the cornea (Updike and Kalnins, 1972), and the adhesion of vesicles and red blood cells to surfaces (Evans, 1980).

2.3.2 Applications of the Elastica Theory

G. M. Griner (1984), in his parametric solution to the pole-vaulting pole problem, recognized the advantages in modeling a fiberglass pole used for pole vaulting as an elastica having an applied concentrated force and moment at the upper end. In his analysis, Griner obtained a parametric solution, expressed in terms of tabulated elliptic integrals, which he believed generated an advantageous pole-vaulting technique that was not normally utilized by coaches or athletes.

In his analysis, Griner depicted the fiberglass pole as a thin elastic column. The upper end of the pole was subject to lateral and transverse forces and a bending moment. To retain static equilibrium, an applied transverse force was used to counteract the applied moment. Furthermore, the Bernoulli-Euler relation for moment, a variation of the classical elastica equation, was used in the analysis. A manipulation of the Bernoulli-Euler moment formula produced equations for the length of the pole, the x and y coordinates, and the inflection point in the pole. This inflection point develops in the upper portion of the pole when a negative applied moment, activated by the pole-vaulter in mid-vault, counteracts the bending which has already occurred.

Griner uses his results to determine the magnitudes of negative moments necessary to cause rapid straightening of the rod under a variety of magnitudes of the compressive force. Additionally, the possibility of snap-through buckling, which occurs when a negative moment becomes large enough to instantaneously reverse the bending of an elastica, was investigated. Through estimates of the maximum bending moment that a vaulter may apply, Griner determined that while rapid rod straightening was a feasible pole-vaulting technique, the danger of snap-through buckling was remote. Therefore, the following pole vaulting technique was outlined by Griner: "Once maximum deflection [of the rod] has been achieved the vaulter would benefit from a powerful straightening of the pole such as would occur if it were suddenly much stiffer. Apparently this can be accomplished by applying a negative moment at this time." A right-handed pole vaulter

should therefore push with his right arm, pull with his left arm, and invert himself with his legs extended in order to create the maximum possible negative moment.

Several other authors have used elastica models and elliptic integrals to solve practical application problems. Vaillette and Adams (1983) chose an infinitely long elastic beam contained within a frictionless, rigid channel and subjected to axially compressive forces to simulate such real world occurrences as paper feeding through a copier machine or film passing through a movie camera. Using variations of the equations discussed above, Vaillette and Adams investigated the maximum permissible axial force that may occur before the beam collapses in the channel. The elastica solution to the beam confined within a channel was then compared to the linear theory (Vaillette, 1982) which was previously used to solve comparable problems. The elastica model clearly represented the physical problem in a more realistic light, due to the fact the linear theory did not differentiate between the length along the curve and the horizontal length the deformed beam occupied. Additionally, the linear theory allowed the length of the beam to become zero, therefore making it possible for the beam to support an infinitely large compressive force. Finally, Vaillette and Adams concluded that for large values of the applied load, the beam became unstable and folded over on itself.

The investigation of the elastica equations for a bar or beam of a given span length but unknown arc length by Chucheepsakul et al. (1995) was motivated by recent activities in offshore engineering and deep ocean mining. The elastica theory was applied to the following situation related to these topics: a riser or bar was used to connect a spot on the seabed to a specified point on the sea surface. Therefore, in the design stage, the span was predetermined whereas the arc length was unknown. The bar was hinged at one support and was free to slide over a second, frictionless support where the reaction was always normal to the beam. A moment was then applied at the hinged support. Using an elliptic-integral formulation, the maximum applied moment the beam can resist was obtained. The actual applied moment was then compared to the calculated maximum or

critical moment. If the applied moment was less than the critical moment, there existed two equilibrium configurations for the beam; of these two configurations, one was stable while the other was not. The stable configuration could be established by visual inspection of the two plotted configurations. Once the stable configuration was known, the length of the arc could be determined. Note that the elliptic-integral method used by Chucheepsakul et al. yielded exact results, whereas other methods led to approximate solutions. The finite element method was also used to solve this problem and yielded results comparable to those obtained in the elliptic-integral method.

The folding of thin elastic sheets, such as paper, sheet metal, or cloth, in the manufacturing process was the primary focus of Wang (1981). By requiring the thickness of the sheet to be small as compared to its minimum radius of curvature, Wang could use the following elastica equations in his analysis:

$$EI \frac{d\theta}{ds} = -M + Fx + Gy$$

$$\frac{dx}{ds} = \cos \theta \quad \frac{dy}{ds} = \sin \theta \quad (2.7 - 2.9)$$

where M , F , and G were the moment, vertical force, and horizontal force, respectively.

Additionally, three different cases of folding were defined within the paper. In Case 1 the folded elastica was compressed by two parallel approaching plates. In Case 2 the elastica was folded between two symmetric rollers. Finally, in Case 3 it was folded between a moving roller and a flat plane. Instead of using the elliptic integral equations to obtain solutions to the three cases above, simple numerical integration was used. The results obtained were as follows: for the same force F and bending stiffness EI , Case 1 had the smallest width, while Case 2 had the smallest height. Case 3 had both the largest width and produced the largest maximum moment and was therefore the least favorable method for the folding manufacturing process.

Thacker et al. (1997) used the elastica theory to determine maximum loads for structures that experience large disturbances. First, a slender elastic column subjected to increasing compressive end loads was discussed. At a certain critical load, the column deviated from its straight shape and buckled. Previously, the bifurcation critical load was used as an indicator for elastic stability. Therefore, if a force on the column was below the bifurcation load, it was assumed that the column would return to its undeformed state after the removal of any sufficiently *small* perturbations. Additionally, a global critical load F_{gc} was defined, below which the column returned to its initial state after *any* applied disturbance (large or small). In some cases, the value of F_{gc} was smaller than the bifurcation load, making the bifurcation load a poor indicator of stability. One such case was a platform supported by two flexible columns subject to earthquake loading.

The effect of the height of the platform on the global critical load was the primary focus of the analysis. First, the columns were defined as slender, perfectly elastic, and with negligible weight. The ends of the columns were fixed to the base and to the rigid solid. The distance between the columns was defined as βL , whereas the length of the columns was defined as L . The total weight of the platform, W , acted at the center of mass which, in the undeformed state, was a distance $\alpha L + L$ from the base. The elastica equations used were similar to those defined by Wang (1981) and differed only by the existence of the two-column system specified in the paper.

By applying the appropriate geometric boundary conditions and manipulating the elastica equations, Thacker et al. derived an equation for the vertical translation, δ , of the center of mass after deformation occurred. As the values for the displacement δ increased, the corresponding vertical load first increased, then decreased, then increased again, indicating the presence of up to three equilibrium solutions. The effect of varying parameters such as the height of the center of mass and the separation of the columns was also examined. It was noted that an increase in the height of the center of mass greatly magnified the nonlinear behavior, therefore drastically decreasing the value of F_{gc} .

However, the value of F_{gc} increased with increasing values of β , but was limited by the bifurcation load, which was independent of β . Therefore, in the case of a platform that experiences earthquake loading, the bifurcation load was totally erroneous in predicting the safe load under finite disturbances and the global critical load should be utilized.

In an effort to avoid the nonlinear equations of equilibrium for plane elastica problems, which were developed by Euler in 1744, Faulkner et al. (1991) used a segmental shooting approach, allowing the separate segments to be loaded in various manners and solved individually. To utilize this technique, a rod with a linear elastic material behavior was assumed to be composed of a number of segments, the ends of which undergo small relative rotations. The small relative rotations in each segment allow the equilibrium equations to be linearized and solved in a straightforward manner. To ensure compatibility between adjacent segments, geometric and force compatibility conditions were applied at the nodes. The original nonlinear problem was divided into small linear segments that could easily be analyzed by a computer. When multiple solutions existed, the segmental shooting technique was capable of determining all solutions and providing insight as to which solution was the most stable. To illustrate their technique, the procedure was applied to both a cantilever and a semi-circular arch example. Benefits derived from this method of analysis included the ability to determine the solution for each segment analytically and the elimination of the need for incremental loading as required by finite element analysis.

2.4 CONCLUSIONS

Although much research has been performed independently on the subjects of surface energies of solids and an elastica, none of authors discussed above have chosen to examine surface and interfacial energies of solids using an elastica. By using a flexible structure, instead of a flexible material as proposed by many authors, a variety of materials may be investigated. The deformed shapes and contact areas between the bent elastica and a rigid surface can then be examined to determine the effects of adhesion.

Chapter 3. Formulation of Analytical Methods

3.1 INTRODUCTION

To investigate the effect of surface energies on the adhesion of solids, an elastica in contact with a flat, rigid surface was chosen. This elastica was assumed to be thin, uniform, smooth, inextensible, and flexible in bending. The extremely flexible structure of the elastica permitted measurable deformation of the solid by relatively small surface attractions. The ends of the elastica strip were lifted, bent, and clamped vertically at an equal height and at a specified distance apart. The ends of the elastica were then moved downward and brought into contact with a flat, horizontal substrate (see Figure 3.1). Additional force was then applied to the ends of the elastica, causing the strip to flatten. Various planar equilibrium shapes were possible, including symmetric and asymmetric shapes with single point contact, symmetric and asymmetric shapes with a flattened region, and symmetric shapes with a buckled region. For the present research, only symmetric shapes were considered. When the effects of adhesion were included in the analysis, the forces of attraction between the elastica and the rigid surface modified the elastica's shape and caused an elongation of the contact length. The effect of adhesion on the contact of the elastica with the rigid surface was determined by comparing values obtained for the contact length of elastica strips subject to surface attractions to those values of the contact length obtained for elastica strips where no adhesion was considered.

The dimensions of the elastica and forces acting on the system were defined as follows. The length of the elastica strip was $2L$, the width of the strip was unity, and the bending stiffness was EI . The initially straight elastica was bent until the ends were a distance $2C$ apart at a fixed height, and the ends were clamped with vertical slopes ($\theta = \pi/2$). The origin of the coordinate system for an elastica strip that has no contact or point contact

with the substrate was placed at the bottom of the strip where the slope was equal to zero. For an elastica strip which has a contact length, $2B$, greater than zero, the origin was placed at the point of separation of the elastica from the rigid substrate. The arc length of the elastica was S , the angle of the tangent with the horizontal was θ , and the horizontal and vertical coordinates were X and Y , respectively. Furthermore, the constant horizontal force was P , the applied vertical force at each end was Q , the vertical deflection due to the load was Δ , the bending moment at the clamped end of the elastica was M_0 , and the moment at the point of separation of the elastica from the rigid surface was M_b . Since only symmetric shapes were examined, this symmetry was utilized and only one-half of the structure was considered. See Figure 3.2 for an illustration of the orientation and location of the variables and forces for an elastica strip in contact with a rigid surface.

In an effort to simplify the comparison between the results obtained from the present analysis with those obtained through experiments on a variety of specimens of differing size and material properties, all elastica dimensions, forces, moments, and energies were nondimensionalized. Table 3.1 illustrates the nondimensionalization process used.

Table 3.1: Nondimensionalized Quantities

Nondimensional Quantity	Definition	Nondimensional Quantity	Definition
s	S / L	δ	Δ / L
x	X / L	p	$PL^2 / (EI)$
y	Y / L	q	$QL^2 / (EI)$
h	H / L	m_0	$M_0L / (EI)$
b	B / L	m_b	$M_bL / (EI)$
c	C / L	u (energy)	$UL / (EI)$

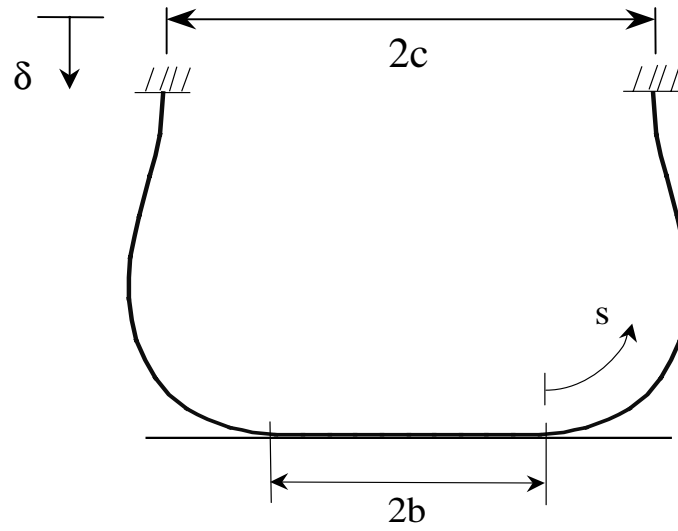


Figure 3.1: Geometry of an elastica in contact with a rigid surface

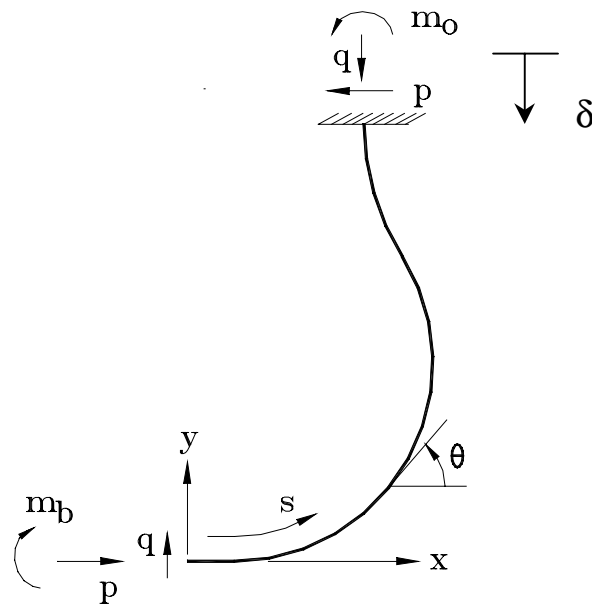


Figure 3.2: Orientation and location of variables and forces for an elastica experiencing line contact

To solve the governing numerical equations and obtain the equilibrium shape of the elastica, a shooting method was utilized. From geometry, the moment-curvature relation, and equilibrium of an element, the governing equations used in the shooting method were:

$$\begin{aligned} \frac{dx}{ds} &= \cos \theta & \frac{dy}{ds} &= \sin \theta \\ \frac{d\theta}{ds} &= m & \frac{dm}{ds} &= -p \sin \theta + q \cos \theta \end{aligned} \quad (3.1 - 3.4)$$

The appropriate end conditions were then applied in order to solve for the desired parameters. For the no contact and the point-contact cases, $x = y = \theta = 0$ at $s=0$ and $x = c$, $\theta = \pi / 2$ at $s=1$. When a contact area greater than zero existed, the boundary conditions were $x = y = \theta = 0$ at $s=0$ and $x = c-b$, $\theta = \pi / 2$ at $s=1-b$. The governing equations, boundary conditions, and values for defined variables (such as b and c) were then entered into a Mathematica file and an equilibrium solution was obtained. Examples of the Mathematica files used can be found in Appendix A.

Two types of analysis were used in order to determine the effects of adhesion on the contact of solids. The first method investigated was a JKR-type analysis where the adhesion forces existed only within the contact region and an energy approach was used to obtain values for the unknown variables. To determine the equilibrium shapes and contact areas, the total energy of the system was minimized. The second method investigated was a DMT-type analysis where the adhesion forces existed in a small region outside of the contact area and an equilibrium approach was used to obtain values for unknown variables. Since the effects of adhesion were contained within the force equations used in the shooting method, the equilibrium shapes and contact areas could be calculated directly. A more detailed description of both analysis methods follows.

3.2 JKR-TYPE ANALYSIS

The analysis method developed by Johnson et al. (1971) was an extension of Hertzian theory and included the effects of surface and interfacial energies. The JKR-type analysis performed in conjunction with the present research was derived from this original JKR method. The elastomer or elastomeric lens required by the experimental technique developed by JKR was replaced with an elastica, which yielded a rectangular contact area (when anticlastic bending is ignored). Additionally, the present research assumed the deformed elastica would retain a smooth, continuous shape. This assumption differed from the original JKR method that predicted a discontinuous slope at the point of separation of the elastomer from the substrate.

3.2.1 Description of Adhesion Forces

The JKR-type analysis was performed using the previously discussed shooting method to solve the governing elastica equations. The weight of the elastica was initially assumed to be negligible. To account for surface and interfacial energies of the materials, an adhesion energy, acting in the region of contact between the rigid surface and the elastica, was considered. This nondimensional adhesion energy was found by multiplying the nondimensional work of adhesion, $\Delta\gamma$, by the contact area. The dimensional work of adhesion is a function of the surface energies of both materials and, therefore, is equal to $\Delta\gamma = \gamma_1 + \gamma_2 - \gamma_{12}$. The term γ_1 is the surface energy of one surface, the term γ_2 is the surface energy of the second surface, and the term γ_{12} represents the interfacial surface tension. The work of adhesion was nondimensionalized using the following formula:

$$\text{Work of Adhesion} = \Delta\gamma = \frac{(\Delta\gamma)_{\text{DIM}} L^2}{E T^3} \quad (3.5)$$

where $(\Delta\gamma)_{\text{DIM}}$ is the dimensional quantity for the work of adhesion (usually given in mJ/m^2) and T is the thickness of the elastica. A range of acceptable, realistic values of $\Delta\gamma$

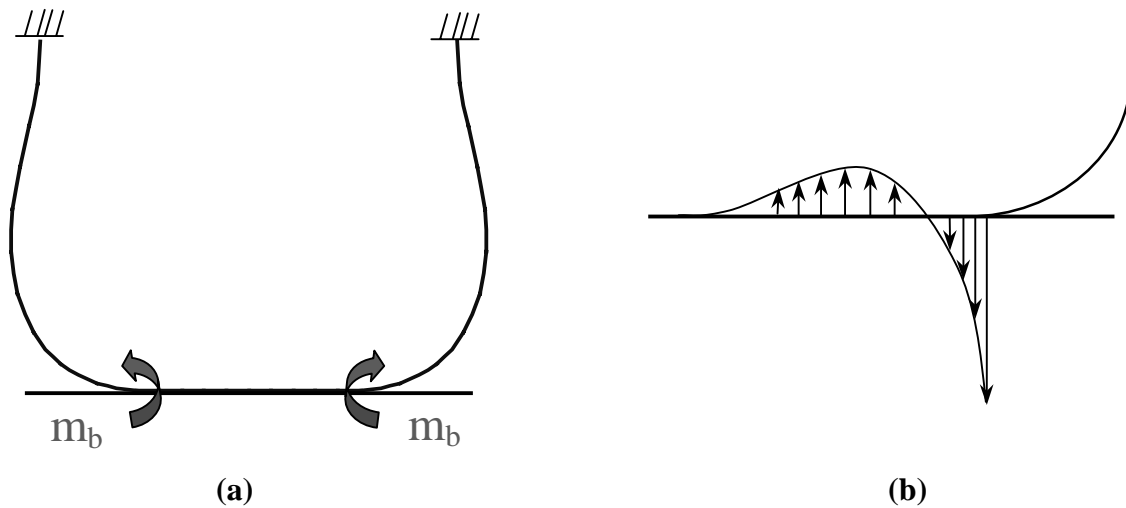


Figure 3.3: (a) Location of moment m_b ; (b) Stress distribution at the point of lift-off due to adhesion forces

which could be used in the analysis was then chosen based on equation (3.5) and a variety of material types. To allow the work of adhesion to deform the elastica and elongate the contact length, a model of the effect of adhesion was developed. At the point of separation of the elastica from the substrate, a moment (m_b) was allowed to assume a non-zero value (Figure 3.3 (a)). The value for m_b was then determined in the process of minimizing the total energy of the system. Figure 3.3 (b) shows the proposed stress distribution due to the adhesion forces. A compressive stress is located in the central region of the contact length, whereas a tensile stress exists at the outer portion of the contact zone. The tensile stress reaches its maximum value at the lift-off point.

3.2.2 Minimization of Energy

Because the effect of the surface energies on the contact of the elastica with the rigid surface was not included in the equations used in the shooting method, it was necessary to use another means to account for their presence. Therefore, an energy method, similar to that employed by Johnson et al. (1971), was utilized. To find the contact equilibrium between the elastica and the rigid solid, the total nondimensional energy of the system,

u_T , was computed. The equation for the total energy consisted of three components: $u_T = u_E + u_M + u_\gamma$. The strain energy due to the bending of the elastica, u_E , was calculated by the Mathematica file. The strain energy was one-half of the integral of the moments squared along the free length of the elastica, or $u_E = \int m^2 ds$, with use of symmetry and the limits of integration extending from $s=0$ to $s=1-b$. The mechanical potential, u_M , was due to the vertical forces, q , moving through the distance δ . Therefore, u_M was equal to $-2q\delta$. Finally, u_γ was the surface or adhesion energy term. The value of u_γ was found by multiplying the work of adhesion ($\Delta\gamma$) by the contact length $2b$ and a factor of 12. This factor of 12 was obtained through the nondimensionalization process when the moment of inertia was broken down into its components, $I=bh^3/12$, and like terms in the denominator and numerator were cancelled. Therefore the value of the adhesion energy term was $u_\gamma = -24b(\Delta\gamma)$.

The total energy of the system, u_T , was calculated for a variety of equilibrium shapes. The values for c , the separation distance between the ends of the elastica, and q , the vertical force, were held constant while the contact length, b , was varied. For each value of b , the total energy was calculated. The values obtained for u_T were then examined. The point where u_T was found to be at its minimum value was considered the equilibrium solution for those particular values of q and c . Once the equilibrium solution was obtained, the values for m_b , b , and the equilibrium shape were determined. This process was then repeated for various values of q and c .

3.2.3 Cases Examined

Using the JKR-type analysis, several different cases were examined. First, a separation distance of $c=0.4$ was considered (Figure 3.4). For this separation distance, five different values for the nondimensional work of adhesion were examined. These values included 0 (indicating no adhesion forces were present), 0.16, 0.32, 0.48, and 0.64. Next, a separation distance of $c=0.8$ was considered (Figure 3.5). The same values of $\Delta\gamma$ were

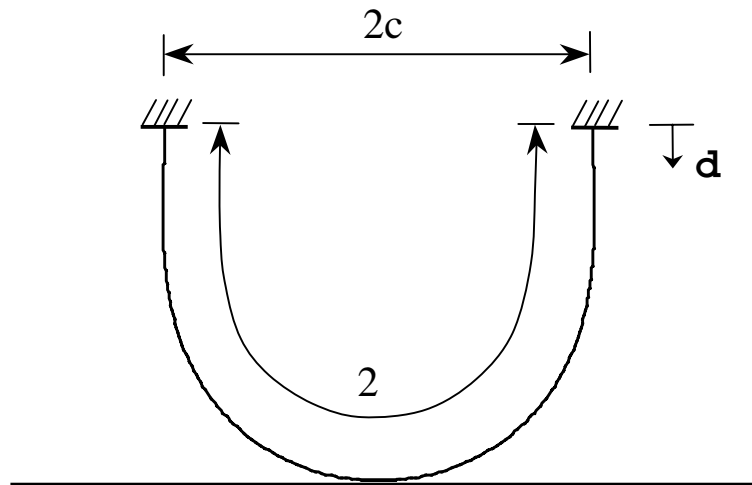


Figure 3.4a: Shape of elastica before contact when $c=0.4$

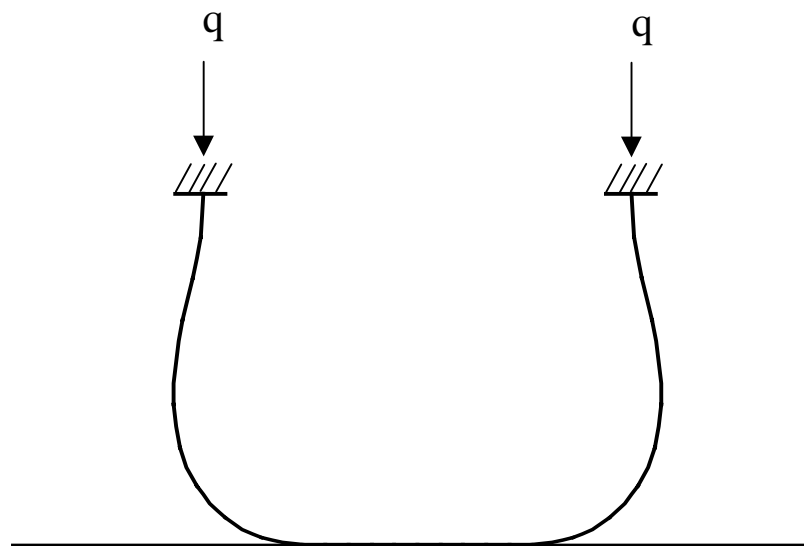


Figure 3.4b: Typical shape of elastica with line contact when $c=0.4$

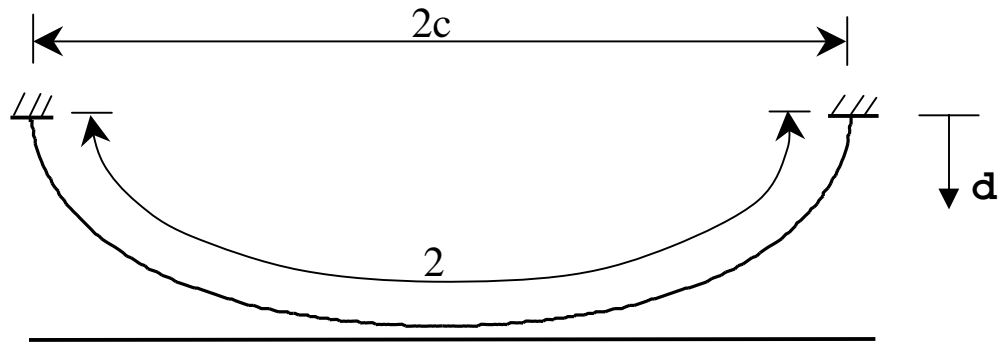


Figure 3.5a: Shape of elastica before contact when $c=0.8$

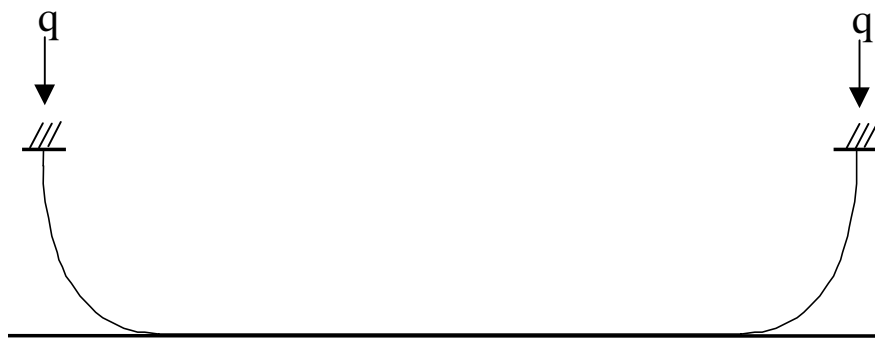


Figure 3.5b: Typical shape of elastica with line contact when $c=0.8$

examined. For each of these cases, a variety of values for the vertical force was considered and values for m_b , b , and p were calculated.

After the initial examination of the equilibrium solutions for $c=0.4$ and $c=0.8$, the equations used in the shooting method were modified to include the self-weight of the elastica. To find acceptable, realistic values to use for the nondimensional self-weight, η , values for the densities of a variety of materials were chosen. The following equation was employed to define the nondimensional self-weight (per unit length):

$$\eta = \frac{12 \rho L^3}{E T^2}$$

where ρ is the density of the specified material. Values chosen for η included -2, -1, 0, 1, and 2. A positive value of η indicated that the elastica was in the orientation shown in Figure 3.1, while a negative value of η indicated that the elastica was rotated 180 degrees and was pushed upwards onto the flat, rigid surface. Again, a separation distance of $c=0.4$ was used and η values were considered for the cases when $\Delta\gamma = 0$ and 0.64 . Note that when the η term was included to account for the self-weight, it was necessary to add an additional term to the total energy equation for the $\Delta\gamma = 0.64$ case. This term, u_G , was found using Mathematica and was equal to $2 \eta \int y(s) ds$ with the limits of integration extending from $s=0$ to $s=1-b$.

3.3 DMT-TYPE ANALYSIS

The second analysis technique used to investigate the effect of surface and interfacial energies was based on a DMT-type theory. The analysis method developed by Derjaguin et al. (1975) presented an alternative analysis method to that which was proposed by JKR. The DMT method, like the JKR method, was an extension of Hertzian theory. The deformation predicted by the DMT method was assumed to follow the Hertzian

prediction and the effect of the attractive forces was assumed to occur in a small zone just outside the contact area. The DMT-type analysis performed in conjunction with the present research was derived from this original DMT method.

3.3.1 Description of Adhesion Forces

The DMT-type analysis was performed using the previously discussed shooting method to solve the governing elastica equations. The weight of the elastica was considered to have a noticeable effect on the outcome of the analysis and was accounted for in the Mathematica file used to solve the governing equations. To account for surface and interfacial energies of the materials, an adhesion force, occurring in a small region just outside of the contact area, was used. Two types of DMT forces were considered: a linear force (relative to the vertical separation) and a Dugdale, or constant, force. These two force types will be discussed in more detail in the following sections. At the point of separation of the elastica from the rigid surface, the linear force experienced its maximum value, while the Dugdale force attained its constant value. When the separation distance between the elastica and the rigid surface reached a value equal to some specified distance, α , both forces were equal to zero. Values for α must be relatively small to indicate that the DMT force acts over an extremely small gap. Unlike the JKR-type analysis, the adhesion forces are included within the equilibrium equations, thereby eliminating the need to minimize the total energy of the system in an effort to find the equilibrium configuration of the elastica.

3.3.2 Linear DMT Force

As stated previously, two different DMT forces were examined within the analysis. First, a linear force was considered. The maximum value of the force, f_0 , occurred at the point of separation of the elastica from the rigid surface. The force varied linearly with the vertical separation distance between the elastica and the substrate. Because the adhesion force varied linearly with respect to $y(x)$, the force is considered a “linear” DMT force.

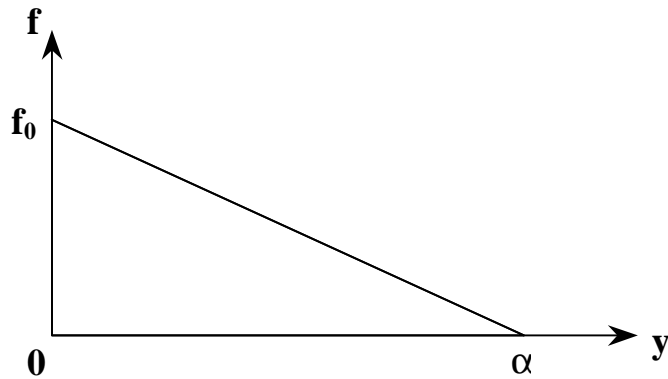


Figure 3.6: Linear force applied in DMT-type analysis

When the separation distance between the elastica and the rigid surface reached a value equal to some specified distance, α , the force became equal to zero (Figure 3.6). As stated previously, values for α remained small to indicate that the DMT force acted over an extremely small gap and to allow for the use of small angle theory in that region. Values of $c=0.4$ and $c=0.8$ were examined, as shown in Figures 3.4 and 3.5.

3.3.3 Dugdale DMT Force

The second DMT force considered was a Dugdale force. The Dugdale force was originally used as a model for crack tip plasticity and described the stresses in the adhesive zone as constant and equal to the yield stress of the material (Maugis, 1992). When applied to the present research, the Dugdale model yielded a constant force, g_0 , which occurred at the point of separation of the elastica from the rigid surface and remained constant until the separation distance between the elastica and the substrate reached the specified value of α . When the vertical separation distance between the two materials was greater than α , the adhesion force was equal to zero (Figure 3.7). To allow direct comparison of the linear and Dugdale force analyses, the same values were used for α ($\alpha = 0.001$, and 0.0001), while values for g_0 were obtained by multiplying f_0 by

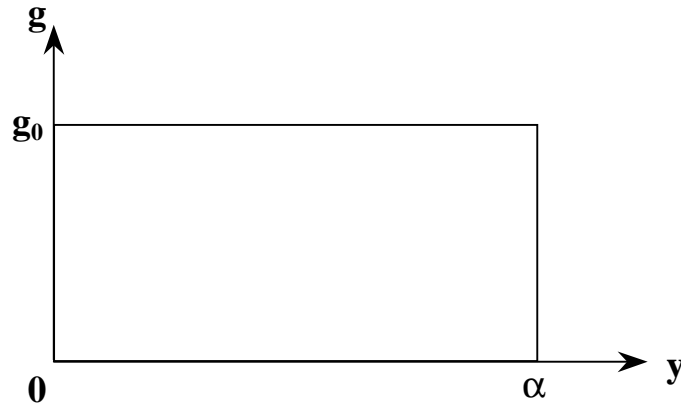


Figure 3.7: Dugdale force applied in DMT-type analysis

one-half. Therefore, the areas under the force curves, and consequently, the adhesion energies, were equal.

3.4 NO CONTACT, POINT CONTACT, AND LINE CONTACT SITUATIONS

For both the JKR- and DMT-type analyses, three stages of contact between the elastica and the substrate were examined. First, the linear contact stage was considered. Linear contact between the elastica and the rigid surface occurred when the ends of the elastica were pushed downward by the vertical force, q , and the value for the contact length, b , was greater than zero. The term linear contact is therefore used to describe the appearance of the contact zone from a two-dimensional perspective. The shooting method, described above, was used for each combination of c and q to obtain values for the contact length, the moment at the point of separation of the elastica from the rigid surface, and the horizontal force. Additionally, the deformed shape of the elastica was obtained for each of these combinations.

Next, the point contact stage was considered. Again, the term point contact is used to describe the appearance of the contact zone from a two-dimensional perspective. Since the adhesion forces in the JKR-type analysis were only active within the contact area, when the contact length, b , became equal to zero, the adhesion forces no longer existed. Therefore, to analyze the elastica experiencing point contact, an analysis technique that ignores adhesion forces must be used. On the contrary, the adhesion forces used in the DMT-type analysis were independent of the contact area and were still active in the point contact stage. Therefore, the series of deformed shapes that occurred when b equaled zero was investigated. To obtain values for the horizontal and vertical forces and the deformed shape of the elastica, the Mathematica file used for the linear contact stage was modified (see Appendix A).

Finally, the no contact, or lift-off, stage was examined. As stated previously, the adhesion forces of the JKR-type analysis were active only when the contact area was greater than zero. Therefore, to analyze the elastica experiencing lift-off, an analysis technique that ignores adhesion forces must be used. Because the DMT forces were independent of the contact area, they continued to act until the elastica was separated from the substrate by a distance of α . When the separation distance between the solids became greater than α , the effect of the adhesion forces vanished. To obtain values for the (upward) vertical force required to separate the solids, the horizontal force experienced by the elastica, and the deformed shape of the elastica, the Mathematica file used for the linear contact case was modified and the shooting method was used to solve for the desired variables. The Mathematica file used in the lift-off stage can be found in Appendix A.

Chapter 4. Results from the JKR-Type Analysis

4.1 INTRODUCTION

Several different cases were examined using the JKR-type analysis. First, a separation distance of $c = 0.4$ was considered. For the case $c = 0.4$, five different values for the work of adhesion were used. These values were 0, 0.16, 0.32, 0.48, and 0.64. For each value of $\Delta\gamma$, values for the horizontal force, the moment at the point of separation, the height of the elastica, and the energy terms u_E , u_M , u_γ , and u_T were obtained using the shooting method. When $\Delta\gamma = 0$, no adhesion forces were present. A majority of the work performed where adhesion forces were ignored was based on the previous analysis by Plaut et al. (1999). A shooting method was used to solve for the specified parameters when there was no contact between the strip and the rigid surface, when point contact existed between the two solids, and when the strip and the rigid surface had formed a line of contact.

When no contact existed between the elastica and the rigid surface and $\Delta\gamma = 0$, the governing equations 3.1-3.3 were applicable. Equation 3.4 was modified by removing the term containing q . The boundary conditions applied were $x = y = \theta = 0$ at $s=0$, and $x = c$, $\theta = \pi/2$ at $s = 1$ (see Figure 3.2). Values for $m(0)$ and p were guessed, the equations were integrated numerically until $s=1$, and the guessed values were then varied using the secant method or Brent's method until the end conditions at $s=1$ were satisfied with sufficient accuracy. The FindRoot command in Mathematica was used to obtain values for the guessed variables that met the specified end conditions. The value for the nondimensional height h_0 was found by evaluating y at $s = 1$.

When point contact between the elastica and the rigid surface was experienced and $\Delta\gamma = 0$, the governing equations 3.1-3.4 were applied. Additionally, the boundary conditions

described above for the no contact situation were also applicable for the point contact case. The same shooting method described for the no contact case was applied, with the additional specification of q . The value of q was increased from zero until the bending moment m_b at the contact point decreased to zero, at which point the contact zone spreads, creating a line contact situation.

When the contact length became greater than zero, line contact between the elastica and the rigid surface formed. Since no adhesion forces were present, the moment at the point of separation of the elastica from the rigid surface was equal to zero. Therefore, the end conditions at $s = 0$ (which was located at the right, clamped end of the elastica) were $x = y = 0$, $\theta = \pi/2$, $m = M$ (the moment at the clamped support), and the end conditions at $s = 1-b$ were $x = c-b$, $\theta = 0$, $m=0$ (see Figure 3.2). A scaled arc length z was introduced in the uplifted region, and was defined by $z = s/t$ and $t = 1-b$. The nondimensional length t was treated as a variable that had a constant value. The governing equations then became

$$\begin{aligned} \frac{dx}{dz} &= t \cos \theta & \frac{dy}{dz} &= t \sin \theta \\ \frac{d\theta}{dz} &= tm & \frac{dm}{dz} &= -tp \sin \theta + tq \cos \theta \\ \frac{dt}{dz} &= 0 & & (4.1-4.5) \end{aligned}$$

and the conditions at the upper end $z = 1$ became $x = c + t - 1$, $\theta = 0$, and $m=0$. The separation parameter c and vertical force q were specified and values were guessed for m_0 , p , and the free length of the elastica. The FindRoot command in Mathematica was then used to obtain values for m_0 , p , and the free length of the elastica. The contact length was calculated by subtracting the free length of the elastica from 1 (the total length of half of the elastica).

When the value of $\Delta\gamma$ was greater than zero, Equations 3.1-3.4 were used as the governing equations. For specified values of c , q , and b , the governing equations were solved by using the shooting method. Values were guessed for p and m_b , and the equations were numerically integrated from $s = 0$ to $s = 1-b$. Boundary conditions were then applied. At $s = 0$ (located at the point of separation of the elastica from the rigid surface, see Figure 3.2), $x = y = \theta = 0$ and $m = m_b$. At $s = 1-b$ (located at the clamped end of the elastica), $\theta = \pi/2$ and $x = c-b$.

Next, the $c = 0.8$ case was analyzed. The governing equations and boundary conditions for the no contact, point contact, and line contact situations described in the $c = 0.4$ case were used again for $c = 0.8$. Additionally, the same values for $\Delta\gamma$ were analyzed. Using the shooting method and Mathematica, values for the horizontal force, the moment at the point of separation, the height of the elastica, and the energy terms u_E , u_M , u_γ , and u_T were obtained.

Finally, the self-weight of the elastica was considered in the analysis. For $c = 0.4$ and $\Delta\gamma = 0$ and 0.64 , η values of -2 , -1 , 0 , 1 , and 2 were examined. To account for the self-weight, the governing equations and Mathematica file used previously were altered. Equations 3.1-3.3 remained the same; however, the self-weight term was added to Equation 3.4 to yield

$$\frac{dm}{ds} = -p \sin \theta + [q + \eta(1-b) - \eta t] \cos \theta \quad (4.6)$$

Note that when $\eta = 0$, Equation 4.6 reverts to Equation 3.4. When the self-weight was considered, the energy term u_G was included in the analysis to account for the work of gravity. The value for u_G was equal to $2 \eta \int y(s) ds$ with the limits of integration extending from $s = 0$ to $s = 1-b$.

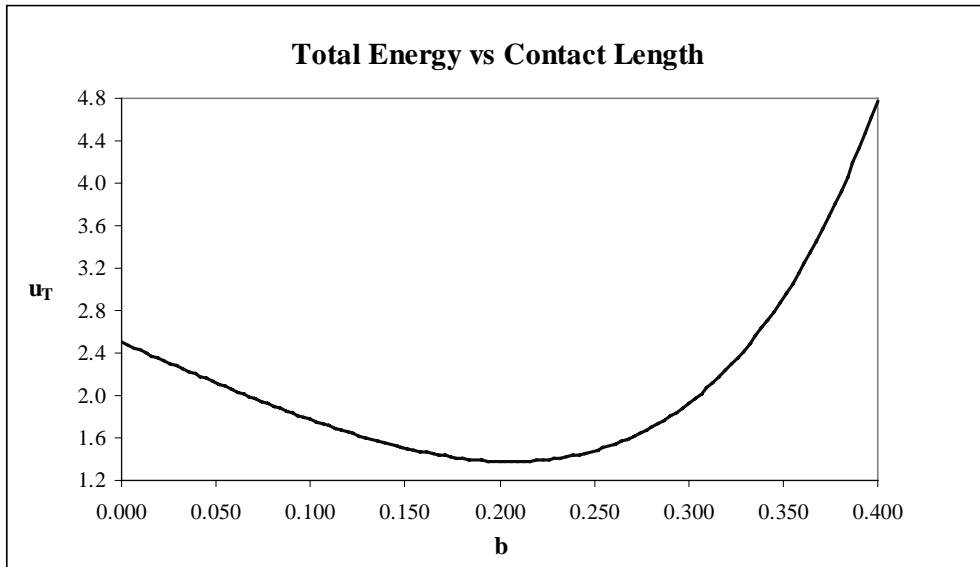


Figure 4.1: Total Energy vs. Contact Length for $c=0.4$, $q=13$, and $\Delta\gamma=0.32$

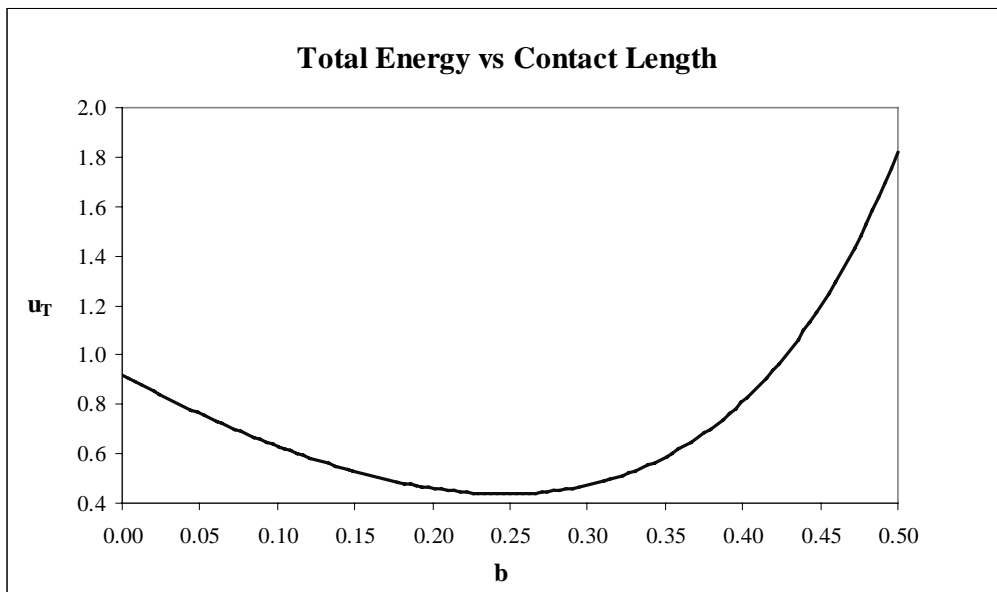


Figure 4.2: Total Energy vs. Contact Length for $c=0.8$, $q=-23.5$, and $\Delta\gamma=0.64$

To find the contact equilibrium between the elastica and the rigid surface using a JKR-type analysis, it was necessary to find the minimum total energy of the system, u_T . To ensure that only one minimum of the total energy occurred for each combination of c , q , and $\Delta\gamma$, the total energy over a large range of b values was examined. Figures 4.1 and 4.2 contain the results of this examination. Figure 4.1 shows that for $c = 0.4$, $q = 13$, and $\Delta\gamma = 0.32$, only one minimum existed in the total energy over the large range of b values investigated. Similarly, Figure 4.2 shows that for $c = 0.8$, $q = -23.5$, and $\Delta\gamma = 0.64$, only one minimum existed in the total energy. Figures 4.1 and 4.2 are typical of the behavior of u_T for other combinations of c , q , and $\Delta\gamma$.

The following sections discuss, in detail, the results obtained from the analyses described above. Results were obtained for $c = 0.4$ and $c = 0.8$ when the self-weight was ignored and for a few limited cases of $c = 0.4$ when the self-weight was included. Since the JKR-type analysis considered only the adhesion forces that acted within the contact zone, when the contact length equaled zero, the effect of the adhesion forces vanished.

4.2 RESULTS FOR THE C=0.4 CASE (NO SELF-WEIGHT INCLUDED)

Using the shooting method, values for the horizontal force, the moment at the point of separation, the height of the elastica, and the energy terms u_E , u_M , u_γ , and u_T were computed. Figures 4.3-4.16 show the results obtained from this analysis. In Figure 4.3, which plots the contact length versus the vertical force, the effect of the adhesion forces can be seen. As the value for the work of adhesion was increased, the value for the contact length, at a constant value of q , also increased. Similarly, Figure 4.4, which plots the contact length versus the vertical deflection, shows that as the value for the work of adhesion increased, the value for the contact length, at a constant value of δ , also increased. The results obtained from Figures 4.3 and 4.4 indicate that the presence of adhesion forces elongated the contact length. The elongation effect produced by the adhesion forces is also evident in Figure 4.11 which shows two different strips of elastica,

both experiencing a vertical deflection of 0.150. The strip that experienced a work of adhesion equal to 0.64 had a total contact length of 0.430, while the strip that experienced a work of adhesion equal to zero had a total contact length of 0.184.

The curves plotted in Figure 4.3 represent the spreading solution where line contact exists between the elastica and the rigid surface ($b > 0$). However, when the elastica strip was pushed onto the rigid surface, the elastica first passed through a stage of point contact with the rigid surface ($b = 0$) before it experienced line contact. During point contact, the contact length was equal to zero. For the $\Delta\gamma = 0$ curve, when there was no contact between the two solids, both b and q equaled zero. As the elastica came into contact with the flat surface, the two solids experienced point contact. Point contact existed until the vertical force, q , was sufficient to cause spreading (line contact). The region of point contact, for $\Delta\gamma = 0$, extended from $b = 0, q = 0$ to $b = 0, q = 12.52$. The regions of no contact and point contact can be seen more clearly in Figure 4.5, which plots the vertical deflection vs. the vertical force. The point contact and no contact ($q = 0, \delta < 0$) regions are denoted on the $\Delta\gamma = 0$ curve by a dashed line.

When $\Delta\gamma > 0$, the elastica experienced the effects of the adhesion forces as long as the contact length was greater than zero. However, once the contact area equaled zero, the effects of the adhesion forces vanished and the elastica behavior reverted to that shown for the $\Delta\gamma = 0$ curve. Additionally, the behavior of the elastica was dependent on two factors: whether the elastica was being pushed onto or pulled off of the rigid surface, and whether the vertical displacement or the vertical force was controlled. “Pulling” here refers to reducing the downward force q until the elastica loses contact with the substrate, which may occur when $q = 0$ or may require $q < 0$, i.e., an upward force. Figures 4.7-4.10 illustrate the possible scenarios. Figure 4.7 shows the path followed by the elastica through the no contact, point contact, and line contact stages. This figure was applicable to the case in which the $\Delta\gamma > 0$ curve did not extend to negative values of δ and where the

vertical displacement was controlled. When the elastica was pushed onto the rigid substrate (lower set of arrows), it experienced the same q and δ values for the no contact and point contact regions as an elastica that ignores adhesion forces. However, once the elastica experienced line contact, the adhesion forces caused an additional attraction between the surfaces, therefore causing a horizontal jump from the $\Delta\gamma=0$ curve to the $\Delta\gamma>0$ curve. When the elastica was pulled off of the rigid surface (upper set of arrows), values for q and δ were obtained from the $\Delta\gamma>0$ curve for line contact. When the value for the contact length approached zero and the adhesion forces vanished, a horizontal jump from the $\Delta\gamma>0$ curve to the $\Delta\gamma=0$ curve occurred. Following the horizontal jump, the values for q and δ were obtained from the $\Delta\gamma=0$ curve.

When the $\Delta\gamma>0$ curve extended into negative values of q and δ , the path followed by the elastica during the pulling phase varied slightly (Figure 4.8). As the elastica was pushed onto the rigid surface, it experienced the same q and δ values as were obtained for the $\Delta\gamma=0$ curve in the no contact and point contact regions. Once the elastica experienced line contact, the adhesion forces caused an additional attraction between the surfaces, therefore causing a horizontal jump from the $\Delta\gamma=0$ curve to the $\Delta\gamma>0$ curve. When the elastica was pulled off of the rigid surface, values for q and δ were obtained from the $\Delta\gamma>0$ curve for line contact. However, when the $\Delta\gamma>0$ curve approached point contact ($b=0$), the path jumped horizontally from the line contact curve for $\Delta\gamma>0$ to the no contact region of the $\Delta\gamma=0$ curve. Therefore, the elastica never experienced a period of point contact during pulling.

Figure 4.9 shows the path followed by the elastica through the no contact, point contact, and line contact stages. Figure 4.9 was applicable when the $\Delta\gamma>0$ curve did not extend to negative values of q and when the vertical force was controlled. When the elastica was pushed onto the rigid substrate, it experienced the same q and δ values for the no contact and point contact regions as an elastica that ignores adhesion forces. However, once the

elastica experienced line contact, the adhesion forces caused an additional attraction between the surfaces, therefore causing a vertical jump from the $\Delta\gamma=0$ curve to the $\Delta\gamma>0$ curve. When the elastica was pulled off of the rigid surface, values for q and δ were obtained from the $\Delta\gamma>0$ curve for line contact. When the value for the contact length approached zero and the adhesion forces vanished, a vertical jump from the $\Delta\gamma>0$ curve to the $\Delta\gamma=0$ curve occurred. Following the vertical jump, the values for q and δ were obtained from the $\Delta\gamma=0$ curve.

When the $\Delta\gamma>0$ curve extended into negative values of q and δ , the path followed by the elastica during the pulling phase varied slightly from the path experienced by the elastica in Figure 4.9 (see Figure 4.10). As the elastica was pushed onto the rigid surface, it experienced the same q and δ values as were obtained for the $\Delta\gamma=0$ curve in the no contact and point contact regions. Once the elastica experienced line contact, the adhesion forces caused an additional attraction between the surfaces, therefore causing a vertical jump from the $\Delta\gamma=0$ curve to the $\Delta\gamma>0$ curve. When the elastica was pulled off of the rigid surface, values for q and δ were obtained from the $\Delta\gamma>0$ curve for line contact. However, when the $\Delta\gamma>0$ curve approached point contact ($b=0$), the path jumped horizontally from the line contact curve for $\Delta\gamma>0$ to the no contact region of the $\Delta\gamma=0$ curve. Therefore, the elastica never experienced a period of point contact during pulling.

Figure 4.6 labels the points of transition between the point and line contact stages that are illustrated in Figures 4.7-4.10. Table 4.1 lists values for the contact length, the vertical force, the vertical displacement, the horizontal force, and the moment at the point of separation of the elastica from the substrate for points A-M. Points B, E, H, and K have the same δ value (0.0966) as point M, and points C, F, I, and L have the same q value (12.52) as point M. Note that when $\Delta\gamma=0.48$ and 0.64 , a negative value was obtained for the vertical force when the contact length was equal to zero (Points A and D). A negative value for q indicates that an upward force was applied at the clamped

ends of the elastica. This upward vertical force required to separate the elastica from the rigid surface is defined as the pull-off force f_p and is equal to $-q$. Therefore, the pull-off forces required to separate the elastica from the rigid surface were $f_p = 2.58$ and 5.85 for $\Delta\gamma=0.48$ and 0.64 , respectively. The positive values obtained for the vertical force at Points G and J indicated that the situation depicted in Figures 4.7 and 4.9 was present. Depending on whether the vertical force or vertical displacement was controlled, a horizontal or vertical jump was made to the $\Delta\gamma=0$ curve. After the jump to the $\Delta\gamma=0$ curve, the values for the vertical force and contact length of the elastica could be obtained from the $\Delta\gamma=0$ case. Therefore, when the value of q was positive at the transition point between point contact and line contact, the pull-off force $f_p=0$.

Table 4.1: Values Corresponding to Points A-M in Figure 4.6

	Point	b	q	δ	p	m_b
$\Delta\gamma=0.64$	A	0.0000	-5.85	-0.0207	1.8315	3.9208
	B	0.1556	2.22	0.0966	8.6423	3.9024
	C	0.2642	12.52	0.1896	14.8224	3.9166
$\Delta\gamma=0.48$	D	0.0000	-2.58	-0.0102	3.1775	3.3979
	E	0.1445	4.52	0.0966	8.9468	3.4000
	F	0.2364	12.52	0.1731	13.7000	3.3834
$\Delta\gamma=0.32$	G	0.0000	0.96	0.0043	4.6694	2.7713
	H	0.1280	7.00	0.0966	9.2851	2.7690
	I	0.2004	12.52	0.1537	12.5734	2.7576
$\Delta\gamma=0.16$	J	0.0000	4.86	0.0255	6.3843	1.9867
	K	0.1030	9.64	0.0966	9.7175	1.9544
	L	0.1500	12.52	0.1307	11.4679	1.9755
$\Delta\gamma=0$	M	0.0000	12.52	0.0966	10.2770	0.0000

Figure 4.12 compares the shape of the elastica when no contact was present to the shape of the elastica in the instant before it separated from the rigid surface for $\Delta\gamma=0.64$. The vertical force experienced at this instant was $q = -5.85$. Therefore, for the elastica shown

in Figure 4.12, a pull-off force $f_p = 5.85$ was experienced. Due to the presence of adhesion forces, the elastica at pull-off experienced a negative δ value of $\delta = -0.0179$, i.e., the height of the elastica was $h=0.8075$ in contrast to the height $h=0.7896$ for no contact.

Another parameter whose values were determined by the shooting method was the moment at the point of separation of the elastica from the rigid surface. As stated previously, when no adhesion forces were considered, the moment $m_b = 0$. When $\Delta\gamma > 0$, m_b assumed a non-zero value to allow for the deformation of the elastica and the elongation of the contact length. The numerical results showed that the moment at the point of separation of the elastica from the rigid surface was essentially independent of the vertical force applied to the clamped ends. The moment m_b was solely dependent on the value of the work of adhesion. Approximate values for m_b were 1.96, 2.77, 3.39, and 3.92 for $\Delta\gamma = 0.16, 0.32, 0.48, \text{ and } 0.64$, respectively. Figures 4.12 and 4.13 illustrate these results. Additionally, Figure 4.13 shows how the value of m_b increased as the value for the work of adhesion increased.

Figure 4.14 shows the effect of increasing values of the work of adhesion in terms of the contact length and the applied vertical force. Each curve in Figure 4.14 represents a constant q value. For a constant value of $\Delta\gamma$, the value for the contact length increased with increasing values of the vertical force. Additionally, when the vertical force was held constant and the value for $\Delta\gamma$ was increased, the contact length also increased. The contact length vs. work of adhesion relationship is shown in Figure 4.15. In this figure, the contact length increases as the work of adhesion increases. Figure 4.16 plots the vertical displacement vs. the work of adhesion while the vertical force is held constant and displays similar results. For a constant value of $\Delta\gamma$, the value for the vertical displacement increased with increasing values of the vertical force. Additionally, when the vertical force was held constant and the value for $\Delta\gamma$ was increased, the vertical displacement also increased.

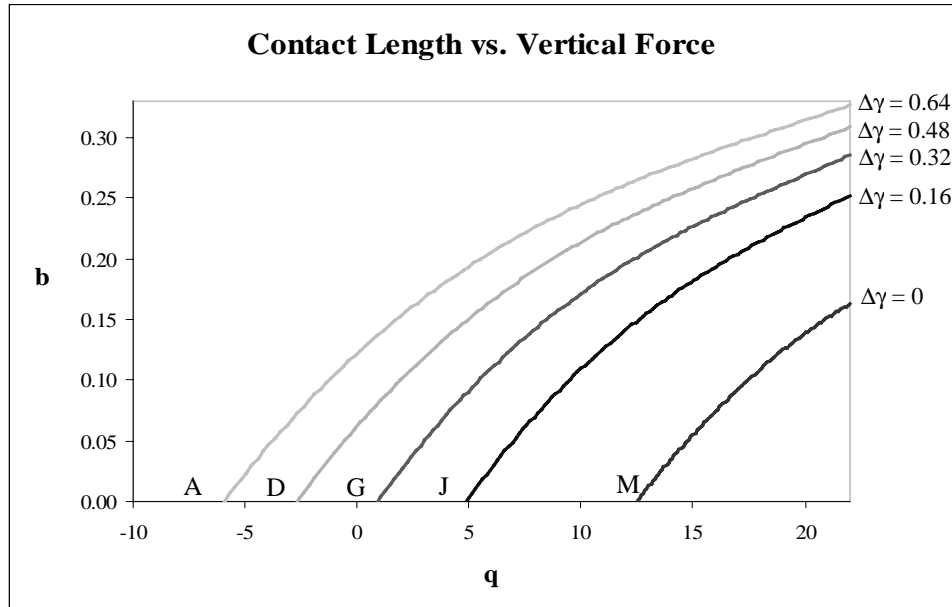


Figure 4.3: Contact Length vs. Vertical Force for $c=0.4$

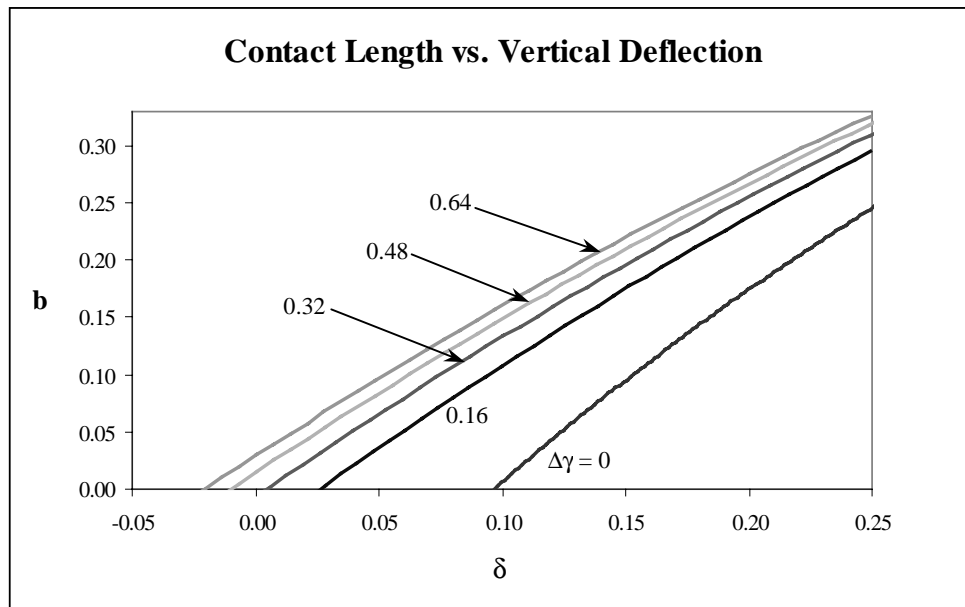


Figure 4.4: Contact Length vs. Vertical Deflection for $c=0.4$

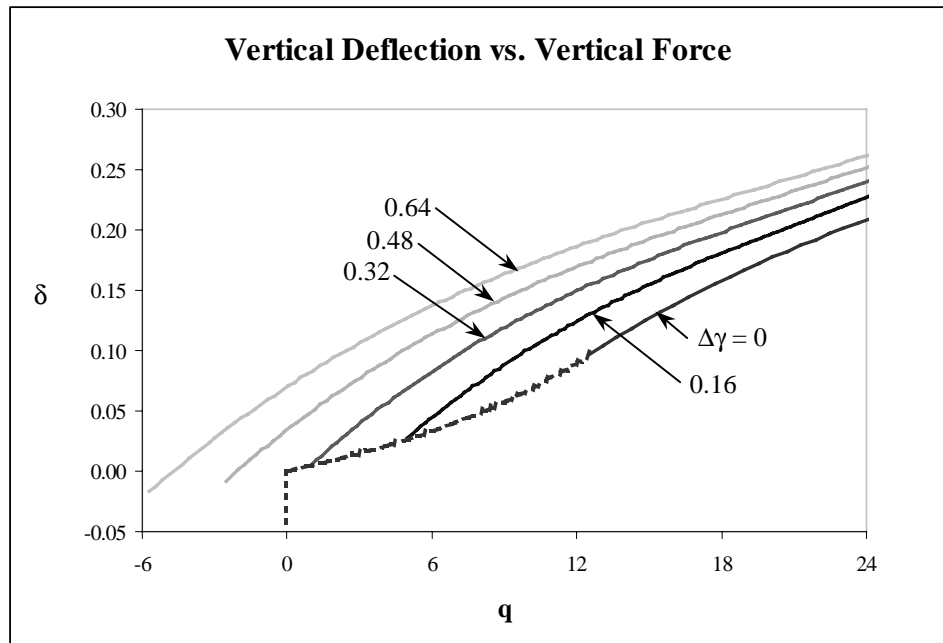


Figure 4.5: Vertical Deflection vs. Vertical Force for $c=0.4$

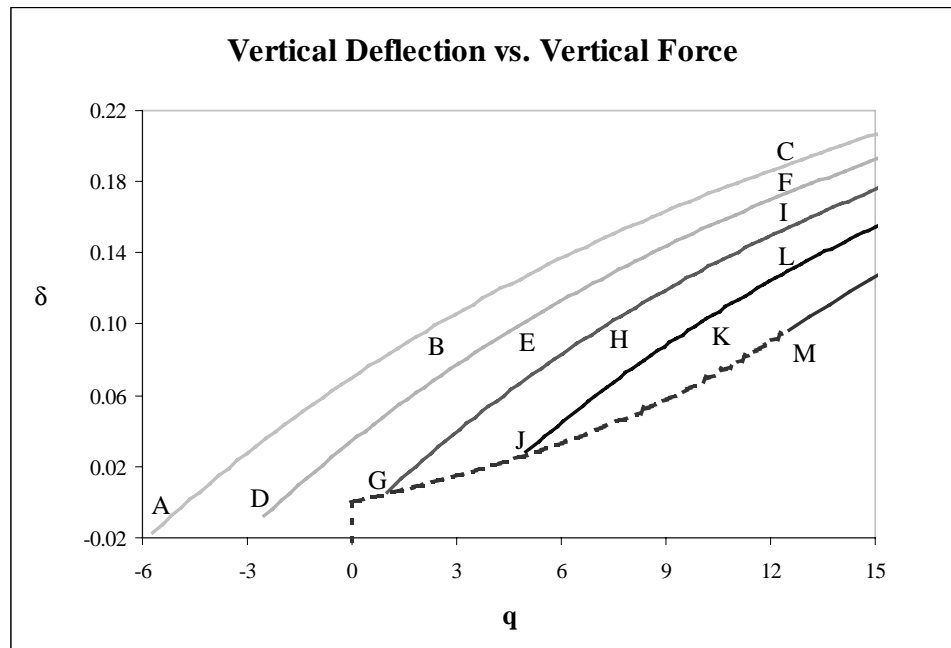


Figure 4.6: Vertical Deflection vs. Vertical Force for $c=0.4$ (Locations of Points A-M: Table 4.1)

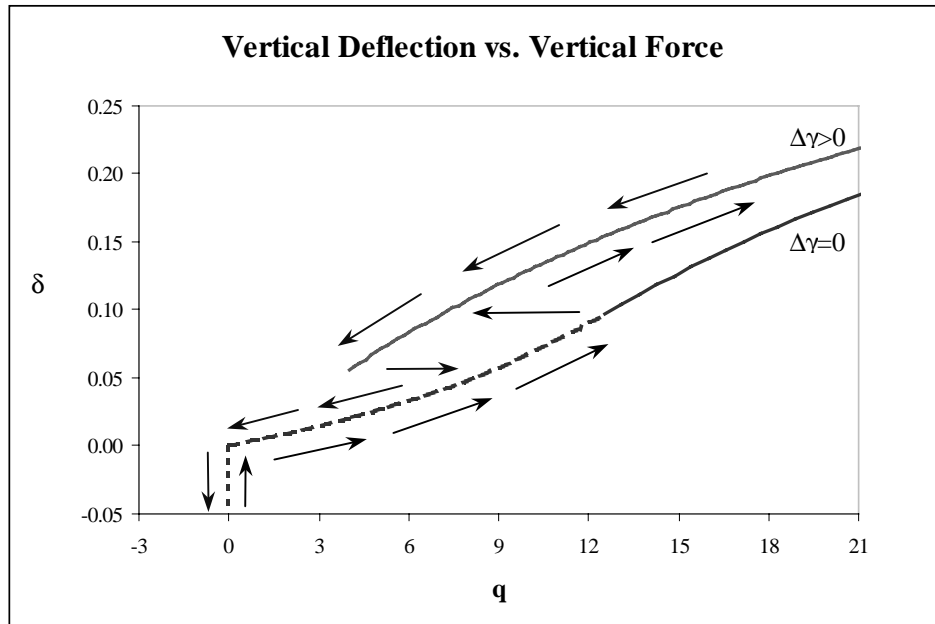


Figure 4.7: Vertical Force Experienced by the Elastica When it is Pushed Onto (lower arrows) or Pulled Off (upper arrows) the Rigid Surface. Vertical Deflection is Controlled.

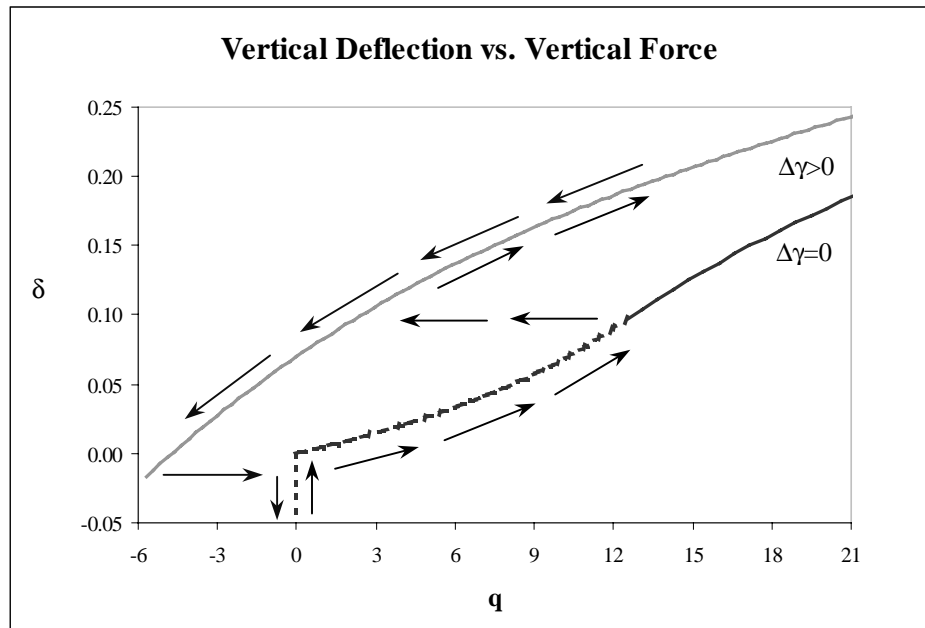


Figure 4.8: Vertical Force Experienced by the Elastica When it is Pushed Onto (lower arrows) or Pulled Off (upper arrows) the Rigid Surface. Vertical Deflection is Controlled. Curve with Adhesion Extends to $\delta < 0$.

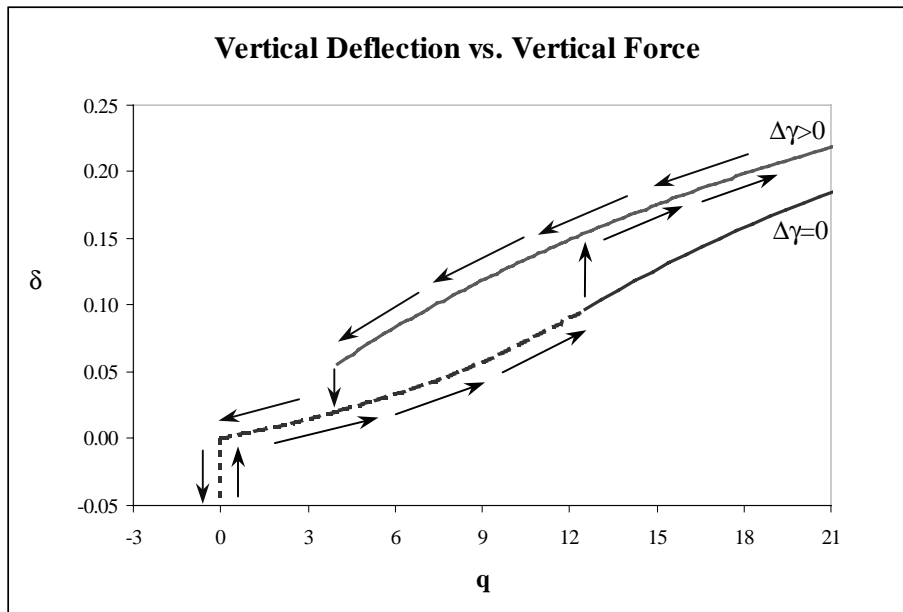


Figure 4.9: Vertical Deflection Experienced by the Elastica When it is Pushed Onto (lower arrows) or Pulled Off (upper arrows) the Rigid Surface. Vertical Force is Controlled.

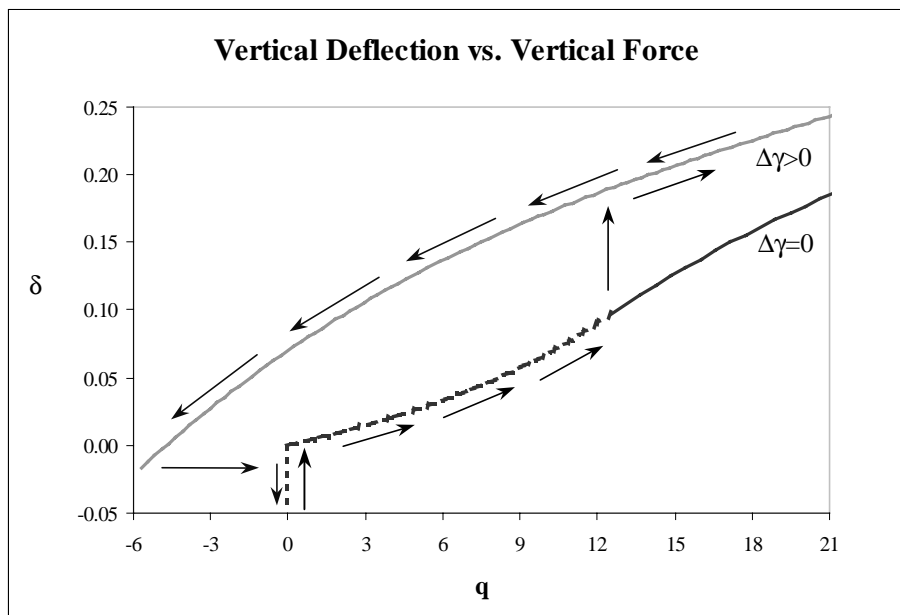


Figure 4.10: Vertical Deflection Experienced by the Elastica When it is Pushed Onto (lower arrows) or Pulled Off (upper arrows) the Rigid Surface. Vertical Force is Controlled. Curve with Adhesion Extends to $\delta < 0$.

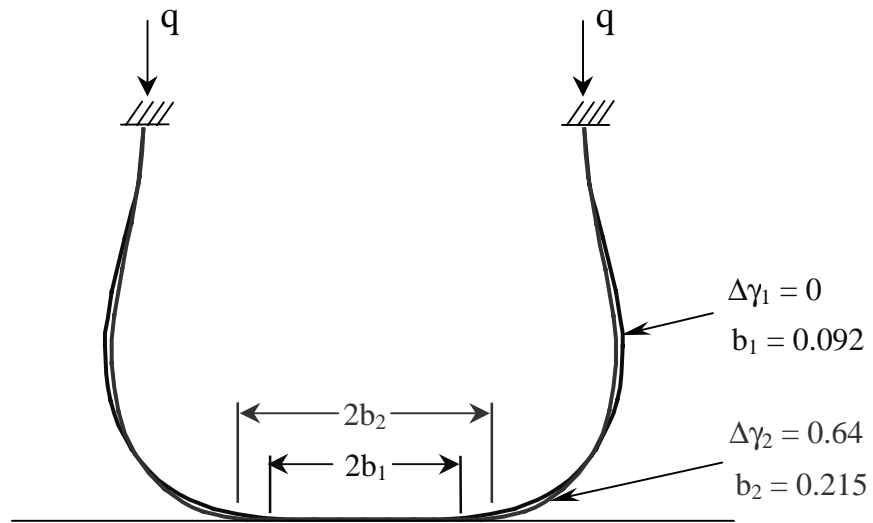


Figure 4.11: Effect of Adhesion on the Contact Length for $c=0.4$, $\delta=0.150$

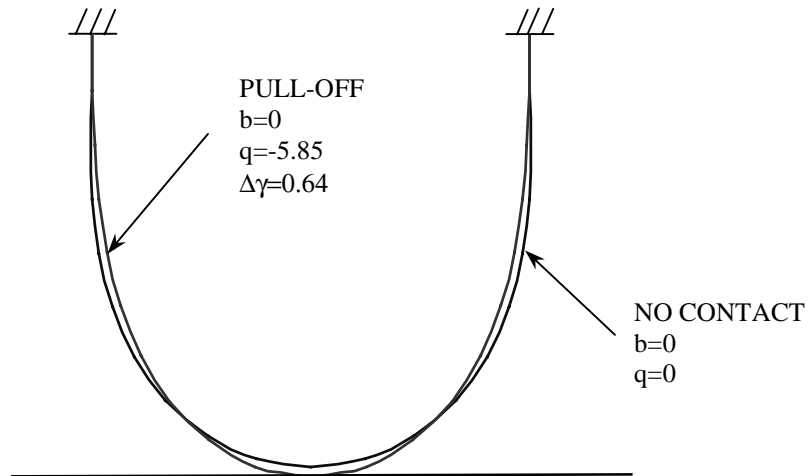


Figure 4.12: Shape of the Elastica at the Pull-Off and No Contact Stages for $c=0.4$

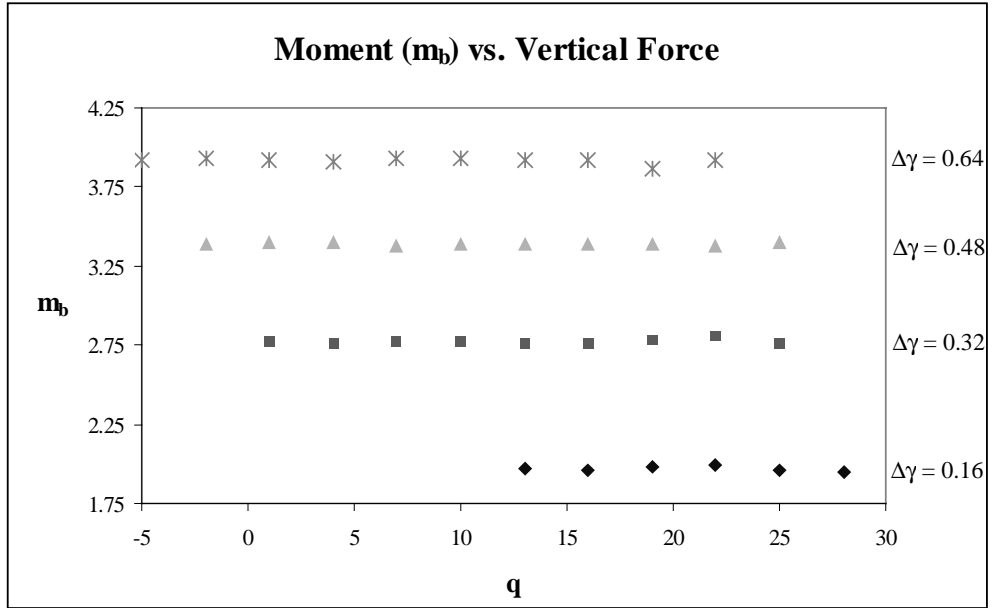


Figure 4.13: Moment vs. Vertical Force for Varying Values of Work of Adhesion ($c=0.4$)

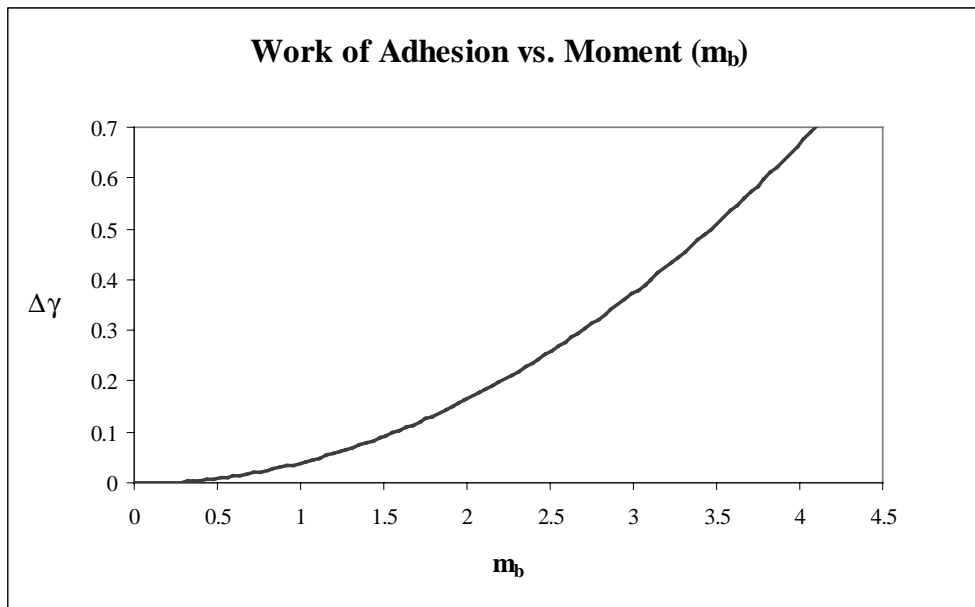


Figure 4.14: Work of Adhesion vs. Moment (m_b) for $c = 0.4$ and $q = 20$

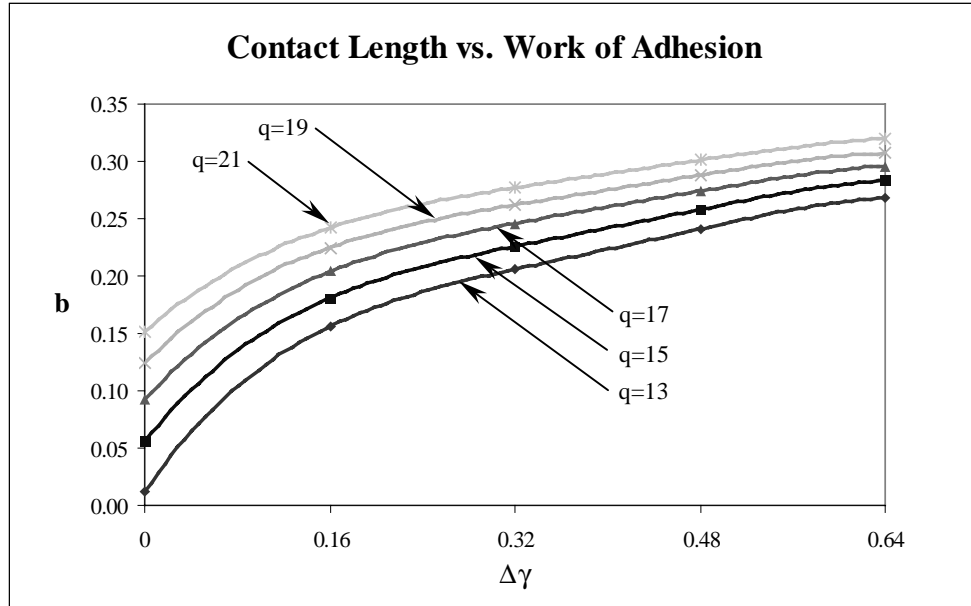


Figure 4.15: Contact Length vs. Work of Adhesion for $c=0.4$

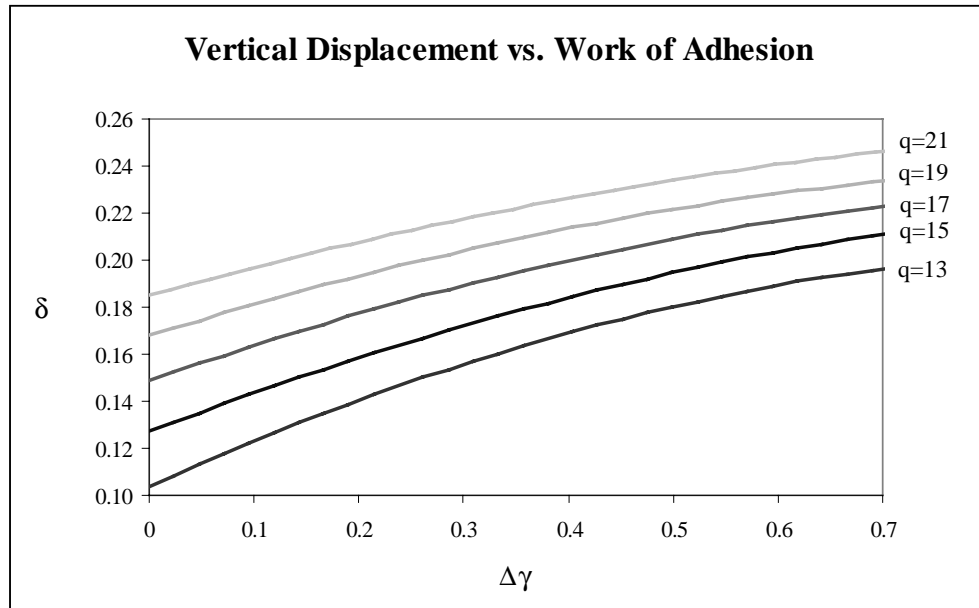


Figure 4.16: Vertical Displacement vs. the Work of Adhesion for $c=0.4$

4.3 RESULTS FOR THE C=0.8 CASE (NO SELF-WEIGHT INCLUDED)

Results obtained for the $c = 0.8$ case, where the self-weight of the elastica was again ignored, resemble those obtained for the $c = 0.4$ case. The shooting method was used to obtain values for the horizontal force, the moment at the point of separation, the height of the elastica, and the energy terms u_E , u_M , u_γ , and u_T . Figures 4.17-4.25 show the results obtained from this analysis. In Figure 4.17, which plots the contact length versus the vertical force for $c=0.8$, the effect of the adhesion forces can be seen. As the value for the work of adhesion $\Delta\gamma$ was increased, the value for the contact length, at a constant value of q , also increased. Similarly, Figure 4.18, which plots the contact length versus the vertical deflection, shows that as the value for the work of adhesion increased, the value for the contact length, at a constant value of δ , also increased. The results obtained from Figures 4.17 and 4.18 indicate that the presence of adhesion forces elongated the contact length. The elongation of the contact length caused by the presence of adhesion forces is also evident in Figure 4.21 which shows two different strips of elastica, both experiencing a vertical deflection of 0.050. The strip that experienced a work of adhesion equal to 0.64 had a total contact length of 0.388, while the strip that experienced a work of adhesion equal to zero had a total contact length of 0.150.

The curves plotted in Figure 4.17, similar to those plotted in Figure 4.3, represent the spreading solution where line contact exists between the elastica and the rigid surface. As discussed in the $c=0.4$ case, when the elastica strip was pushed onto the rigid surface, the elastica first passed through a stage of point contact with the rigid surface before it experienced line contact. During point contact, the contact length was equal to zero. For the $\Delta\gamma=0$ curve, when there was no contact between the two solids, both b and q equaled zero. As the elastica came into contact with the flat surface, the two solids experienced point contact. Point contact existed until the vertical force, q , was sufficient enough to cause spreading (line contact). The region of point contact, for $\Delta\gamma=0$, extended from $b=0$, $q=0$ to $b=0$, $q=2.49$. The regions of no contact and point contact can be seen more clearly

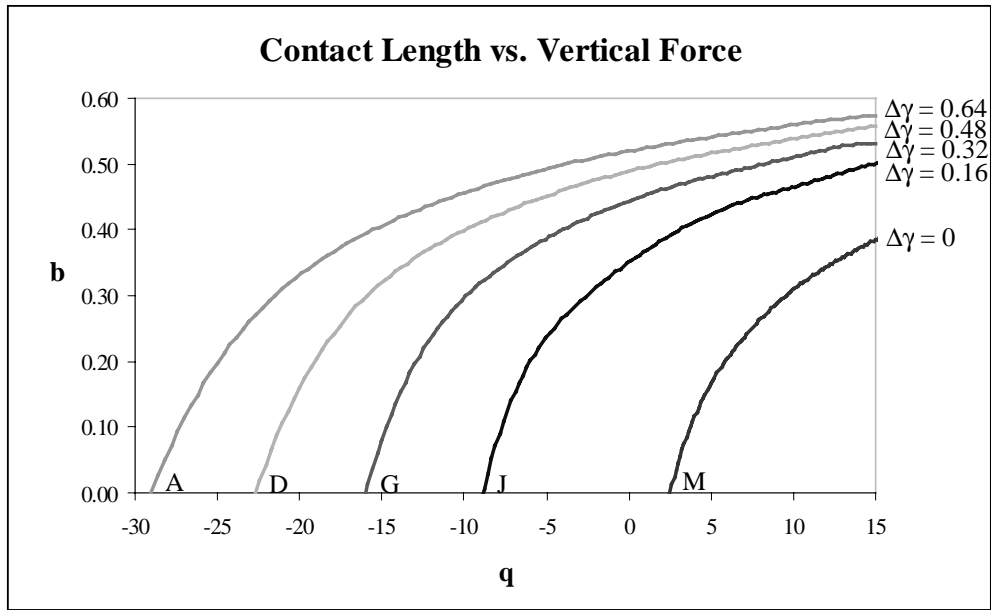


Figure 4.17: Contact Length vs. Vertical Force for $c=0.8$

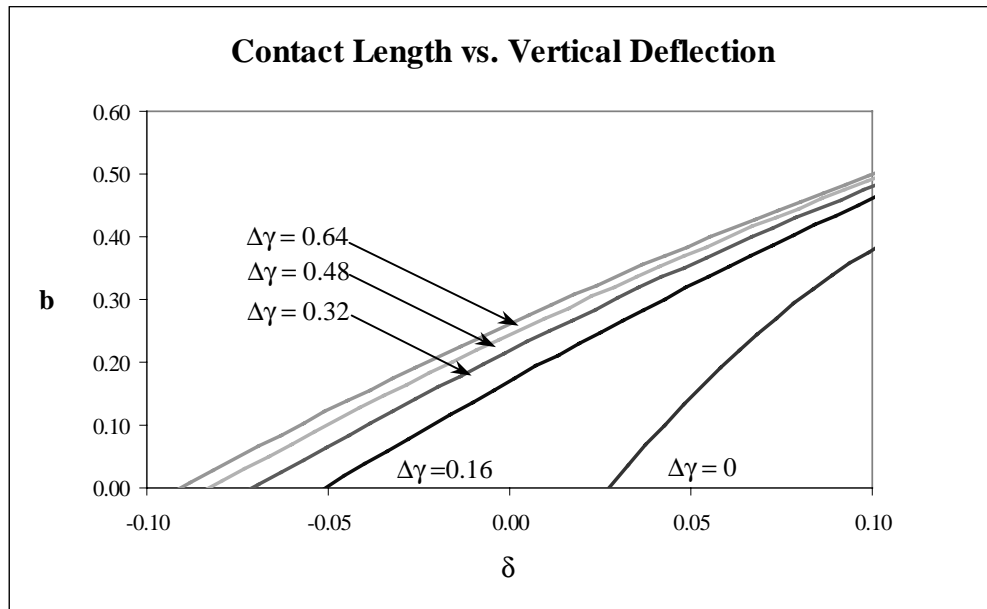


Figure 4.18: Contact Length vs. Vertical Deflection for $c=0.8$

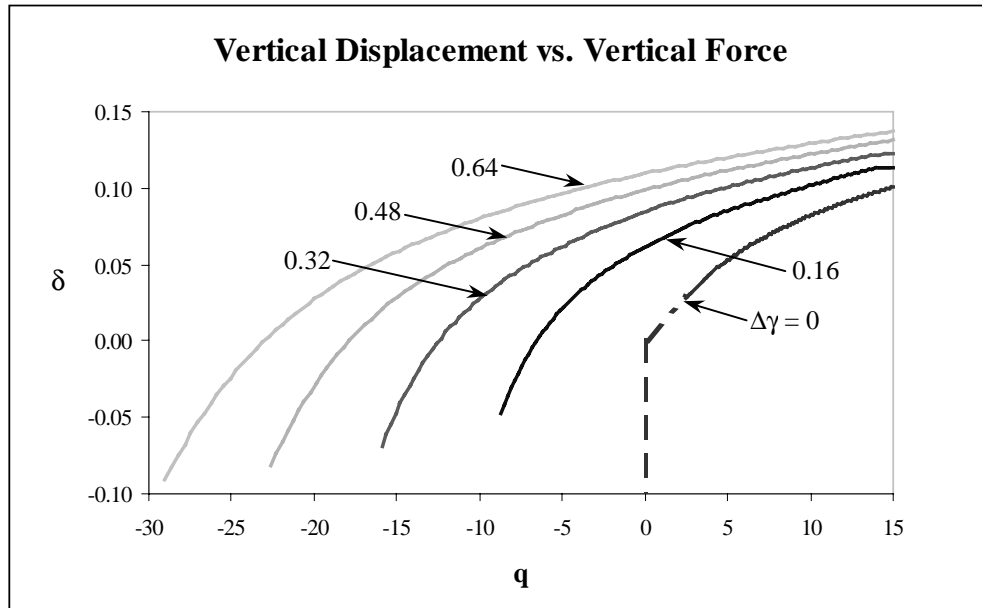


Figure 4.19: Vertical Displacement vs. Vertical Force for $c=0.8$

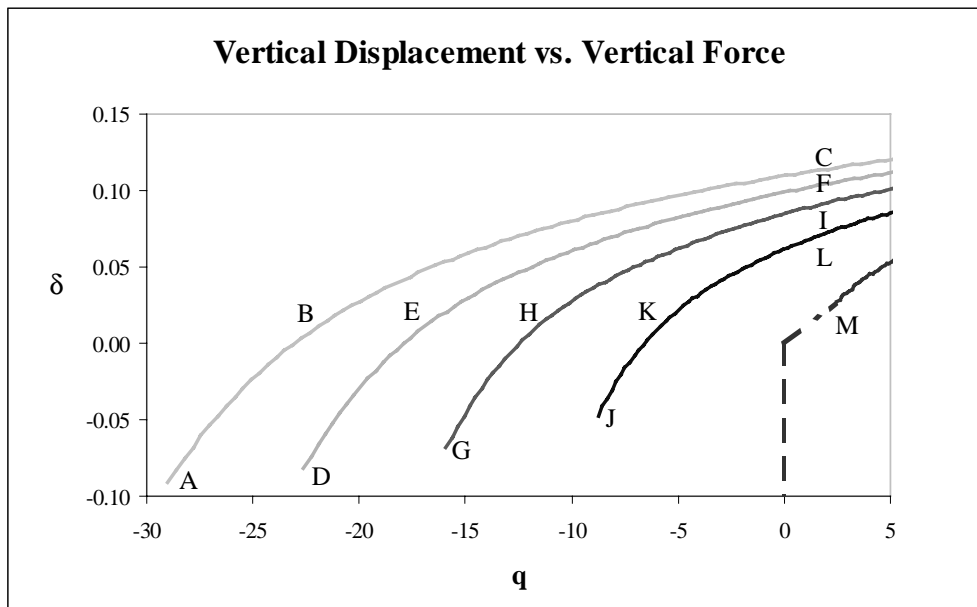


Figure 4.20: Vertical Displacement vs. Vertical Force for $c=0.8$ (Locations of Points A-M: Table 4.2)

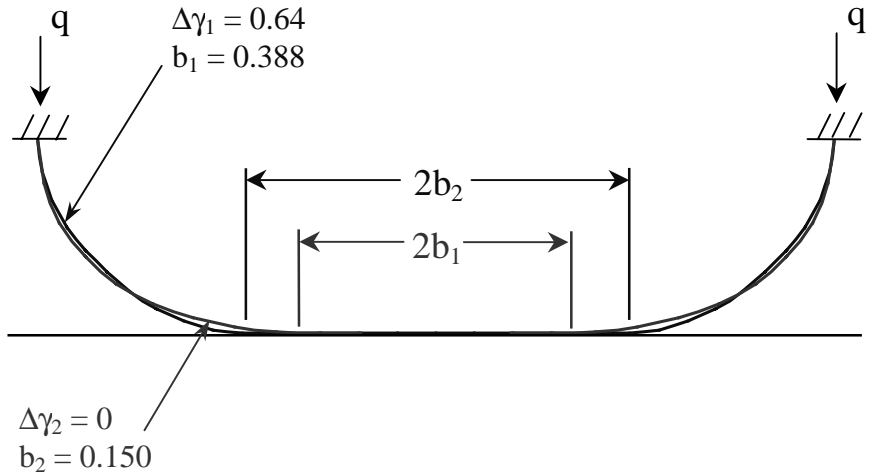


Figure 4.21: Effect of Adhesion on the Contact Length for $c=0.8$, $\delta=0.050$

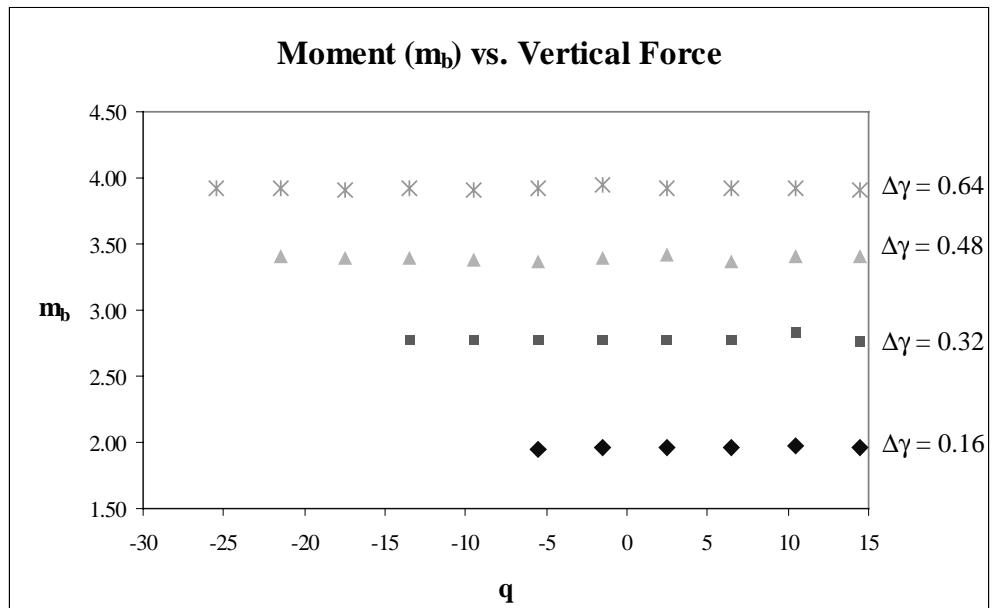


Figure 4.22: Moment (m_b) vs. Vertical Force for Various Values of Work of Adhesion ($c=0.8$)

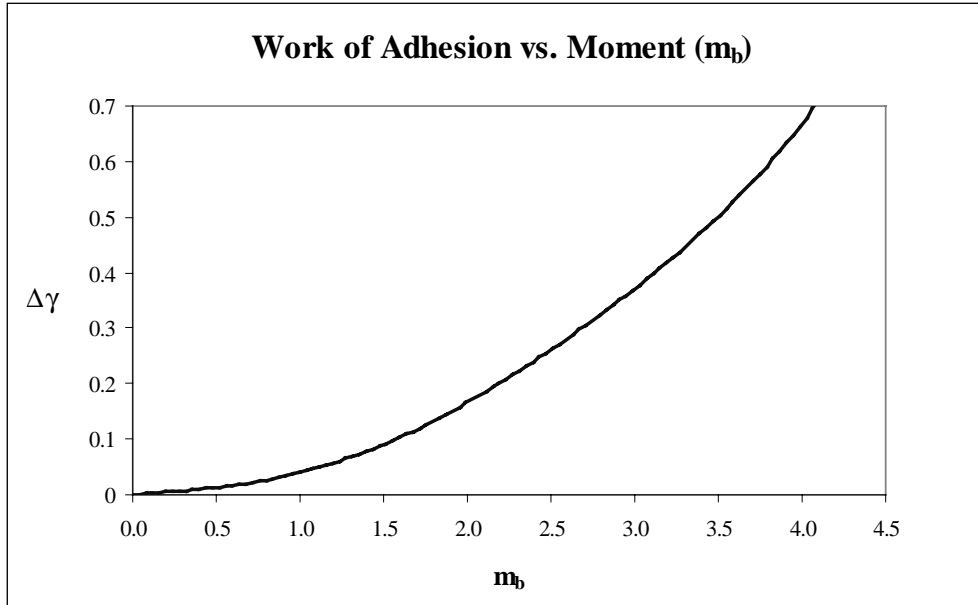


Figure 4.23: Work of Adhesion vs. Moment (m_b) for $c=0.8$ and $q=2.5$

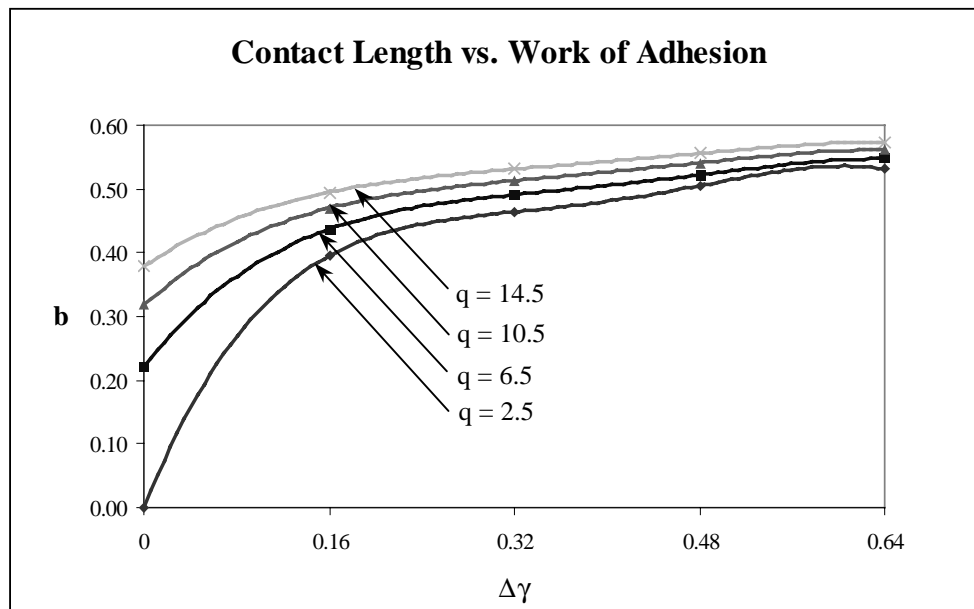


Figure 4.24: Contact Length vs. Work of Adhesion for $c=0.8$

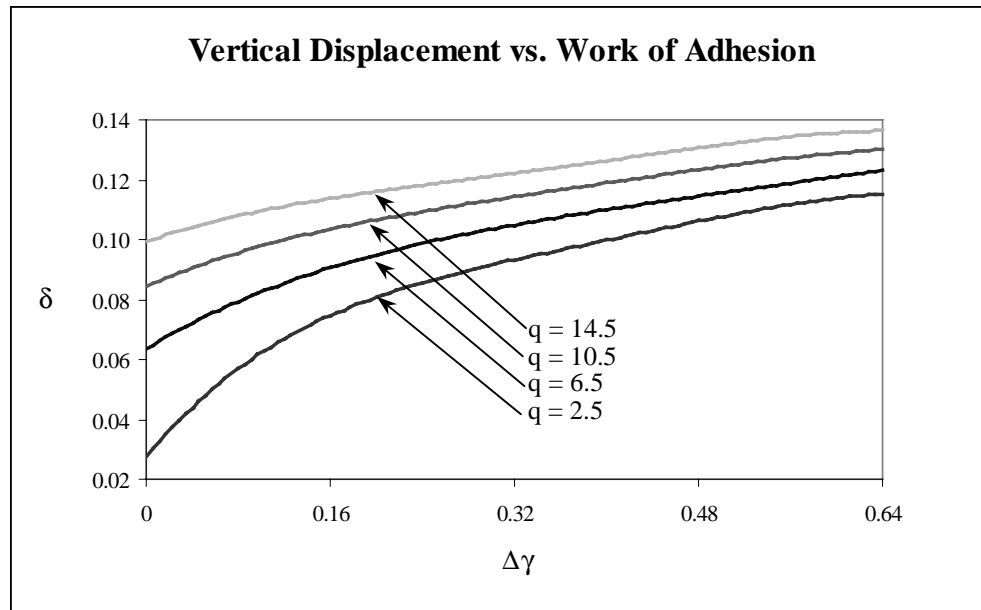


Figure 4.25: Vertical Displacement vs. the Work of Adhesion for $c=0.8$

in Figure 4.19, which plots the vertical deflection vs. the vertical force. The point contact and no contact regions are denoted on the $\Delta\gamma=0$ curve by a dashed line.

When $\Delta\gamma>0$, the elastica experienced the effects of the adhesion forces as long as the contact length was greater than zero. However, once the contact area equaled zero, the effects of the adhesion forces vanished and the elastica behavior reverted to that shown for the $\Delta\gamma=0$ curve. Additionally, the behavior of the elastica depended on two factors: whether the elastica was being pushed onto or pulled off of the rigid surface, and whether the vertical displacement or the vertical force was controlled. Since all the $\Delta\gamma$ curves examined in the analysis for $c=0.8$ extend into a region of negative q and δ values, Figures 4.8 and 4.10 describe the path followed by the elastica. When the elastica was pushed onto the rigid surface (while the vertical displacement was controlled), it

experienced the same q and δ values as were obtained for the $\Delta\gamma=0$ curve in the no contact and point contact regions. Once the elastica experienced line contact, the adhesion forces caused an additional attraction between the surfaces, therefore causing a horizontal jump from the $\Delta\gamma=0$ curve to the $\Delta\gamma>0$ curve. When the elastica was pulled off of the rigid surface, values for q and δ were obtained from the $\Delta\gamma>0$ curve for line contact. However, when the $\Delta\gamma>0$ curve approached point contact ($b=0$), the path jumped horizontally from the line contact curve for $\Delta\gamma>0$ to the no contact region of the $\Delta\gamma=0$ curve. Therefore, the elastica never experienced a period of point contact during pulling.

Figure 4.10 examines the path followed by the elastica when the vertical force is controlled. As the elastica was pushed onto the rigid surface, it experienced the same q and δ values as were obtained for the $\Delta\gamma=0$ curve in the no contact and point contact regions. Once the elastica experienced line contact, the adhesion forces caused an additional attraction between the surfaces, therefore causing a vertical jump from the $\Delta\gamma=0$ curve to the $\Delta\gamma>0$ curve. When the elastica was pulled off of the rigid surface, values for q and δ were obtained from the $\Delta\gamma>0$ curve for line contact. However, when the $\Delta\gamma>0$ curve approached point contact ($b=0$), the path jumped horizontally from the line contact curve for $\Delta\gamma>0$ to the no contact region of the $\Delta\gamma=0$ curve. Therefore, the elastica never experienced a period of point contact during pulling.

Figure 4.20 labels the points of transition between the point and line contact stages that are illustrated in Figures 4.8 and 4.10. Table 4.2 lists values for the contact length, the vertical force, the vertical displacement, the horizontal force, and the moment at the point of separation of the elastica from the substrate for points A-M. Note that when $\Delta\gamma>0$, a negative value was obtained for the vertical force when the contact length was equal to zero (Points A, D, G, and J). A negative value for q indicates that an upward force was applied at the clamped ends of the elastica. This upward vertical force required to separate the elastica from the rigid surface is defined as the pull-off force f_p and is equal to $-q$. Therefore, the pull-off forces required to separate the elastica from the rigid

surface were $f_p = 8.83, 15.9, 22.6,$ and 28.9 for $\Delta\gamma=0.16, 0.32, 0.48,$ and $0.64,$ respectively.

Another parameter whose values were determined by the shooting method was the moment at the point of separation of the elastica from the rigid surface. As stated previously, when no adhesion forces were considered, the moment $m_b = 0$. When $\Delta\gamma > 0$, m_b assumed a non-zero value to allow for the deformation of the elastica and the elongation of the contact length. The results from the $c=0.8$ analysis showed that the moment at the point of separation of the elastica from the rigid surface was not only essentially independent of the vertical force applied to the clamped ends, but also

Table 4.2: Values Corresponding to Points A-M in Figure 4.20

	Point	b	q	δ	p	m_b
$\Delta\gamma=0.64$	A	0.000	-28.90	-0.0886	-50.7830	3.9181
	B	0.331	-19.79	0.0275	-25.9103	3.9172
	C	0.531	2.49	0.1150	8.4220	3.9250
$\Delta\gamma=0.48$	D	0.000	-22.60	-0.0817	-41.8175	3.3972
	E	0.317	-14.91	0.0275	-21.4050	3.3973
	F	0.505	2.49	0.1061	5.9809	3.4258
$\Delta\gamma=0.32$	G	0.000	-15.90	-0.0689	-31.9523	2.7704
	H	0.296	-9.98	0.0275	-16.8038	2.7727
	I	0.464	2.49	0.0932	3.0983	2.7776
$\Delta\gamma=0.16$	J	0.000	-8.83	-0.0496	-21.5327	1.9626
	K	0.257	-4.17	0.0275	-11.0496	1.9541
	L	0.395	2.49	0.0746	0.0233	1.9647
$\Delta\gamma=0$	M	0.000	2.49	0.0275	3.7852	0.0000

had the same value as for the separation distance $c=0.4$ between the ends of the elastica. The moment m_b was solely dependent on the value of the work of adhesion. As before, the moment at the point of separation of the elastica from the rigid surface was equal to 1.96, 2.77, 3.39, and 3.92 for $\Delta\gamma = 0.16, 0.32, 0.48,$ and $0.64,$ respectively. Figures 4.22

and 4.23 illustrate these results. Additionally, Figure 4.23 shows that the value of m_0 increased as the value for the work of adhesion increased.

Figure 4.24 shows the effect of increasing values of the work of adhesion in terms of the contact length and the applied vertical force. Each curve in Figure 4.23 represents a constant q value. For a constant value of $\Delta\gamma$, the value for the contact length increased with increasing values of the vertical force. Additionally, when the vertical force was held constant and the value for $\Delta\gamma$ was increased, the contact length also increased.

Figure 4.25 plots the vertical displacement vs. the work of adhesion while the vertical force is held constant and displays similar results. For a constant value of $\Delta\gamma$, the value for the vertical displacement increased with increasing values of the vertical force. Additionally, when the vertical force was held constant and the value for $\Delta\gamma$ was increased, the vertical displacement also increased.

4.4 RESULTS FOR THE C=0.4 CASE (SELF-WEIGHT INCLUDED)

The final case studied in the JKR-type analysis included the self-weight of the elastica in the governing equations (see Equation 4.6). Values of $\eta = -2, -1, 0, 1,$ and 2 were considered for $c=0.4$ with $\Delta\gamma=0$ and 0.64 . Positive values of η indicate that the elastica was oriented in the manner shown in Figure 3.1, while negative values of η indicate that the elastica was rotated 180 degrees and was pushed upward onto a rigid plate. To include the self-weight of the elastica in the analysis, an energy term was added to the u_T equation. The term u_G was included in the analysis to account for the work of gravity and was equal to $2 \eta \int y(s) ds$ with the limits of integration extending from $s=0$ to $s=1-b$.

Results from the JKR-type analysis, which included the self-weight of the elastica, can be found in Figures 4.26-4.31. Figure 4.26 plots the contact length vs. the applied vertical force for $c=0.4$ and $\Delta\gamma=0$ (i.e., in the absence of adhesion). When positive values for η were used, the contact length at a fixed value of q increased. Therefore, the self-weight

was added to the vertical force that was applied in the downward direction, creating a larger contact area. Conversely, when negative values for η were used, the contact length at a fixed value of q decreased. Therefore, the self-weight was subtracted from the vertical force applied in the downward direction, decreasing the value for the contact length. Values for q at points A, B, C, D, and E are 10.90, 11.73, 12.52, 13.33, and 14.13, respectively.

When the self-weight was included in the analysis and the adhesion forces were ignored, values in Figure 4.26 for the vertical force at a fixed contact length shifted either to the left or to the right. This shift depended on the sign of η . However, the addition of the self-weight to the analysis had no visible effect on the contact length vs. vertical displacement relationship (Figure 4.27). The curve obtained in Figure 4.27 is the same as the $\Delta\gamma=0$ curve in Figure 4.4. The contact length vs. the vertical displacement curve remained approximately the same regardless of the values used for η in this analysis. This implies that the η values used for this analysis were not large enough to create a noticeable difference in the b vs. δ curve. The value of δ at the transition point between the point contact and line contact stages (Point M) is approximately 0.0966 (as in Table 4.1).

In addition to the contact length vs. vertical force and the contact length vs. vertical displacement plots, the vertical displacement vs. vertical force was plotted (Figure 4.28). When the self-weight of the elastica was added to the analysis, the values for the vertical displacement, at a constant value of q , increased with increasing values of η and decreased with decreasing values of η . The curves shown in Figure 4.28 represent the spreading solution for $c=0.4$ and $\Delta\gamma=0$ only. An analysis of the no contact condition was performed in order to determine the initial height, h_0 . Values for the initial height were 0.7912, 0.7904, 0.7896, 0.7887, and 0.7878 for $\eta=2, 1, 0, -1,$ and 2 , respectively. Values for h_0 were solely dependent on the value used for η . Once the value of h_0 was obtained, it was used in the equation $h_0 - h = \delta$ to find the vertical displacement of the

elastica, where h was the height of the elastica at a specified point. No analysis was conducted to determine the point contact solution when the self-weight was included.

Next, an analysis was conducted which combined the effects of the addition of self-weight and the presence of adhesion forces. Figure 4.29 illustrates the effects of the self-weight when $\eta=2, 0,$ and $-2,$ and $\Delta\gamma=0.64.$ Values for the contact length, at a fixed value of $q,$ increased as the value of η increased, and decreased as values for η decreased. With the addition of the adhesion forces, values for q at $b=0$ became negative. At points G, H, and I, the vertical force equaled $-7.5, -5.7,$ and $-3.8,$ respectively.

Figure 4.30, like Figure 4.27, shows that for $\eta=2, 0,$ and $-2,$ and $\Delta\gamma=0.64,$ the contact length vs. vertical displacement relationship is approximately the same regardless of the value of η used. The curve obtained in Figure 4.30 is the same as the $\Delta\gamma=0.64$ curve in Figure 4.4. The value of δ at the transition point between the point contact and line contact stages (point J) is $-0.0207.$

The vertical displacement vs. vertical force curve for $c=0.4$ and $\Delta\gamma=0.64$ (Figure 4.31) shows that for a constant value of $q,$ the vertical displacement increased with increasing values of η and decreased with decreasing values of $\eta.$ Additionally, for a constant value of $\delta,$ the value of q increased with decreasing values of η and decreased with increasing values of $\delta.$ The curves shown in Figure 4.31 terminate at $b=0$ and only represent the spreading solution for $c=0.4$ and $\Delta\gamma=0.64.$

Finally, Figure 4.32 illustrates the effect of adhesion for a specific value of $\eta.$ The curves shown represent $\Delta\gamma=0$ and $\Delta\gamma=0.64.$ For constant values of η and $q,$ values for the contact length increased with increasing values of $\Delta\gamma.$ This indicates that when adhesion forces are present (and η is held constant), an elongation of the contact length occurs.

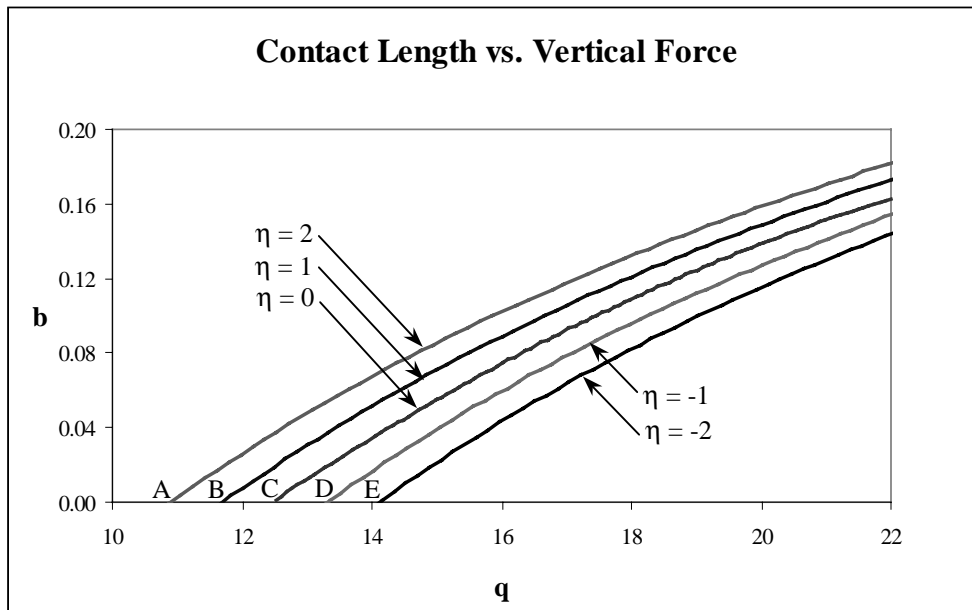


Figure 4.26: Contact Length vs. Vertical Force for $c=0.4$ and $\Delta\gamma=0$

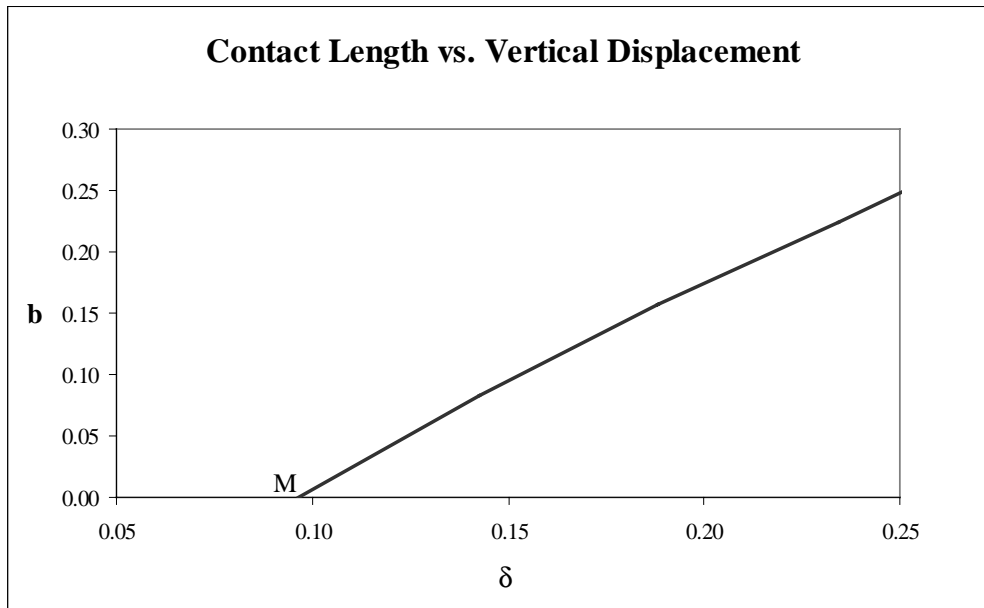


Figure 4.27: Contact Length vs. Vertical Displacement for $c=0.4$ and $\Delta\gamma=0$

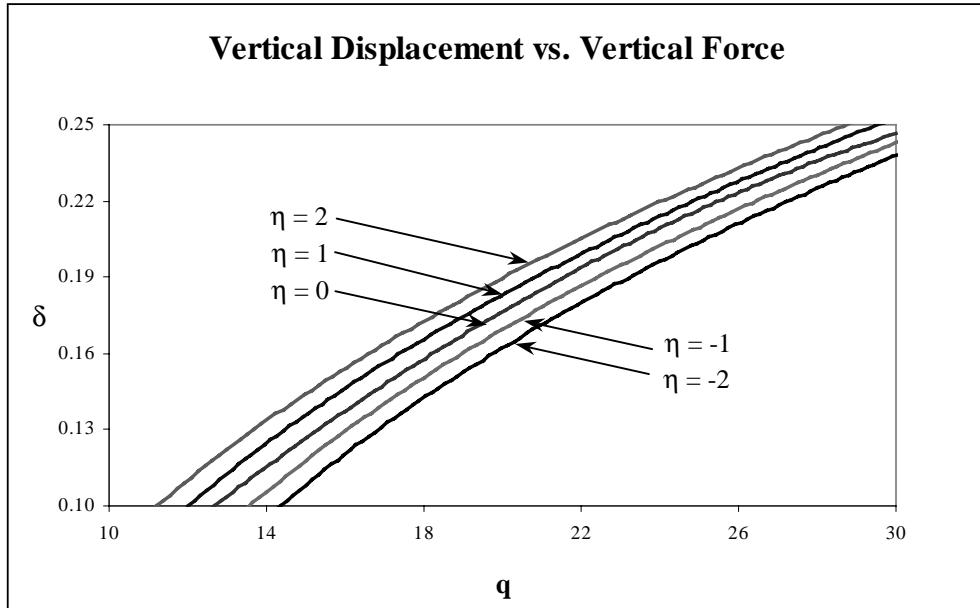


Figure 4.28: Vertical Displacement vs. Vertical Force for $c=0.4$ and $\Delta\gamma=0$

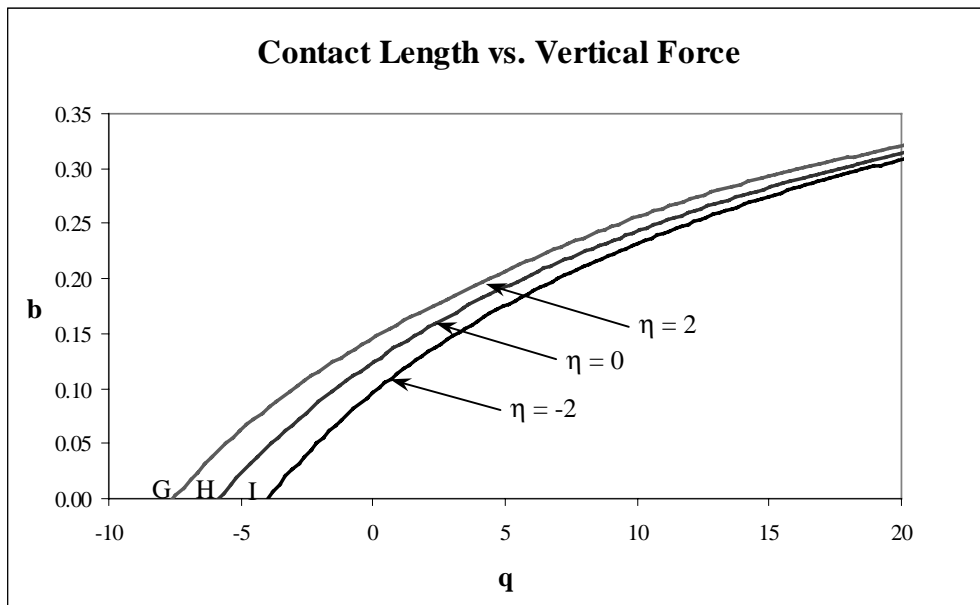


Figure 4.29: Contact Length vs. Vertical Force for $c=0.4$ and $\Delta\gamma=0.64$

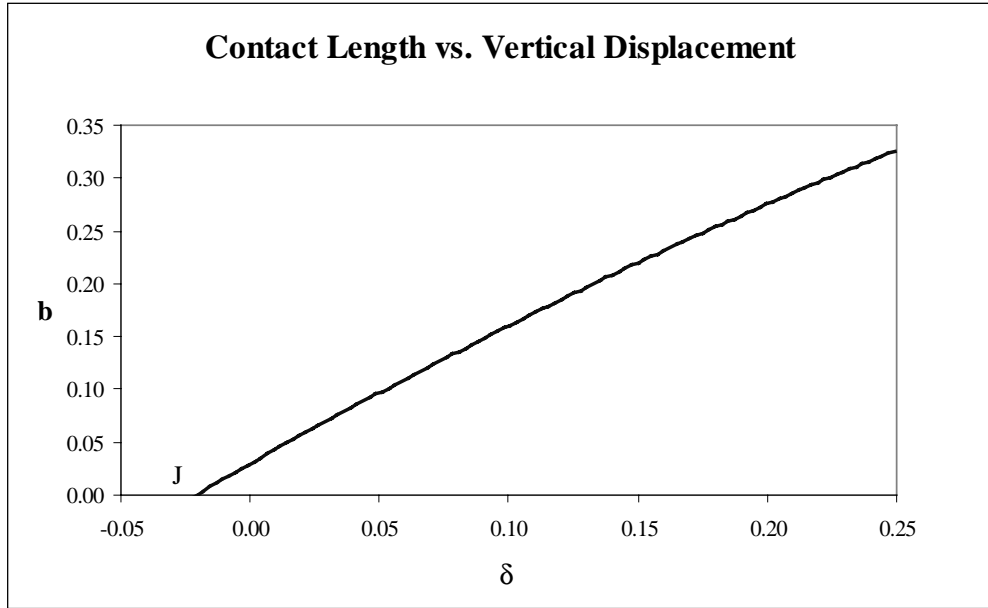


Figure 4.30: Contact Length vs. Vertical Displacement for $c=0.4$ and $\Delta\gamma=0.64$

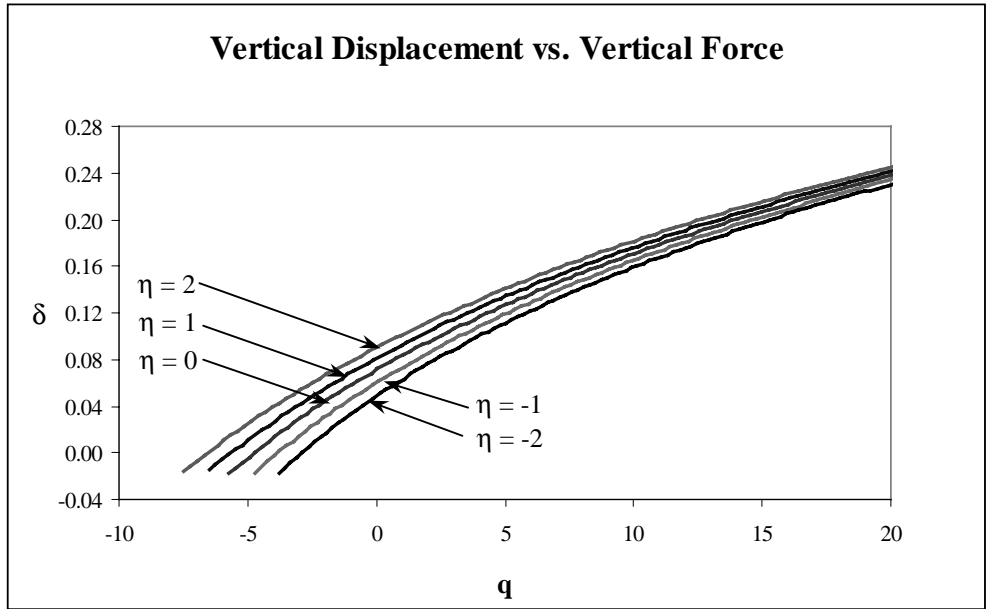


Figure 4.31: Vertical Displacement vs. Vertical Force for $c=0.4$ and $\Delta\gamma=0.64$

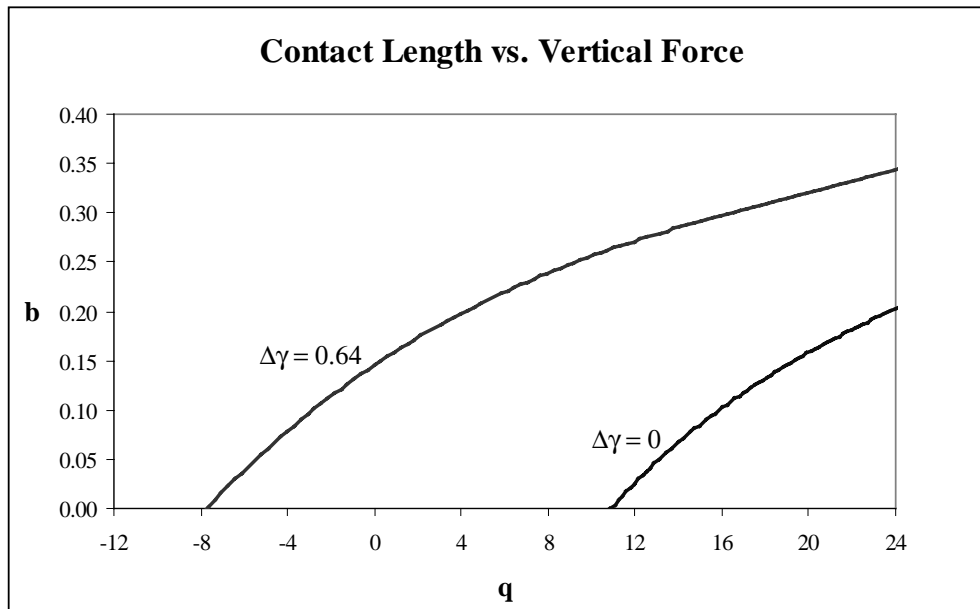


Figure 4.32: Contact Length vs. Vertical Force for $c=0.4$ and $\eta=2$

Chapter 5. Results from the DMT-Type Analysis

5.1 INTRODUCTION

Using a DMT-type analysis, several different cases were examined. First, a linear DMT force was used (see Figure 5.1(a)). For the linear DMT force, the maximum value of the force occurred at the point of separation of the elastica from the rigid surface. The term linear was used to describe this force due to the linear relationship between the adhesion force and $y(x)$. Several different values for the maximum force, f_0 , were investigated including $f_0=100$, 1000, and 10,000 for $c=0.4$, and $f_0=10$, 100, and 1000 for $c=0.8$. For each value of f_0 , three different values for α , the maximum separation distance between the elastica and the substrate over which the DMT forces acted, were examined. Values for α included $\alpha=0.01$, 0.001, and 0.0001. Additionally, values of $c=0.4$ and $c=0.8$ were considered, as were values of $\eta=2$, 0, and -2 . Values used for α and f_0 , as well as the combinations of η , α , and f_0 that were examined, can be found in Tables 5.1 and 5.2.

Table 5.1 : Values Used for the Linear DMT Force when $c=0.4$

η	α	f_0	η	α	f_0	η	α	f_0
2	0.01	100	0	0.01	100	-2	0.01	100
		1000			1000			1000
		10000			10000			10000
2	0.001	100	0	0.001	100	-2	0.001	100
		1000			1000			1000
		10000			10000			10000
2	0.0001	100	0	0.0001	100	-2	0.0001	100
		1000			1000			1000
		10000			10000			10000

Table 5.2: Values Used for the Linear DMT Force when $c=0.8$

η	α	f_0	η	α	f_0	η	α	f_0
2	0.01	10	0	0.01	10	-2	0.01	10
		100			100			100
		1000			1000			1000
2	0.001	10	0	0.001	10	-2	0.001	10
		100			100			100
		1000			1000			1000
2	0.0001	10	0	0.0001	10	-2	0.0001	10
		100			100			100
		1000			1000			1000

Since the adhesion forces were included within the equilibrium equations, the need to minimize the total energy of the system in order to find the equilibrium configuration of the elastica was eliminated. The linear force DMT-type analysis used the previously discussed shooting method to solve the governing elastica equations for three cases: when there was no contact between the strip and the rigid surface, when point contact existed between the two solids, and when the strip and the rigid surface had formed line contact. The curves obtained by using the combinations of f_0 , α , and η described in Table 5.1 were compared to the curves which ignored the effects of adhesion ($f_0=0$, $\alpha=0$) that were derived for the JKR-type analysis (i.e., when $\Delta\gamma=0$).

The horizontal length over which the DMT-type force acted, beginning at the point $x=0$, $y=0$ (see Figure 3.2), was denoted d . Over this length, the vertical gap between the substrate and the elastica varied from $y=0$ at the left end to $y=\alpha$ at the right end. It was assumed that the slope of the elastica in this region was very small, so that a linear analysis could be carried out, and $x=s$. This analysis is described in Appendix B. The conditions at the right end of this region were obtained from the linear analysis, i.e., $x=d$, $y=\alpha$, $\theta=d^2y/dx^2$, and $m=d^2y/dx^2$. These conditions became the initial conditions for the

shooting method solution of the elastica equations. The end conditions were specified for the right clamped end of the strip. Figure 5.1 (a, b, c) shows the linear force as it varied with y , the linear force as it varied with x , and the shape of the elastica from $x=0$ to $x=d$.

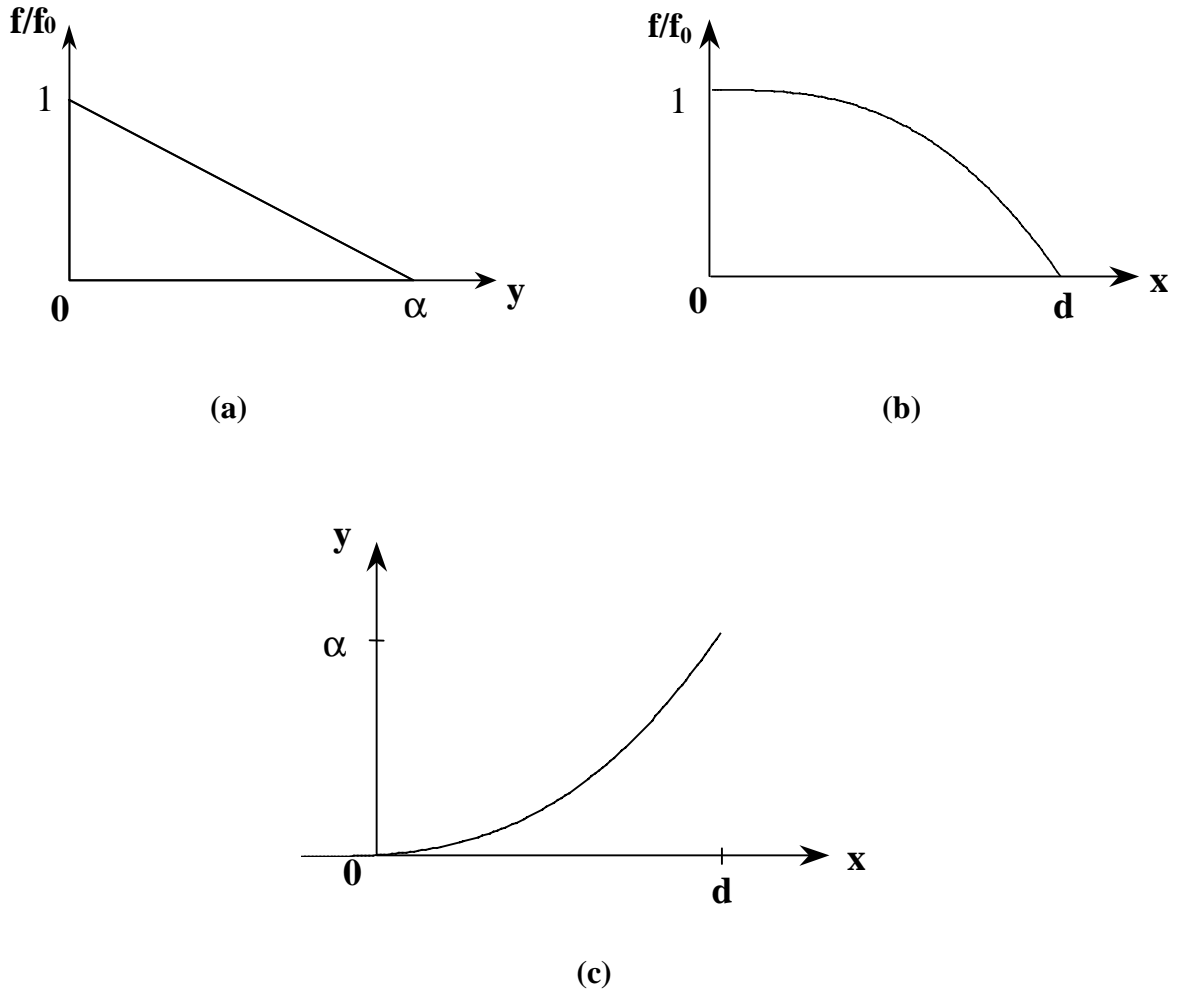


Figure 5.1: (a) Linear force vs. y for DMT-type analysis; (b) Typical corresponding adhesion force vs. x plot for linear force DMT-type analysis; (c) Typical y vs. x plot from $x=0$ to $x= d$ for linear force DMT-type analysis

When no contact existed between the elastica and the rigid surface, Equations 3.1-3.3 and Equation 4.6 were used as the governing equations. The DMT force experienced its

maximum value at the center of the elastica ($x=0$), where y is denoted y_0 with $0 < y_0 < \alpha$, and acted until the vertical separation distance between the elastica and the substrate reached a value α ($y=\alpha$). Therefore, end conditions were specified at $s=d$ and $s=1$. The values for θ and m at $s=d$ depended on y_0 . When $s=1$, the end conditions were $x=c$ and $\theta=\pi/2$. Values for c , d , η , f_0 , and α were specified and values were guessed for p and y_0 . The FindRoot command in Mathematica was used to obtain values for p and y_0 .

When point contact between the elastica and the rigid surface was experienced, the governing equations used in the no contact case were again applied (Equations 3.1-3.3 and Equation 4.6). The end conditions at $s=1$ were $x=c$ and $\theta=\pi/2$. Values for c , d , η , f_0 , and α were specified and values were guessed for p and M , where M was a constant representing the magnitude of $y(x)$. Here $y=0$ at $x=0$. The FindRoot command in Mathematica was used to obtain values for the guessed variables that met the specified end conditions.

When the contact length became greater than zero, line contact formed between the elastica and the rigid surface. At the point of separation of the elastica from the rigid surface ($x=0$, $y=0$), the linear force experienced its maximum value. This force acted until the vertical separation distance between the elastica and the substrate reached a value of α ($x=d$, $y=\alpha$). When the vertical separation distance between the elastica and the substrate became greater than α , the adhesion force equaled zero. Therefore, end conditions were specified at $s=d$ and $s=1-b$. When $s=1-b$, the end conditions were $x=c-b$ and $\theta=\pi/2$. A scaled arc length t was introduced in the uplifted region when $s > d$, and was defined by $t=(s-d)/u$ where $u=1-d-b$ and $0 < t < 1$. The non-dimensional length u was treated as a variable that had a constant value. The governing equations then became

$$\frac{dx}{dt} = u \cos \theta \qquad \frac{dy}{dt} = u \sin \theta$$

$$\frac{d\theta}{dt} = u m$$

$$\frac{dm}{dt} = -u p \sin \theta + u[q + \eta(1-b) - \eta(d+ut)] \cos \theta$$

$$\frac{du}{dt} = 0 \tag{5.1-5.5}$$

and the conditions at the upper end $t=1$ became $x=c+d+u-1$ and $\theta=\pi/2$. The separation parameter c , the distance d along the elastica over which the DMT force acted, the self-weight η , the DMT force f_0 , and the vertical separation distance α were specified and values were guessed for p and u . The FindRoot command in Mathematica was used to obtain values for p and u . The contact length was then calculated using the formula $b=1-d-u$.

The second DMT force considered was a Dugdale force. The Dugdale force, g_0 , was a constant force which began at the point of separation of the elastica from the rigid surface and remained constant until the separation distance between the elastica and the substrate reached the specified value of α . When the vertical separation distance between the elastica and the rigid surface became greater than α , the adhesion forces vanished. Therefore, the plot of the normalized Dugdale force (f/g_0) vs. y produced a constant value of 1 from $0 < y < \alpha$. When $y > \alpha$, the Dugdale force was equal to zero. The plot of the normalized Dugdale force (f/g_0) vs. x also produced a constant value of 1 from $0 < x < d$. When $x > d$, the Dugdale force was equal to zero. Finally, when the x and y values of the elastica were plotted for $0 < x < d$ (or, $0 < y < \alpha$), the shape of the elastica resembled that shown in Figure 5.1 (c).

Several different values for the maximum force, g_0 , were investigated including $g_0=500$ and 5000. For each value of g_0 , the following α values were examined: $\alpha=0.001$ and 0.0001. Additionally, values of $\eta=2, 0$, and -2 were considered, with $c=0.4$. Values used

for α and g_0 , as well as the combinations of η , α , and g_0 that were examined, can be found in Table 5.3.

Since the adhesion forces were included within the equilibrium equations, the need to minimize the total energy of the system in order to find the equilibrium configuration of the elastica was eliminated. The Dugdale force DMT-type analysis used the previously discussed shooting method to solve the governing elastica equations for three cases: no contact between the strip and the rigid surface, point contact between the two solids, and line contact formation between the strip and the rigid surface. The curves obtained by

Table 5.3: Values Used for the Dugdale DMT Force

η	α	g_0	η	α	g_0	η	α	g_0
2	0.001	500	0	0.001	500	-2	0.001	500
		5000			5000			5000
2	0.0001	500	0	0.0001	500	-2	0.0001	500
		5000			5000			5000

using the combinations of g_0 , α , and η described in Table 5.3 were compared to the curves which ignored the effects of adhesion ($g_0=0$, $\alpha=0$) that were derived for the JKR-type analysis (i.e., when $\Delta\gamma=0$).

The governing equations and boundary conditions used to obtain solutions for the no contact, point contact, and line contact stages of the Dugdale force DMT-type analysis are the same as those used in the linear force DMT-type analysis for the no contact, point contact, and line contact stages, respectively. The difference in the two analyses lies in the types of forces used (linear vs. constant). Therefore, the differences between the two analyses were reflected in the equation obtained for $y(x)$. Although the end conditions at $s=d$ remained $x=d$, $y=\alpha$, $\theta=dy/dx$, and $m=d^2y/dx^2$, the actual values calculated for θ and m changed according the equation used for $y(x)$. The linear analysis used to determine $y(x)$ for $0<x<d$ is described in Appendix C for the Dugdale DMT model.

5.2 RESULTS FOR THE LINEAR DMT-TYPE FORCE

Using the shooting method, and the governing equations and end conditions described for the linear force with line contact, values for the free length u of the elastica, the vertical force q , the horizontal force p , the height h of the elastica, and the moment m_d at d were obtained. The contact length was then calculated using $b = 1 - d - u$, and the vertical displacement was calculated by subtracting the height of the elastica from its initial height when there was no contact between the elastica and the rigid surface ($\delta = h_0 - h$). For the linear force, separation distances of $c=0.4$ and $c=0.8$ between the clamped ends were considered. Additionally, for each value of c , three η values were examined: $\eta=2$, 0 , and -2 . The values of h_0 corresponding to $\eta=2$, 0 , and -2 were $h_0=0.7912$, 0.7896 , and 0.7878 , respectively, for $c=0.4$, and $h_0=0.4408$, 0.4368 , and 0.4324 , respectively, for $c=0.8$.

5.2.1 Results for $c=0.4$ and $\eta=0$ (Line Contact Only)

The results obtained for the line contact case when $c=0.4$ and $\eta=0$ can be found in Figures 5.2- 5.11. Values of $\alpha=0.001$ and 0.0001 were examined. The original analysis also included an examination of the $\alpha=0.01$ case. However, it was later discovered that values for θ at $s=d$ were significantly larger than θ values at $s=d$ for $\alpha=0.001$ and $\alpha=0.0001$. Since a linear analysis from $s=0$ to $s=d$ was possible due to small angle theory, $\alpha=0.01$ was eliminated due to the larger values of θ that were present at $s=d$. Table 5.4 presents values for θ and m_d when $\alpha=0.01$, 0.001 , and 0.0001 for $c=0.4$, $\eta=0$, $b=0$ (approximately), and $f_0=100$, 1000 , and $10,000$.

For each value of α , maximum force values $f_0=0$, 100 , 1000 , and $10,000$ were considered. In Figure 5.2, which plots the contact length vs. the vertical force for $\alpha=0.001$, the effect of the adhesion forces can be seen. As the value for the maximum linear force f_0 was increased, the value for the contact length b , at a constant value of q , also increased.

Table 5.4: Values for d , θ , and m_d when $c=0.4$, $\eta=0$, and $b=0$

α	$f_0=100$			$f_0=1000$			$f_0=10,000$		
	d	θ	m_d	d	θ	m_d	d	θ	m_d
0.01	0.153	0.183	2.0847	0.106	0.2401	3.0838	0.063	0.38953	7.387
0.001	0.073	0.0397	1.0163	0.055	0.0485	1.3708	0.033	0.0764	3.1374
0.0001	0.035	0.0085	0.4704	0.029	0.0097	0.5731	0.018	0.0142	1.1222

When $f_0=100$, the values obtained through the analysis were very close to those obtained for $f_0=0$ (i.e. no adhesion forces present). Figure 5.3 presents results similar to those in Figure 5.2. This plot of contact length b vs. vertical deflection δ shows that as the value for the maximum linear force increased, the value for the contact length, at a constant value of δ , also increased. The results obtained from Figures 5.2 and 5.3 indicate that the presence of adhesion forces elongated the contact length.

The results of the line contact analysis (or spreading solution) can also be seen in Figure 5.4 which plots the vertical displacement δ vs. the vertical force q . All curves in Figure 5.4 terminated when the contact length equaled zero and the elastica reached the transition point from line contact to point contact. Values of d , q , δ , p , and m_d at the transition point between point and line contact can be found in Table 5.5.

Table 5.5: Values Corresponding to the Transition Point Between Line Contact ($b>0$) and Point Contact ($b=0$) for $c=0.4$ and $\eta=0$

	Curve	d	q	δ	p	m_d
$\alpha = 0$	$f_0 = 0$	0.0000	12.52	0.0966	10.277	NA
$\alpha = 0.001$	$f_0 = 100$	0.0731	12.10	0.0919	10.052	1.0163
	$f_0 = 1000$	0.0549	9.62	0.0667	8.765	1.3708
	$f_0 = 10000$	0.0334	-0.83	0.0018	4.088	3.1374
$\alpha = 0.0001$	$f_0 = 100$	0.0349	12.42	0.0953	10.220	0.4704
	$f_0 = 1000$	0.0290	11.77	0.0875	9.860	0.5731
	$f_0 = 10000$	0.0183	9.23	0.0608	8.510	1.1222

Since the moment at the point of separation of the elastica from the rigid surface was equal to zero ($m_b=0$) for line contact, values were calculated for the moment at $s=d$. Figure 5.5 plots the moment m_d vs. the vertical force q for $\alpha=0.001$. As the value of f_0 increased, the moment m_d also increased for a fixed value of q . Unlike the moment m_b , which was calculated in the JKR-type analysis, the value of m_d is dependent on the vertical force applied to the clamped ends. Values for m_d increased as the applied vertical force increased (for a fixed value of f_0).

Figure 5.6 shows the relationship between the moment at $s=d$ and the vertical displacement for $c=0.4$, $\eta=0$, and $\alpha=0.001$. As the value of f_0 increased, the moment m_d also increased for a fixed value of δ . Additionally, as the value of m_d increased, the value of the vertical displacement increased (for a fixed value of f_0). Values for the moment m_d , the vertical force q , and the vertical displacement δ at $b=0$ (i.e. at the left end of the curves) can be found in Table 5.5.

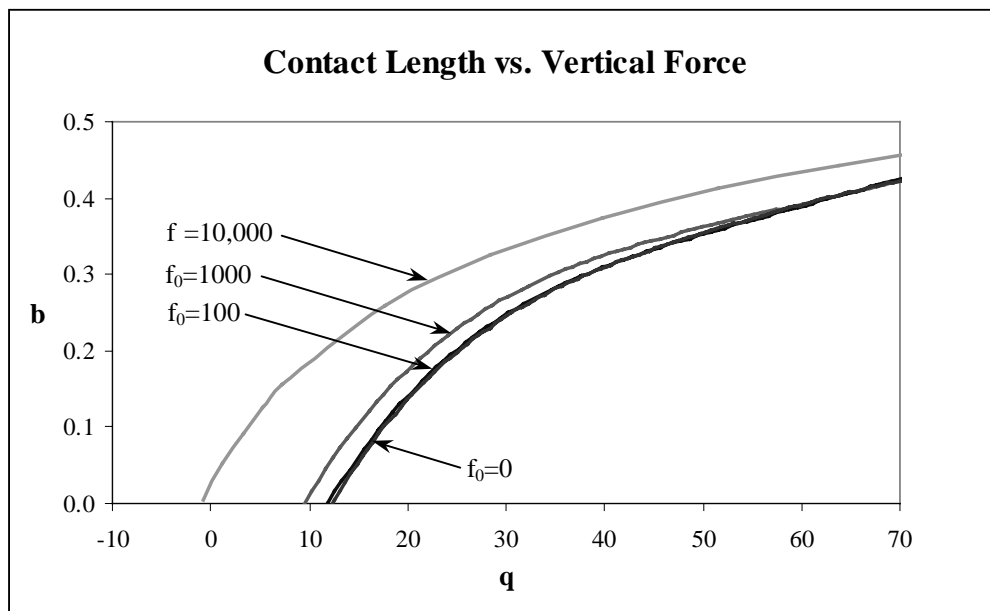


Figure 5.2: Contact Length vs. Vertical Force for $c=0.4$, $\eta=0$, and $\alpha=0.001$

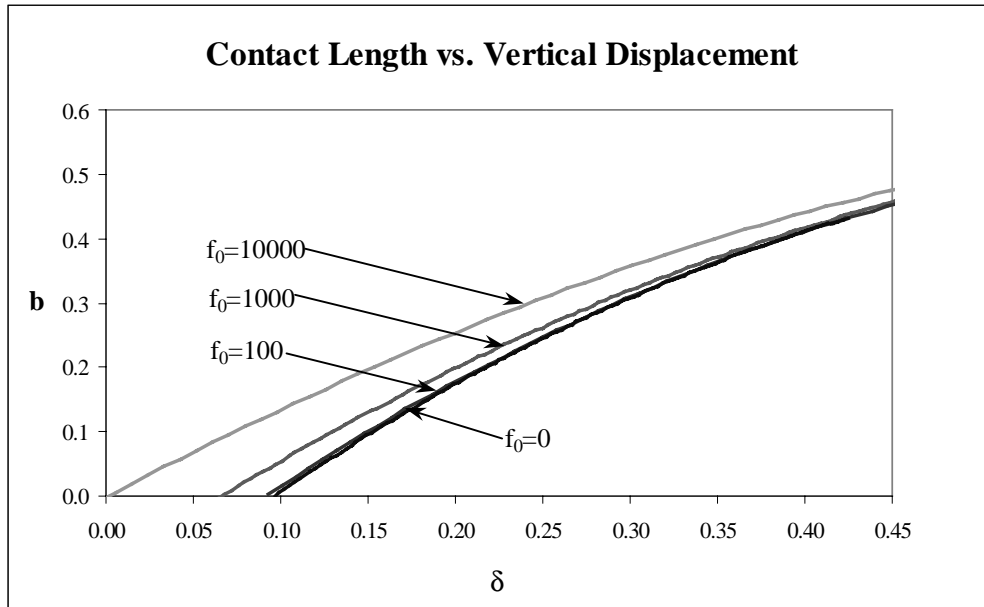


Figure 5.3: Contact Length vs. Vertical Displacement for $c=0.4$, $\eta=0$, and $\alpha=0.001$

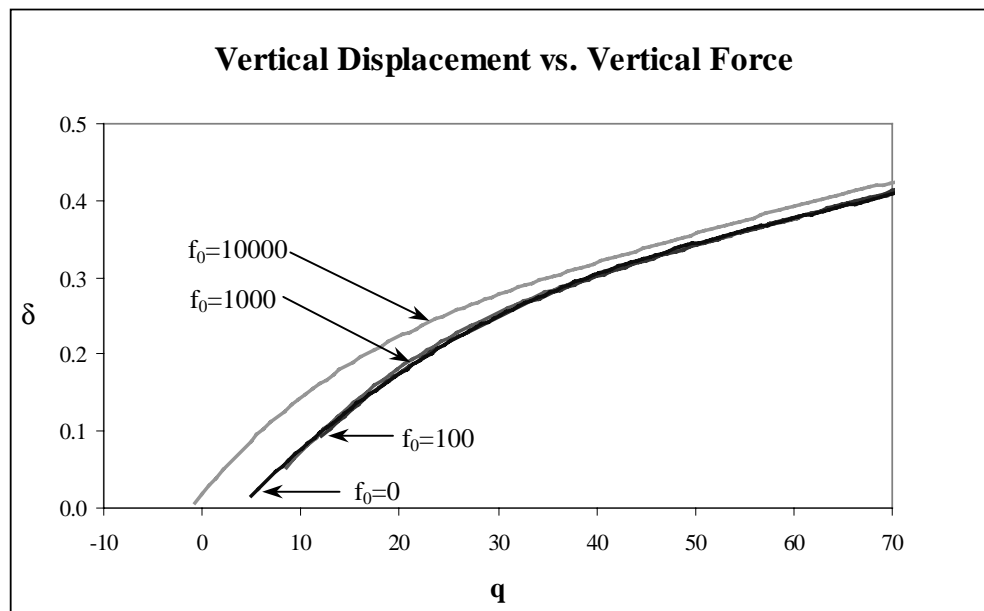


Figure 5.4: Vertical Displacement vs. Vertical Force for $c=0.4$, $\eta=0$, and $\alpha=0.001$

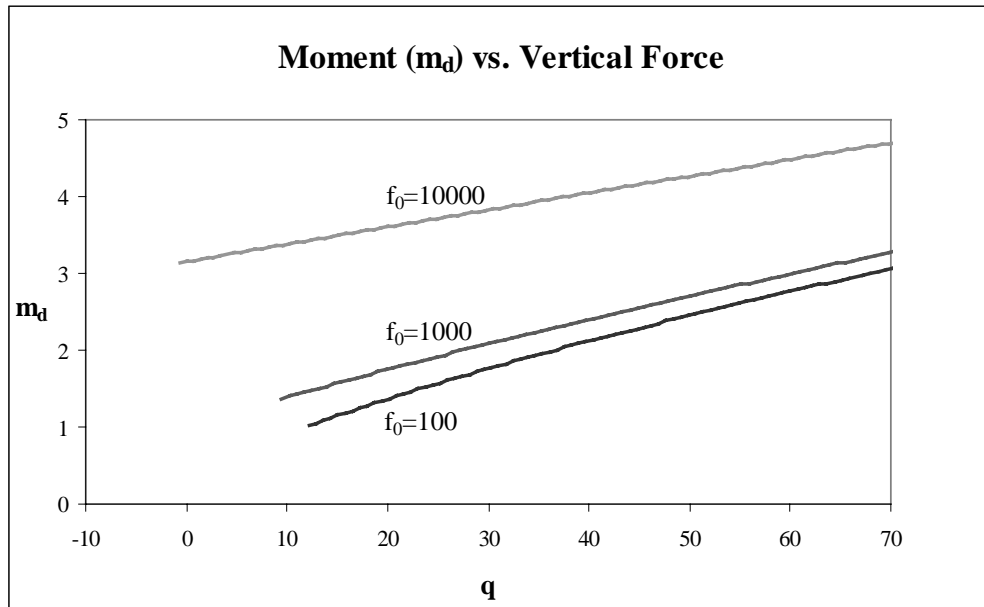


Figure 5.5: Moment (m_d) vs. Vertical Force for $c=0.4$, $\eta=0$, and $\alpha=0.001$

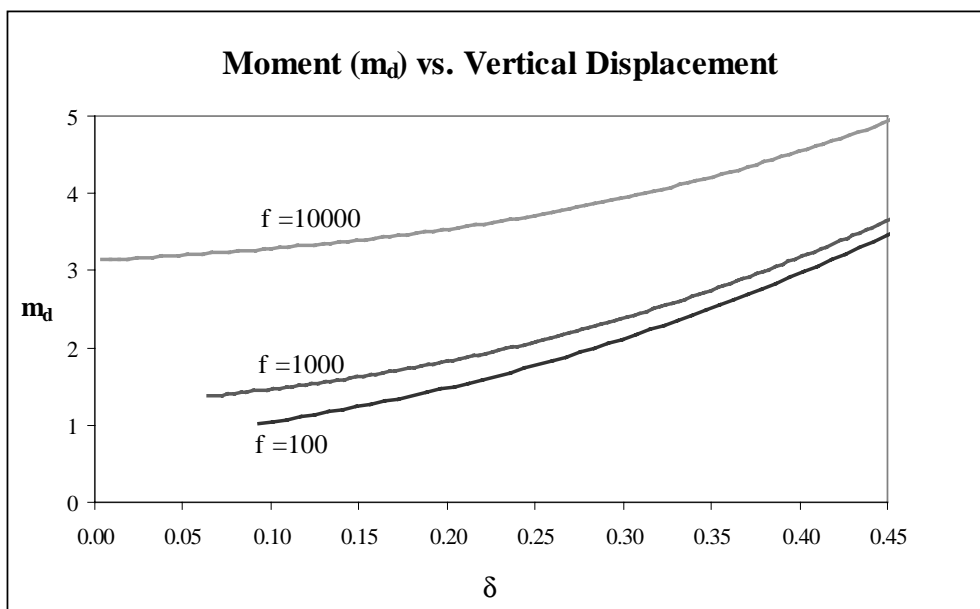


Figure 5.6: Moment (m_d) vs. Vertical Displacement for $c=0.4$, $\eta=0$, and $\alpha=0.001$

Results for the linear force DMT-type analysis when $c=0.4$, $\eta=0$, and $\alpha=0.0001$ can be found in Figures 5.7-5.11. Figure 5.7 plots the contact length vs. the vertical force for $\alpha=0.0001$. As the value for the maximum linear force f_0 was increased, the value for the contact length b , at a constant value of q , also increased. When $f_0=100$ and $f_0=1000$, the values obtained through the analysis were very close to those obtained for $f_0=0$ (i.e. no adhesion forces present). Figure 5.8 presents results similar to those in Figure 5.7. This plot of contact length b vs. vertical deflection δ shows that as the value for the maximum linear force increased, the value for the contact length, at a constant value of δ , also increased. The results obtained from Figures 5.7 and 5.8 indicate that the presence of adhesion forces elongated the contact length.

The results of the line contact analysis (or spreading solution) for $c=0.4$, $\eta=0$, and $\alpha=0.0001$ can also be seen in Figure 5.9 which plots the vertical displacement δ vs. the vertical force q . All curves in Figure 5.9 terminated when the contact length equaled zero and the elastica reached the transition point from line contact to point contact. Additionally, the values obtained for the curves $f_0=100$, 1000 , and $10,000$ were very close to those obtained for $f_0=0$ (i.e. no adhesion forces present). Values of d , q , δ , p , and m_d at the transition point between point and line contact can be found in Table 5.5.

Since the moment at the point of separation of the elastica from the rigid surface was equal to zero ($m_b=0$), values were calculated for the moment at $s=d$. Figure 5.10 plots the moment m_d vs. the vertical force q for $\alpha=0.0001$. As the value of f_0 increased, the moment m_d also increased for a fixed value of q . Unlike the moment m_b , which was calculated in the JKR-type analysis, the value of m_d was dependent on the vertical force applied to the clamped ends. Values for m_d increased as the applied vertical force increased (for a fixed value of f_0). The curves in Figure 5.10 for $f_0=100$, 1000 , and $10,000$ terminate when the transition point from line contact to point contact has been attained ($b=0$).

Figure 5.11 shows the relationship between the moment at $s=d$ and the vertical displacement for $c=0.4$, $\eta=0$, and $\alpha=0.0001$. As the value of f_0 increased, the moment m_d also increased for a fixed value of δ . Additionally, as the value of m_d increased, the value of the vertical displacement increased (for a fixed value of f_0). Values for the moment m_d , the vertical force q , and the vertical displacement δ at $b=0$ can be found in Table 5.5. The curves in Figure 5.11 for $f_0=100$, 1000, and 10,000 terminate when the transition point from line contact to point contact has been attained ($b=0$).

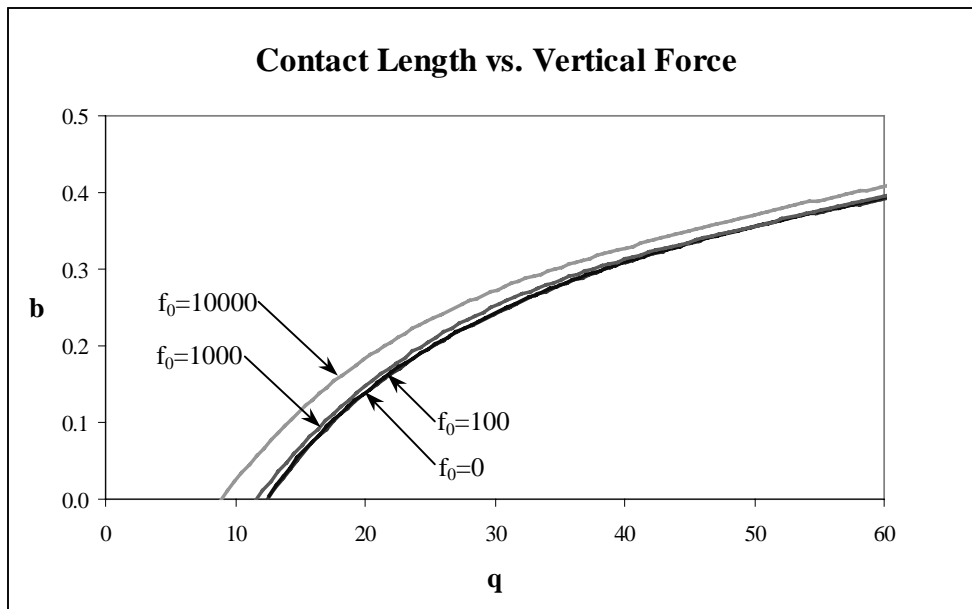


Figure 5.7: Contact Length vs. Vertical Force for $c=0.4$, $\eta=0$, and $\alpha=0.0001$

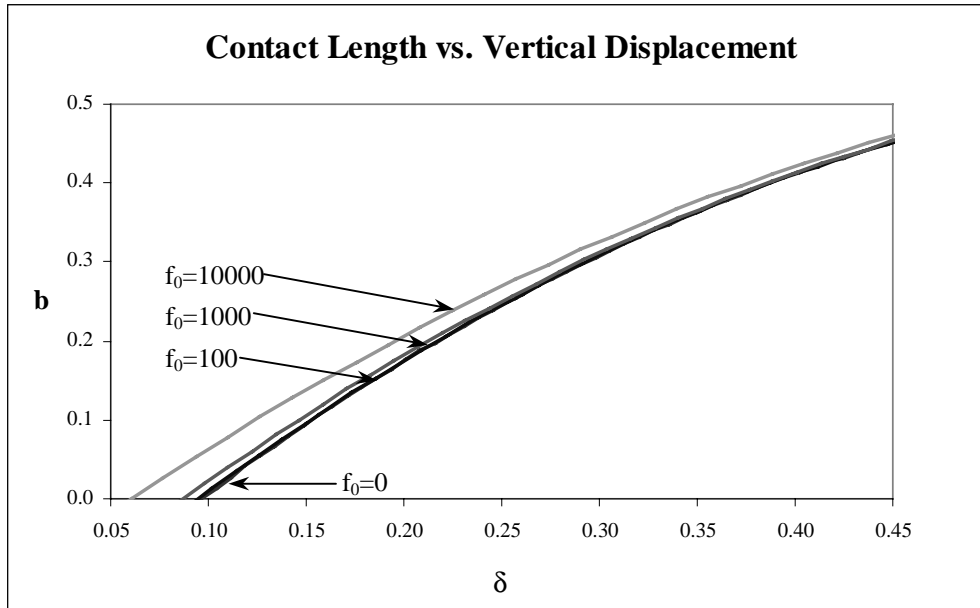


Figure 5.8: Contact Length vs. Vertical Displacement for $c=0.4$, $\eta=0$, and $\alpha=0.0001$

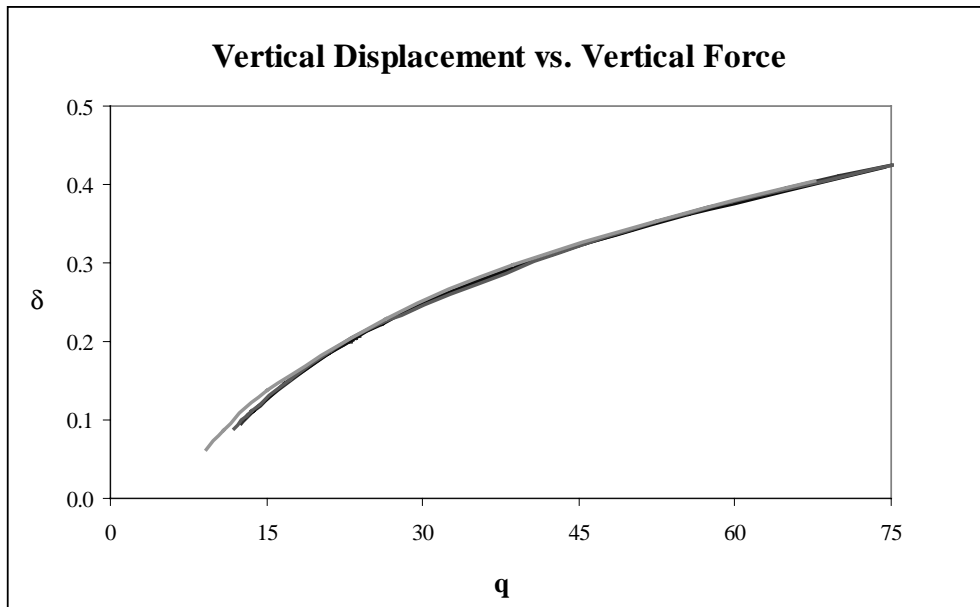


Figure 5.9: Vertical Displacement vs. Vertical Force for $c=0.4$, $\eta=0$, and $\alpha=0.0001$

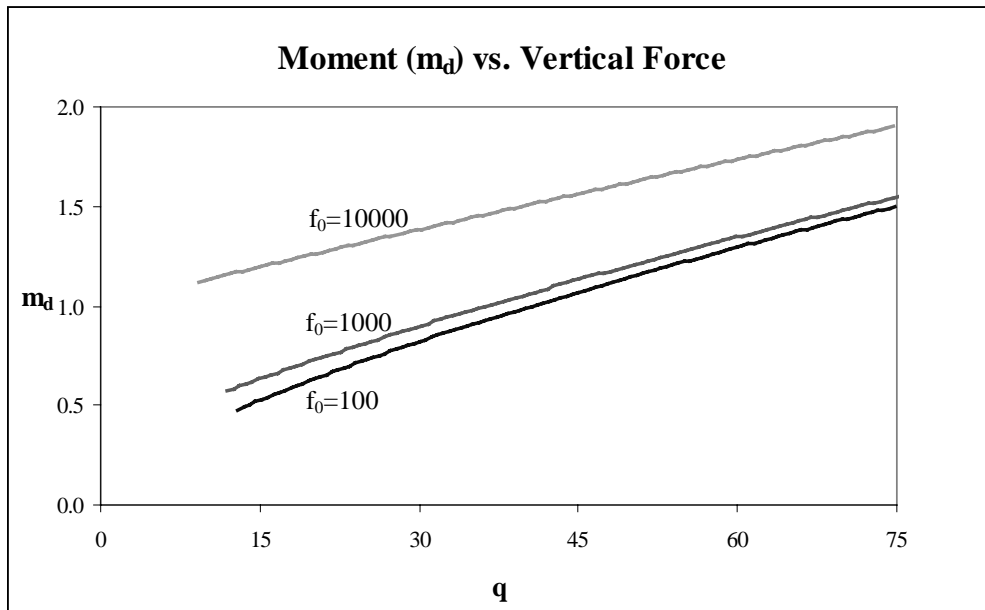


Figure 5.10: Moment (m_d) vs. Vertical Force for $c=0.4$, $\eta=0$, and $\alpha=0.0001$

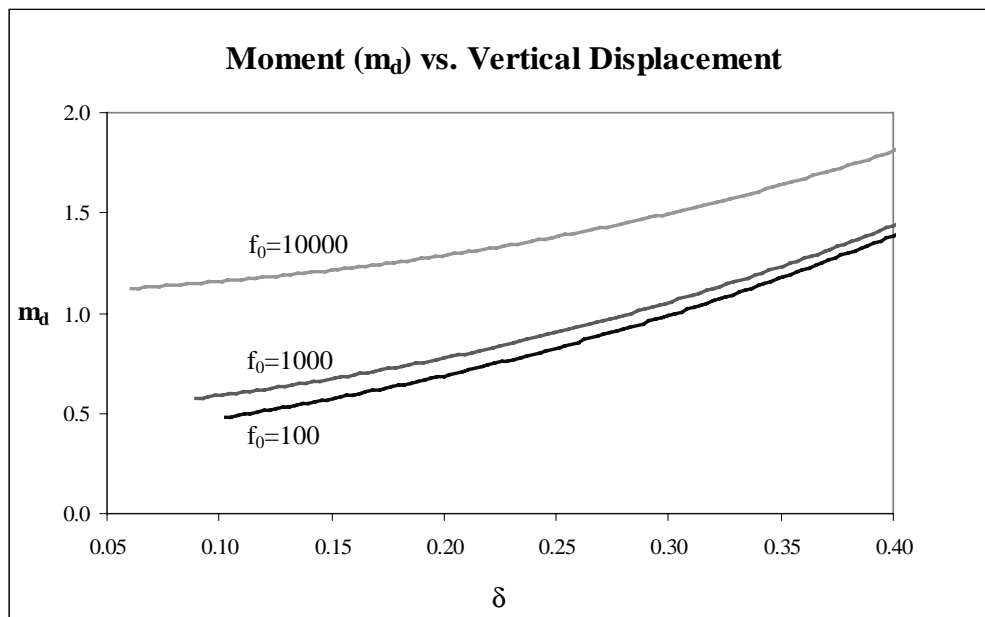


Figure 5.11: Moment (m_d) vs. Vertical Displacement for $c=0.4$, $\eta=0$, and $\alpha=0.0001$

5.2.2 Results for $c=0.4$ and $\eta=2$ (Line Contact Only)

The results obtained for the line contact case when $c=0.4$ and $\eta=2$ can be found in Figures 5.12-5.21. Values of $\alpha=0.001$ and 0.0001 were examined. For each value of α , maximum force values of $f_0=0, 100, 1000$, and $10,000$ were considered. The results obtained for $c=0.4$ and $\eta=2$ were comparable to those obtained when $c=0.4$ and $\eta=0$. The presence of adhesion forces caused an elongation of the contact area. For increasing values of f_0 , the contact length also increased when the values of q and δ were fixed (see Figures 5.12, 5.13, 5.17, and 5.18). Figures 5.14 and 5.19, for $\alpha=0.001$ and 0.0001 , respectively, plot the vertical displacement δ vs. the vertical force q . All curves in Figures 5.14 and 5.19 terminated when the contact length equaled zero and the elastica reached the transition point from line contact to point contact. Values d, q, δ, p , and m_d at the transition point when $\alpha=0.001$ and 0.0001 can be found in Table 5.6.

Table 5.6: Values Corresponding to the Transition Point Between Line Contact ($b>0$) and Point Contact ($b=0$) for $c=0.4$ and $\eta=2$

	Curve	d	q	δ	p	m_d
$\alpha = 0$	$f_0 = 0$	0.0000	10.90	0.0960	10.178	NA
$\alpha = 0.001$	$f_0 = 100$	0.0726	10.48	0.0914	9.952	1.0273
	$f_0 = 1000$	0.0548	7.96	0.0664	8.643	1.3862
	$f_0 = 10000$	0.0334	-2.62	0.0024	3.888	3.1391
$\alpha = 0.0001$	$f_0 = 100$	0.0346	10.81	0.0949	10.125	0.4753
	$f_0 = 1000$	0.0284	10.17	0.0874	9.767	0.5772
	$f_0 = 10000$	0.0183	7.56	0.0607	8.384	1.1260

Values for the moment at $s=d$ were calculated using the shooting method. These values were then plotted against the vertical force and the vertical displacement (Figures 5.15, 5.16, 5.20, and 5.21). As the value of f_0 increased, the moment m_d increased when values of q and δ were fixed. Additionally, as the value of m_d increased, the values of the vertical force and the vertical displacement also increased. Unlike the moment m_b , which

was calculated in the JKR-type analysis, the value of m_d was dependent on the vertical force applied to the clamped ends, as well as the value of the maximum linear force f_0 .

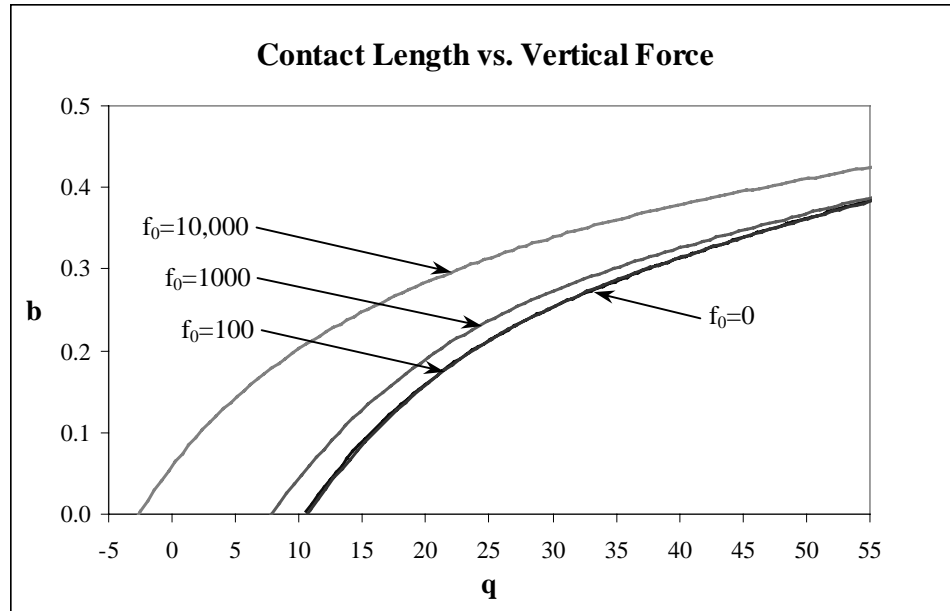


Figure 5.12: Contact Length vs. Vertical Force for $c=0.4$, $\eta=2$, and $\alpha=0.001$

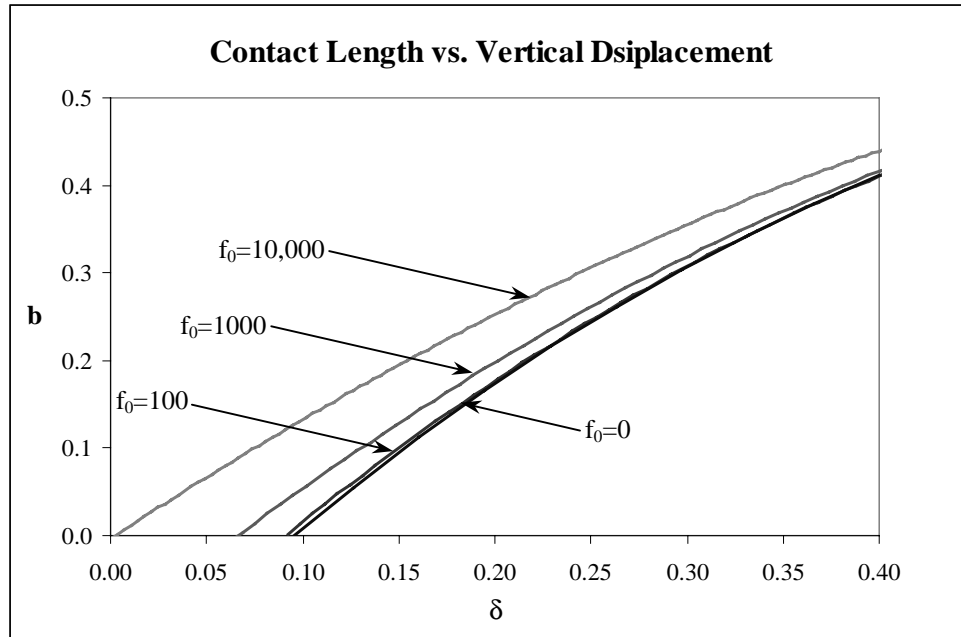


Figure 5.13: Contact Length vs. Vertical Displacement for $c=0.4$, $\eta=2$, and $\alpha=0.001$

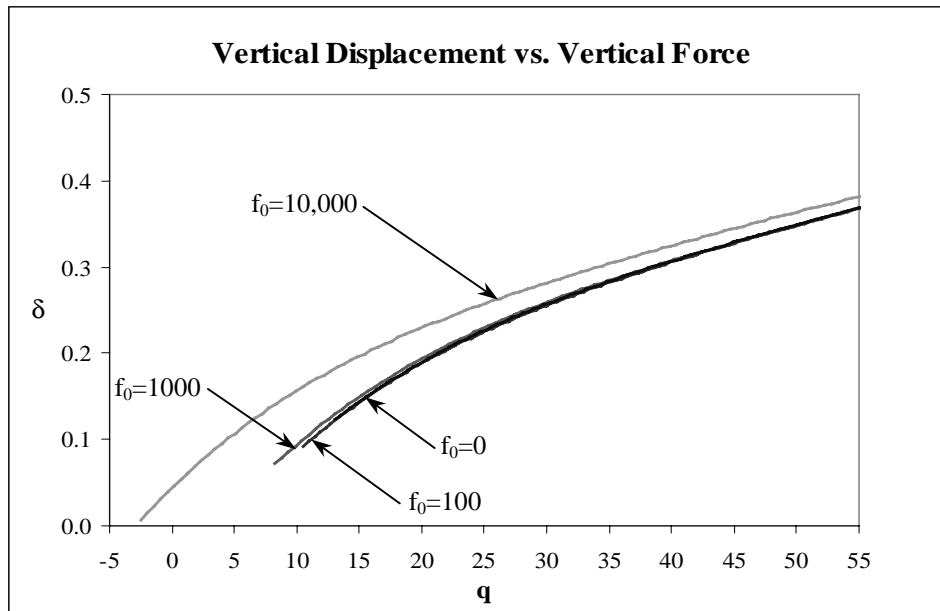


Figure 5.14: Vertical Displacement vs. Vertical Force for $c=0.4$, $\eta=2$, and $\alpha=0.001$

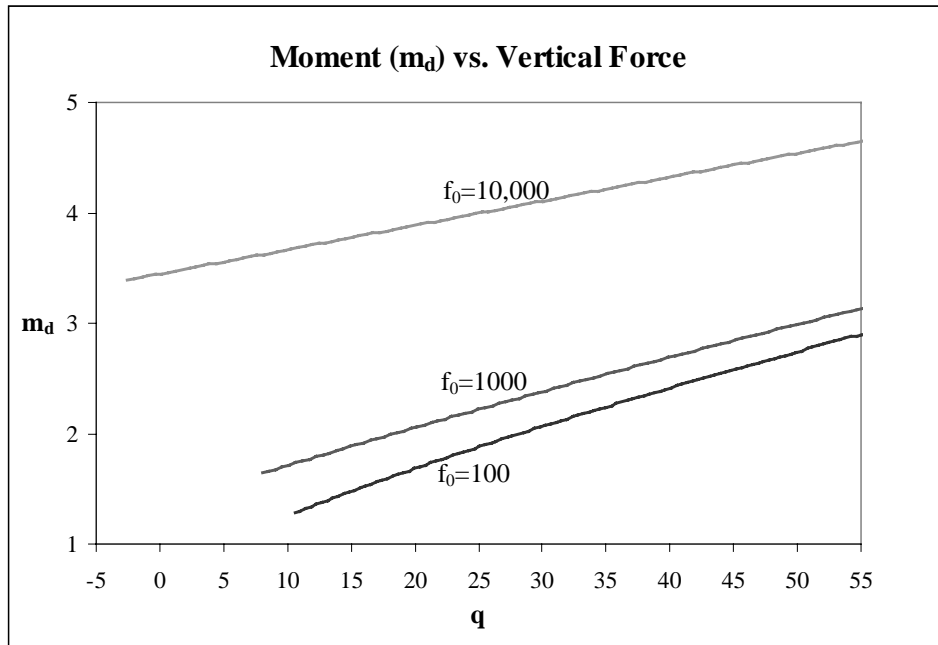


Figure 5.15: Moment (m_d) vs. Vertical Force for $c=0.4$, $\eta=2$, and $\alpha=0.001$

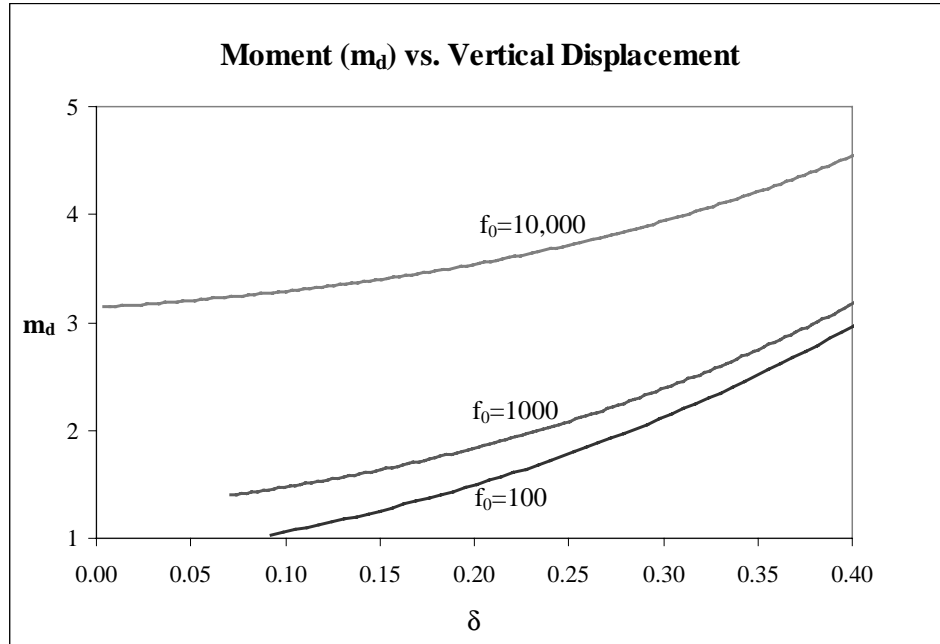


Figure 5.16: Moment (m_d) vs. Vertical Displacement for $c=0.4$, $\eta=2$, and $\alpha=0.001$

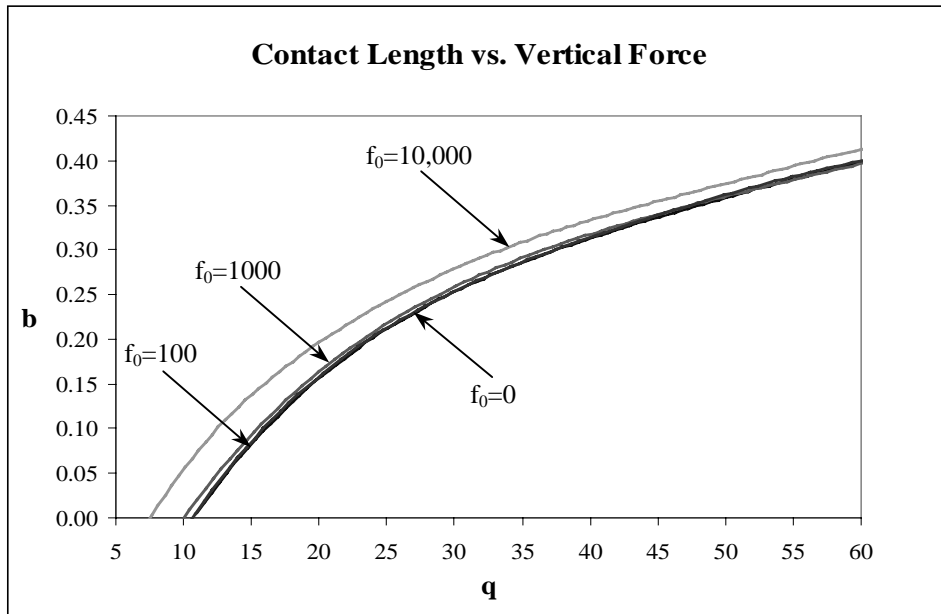


Figure 5.17: Contact Length vs. Vertical Force for $c=0.4$, $\eta=2$, and $\alpha=0.0001$

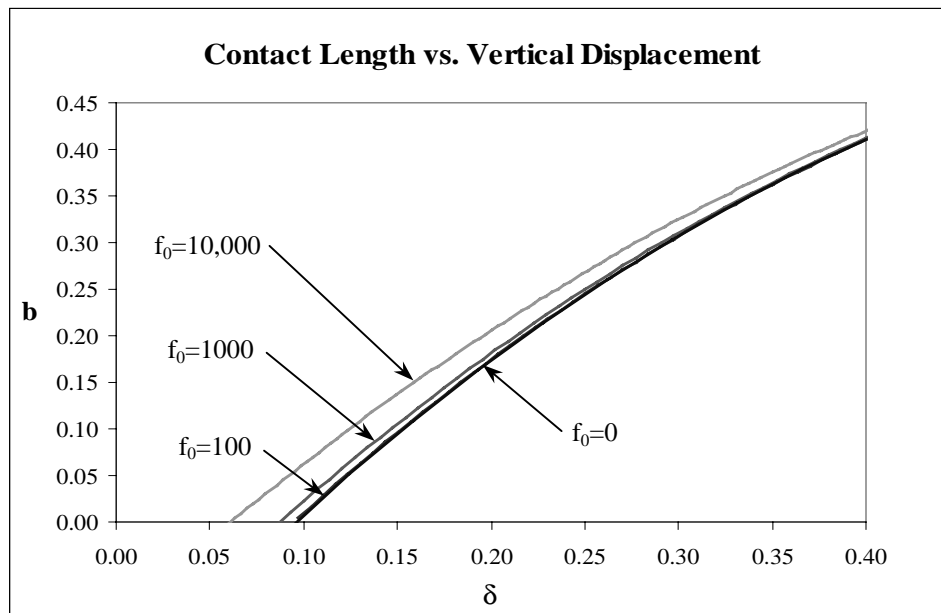


Figure 5.18: Contact Length vs. Vertical Displacement for $c=0.4$, $\eta=2$, and $\alpha=0.0001$

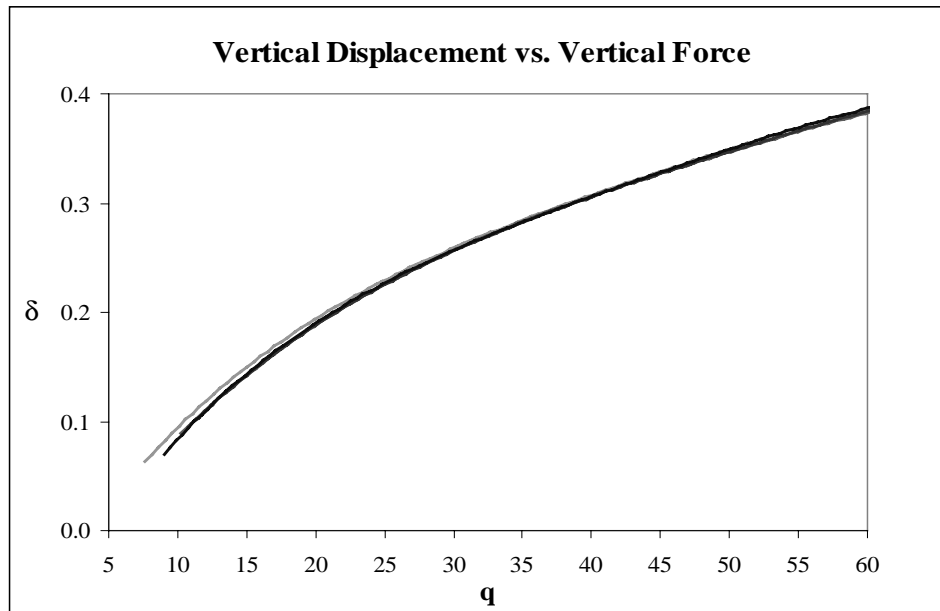


Figure 5.19: Vertical Displacement vs. Vertical Force for $c=0.4$, $\eta=2$, and $\alpha=0.0001$

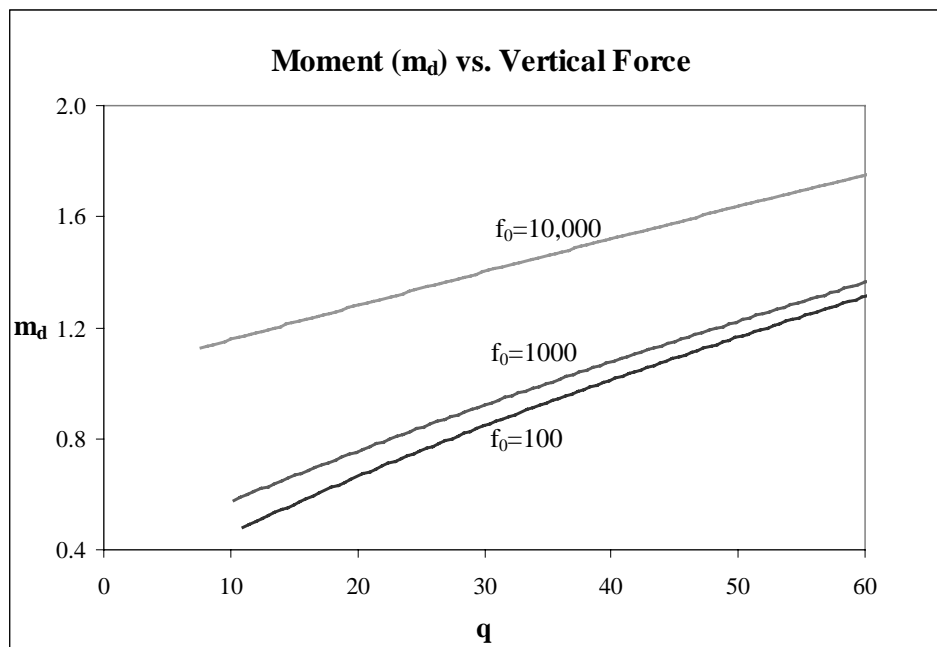


Figure 5.20: Moment (m_d) vs. Vertical Force for $c=0.4$, $\eta=2$, and $\alpha=0.0001$

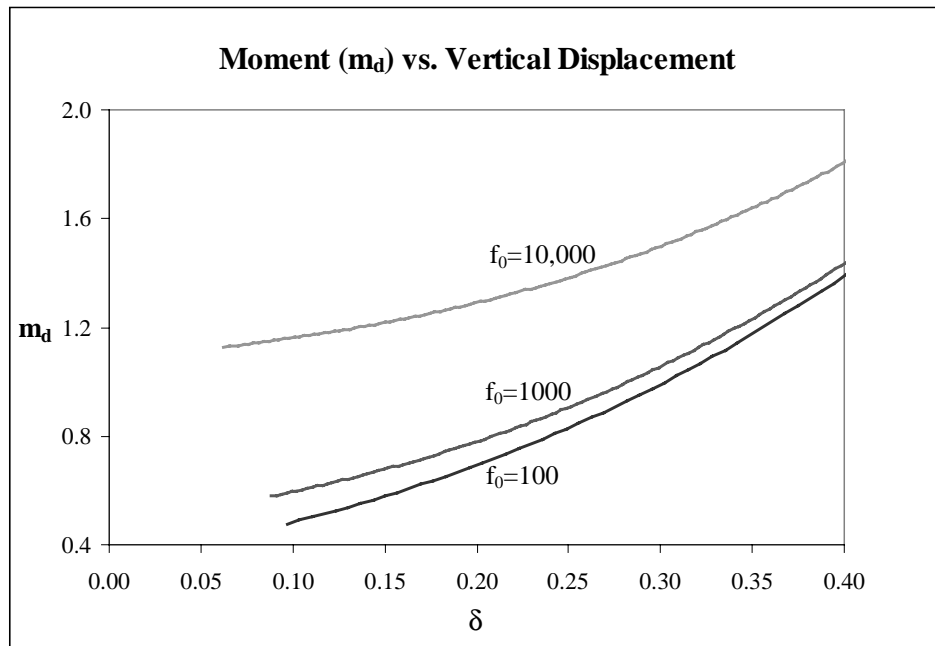


Figure 5.21: Moment (m_d) vs. Vertical Displacement for $c=0.4$, $\eta=2$, and $\alpha=0.0001$

5.2.3 Results for $c=0.4$ and $\eta=-2$ (Line Contact Only)

The results obtained for $c=0.4$ and $\eta=-2$ were comparable to those obtained when $c=0.4$ and $\eta=0$. When adhesion forces were included in the analysis, an elongation of the contact length occurred. The analysis included an investigation of $\alpha=0.001$ and 0.0001 when $f_0=100$, 1000 , and $10,000$. Values were obtained for d , q , δ , p , and m_d through a shooting analysis. The results obtained for $c=0.4$, $\eta=-2$, and $\alpha=0.001$ and 0.0001 can be found in Figures 5.22-5.31. Additionally, tabular results for d , q , δ , p , and m_d at $c=0.4$, $\eta=-2$ and $b=0$ are located in Table 5.7.

Table 5.7: Values Corresponding to the Transition Point Between Line Contact ($b>0$) and Point Contact ($b=0$) for $c=0.4$ and $\eta=-2$

	Curve	d	q	δ	p	m_d
$\alpha = 0$	$f_0 = 0$	0.0000	14.13	0.0972	10.375	NA
$\alpha = 0.001$	$f_0 = 100$	0.0737	13.69	0.0921	10.140	0.9969
	$f_0 = 1000$	0.0551	11.26	0.0666	8.872	1.3639
	$f_0 = 10000$	0.0334	0.93	0.0006	4.253	3.1297
$\alpha = 0.0001$	$f_0 = 100$	0.0352	14.03	0.0958	10.316	0.4587
	$f_0 = 1000$	0.0287	13.38	0.0878	9.948	0.5635
	$f_0 = 10000$	0.0183	10.87	0.0606	8.619	1.1175

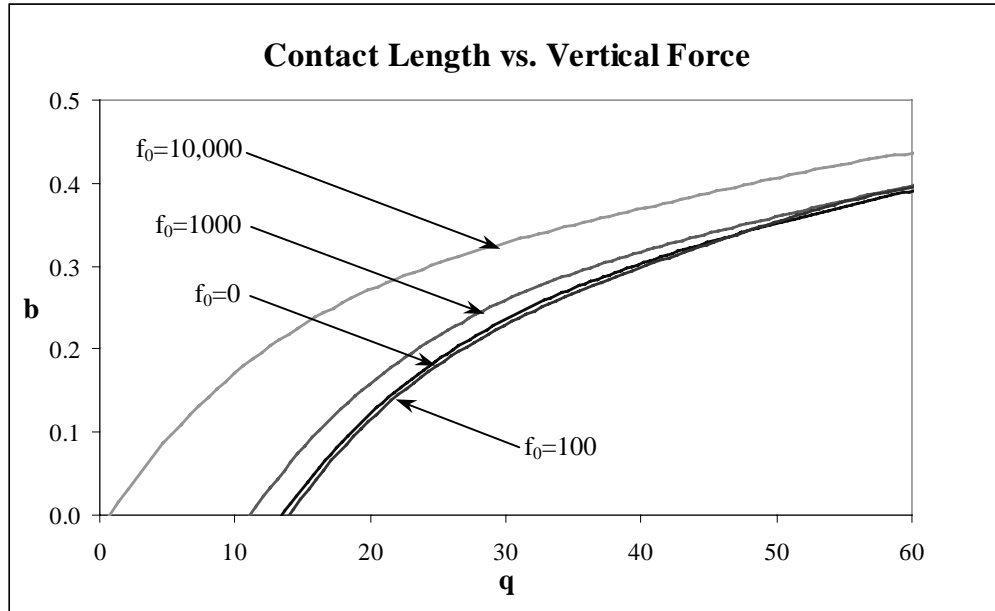


Figure 5.22: Contact Length vs. Vertical Force for $c=0.4$, $\eta=-2$, and $\alpha=0.001$

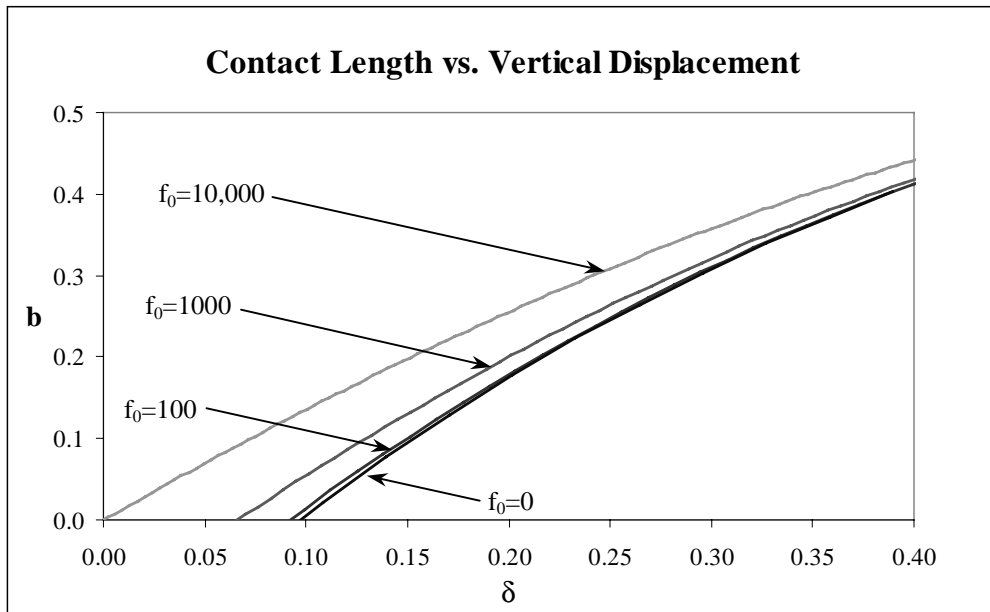


Figure 5.23: Contact Length vs. Vertical Displacement for $c=0.4$, $\eta=-2$, and $\alpha=0.001$

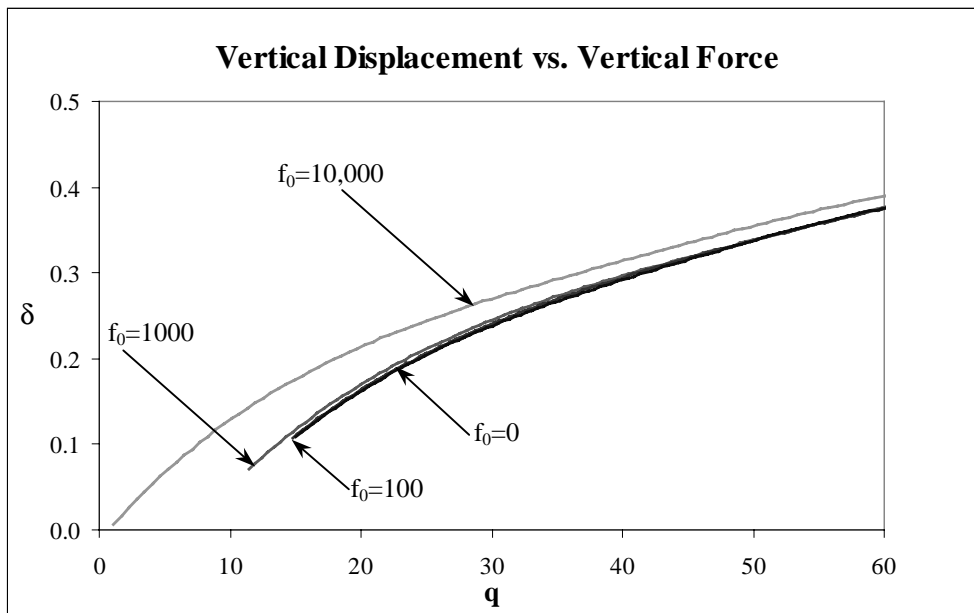


Figure 5.24: Vertical Displacement vs. Vertical Force for $c=0.4$, $\eta=-2$, and $\alpha=0.001$

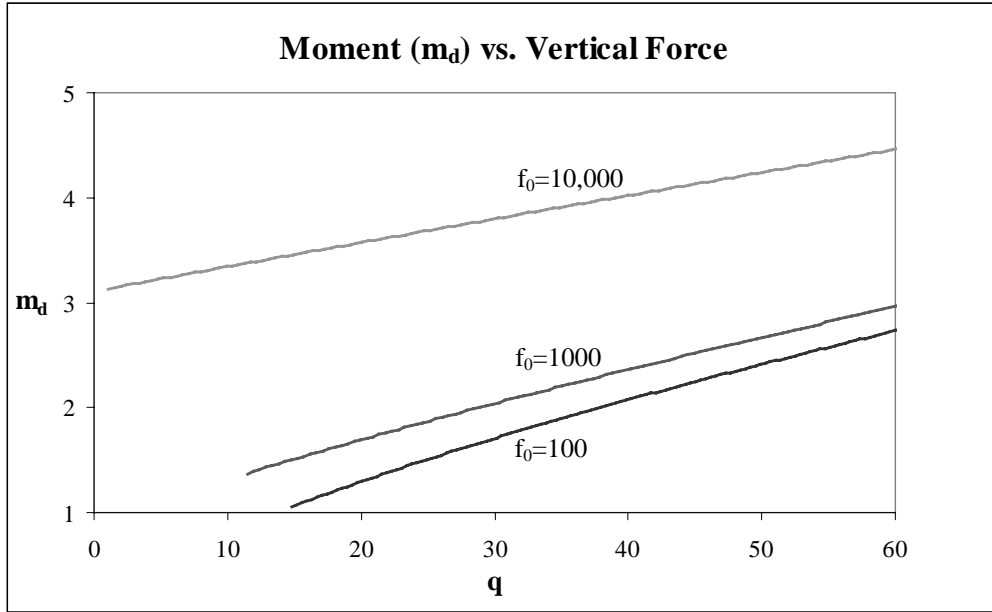


Figure 5.25: Moment (m_d) vs. Vertical Force for $c=0.4$, $\eta=-2$, and $\alpha=0.001$

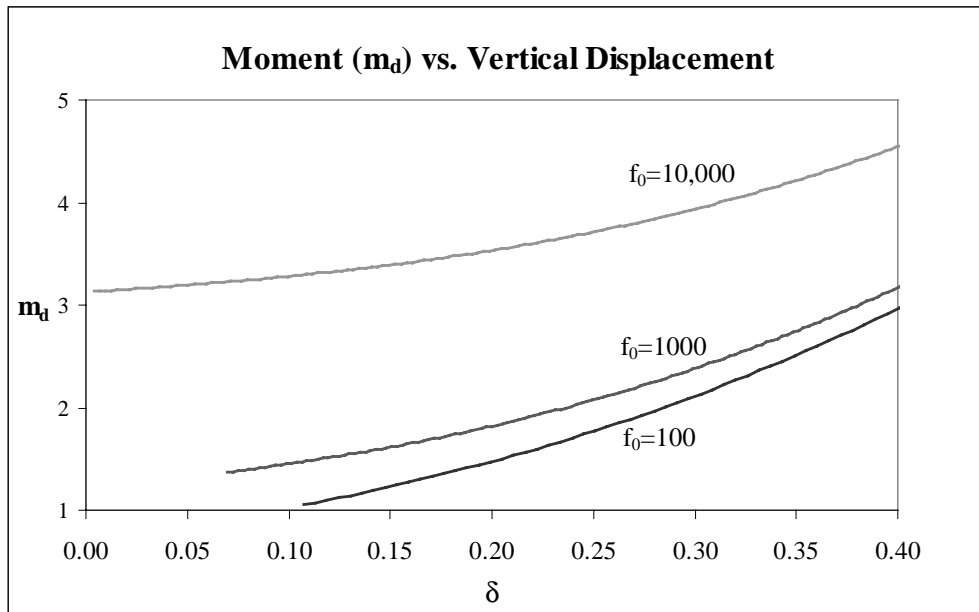


Figure 5.26: Moment (m_d) vs. Vertical Displacement for $c=0.4$, $\eta=-2$, and $\alpha=0.001$

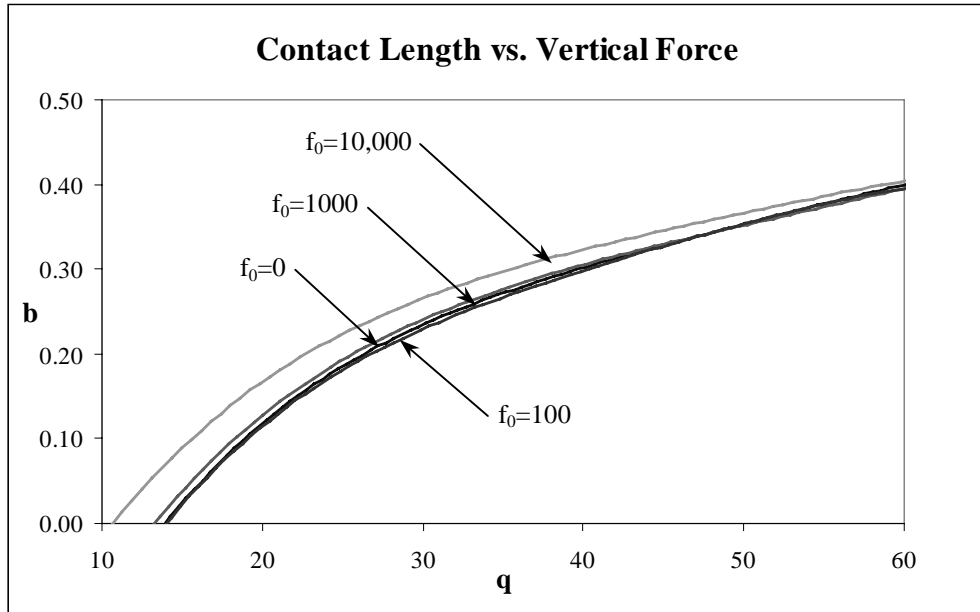


Figure 5.27: Contact Length vs. Vertical Force for $c=0.4$, $\eta=-2$, and $\alpha=0.0001$

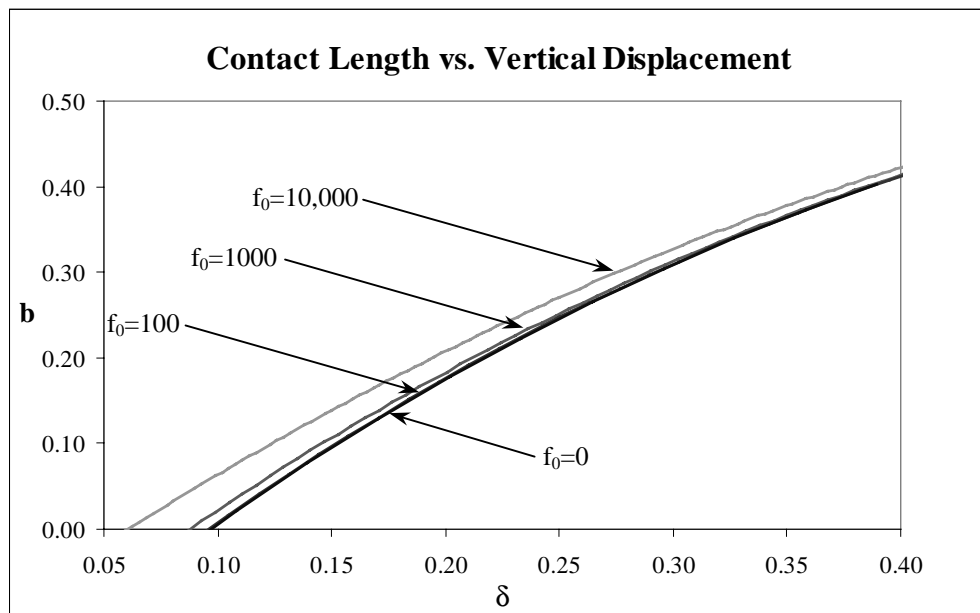


Figure 5.28: Contact Length vs. Vertical Displacement for $c=0.4$, $\eta=-2$, and $\alpha=0.0001$

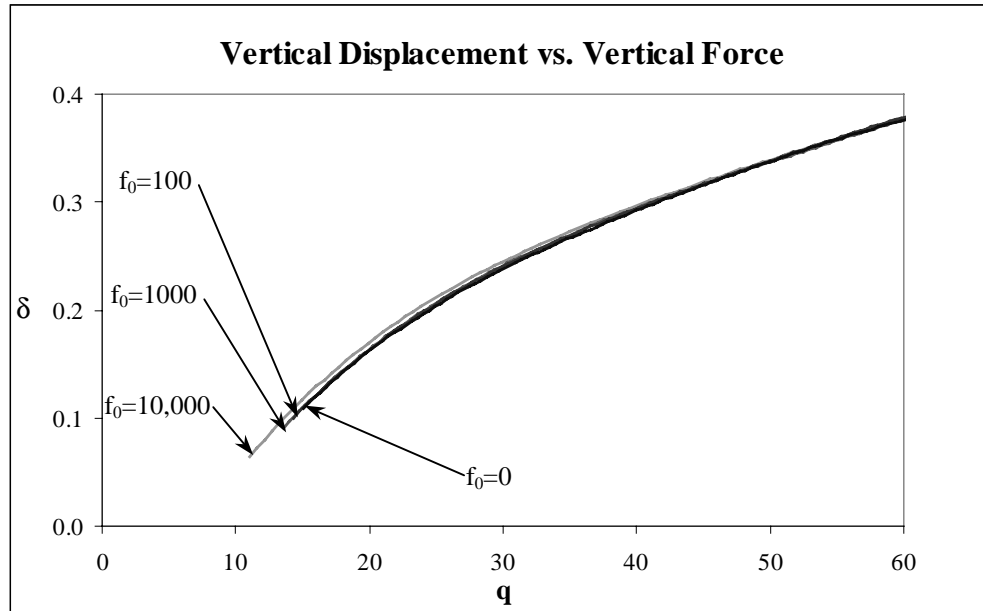


Figure 5.29: Vertical Displacement vs. Vertical Force for $c=0.4$, $\eta=-2$, and $\alpha=0.0001$

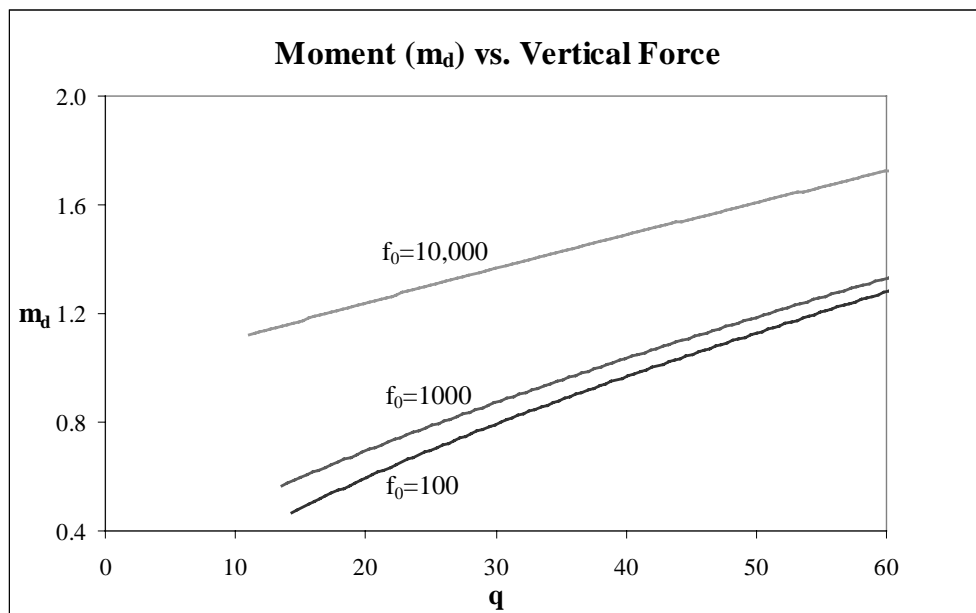


Figure 5.30: Moment (m_d) vs. Vertical Force for $c=0.4$, $\eta=-2$, and $\alpha=0.0001$

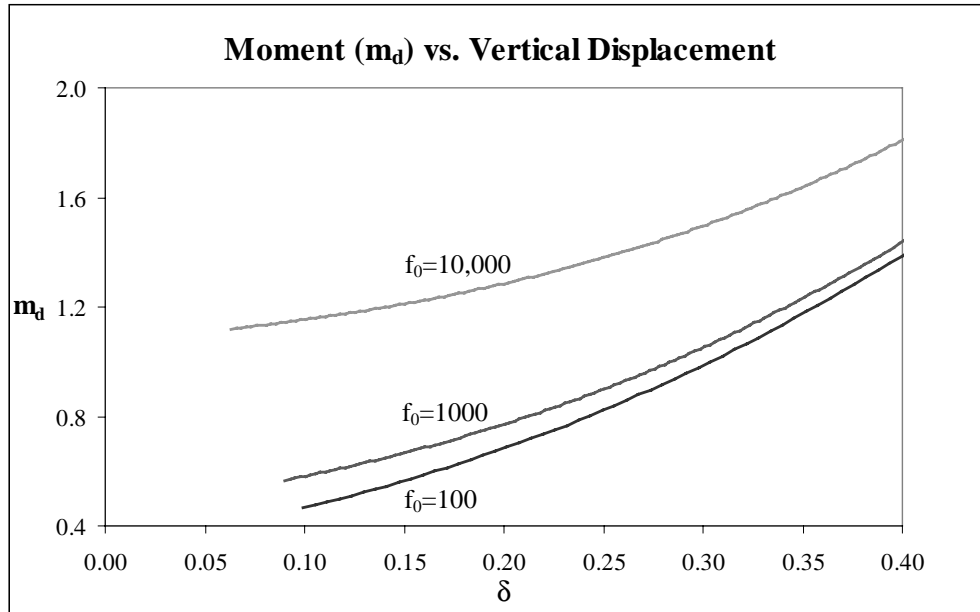


Figure 5.31: Moment (m_d) vs. Vertical Displacement for $c=0.4$, $\eta=-2$, and $\alpha=0.0001$

The effect of the self-weight term η on the DMT-type analysis can be seen in Figure 5.32. Three η values, including $\eta=2$, 0, and -2 , were examined when $c=0.4$, $\alpha=0.001$, and $f_0=1000$. Figure 5.32, which plots the contact length b vs. the vertical force q , shows that when a positive value for the self-weight is added to the analysis, the value of b increased when the value of q was fixed. Also, when a negative value was used for η , the contact length decreased when the value of q was fixed.

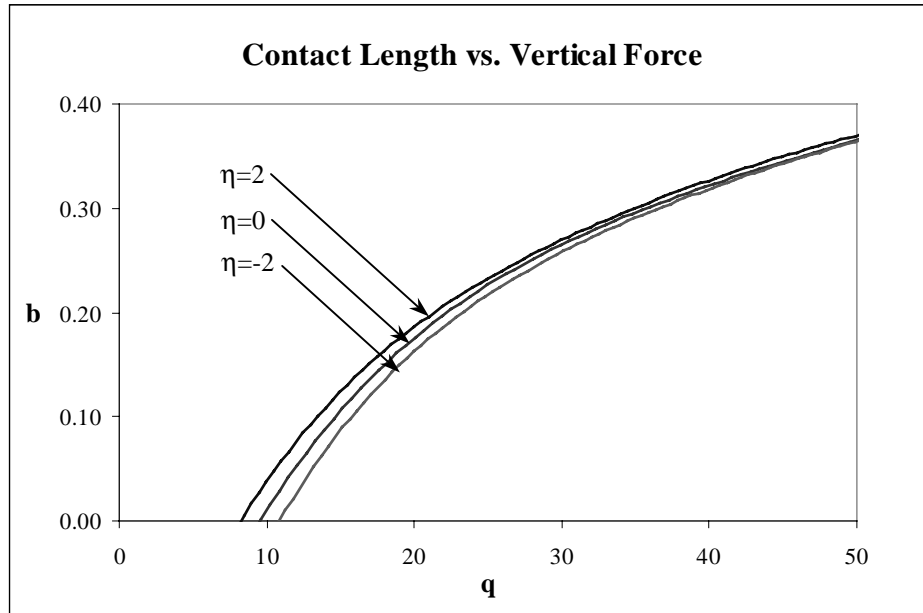


Figure 5.32: Contact Length vs. Vertical Force for $c=0.4$, $\alpha=0.001$, and $f_0=1000$.

5.2.4 Results for $c=0.8$ and $\eta=0$ (Line Contact Only)

The results obtained for the line contact case when $c=0.8$ and $\eta=0$ can be found in Figures 5.33-5.42. Values of $\alpha=0.001$ and 0.0001 were examined. The original analysis also included an examination of the $\alpha=0.01$ case. However, it was later discovered that values for θ at $s=d$ when $\alpha=0.01$ were significantly larger than θ values at $s=d$ for $\alpha=0.001$ and 0.0001 . Since a linear analysis was conducted to find values for x , y , θ , and m when $0 < s < d$, and the linear analysis was contingent upon the existence of small θ values in this region, the $\alpha=0.01$ case was eliminated due to the larger values of θ that were present at $s=d$. Table 5.8 presents values for θ and m_d when $\alpha=0.01$, 0.001 , and 0.0001 for $c=0.8$, $\eta=0$, $b=0$ (approximately), and $f_0=10$, 100 , and 1000 .

Table 5.8: Values for d , θ , and m_d when $c=0.8$, $\eta=0$, and $b=0$

α	$f_0=10$			$f_0=100$			$f_0=1000$		
	d	θ	m_d	d	θ	m_d	d	θ	m_d
0.01	0.261	0.1084	0.7413	0.192	0.1304	0.8814	0.114	0.2109	2.0572
0.001	0.126	0.0231	0.3472	0.098	0.0271	0.4276	0.060	0.0419	0.9221
0.0001	0.060	0.0049	0.1592	0.050	0.0055	0.1859	0.033	0.0079	0.3467

For each value of α examined in this analysis, maximum adhesion force values of $f_0=0$, 10, 100, and 1000 were considered. Figure 5.33 plots the contact length b vs. the vertical force q when $c=0.8$, $\eta=0$, and $\alpha=0.001$. From this plot, the effect of the adhesion forces can be seen. As the value for the maximum linear force f_0 was increased, the contact length, at a fixed value of q , also increased. When $f_0=10$, the values obtained from the analysis were very close to those obtained for $f_0=0$ (i.e. no adhesion forces present). Figure 5.34, which plots the contact length b vs. the vertical displacement δ , also demonstrates the effect of the adhesion forces on the contact length. Again, as the value of f_0 was increased, the contact length, at a fixed value of δ , also increased. The results obtained from Figures 5.33 and 5.34 indicated that the presence of adhesion forces elongated the contact length.

The relationship between the vertical displacement and the vertical force for $c=0.8$, $\eta=0$, and $\alpha=0.001$ is plotted in Figure 5.35. The curves in this figure represent the result from the spreading solution only (the point contact and no contact analyses will be presented in a later section). Figure 5.35 verifies that as the vertical force at the clamped ends was increased, the vertical displacement experienced by the elastica also increased. Additionally, as the value of the maximum linear force f_0 was increased, the vertical displacement, at a fixed value of q , also increased. All curves in Figure 5.35 terminated when the contact length equaled zero and the elastica experienced the transition from line contact to point contact. Values of d , q , δ , p , and m_d at the transition point can be found in Table 5.9.

Table 5.9: Values Corresponding to the Transition Point Between Line Contact ($b>0$) and Point Contact ($b=0$) for $c=0.8$ and $\eta=0$

	Curve	d	q	δ	p	m_d
$\alpha = 0$	$f_0 = 0$	0.0000	2.49	0.0275	-3.785	NA
$\alpha = 0.001$	$f_0 = 10$	0.1257	2.29	0.0253	-4.110	0.3472
	$f_0 = 100$	0.0982	1.38	0.0155	-5.620	0.4276
	$f_0 = 1000$	0.0603	-2.27	-0.0150	-11.424	0.9221
$\alpha = 0.0001$	$f_0 = 10$	0.0600	2.46	0.0271	-3.847	0.1592
	$f_0 = 100$	0.0503	2.21	0.0240	-4.265	0.1859
	$f_0 = 1000$	0.0327	1.23	0.0129	-5.895	0.3467

Figures 5.36 and 5.37 plot the moment m_d vs. the vertical force q and the vertical displacement δ , respectively. Various values of f_0 were examined, including $f_0=10, 100,$ and 1000 . Figure 5.36 shows that as the value of f_0 increased, the moment m_d also increased when q remained constant. Additionally, at a constant value of f_0 , the moment m_d increased with increasing values of q . The relationship between the moment at $s=d$ and the vertical displacement δ for $c=0.8, \eta=0,$ and $\alpha=0.001$ is presented in Figure 5.37. In this figure, as the value of f_0 increased, the moment m_d increased for a fixed value of δ . Also, as the value of m_d increased, the value of the vertical displacement increased (for a fixed value of f_0). Therefore, unlike the moment m_b which was calculated in the JKR-type analysis, the moment at $s=d$ was not independent of the applied vertical force or the separation distance between the clamped ends of the elastica.

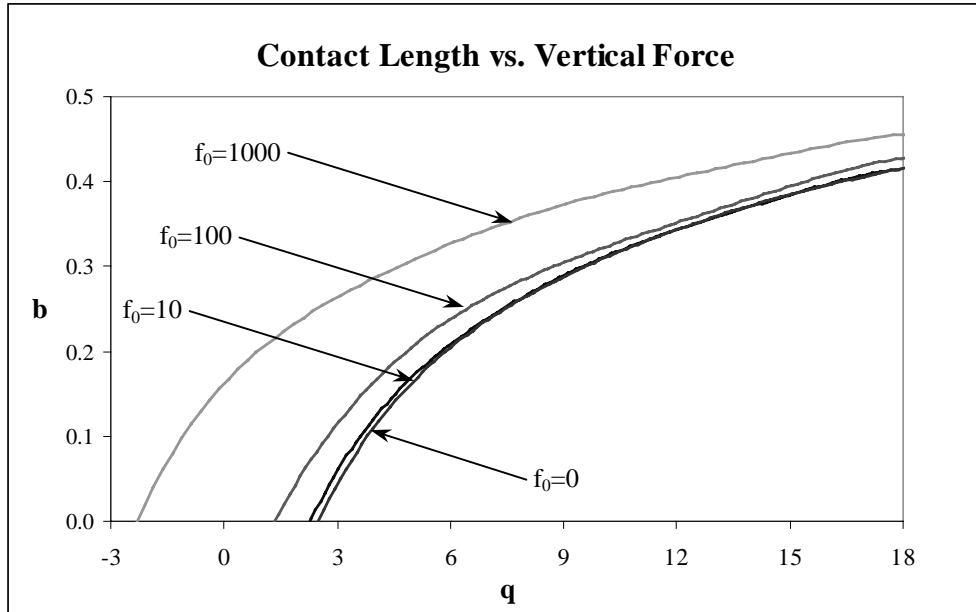


Figure 5.33: Contact Length vs. Vertical Force for $c=0.8$, $\eta=0$, and $\alpha=0.001$

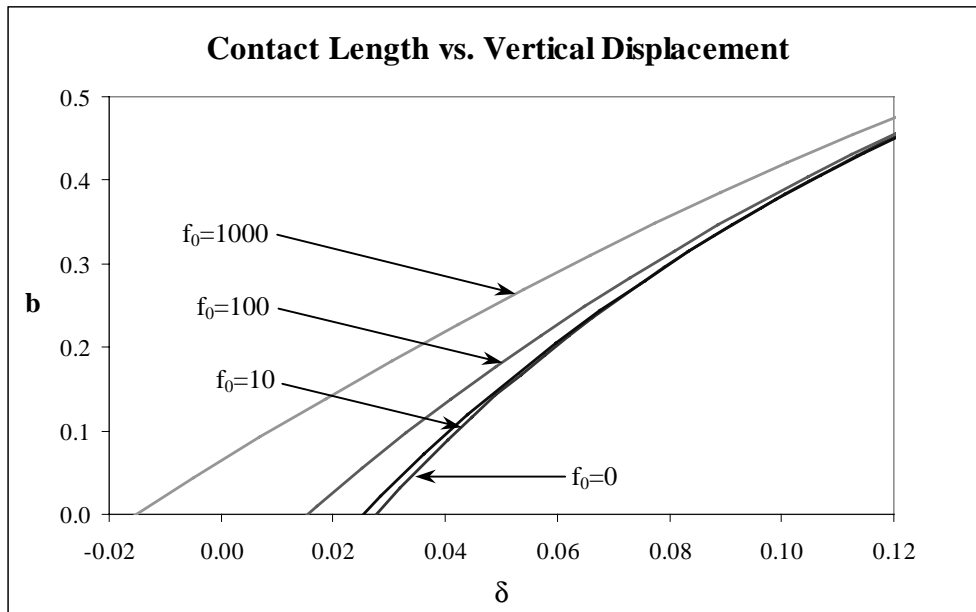


Figure 5.34: Contact Length vs. Vertical Displacement for $c=0.8$, $\eta=0$, and $\alpha=0.001$

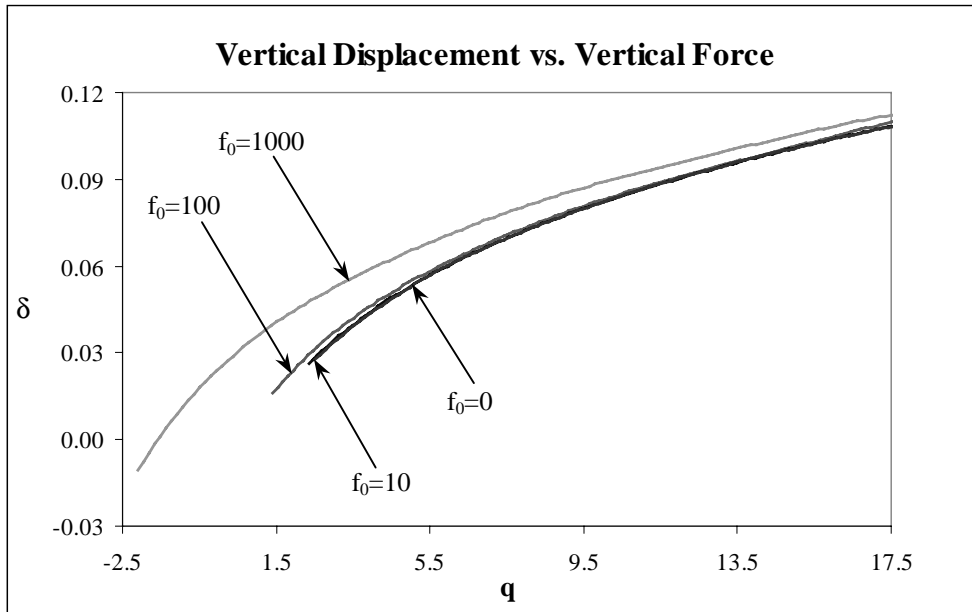


Figure 5.35: Vertical Displacement vs. Vertical Force for $c=0.8$, $\eta=0$, and $\alpha=0.001$

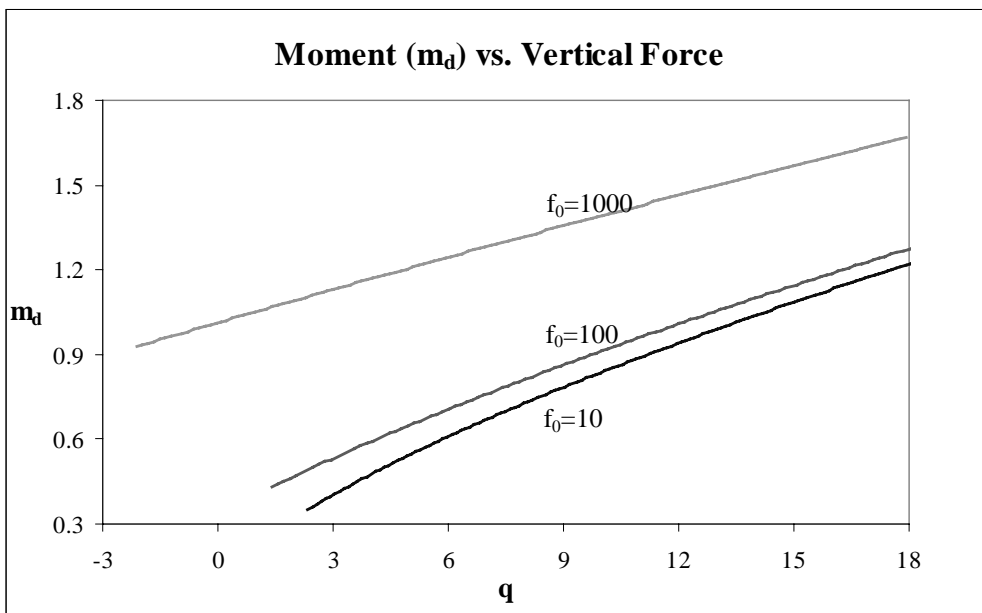


Figure 5.36: Moment (m_d) vs. Vertical Force for $c=0.8$, $\eta=0$, and $\alpha=0.001$

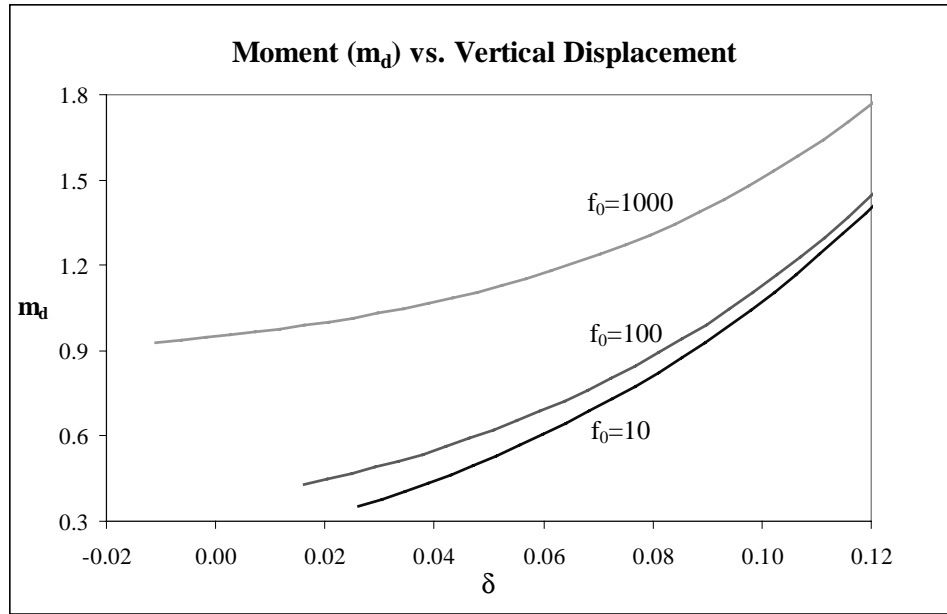


Figure 5.37: Moment (m_d) vs. Vertical Displacement for $c=0.8$, $\eta=0$, and $\alpha=0.001$

The results for the linear force DMT-type analysis when $c=0.8$, $\eta=0$, and $\alpha=0.0001$ can be found in Figures 5.38-5.42. Values used for the maximum adhesion force were $f_0=0$, 10, 100, and 1000. Figure 5.38 is a plot of the contact length b vs. the vertical force q . As the value of the maximum force f_0 increased, the contact length also increased (for a fixed value of q). When $f_0=10$, the values obtained through the DMT-type analysis for b and q were very close to those obtained for $f_0=0$ when adhesion forces were ignored. Therefore, relative to $f_0=100$ and $f_0=1000$, $f_0=10$ was a small adhesion force.

Figure 5.39 yielded results similar to those obtained from Figure 5.38. This figure (which plots the contact length vs. the vertical displacement) shows that as the value for the maximum linear force increased, the value for the contact length, at a constant value of δ , also increased. Again, when $f_0=10$, the values obtained through the DMT-type analysis for b and δ were very close to those obtained for $f_0=0$ when adhesion forces were ignored. Therefore, the adhesion force $f_0=10$ produced minimal additional deformation

in the shape of the elastica. The results obtained from Figures 5.38 and 5.39 indicated that the presence of adhesion forces elongated the contact length.

The relationship between the vertical displacement and the vertical force can be located in Figure 5.40. All curves in Figure 5.40 represented the line contact solution only and terminated when the contact length became zero. As the contact length approached zero, the elastica experienced a transition from line contact to point contact. Values of d , q , δ , p , and m_d at this transition point are located in Table 5.9. When the vertical force was held constant, the vertical displacement increased with increasing values of f_0 .

Additionally, the values obtained for δ and q when $f_0=10$, 100, and 1000 were very close to those obtained when $f_0=0$, especially when q was greater than 8.

Using the shooting method, values were obtained for the moment at $s=d$. A plot of the moment m_d vs. the vertical force q when $c=0.8$, $\eta=0$, and $\alpha=0.0001$ shows that for a constant value of q , the moment m_d increased with increasing values of f_0 . Furthermore, as values for the vertical force q increased, the moment m_d also increased (when f_0 was held constant), as seen in Figure 5.41. The moment m_d was also plotted against the vertical displacement δ . Figure 5.42 shows that for a constant value of δ , m_d increased with increasing values of f_0 . Values for the moment m_d , the vertical force q , and the vertical displacement δ at $b=0$ can be found in Table 5.9.

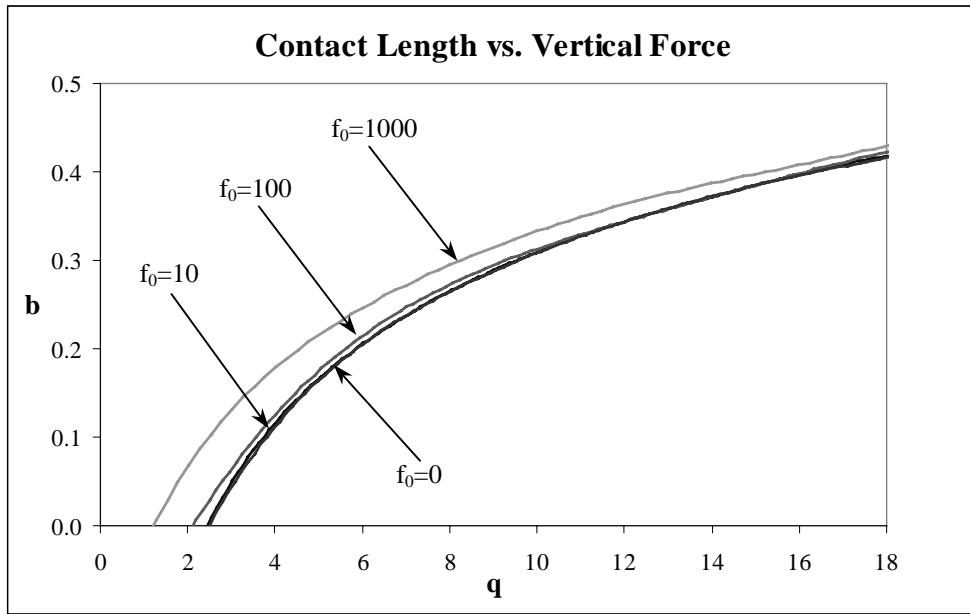


Figure 5.38: Contact Length vs. Vertical Force for $c=0.8$, $\eta=0$, and $\alpha=0.0001$

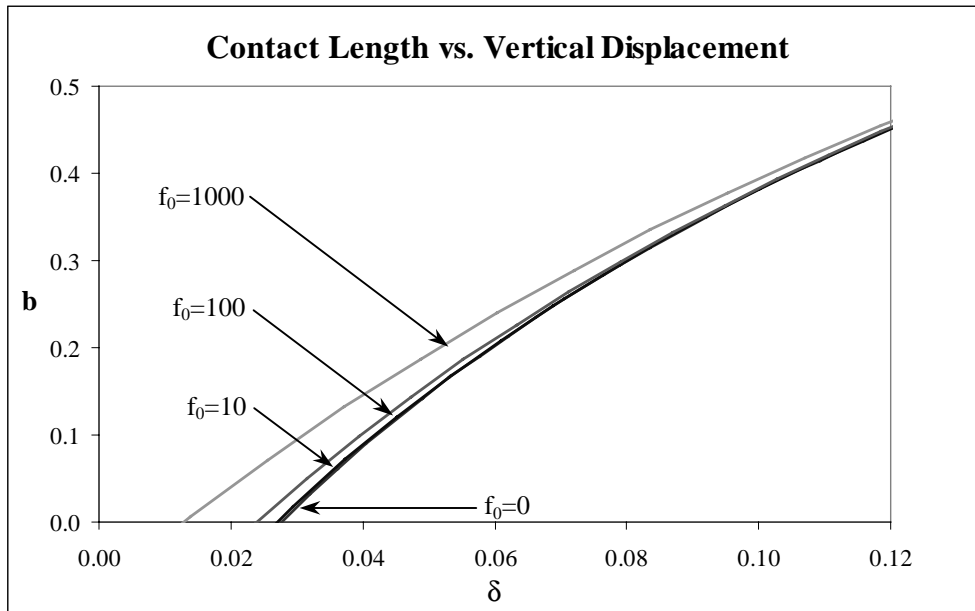


Figure 5.39: Contact Length vs. Vertical Displacement for $c=0.8$, $\eta=0$, and $\alpha=0.0001$

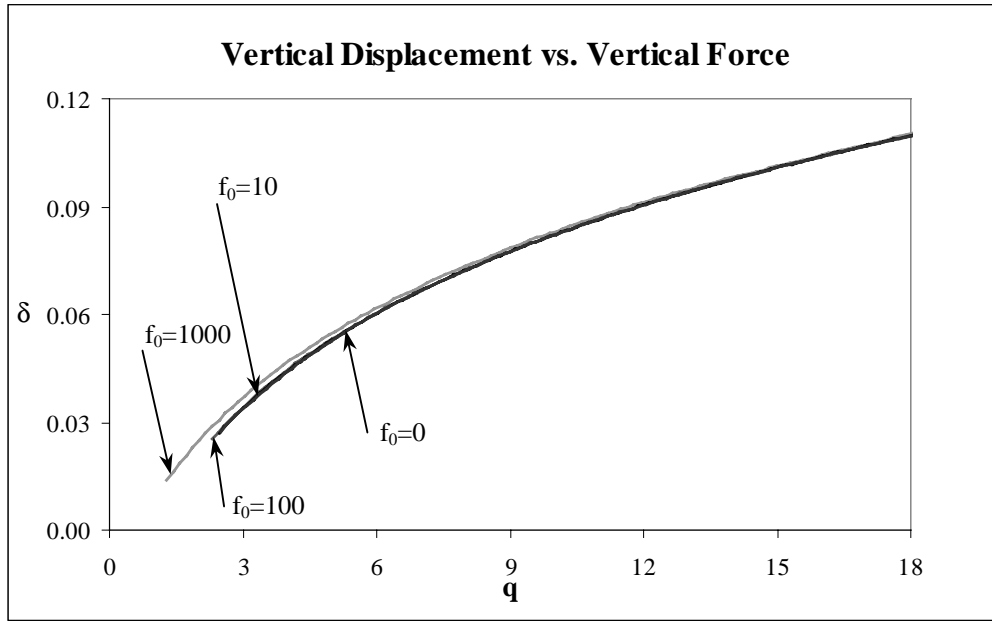


Figure 5.40: Vertical Displacement vs. Vertical Force for $c=0.8$, $\eta=0$, and $\alpha=0.0001$

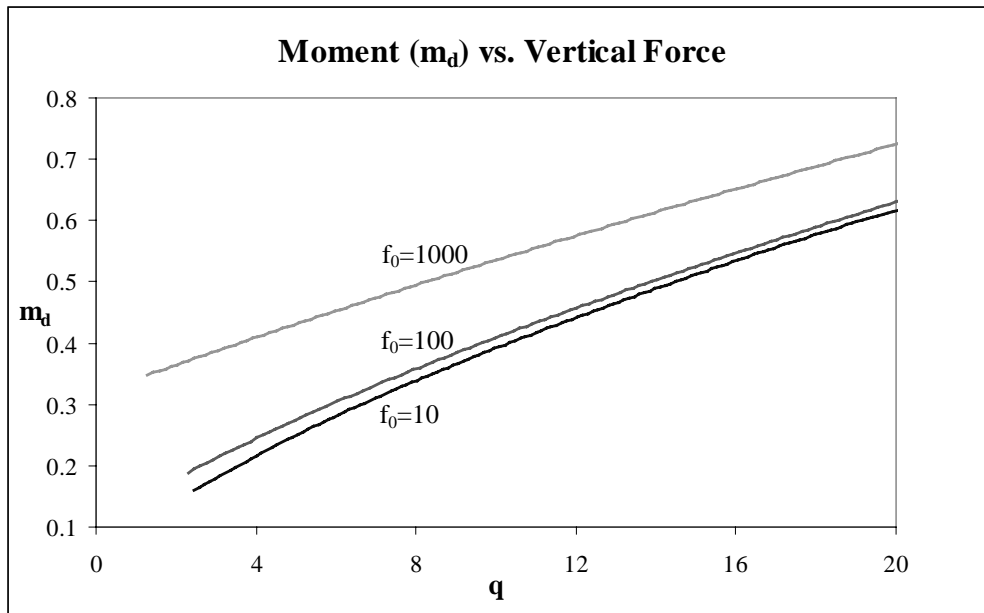


Figure 5.41: Moment (m_d) vs. Vertical Force for $c=0.8$, $\eta=0$, and $\alpha=0.0001$

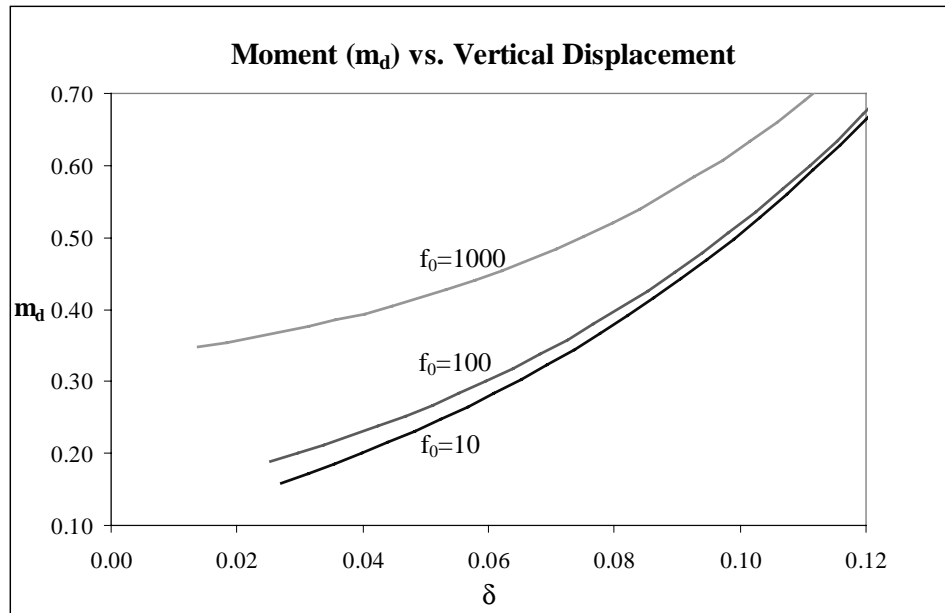


Figure 5.42: Moment (m_d) vs. Vertical Displacement for $c=0.8$, $\eta=0$, and $\alpha=0.0001$

5.2.5 Results for $c=0.8$ and $\eta=2$ (Line Contact Only)

The results obtained for the line contact case when $c=0.8$ and $\eta=2$ can be found in Figures 5.43-5.52. Values of $\alpha=0.001$ and 0.0001 were examined. Similar to the cases discussed previously which involved a DMT-type analysis, the original analysis also included an examination of the $\alpha=0.01$ case. Since the values for θ at $s=d$ when $\alpha=0.01$ were significantly larger than θ values at $s=d$ for $\alpha=0.001$ and 0.0001 , this portion of the analysis has been omitted.

For each value of α examined, maximum force values of $f_0=0$, 100, 1000, and 10,000 were considered. The results obtained for $c=0.8$ and $\eta=2$ were comparable to those obtained when $c=0.8$ and $\eta=0$. Figure 5.43 is a plot of the contact length vs. the vertical force for $c=0.8$, $\eta=2$, and $\alpha=0.001$. In general, when the vertical force was held constant,

increasing values of f_0 produced an increase in the contact length. However, when q was equal to 2.5 (approximately), the $f_0=0$ curve crossed the $f_0=10$ curve. Therefore, when $q>2.5$, a larger contact length existed when $f_0=0$ than when $f_0=10$ for a fixed value of q . Additionally, at approximately $q=11$, the $f_0=0$ curve crossed the $f_0=100$ curve. Therefore, when $q>11$, a larger contact length existed when $f_0=0$ than when $f_0=100$. Although the b vs. q plot for $c=0.8$, $\eta=2$, and $\alpha=0.001$ varied from the trend seen in all the previous contact length vs. vertical force plots, the relationship between the contact length and the vertical displacement for $f_0=0$, 10, 100, and 1000 remained consistent with the previous b vs. δ plots (see Figure 5.44). As the value of f_0 increased, the value of the contact length, at a fixed value of δ , also increased.

The results of the line contact analysis can also be seen in Figure 5.45, which plots the vertical displacement δ vs. the vertical force q . For a fixed value of q , the $f_0=0$ curve, which lies above the $f_0=10$ throughout its entirety, produced larger vertical displacements than the $f_0=10$ curve. Furthermore, when $q=3$ (approximately), the $f_0=0$ curve crossed the $f_0=100$ curve. Therefore, for $q>3$, the $f_0=0$ curve produced larger vertical displacements than the $f_0=100$ curve. Finally, the $f_0=0$ curve approached the $f_0=1000$ curve; however, for the values of q examined, it did not cross the $f_0=1000$ curve. All curves in Figure 5.45 terminated when the elastica approached point contact ($b=0$). The values of d , q , δ , p , and m_d at the transition from point contact to line contact can be found in Table 5.10.

The moment m_d vs. the vertical force q and the moment m_d vs. the vertical displacement relationships found in Figures 5.46 and 5.47 resemble those when $c=0.8$ and $\eta=0$. For a fixed value of q , m_d increased with increasing values of f_0 . Additionally, for a fixed value of δ , m_d also increased with increasing values of f_0 . Finally, for a fixed value of f_0 , the moment at $s=d$ increased with increasing values of q and δ . Values for m_d , q , and δ when $c=0.8$, $\eta=2$, and $b=0$ can be found in Table 5.10.

Table 5.10: Values Corresponding to the Transition Point Between Line Contact ($b>0$) and Point Contact ($b=0$) for $c=0.8$ and $\eta=2$.

	Curve	d	q	δ	p	m_d
$\alpha = 0$	$f_0 = 0$	0.0000	0.81	0.0287	-5.017	NA
$\alpha = 0.001$	$f_0 = 10$	0.1223	0.60	0.0266	-5.345	0.3629
	$f_0 = 100$	0.0970	-0.34	0.0171	-6.865	0.4419
	$f_0 = 1000$	0.0602	-4.09	-0.0126	-12.776	0.9294
$\alpha = 0.0001$	$f_0 = 10$	0.0582	0.75	0.0281	-5.105	0.1684
	$f_0 = 100$	0.0494	0.51	0.0254	-5.501	0.1946
	$f_0 = 1000$	0.0325	-0.49	0.0146	-7.149	0.3525

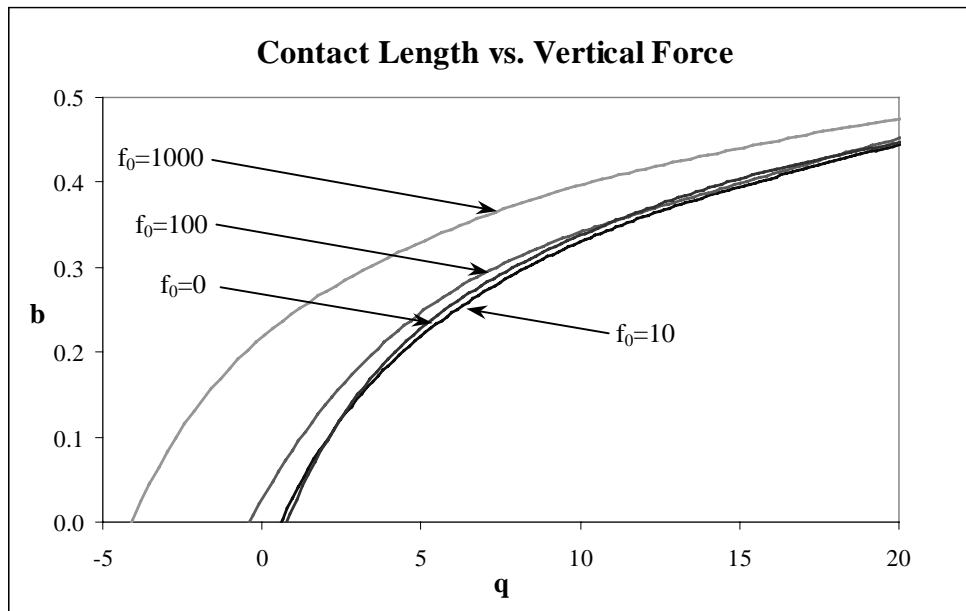


Figure 5.43: Contact Length vs. Vertical Force for $c=0.8$, $\eta=2$, and $\alpha=0.001$

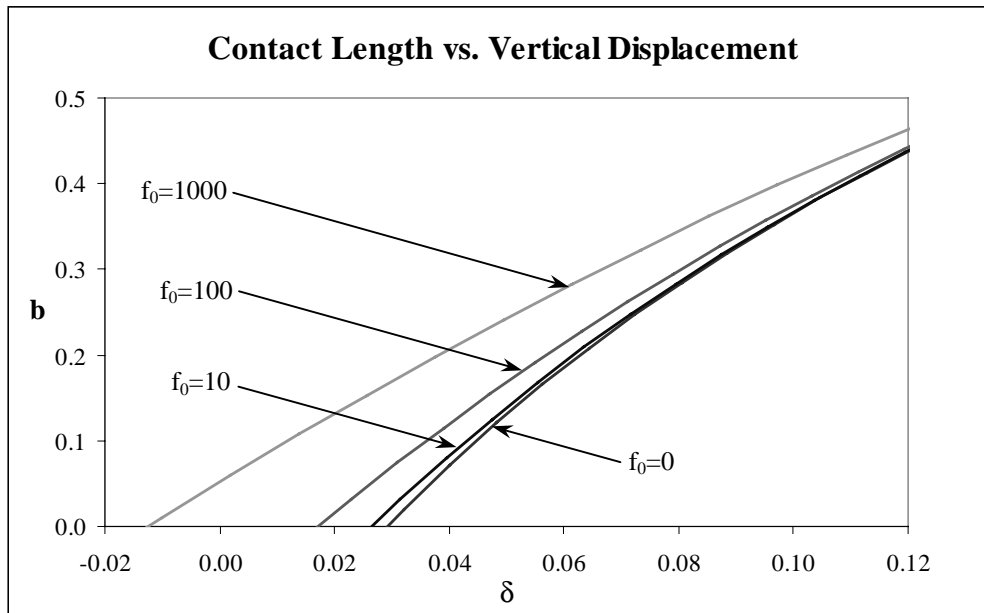


Figure 5.44: Contact Length vs. Vertical Displacement for $c=0.8$, $\eta=2$, and $\alpha=0.001$

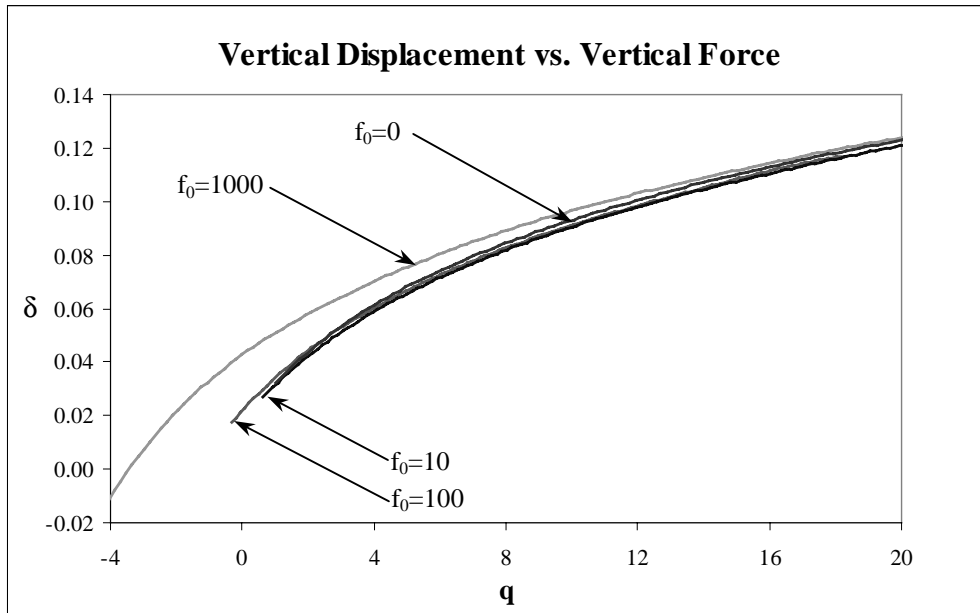


Figure 5.45: Vertical Displacement vs. Vertical Force for $c=0.8$, $\eta=2$, and $\alpha=0.001$

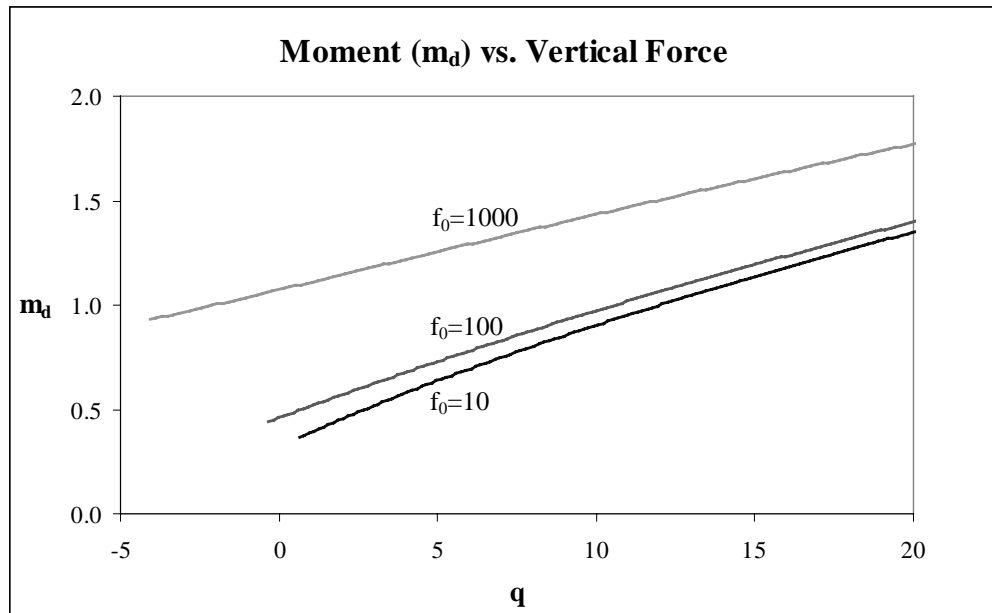


Figure 5.46: Moment (m_d) vs. Vertical Force for $c=0.8$, $\eta=2$, and $\alpha=0.001$

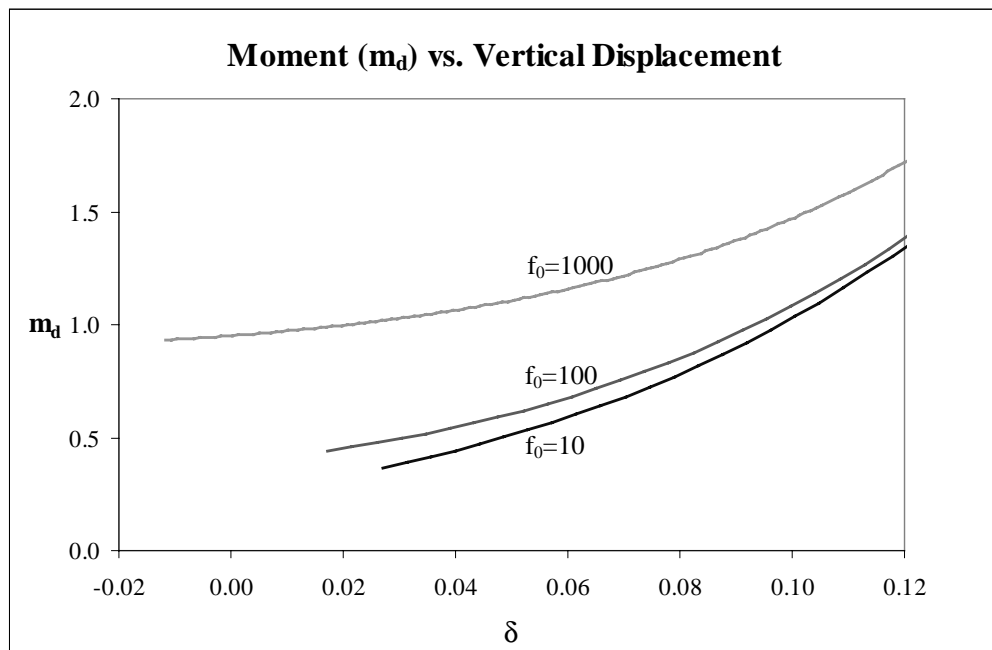


Figure 5.47: Moment (m_d) vs. Vertical Displacement for $c=0.8$, $\eta=2$, and $\alpha=0.001$

The results for the linear force DMT-type analysis when $c=0.8$, $\eta=2$, and $\alpha=0.0001$ can be found in Figures 5.48-5.52. Values used for the maximum adhesion force were $f_0=0$, 10, 100, and 1000. Figure 5.48 is a plot of the contact length b vs. the vertical force q . For $f_0>0$, as the value of the maximum force f_0 increased, the contact length also increased (for a fixed value of q). However, the $f_0=0$ curve produced b values greater than those obtained through the DMT-type analysis when $f_0=10$ for the entire range of q values examined in this analysis. Additionally, the $f_0=0$ curve crossed the $f_0=100$ curve at approximately $q=2.5$. Therefore, when $q>2.5$, the contact length was longer when $f_0=0$ than when $f_0=100$. The $f_0=0$ curve approached the $f_0=1000$ curve but did not cross it for the values of q which were examined in this analysis.

The relationship between the contact length and the vertical displacement for $f_0=0$, 10, 100, and 1000 remained consistent with the previous b vs. δ plots (see Figure 5.49). As the value of f_0 increased, the value of the contact length, at a fixed value of δ , also increased. When $f_0=10$, the values obtained through the DMT-type analysis for b and δ were very close to those obtained for $f_0=0$ when adhesion forces were ignored. Therefore, the adhesion force $f_0=10$ produced minimal additional deformation in the shape of the elastica. As values of δ grew larger, the $f_0=100$ curve also yielded values close to those obtained when $f_0=0$. The results obtained from Figure 5.49 indicated that the presence of adhesion forces elongated the contact length.

The relationship between the vertical displacement and the vertical force can be located in Figure 5.50. All curves in Figure 5.50 represented the line contact solution only and terminated when the contact length became zero. As the contact length approached zero, the elastica experienced a transition from line contact to point contact. Values of d , q , δ , p , and m_d at this transition point are located in Table 5.11. For $f_0>0$, when the vertical force was held constant, the vertical displacement increased slightly with increasing values of f_0 . However, the $f_0=0$ curve produced larger vertical displacements along its

entirety than those produced by the $f_0=10$ and $f_0=100$ curves at corresponding q values. The $f_0=0$ curve also crossed the $f_0=1000$ curve at approximately $q=3$. Therefore, when $q>3$, the vertical displacements when $f_0=0$ were larger than the vertical displacements when $f_0=1000$ for the same value of q .

Using the shooting method, values were obtained for the moment at $s=d$. A plot of the moment m_d vs. the vertical force q when $c=0.8$, $\eta=2$, and $\alpha=0.0001$ shows that for a constant value of q , the moment m_d increased with increasing values of f_0 . Furthermore, as values for the vertical force q increased, the moment m_d also increased (when f_0 was held constant) as seen in Figure 5.51. The moment m_d was also plotted against the vertical displacement δ . Figure 5.52 shows that for a constant value of δ , m_d increased with increasing values of f_0 . Values for the moment m_d , the vertical force q , and the vertical displacement δ at $b=0$ can be found in Table 5.10.

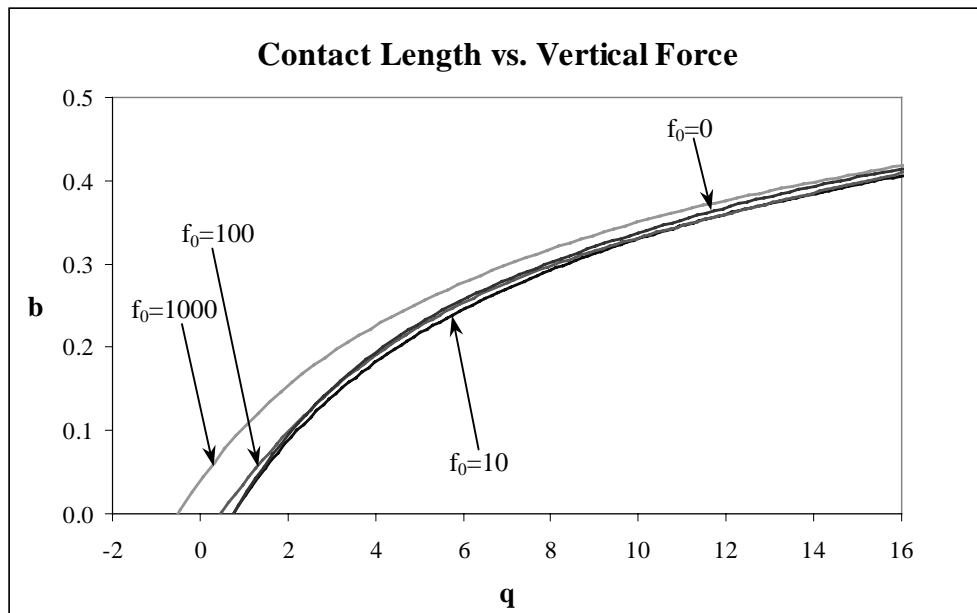


Figure 5.48: Contact Length vs. Vertical Force for $c=0.8$, $\eta=2$, and $\alpha=0.0001$

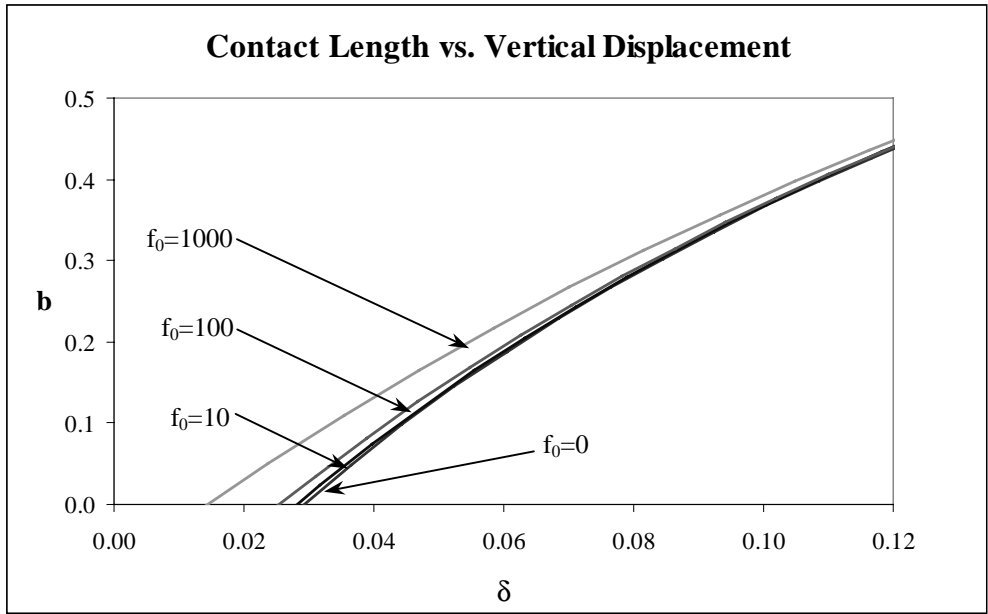


Figure 5.49: Contact Length vs. Vertical Displacement for $c=0.8$, $\eta=2$, and $\alpha=0.0001$

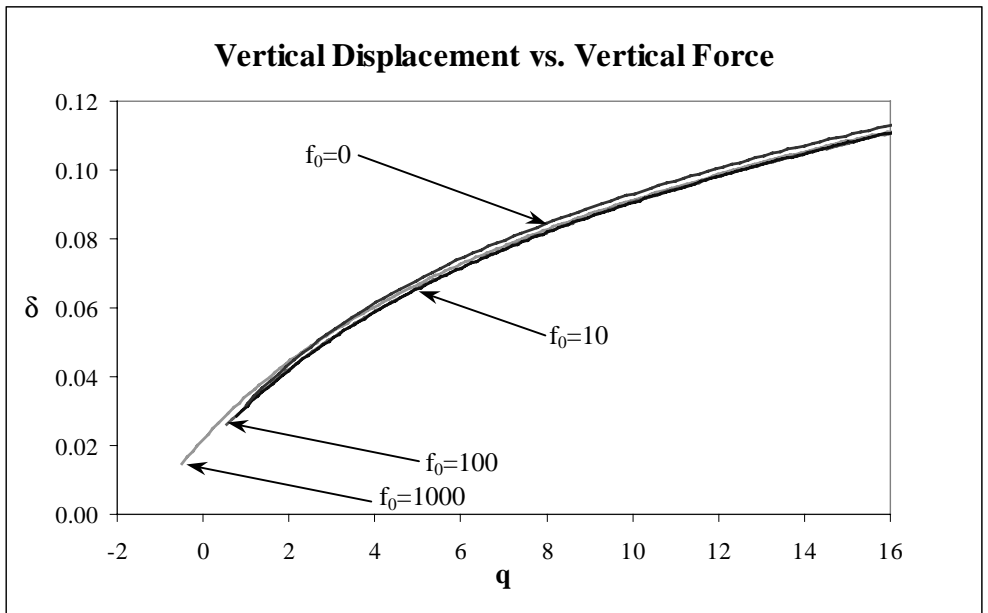


Figure 5.50: Vertical Displacement vs. Vertical Force for $c=0.8$, $\eta=2$, and $\alpha=0.0001$

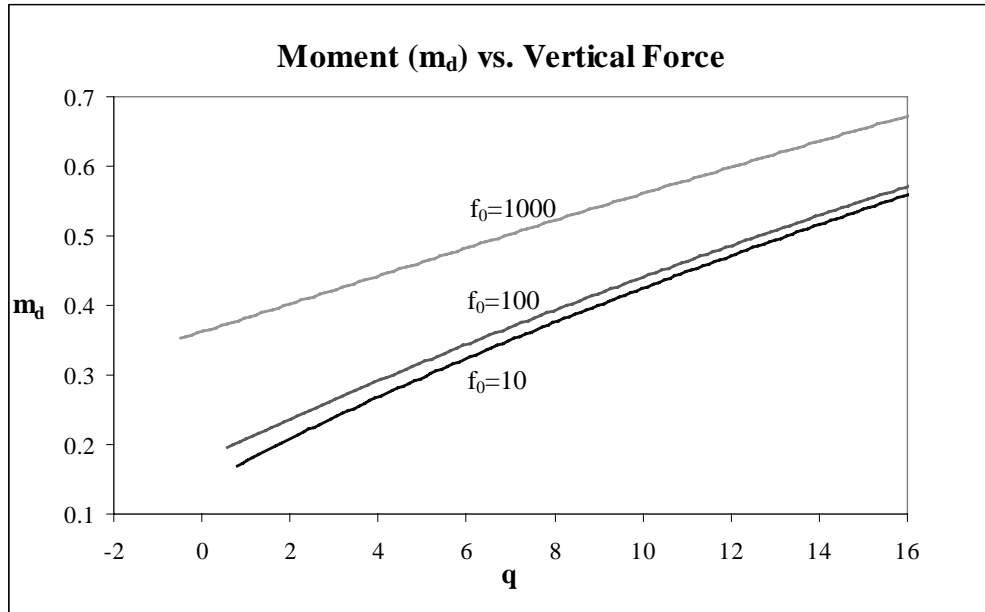


Figure 5.51: Moment (m_b) vs. Vertical Force for $c=0.8$, $\eta=2$, and $\alpha=0.0001$

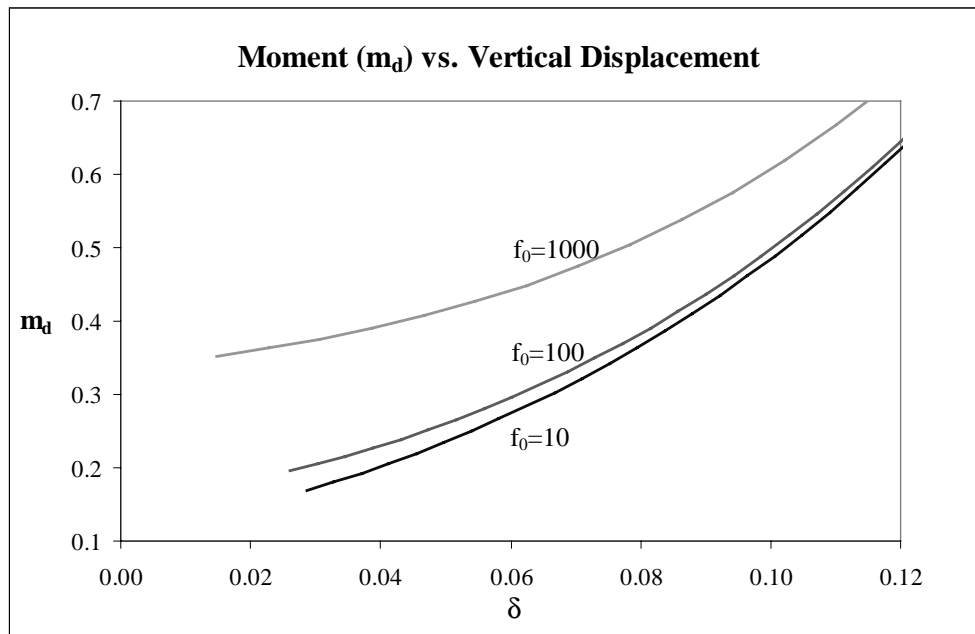


Figure 5.52: Moment (m_b) vs. Vertical Displacement for $c=0.8$, $\eta=2$, and $\alpha=0.0001$

5.2.6 Results for $c=0.8$ and $\eta=-2$ (Line Contact Only)

The results obtained for the line contact case when $c=0.8$ and $\eta=-2$ can be found in Figures 5.53-5.62. Values of $\alpha=0.001$ and 0.0001 were examined. Similar to the cases discussed previously which involved a DMT-type analysis, the original analysis also included an examination of the $\alpha=0.01$ case. Since the values for θ at $s=d$ when $\alpha=0.01$ were significantly larger than θ values at $s=d$ for $\alpha=0.001$ and 0.0001 , this portion of the analysis has been omitted.

For each value of α examined, maximum force values of $f_0=0, 100, 1000,$ and $10,000$ were considered. The trends observed in the plots for $\alpha=0.001$ and $\alpha=0.0001$ when $c=0.8$ and $\eta=-2$ were the same as the general trends discussed in previous sections. For the contact length vs. vertical force plots, the contact length increased with increasing values of f_0 (when q was fixed). Similarly, when the contact length was plotted against the vertical displacement, the contact length increased with increasing values of f_0 (when δ was fixed).

The trends observed in previous sections for the relationship between the vertical displacement δ and the vertical force q also remained the same for the DMT-type analysis when $c=0.8, \eta=-2,$ and $\alpha=0.001$ and 0.0001 . All curves in the vertical displacement vs. vertical force plots represented the line contact solution only and terminated when the transition from line contact to point contact was reached. Values for $d, q, \delta, p,$ and m_d for $c=0.8, \eta=-2,$ and $b=0$ can be located in Table 5.11.

Plots were also obtained for the moment m_d vs. the vertical force and the moment m_d vs. the vertical displacement. When q and δ were fixed, the value of the moment m_d increased with increasing values of f_0 . Also, m_d increased with increasing values of q and δ . Unlike the moment m_b , which was calculated for the JKR-type analysis, the moment m_d was not independent of the vertical force applied at the clamped ends of the elastica, nor was it independent of the separation distance c between the clamped ends. All results

of the linear force DMT-type analysis when $c=0.8$ and $\eta=-2$ can be found in Figures 5.53-5.62.

Table 5.11: Values Corresponding to the Transition Point Between Line Contact ($b>0$) and Point Contact ($b=0$) for $c=0.8$ and $\eta=-2$.

	Curve	d	q	δ	p	m_d
$\alpha = 0$	$f_0 = 0$	0.0000	4.17	0.0260	-2.557	NA
$\alpha = 0.001$	$f_0 = 10$	0.1296	3.97	0.0237	-2.883	0.3310
	$f_0 = 100$	0.0994	3.07	0.0134	-4.391	0.4125
	$f_0 = 1000$	0.0604	-0.45	-0.0178	-10.070	0.9147
$\alpha = 0.0001$	$f_0 = 10$	0.0623	4.13	0.0254	-2.628	0.1488
	$f_0 = 100$	0.0512	3.88	0.0222	-3.054	0.1763
	$f_0 = 1000$	0.0328	2.94	0.0108	-4.639	0.3407

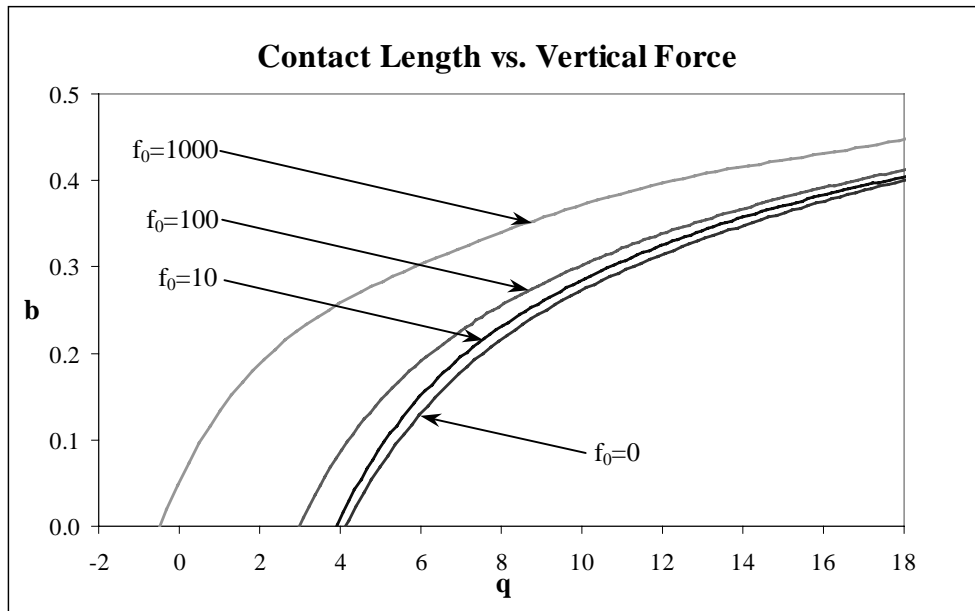


Figure 5.53: Contact Length vs. Vertical Force for $c=0.8$, $\eta=-2$, and $\alpha=0.001$

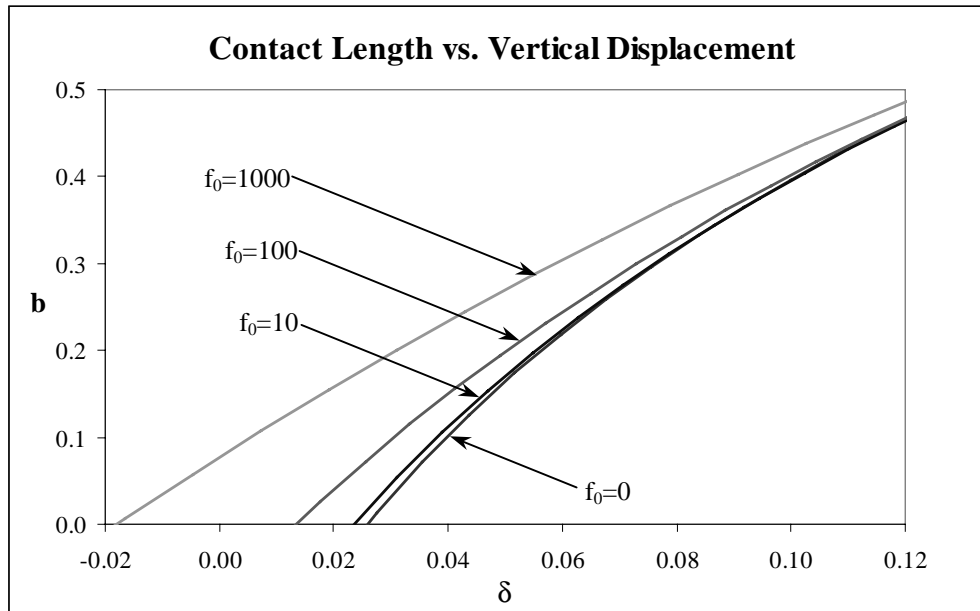


Figure 5.54: Contact Length vs. Vertical Displacement for $c=0.8$, $\eta=-2$, and $\alpha=0.001$

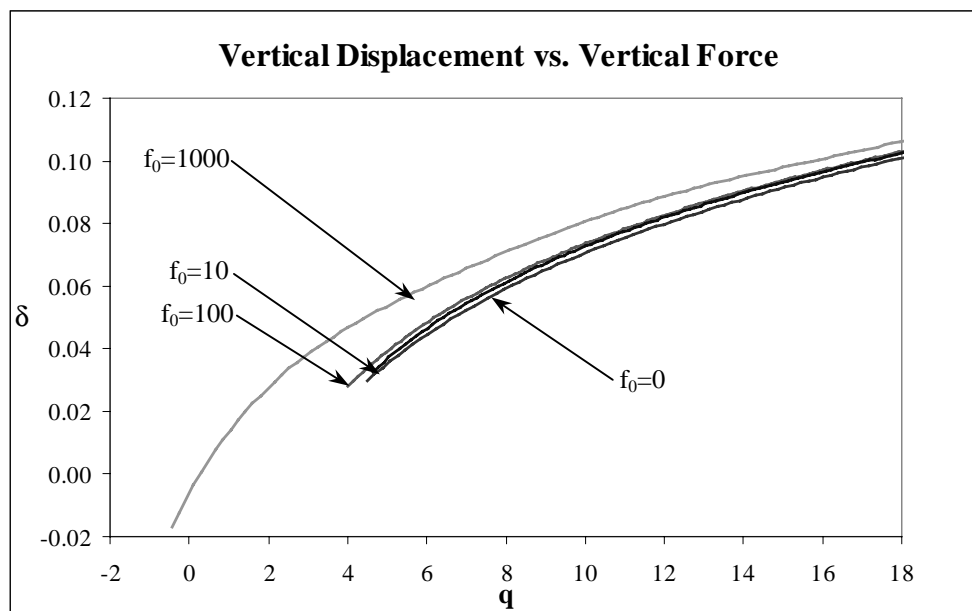


Figure 5.55: Vertical Displacement vs. Vertical Force for $c=0.8$, $\eta=-2$, and $\alpha=0.001$

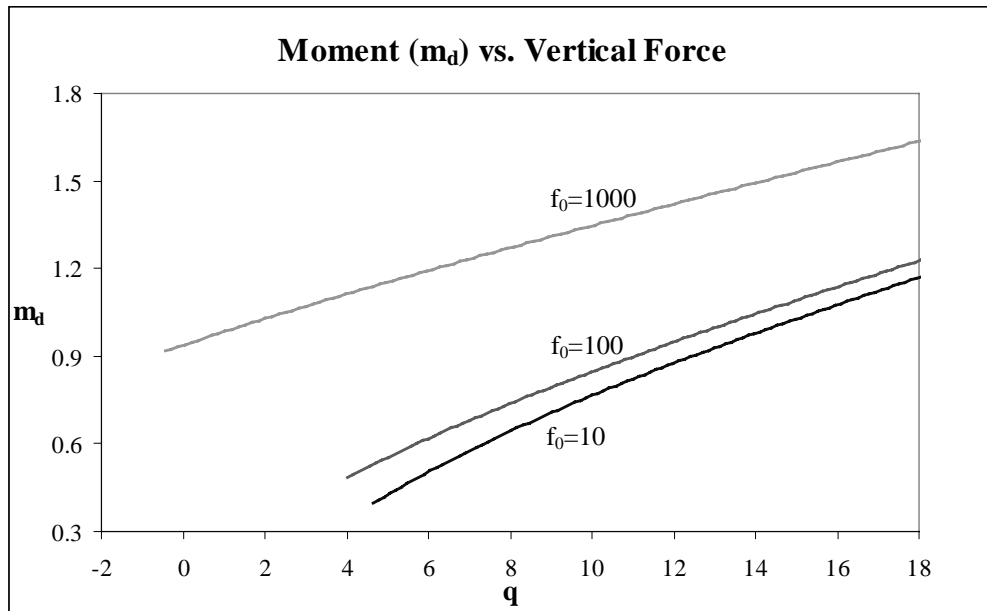


Figure 5.56: Moment (m_d) vs. Vertical Force for $c=0.8$, $\eta=-2$, and $\alpha=0.001$

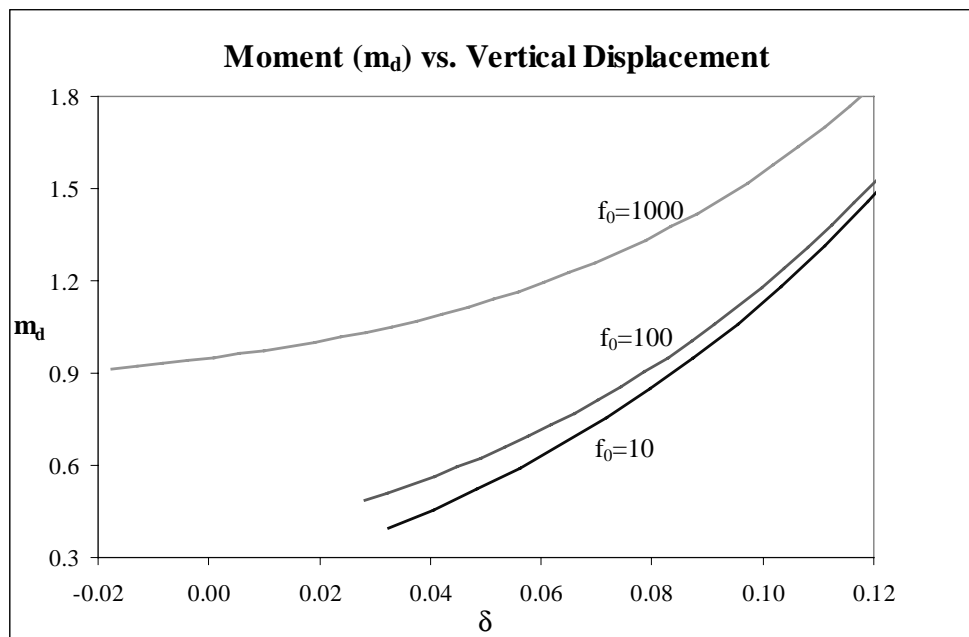


Figure 5.57: Moment (m_d) vs. Vertical Displacement for $c=0.8$, $\eta=-2$, and $\alpha=0.001$

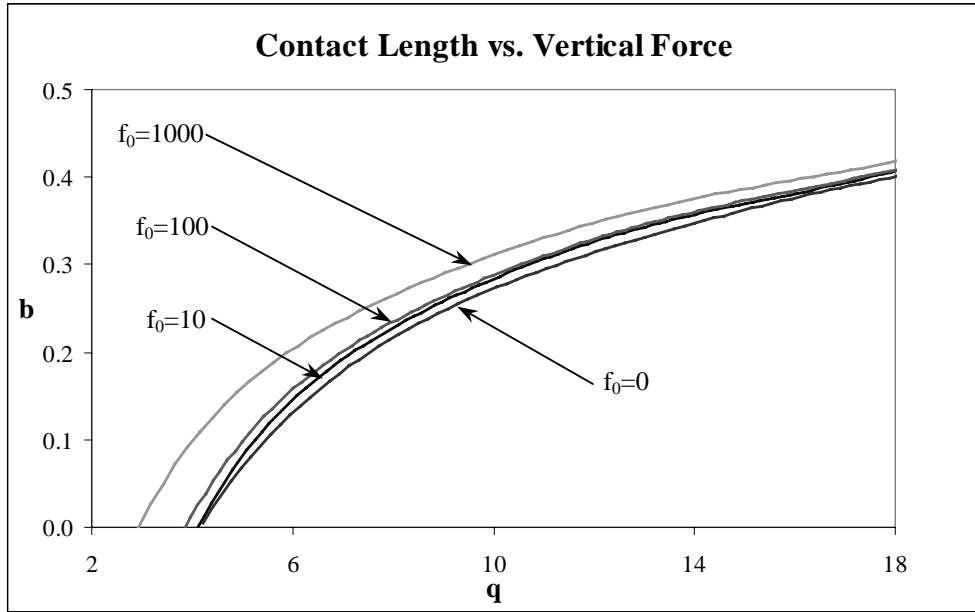


Figure 5.58: Contact Length vs. Vertical Force for $c=0.8$, $\eta=-2$, and $\alpha=0.0001$

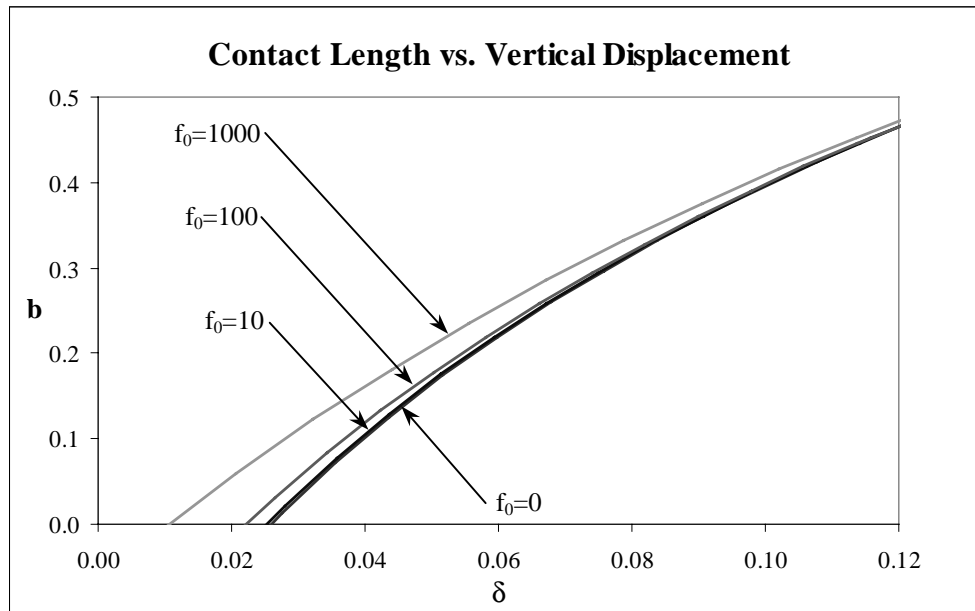


Figure 5.59: Contact Length vs. Vertical Displacement for $c=0.8$, $\eta=-2$, and $\alpha=0.0001$

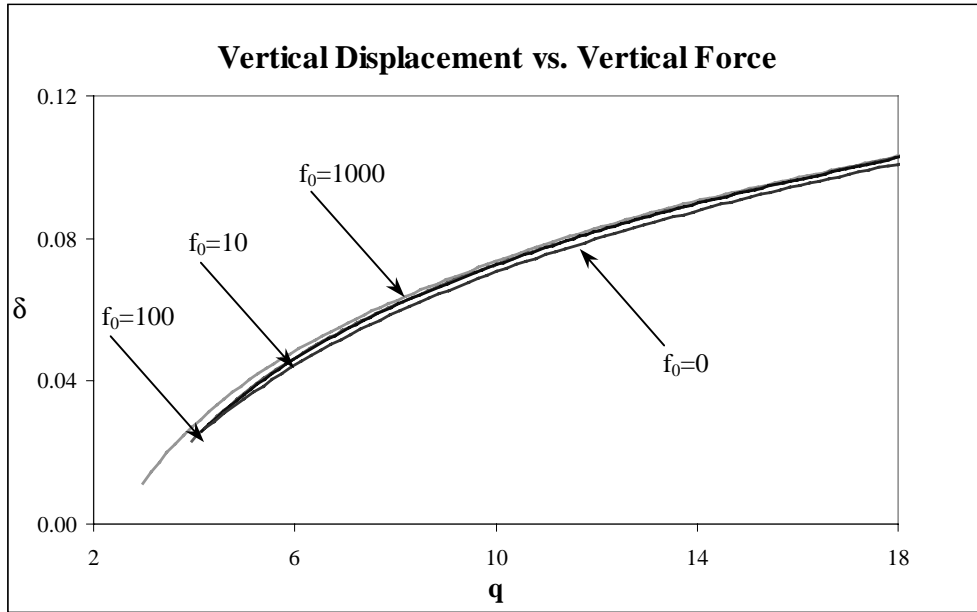


Figure 5.60: Vertical Displacement vs. Vertical Force for $c=0.8$, $\eta=-2$, and $\alpha=0.0001$

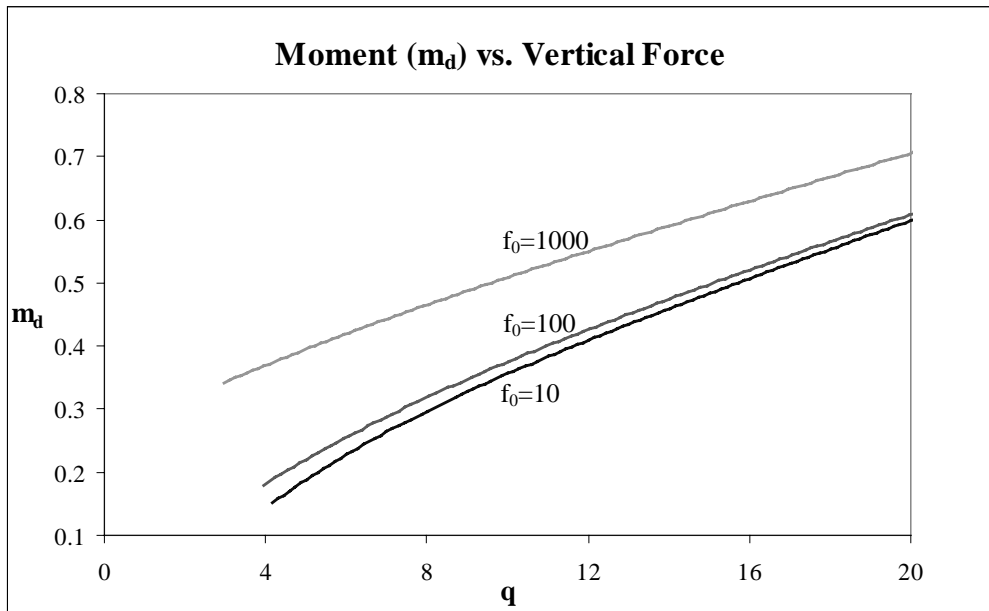


Figure 5.61: Moment (m_d) vs. Vertical Force for $c=0.8$, $\eta=-2$, and $\alpha=0.0001$

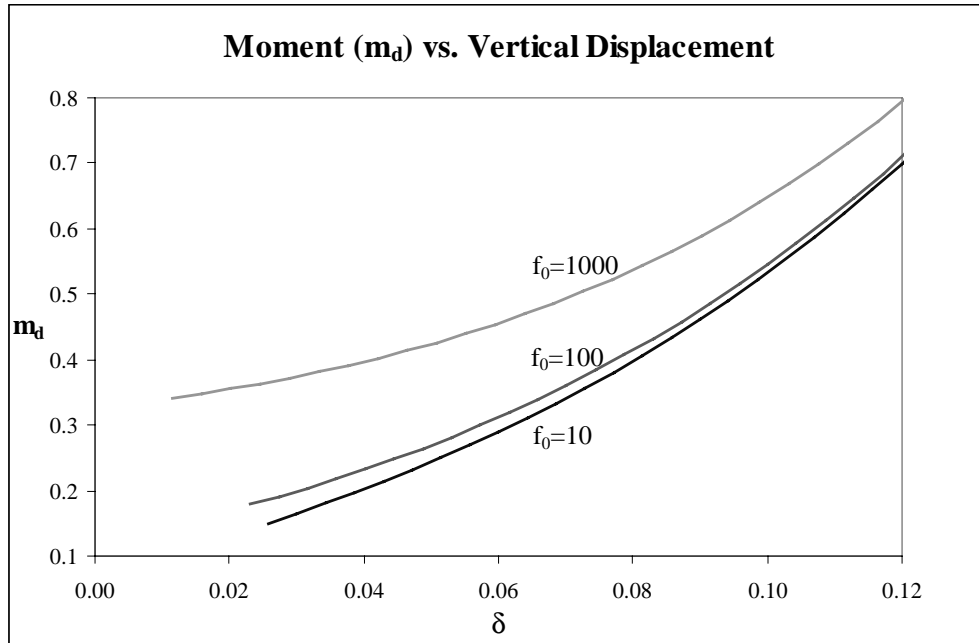


Figure 5.62: Moment (m_d) vs. Vertical Displacement for $c=0.8$, $\eta=-2$, and $\alpha=0.0001$

5.3 RESULTS FOR THE DUGDALE DMT-TYPE FORCE

Using the shooting method and the governing equations discussed in Section 5.1 of this chapter, values for the free length u of the elastica, the vertical force q , the horizontal force p , the height of the elastica h , and the moment m_d at $s=d$ were obtained for the line contact case. The contact length was then calculated using $b = 1 - d - u$, and the vertical displacement was calculated by subtracting the height of the elastica from its initial height when there was no contact between the elastica and the rigid surface ($\delta = h_0 - h$). For the Dugdale force, a separation distance of $c=0.4$ between the clamped ends of the elastica was considered. Additionally, three η values were examined: $\eta=2$, 0, and -2 . The values of h_0 corresponding to $\eta=2$, 0, and -2 were $h_0=0.7912$, 0.7896 , and 0.7878 when $c=0.4$.

5.3.1 Results for $c=0.4$ and $\eta=0$ (Line Contact Only)

The results obtained for the line contact case when $c=0.4$ and $\eta=0$ can be found in Figures 5.63-5.72. Values of $\alpha=0.001$ and 0.0001 were examined. For each value of α , Dugdale force values of $g_0=500$ and $g_0=5000$ were considered. The effect of the adhesion forces can be seen in Figure 5.63, which plots the contact length vs. the vertical force when $\alpha=0.001$. For a fixed value of q , as the adhesion force g_0 increased, the contact length b also increased. Figure 5.64 presents similar results. The contact length vs. vertical displacement relationship presented in Figure 5.64 shows that as the value of the adhesion force g_0 increased, the contact length also increased (for a fixed value of δ). The results obtained in Figures 5.63 and 5.64 indicate that the presence of adhesion forces elongated the contact length.

Figure 5.65 represents the line contact solution for $c=0.4$, $\eta=0$, and $\alpha=0.001$. All curves contained in Figure 5.65 terminated when the elastica experienced the transition from point contact ($b=0$) to line contact ($b>0$). Values of d , q , δ , p , and m_d at this transition point can be found in Table 5.12. Figure 5.65 shows the relationship between the vertical displacement and the vertical force. For a fixed value of q , the vertical displacement δ increased with increasing values of the adhesion force g_0 . Additionally, as the vertical force increased, the vertical displacement also increased.

Table 5.12: Values Corresponding to the Transition Point From Line Contact ($b>0$) to Point Contact ($b=0$) for $c=0.4$ and $\eta=0$ (Dugdale Force)

	Curve	d	q	δ	p	m_d
$\alpha = 0$	$g_0 = 0$	0.0000	12.52	0.0966	10.277	NA
$\alpha = 0.001$	$g_0 = 500$	0.0578	9.75	0.0687	8.854	1.3753
	$g_0 = 5000$	0.0356	-0.73	0.0037	4.178	3.1376
$\alpha = 0.0001$	$g_0 = 500$	0.0297	11.83	0.0884	9.895	0.5694
	$g_0 = 5000$	0.0194	9.27	0.0614	8.535	1.1202

Using the shooting method, the governing equations, and the end conditions specified for the Dugdale force line contact case, values were obtained for the moment at $s=d$. The values for this moment were then plotted against the vertical force and the vertical displacement. Figure 5.66 plots the moment m_d vs. the vertical force q for $c=0.4$, $\eta=0$, $\alpha=0.001$, and $g_0=500$ and 5000 . As g_0 increased, the contact length also increased when q was fixed. Additionally, when the vertical force increased, the contact length increased (when g_0 was held constant). Figure 5.67 plots the moment m_d vs. the vertical displacement δ for $c=0.4$, $\eta=0$, $\alpha=0.001$, and $g_0=500$ and 5000 . As g_0 increased, the contact length also increased when δ was fixed. Furthermore, when the vertical displacement increased, the contact length increased (when g_0 was held constant).

The results obtained for the Dugdale force DMT-type analysis when $c=0.4$, $\eta=0$, and $\alpha=0.0001$ were comparable to those obtained when $\alpha=0.001$. Additionally, the trends experienced in plots for $\alpha=0.0001$ were identical to those experienced in the corresponding plots for $\alpha=0.001$. Results from the Dugdale force analysis for $\alpha=0.0001$ can be found in Figures 5.68-5.72.

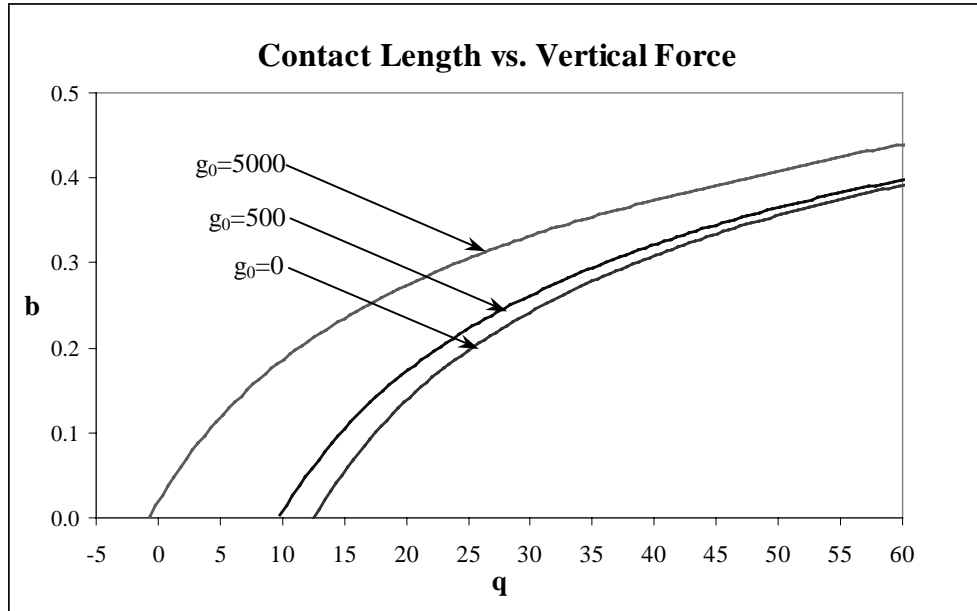


Figure 5.63: Contact Length vs. Vertical Force for $c=0.4$, $\eta=0$, and $\alpha=0.001$ (Dugdale Force)

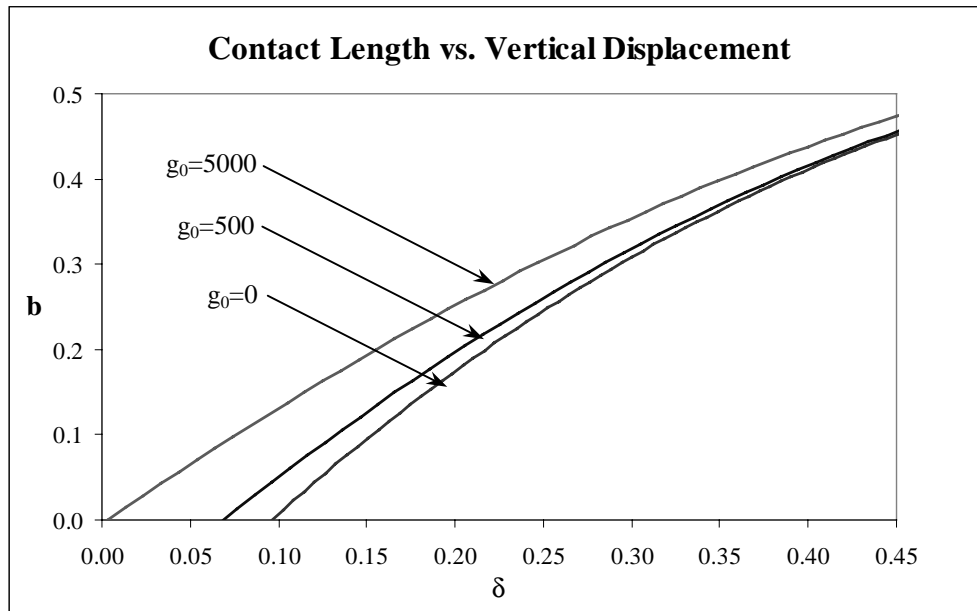


Figure 5.64: Contact Length vs. Vertical Displacement for $c=0.4$, $\eta=0$, and $\alpha=0.001$ (Dugdale Force)

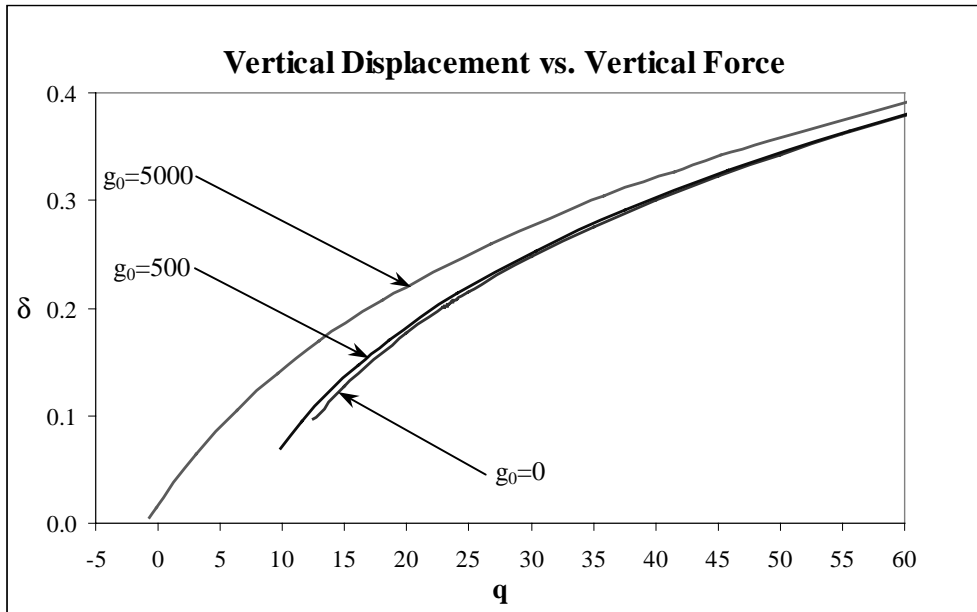


Figure 5.65: Vertical Displacement vs. Vertical Force for $c=0.4$, $\eta=0$, and $\alpha=0.001$ (Dugdale Force)

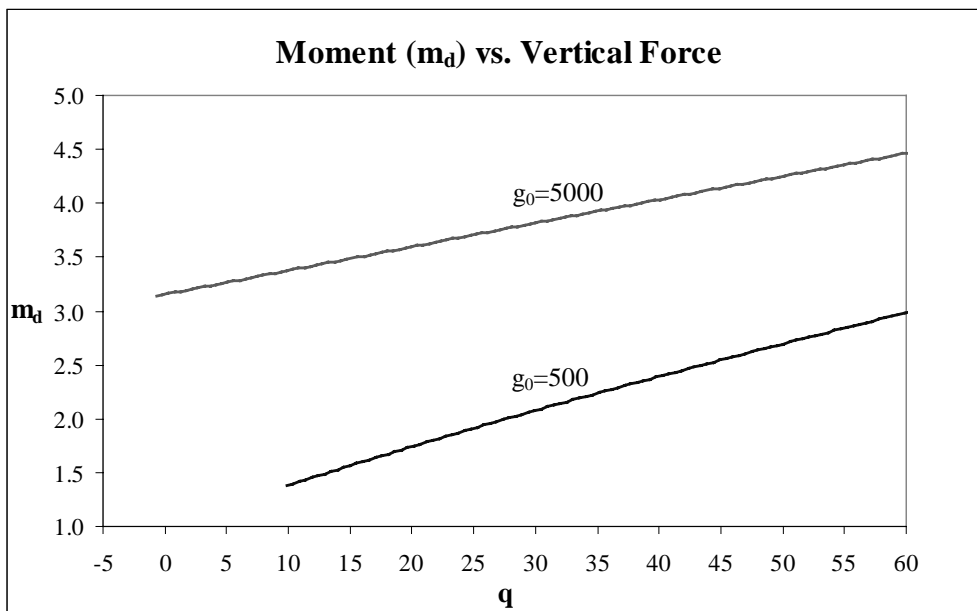


Figure 5.66: Moment (m_d) vs. Vertical Force for $c=0.4$, $\eta=0$, and $\alpha=0.001$ (Dugdale Force)

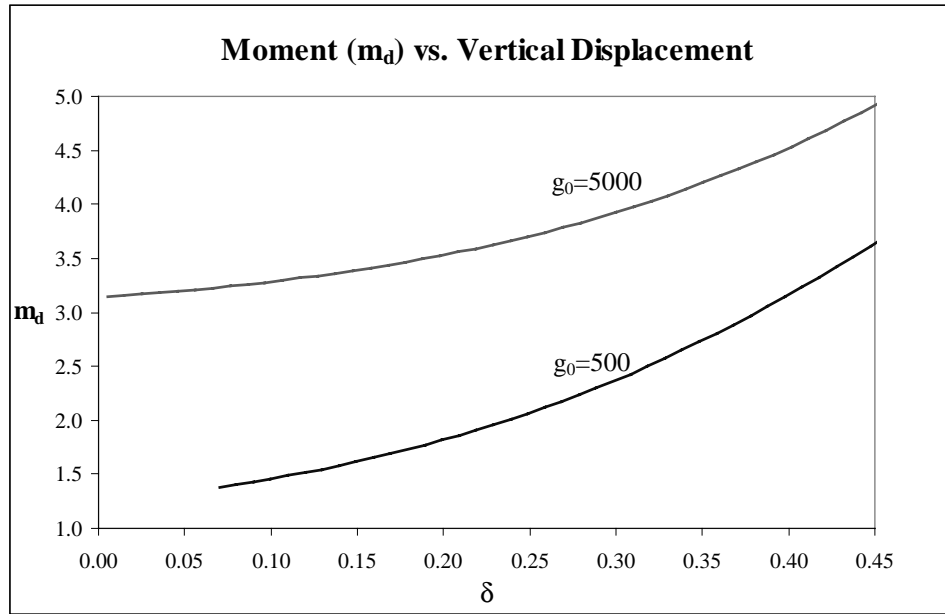


Figure 5.67: Moment (m_d) vs. Vertical Displacement for $c=0.4$, $\eta=0$, and $\alpha=0.001$ (Dugdale Force)

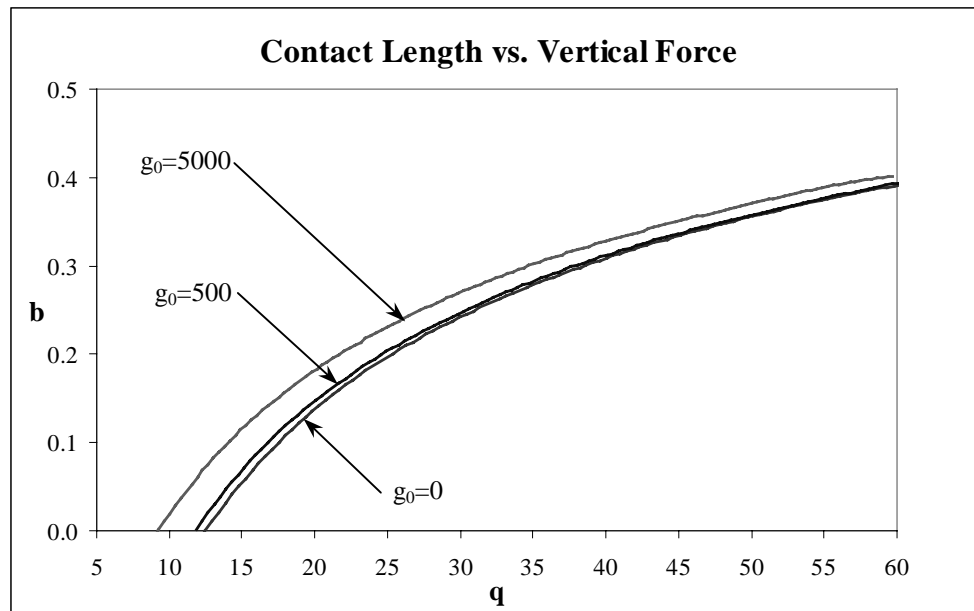


Figure 5.68: Contact Length vs. Vertical Force for $c=0.4$, $\eta=0$, and $\alpha=0.0001$ (Dugdale Force)

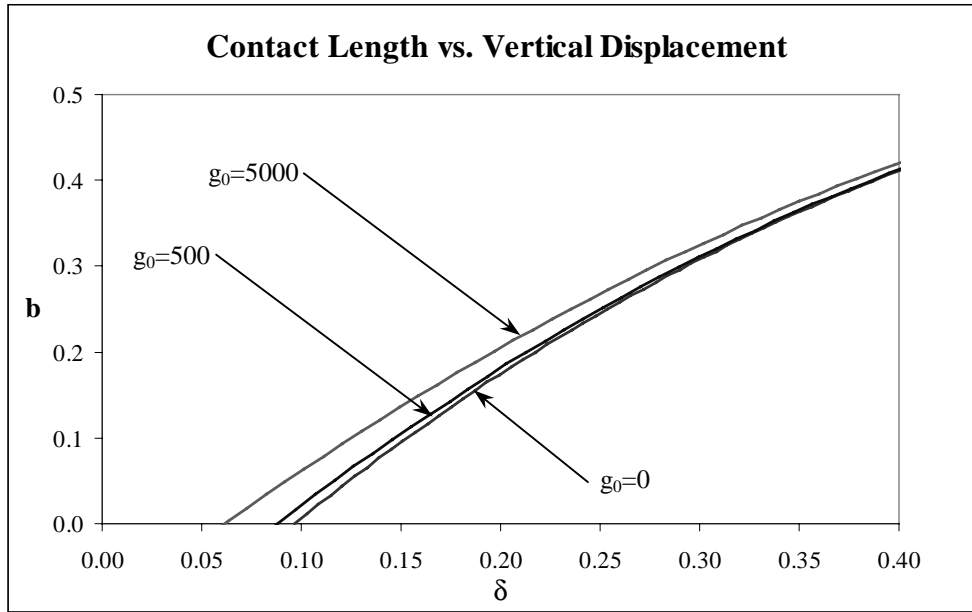


Figure 5.69: Contact Length vs. Vertical Displacement for $c=0.4$, $\eta=0$, and $\alpha=0.0001$ (Dugdale Force)

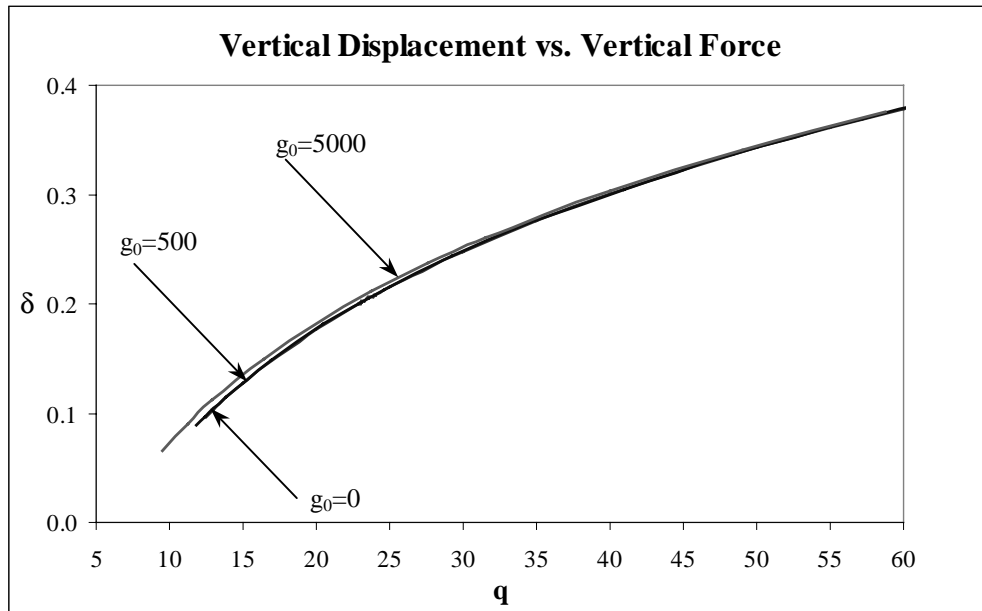


Figure 5.70: Vertical Displacement vs. Vertical Force for $c=0.4$, $\eta=0$, and $\alpha=0.0001$ (Dugdale Force)

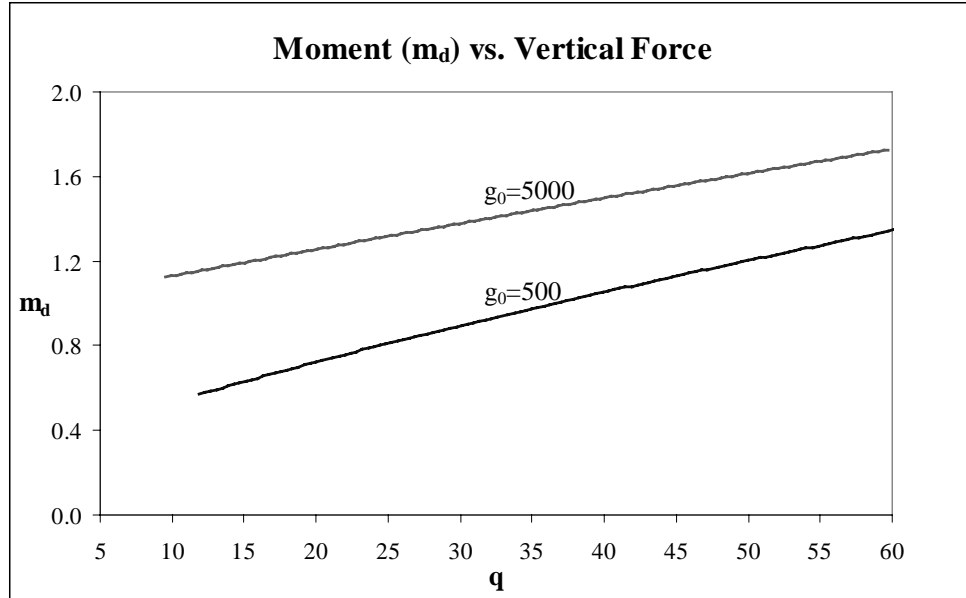


Figure 5.71: Moment (m_d) vs. Vertical Force for $c=0.4$, $\eta=0$, and $\alpha=0.0001$ (Dugdale Force)

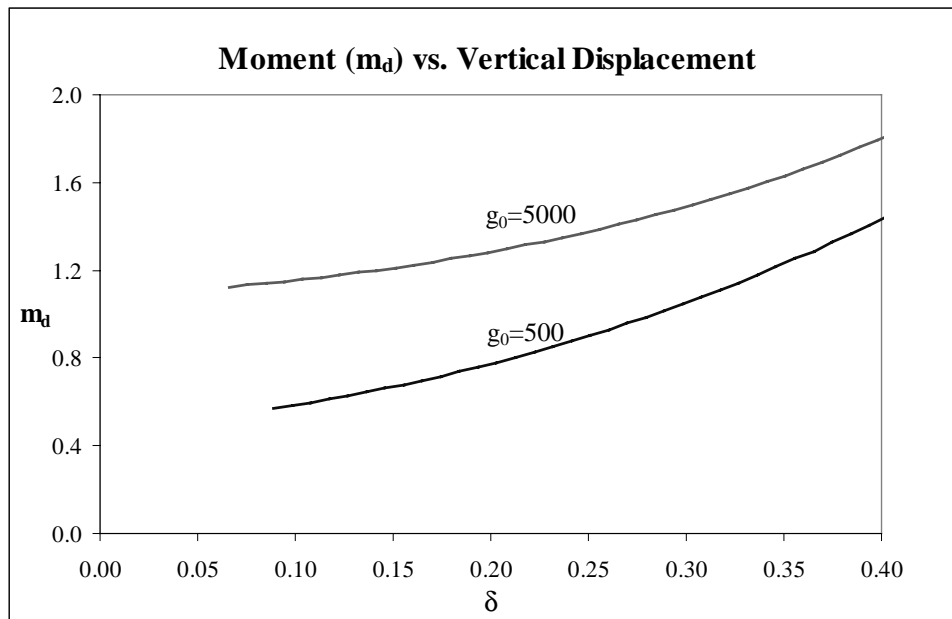


Figure 5.72: Moment (m_d) vs. Vertical Displacement for $c=0.4$, $\eta=0$, and $\alpha=0.0001$ (Dugdale Force)

5.3.2 Results for $c=0.4$ and $\eta=2$ (Line Contact Only)

The results obtained for the Dugdale force, line contact case when $c=0.4$ and $\eta=2$ can be found in Figures 5.73-5.82. Values of $\alpha=0.001$ and 0.0001 were examined. For each value of α examined, maximum force values of $g_0=0, 500, \text{ and } 5000$ were considered. The trends observed in the plots for $\alpha=0.001$ and $\alpha=0.0001$ when $c=0.4$ and $\eta=2$ were the same as the general trends discussed in Section 5.3.1 ($c=0.4$ and $\eta=0$). For the contact length vs. vertical force plots, the contact length increased with increasing values of g_0 (when q was fixed). Similarly, when the contact length was plotted against the vertical displacement, the contact length increased with increasing values of g_0 (when δ was fixed).

The trends observed in Section 3.5.1 for the relationship between the vertical displacement δ and the vertical force q also remained the same for the DMT-type analysis when $c=0.4, \eta=2, \text{ and } \alpha=0.001 \text{ and } 0.0001$. All curves in the vertical displacement vs. vertical force plots represented the line contact solution only and terminated when the transition from line contact to point contact was reached. Values for $d, q, \delta, p, \text{ and } m_d$ for $c=0.4, \eta=2, \text{ and } b=0$ can be located in Table 5.13.

Table 5.13: Values Corresponding to the Transition Point From Line Contact ($b>0$) to Point Contact ($b=0$) for $c=0.4$ and $\eta=2$ (Dugdale Force)

	Curve	d	q	δ	p	m_d
$\alpha = 0$	$g_0 = 0$	0.0000	10.90	0.0960	10.178	NA
$\alpha = 0.001$	$g_0 = 500$	0.0577	8.12	0.0688	8.748	1.3867
	$g_0 = 5000$	0.0356	-2.50	0.0045	3.995	3.1423
$\alpha = 0.0001$	$g_0 = 500$	0.0296	10.20	0.0879	9.787	0.5759
	$g_0 = 5000$	0.0194	7.62	0.0616	8.426	1.1244

Plots were also obtained for the moment m_d vs. the vertical force and the moment m_d vs. the vertical displacement. When q and δ were fixed, the value of the moment m_d increased with increasing values of g_0 . Also, m_d increased with increasing values of q and δ . Unlike the moment m_b , which was calculated for the JKR-type analysis, the moment m_d was not independent of the vertical force applied at the clamped ends of the elastica, nor was it independent of the separation distance c between clamped ends. All results of the Dugdale force DMT-type analysis when $c=0.4$ and $\eta=2$ can be found in Figures 5.73-5.82.

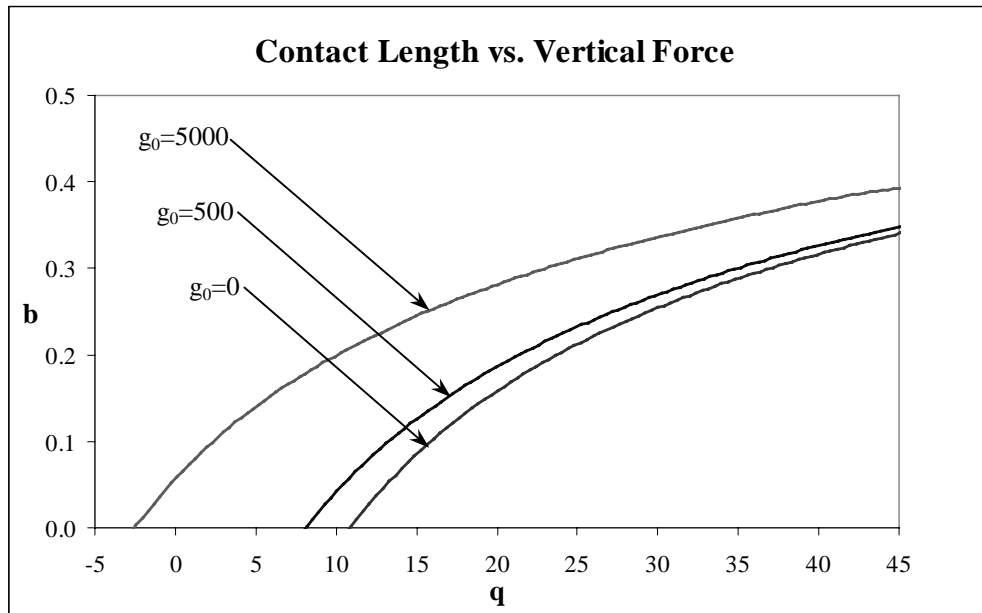


Figure 5.73: Contact Length vs. Vertical Force for $c=0.4$, $\eta=2$, and $\alpha=0.001$ (Dugdale Force)

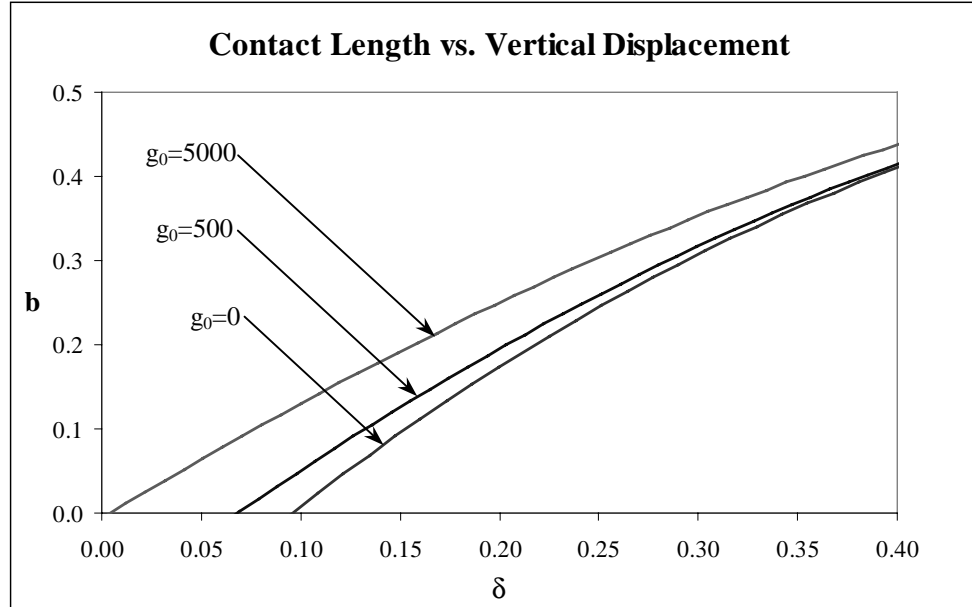


Figure 5.74: Contact Length vs. Vertical Displacement for $c=0.4$, $\eta=2$, and $\alpha=0.001$ (Dugdale Force)

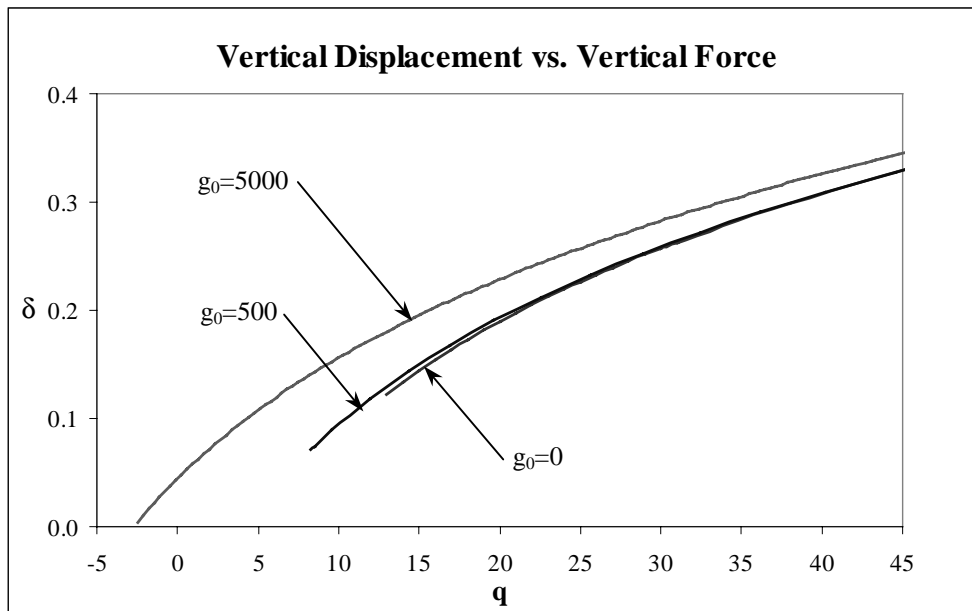


Figure 5.75: Vertical Displacement vs. Vertical Force for $c=0.4$, $\eta=2$, and $\alpha=0.001$ (Dugdale Force)

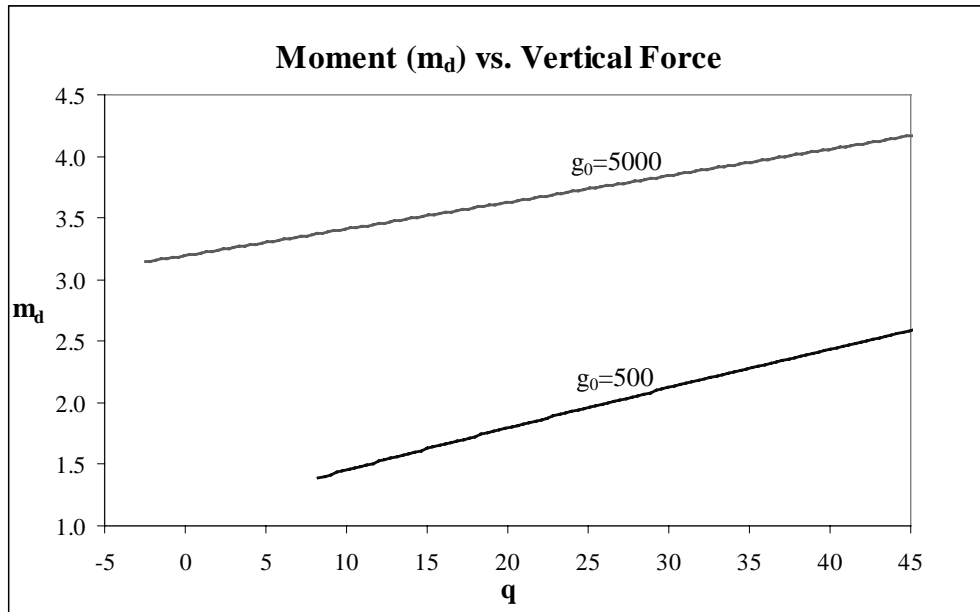


Figure 5.76: Moment (m_d) vs. Vertical Force for $c=0.4$, $\eta=2$, and $\alpha=0.001$ (Dugdale Force)

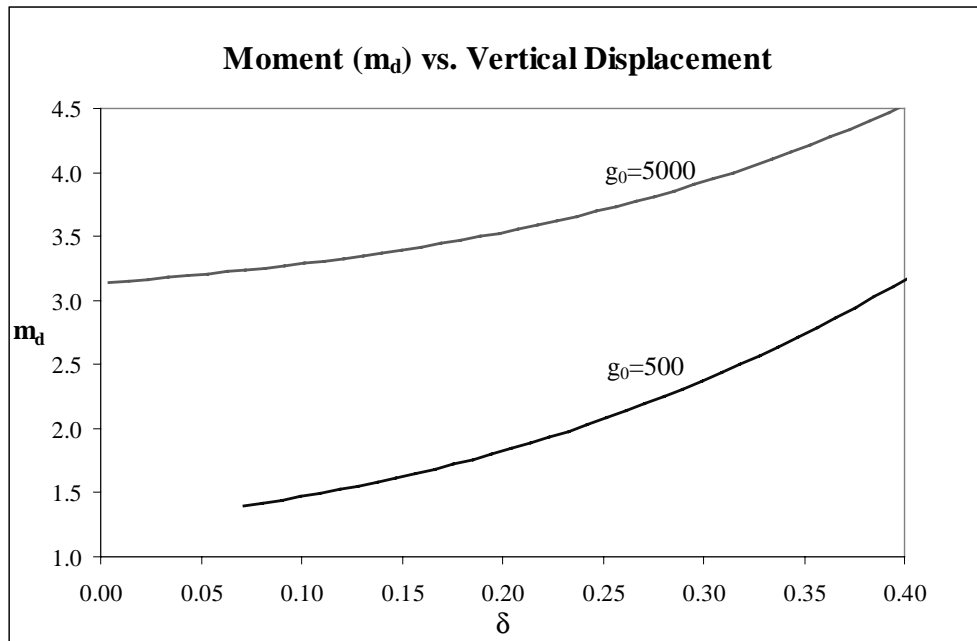


Figure 5.77: Moment (m_d) vs. Vertical Displacement for $c=0.4$, $\eta=2$, and $\alpha=0.001$ (Dugdale Force)

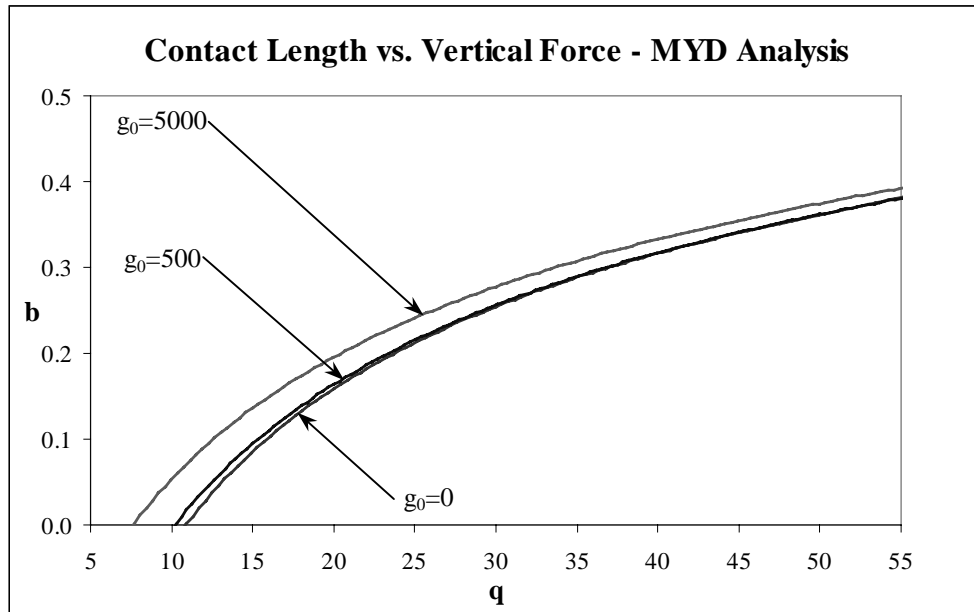


Figure 5.78: Contact Length vs. Vertical Force for $c=0.4$, $\eta=2$, and $\alpha=0.0001$ (Dugdale Force)

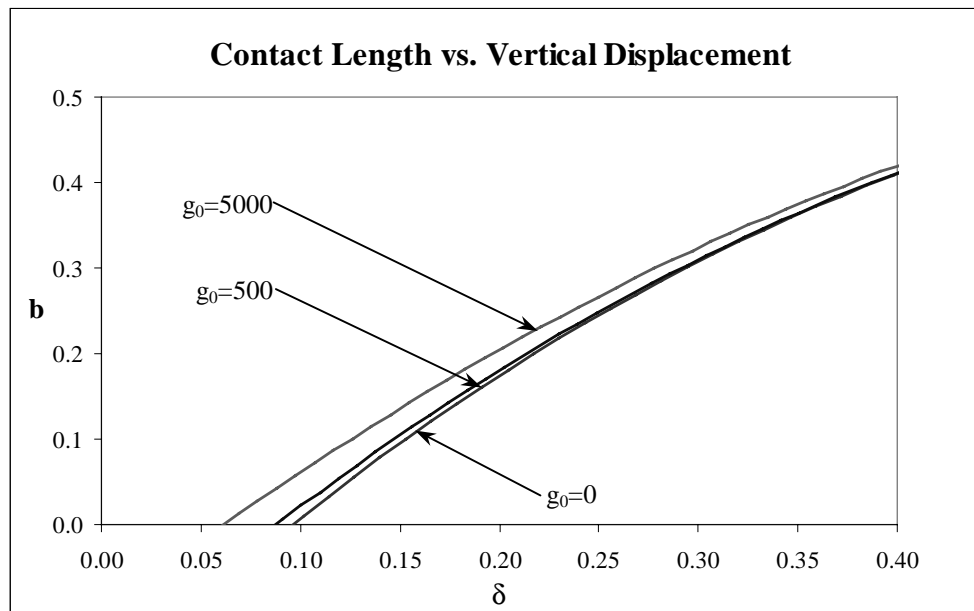


Figure 5.79: Contact Length vs. Vertical Displacement for $c=0.4$, $\eta=2$, and $\alpha=0.0001$ (Dugdale Force)

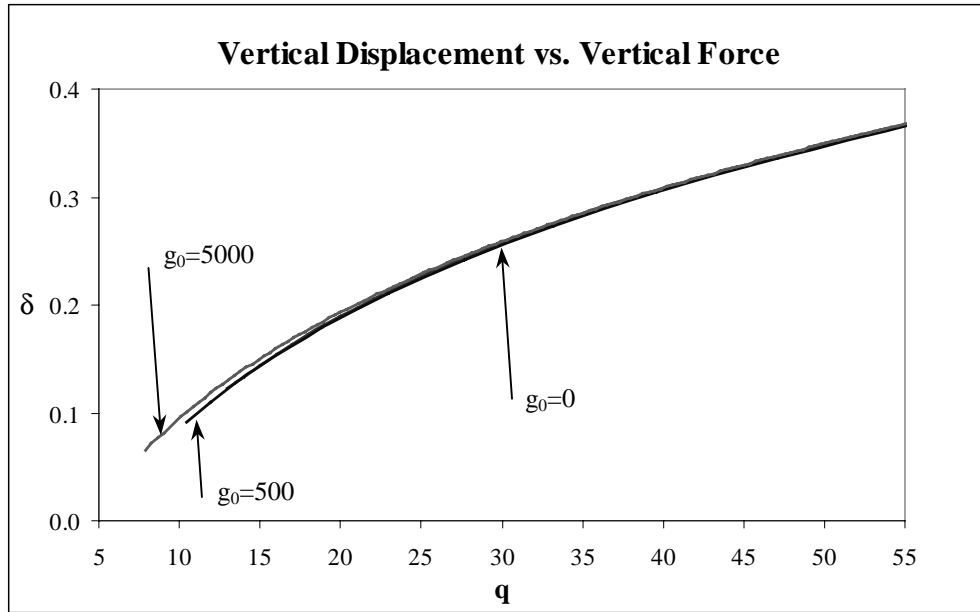


Figure 5.80: Vertical Displacement vs. Vertical Force for $c=0.4$, $\eta=2$, and $\alpha=0.0001$ (Dugdale Force)

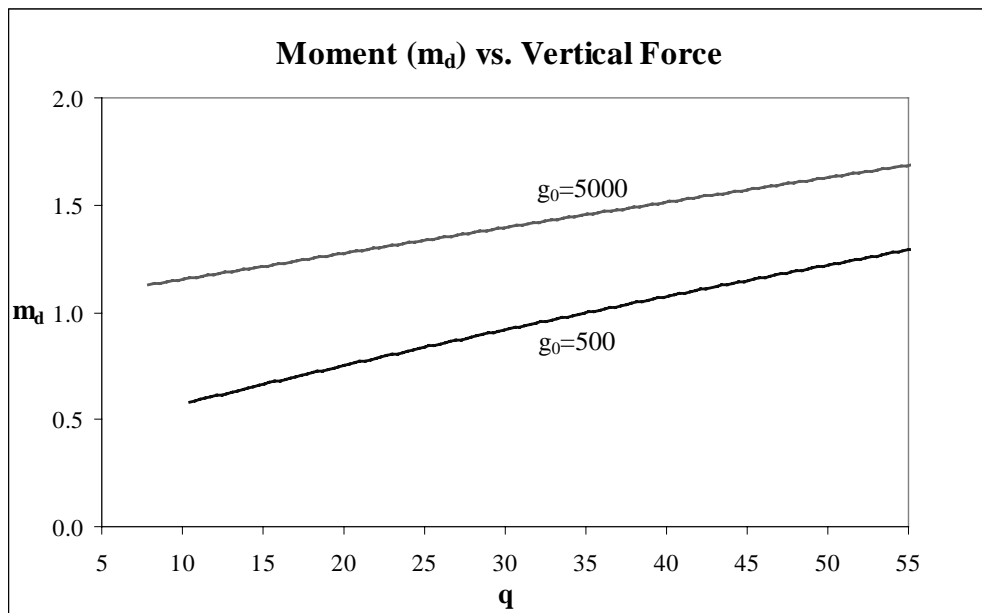


Figure 5.81: Moment (m_d) vs. Vertical Force for $c=0.4$, $\eta=2$, and $\alpha=0.0001$ (Dugdale Force)

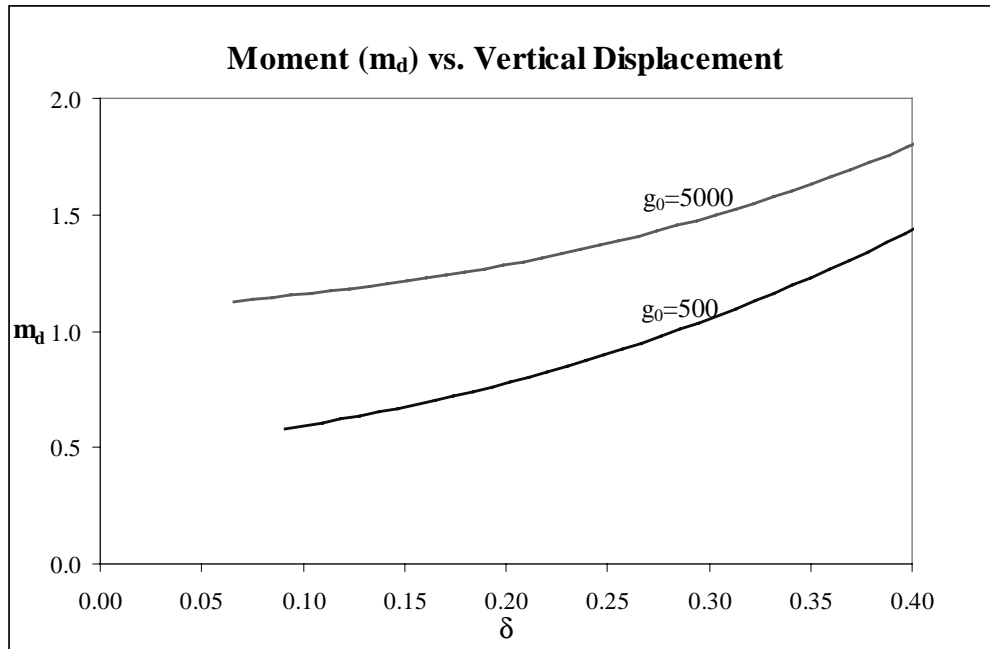


Figure 5.82: Moment (m_d) vs. Vertical Displacement for $c=0.4$, $\eta=2$, and $\alpha=0.0001$ (Dugdale Force)

5.3.3 Results for $c=0.4$ and $\eta=-2$ (Line Contact Only)

The results obtained for the Dugdale force, line contact solution when $c=0.4$ and $\eta=-2$ can be found in Figures 5.83-5.92. Again, $\alpha=0.001$ and $\alpha=0.0001$ were investigated, and for each α considered, adhesion force values of $g_0=500$ and $g_0=5000$ were examined. The trends observed in b vs. q , b vs. δ , δ vs. q , m_d vs. q , and m_d vs. δ plots for $c=0.4$, $\eta=-2$ were the same as those observed when $c=0.4$, $\eta=0$ and $c=0.4$, $\eta=2$ (Sections 5.3.1 and 5.3.2). The contact length b vs. vertical force q plots showed that for a fixed value of q , the contact length increased with increasing values for the adhesion force. The contact length b vs. vertical displacement δ plots showed that for a fixed value of δ , the contact length also increased with increasing values for the adhesion force. Additionally, the vertical displacement was plotted against the vertical force for the Dugdale force DMT-

type analysis. All curves in the d vs. q plot represented the line contact solution only and terminated when the elastica experienced the transition from line contact ($b>0$) to point contact ($b=0$). Values for d , p , δ , q , and m_d at the transition point ($b=0$) are located in Table 5.14

Table 5.14: Values Corresponding to the Transition Point From Line Contact ($b>0$) to Point Contact ($b=0$) for $c=0.4$ and $\eta=-2$ (Dugdale Force)

	Curve	d	q	δ	p	m_d
$\alpha = 0$	$g_0 = 0$	0.0000	14.13	0.0972	10.375	NA
$\alpha = 0.001$	$g_0 = 500$	0.0580	11.37	0.0684	8.949	1.3633
	$g_0 = 5000$	0.0357	1.01	0.0022	4.333	3.1323
$\alpha = 0.0001$	$g_0 = 500$	0.0299	13.44	0.0887	9.990	0.5625
	$g_0 = 5000$	0.0194	10.93	0.0616	8.657	1.1161

The moment at $s=d$ was plotted against both the vertical force and the vertical displacement for $c=0.4$, $\eta=-2$, and $\alpha=0.001$ and 0.0001 . When q was held constant, the moment m_d increased with increasing values of g_0 . Additionally, the moment at $s=d$ increased with increasing values of q for a constant value of g_0 . Similarly, when δ was held constant, the moment m_d increased with increasing values of g_0 . The moment m_d also increased with increasing values of δ (for a constant g_0).

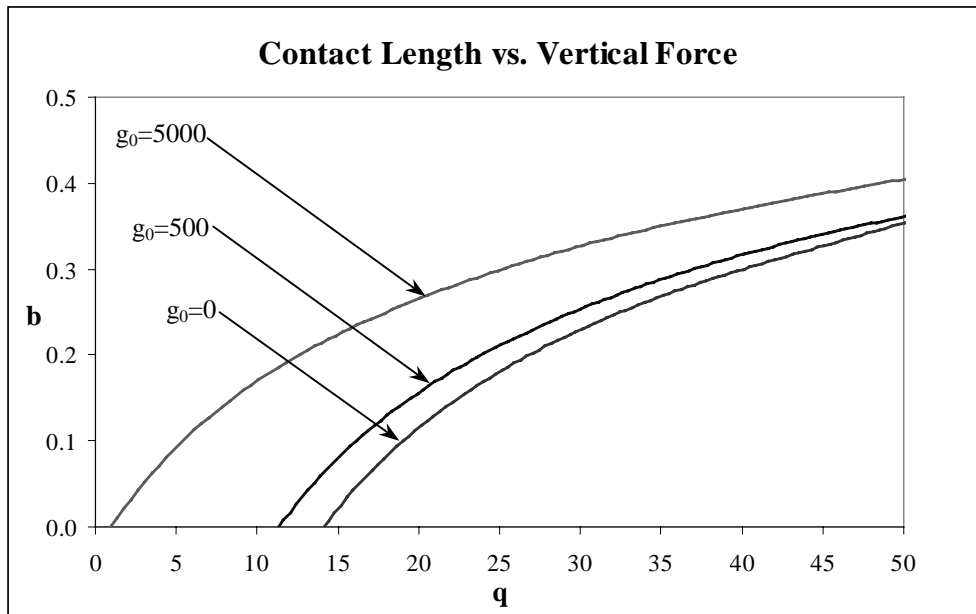


Figure 5.83: Contact Length vs. Vertical Force for $c=0.4$, $\eta=-2$, and $\alpha=0.001$ (Dugdale Force)

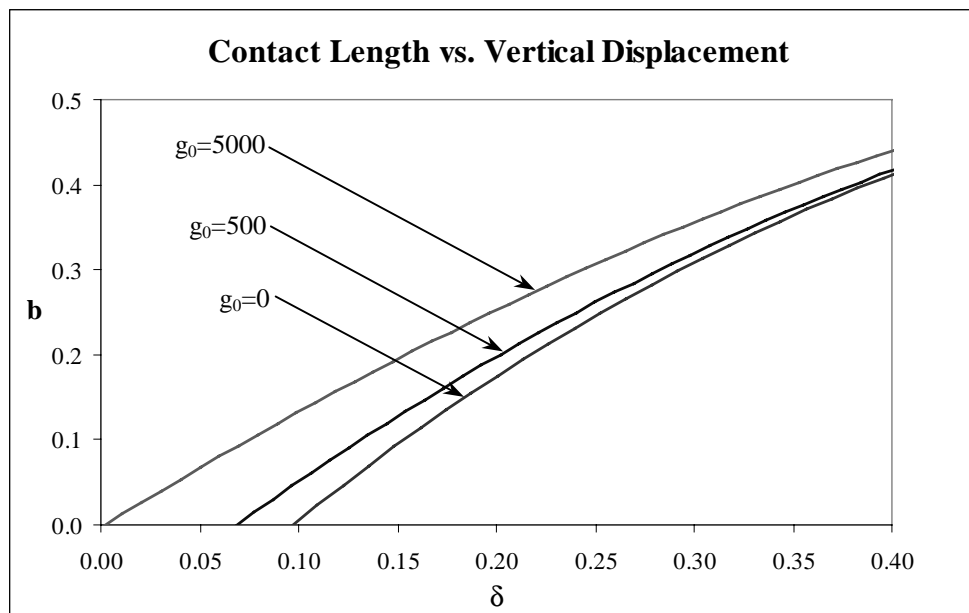


Figure 5.84: Contact Length vs. Vertical Displacement for $c=0.4$, $\eta=-2$, and $\alpha=0.001$ (Dugdale Force)

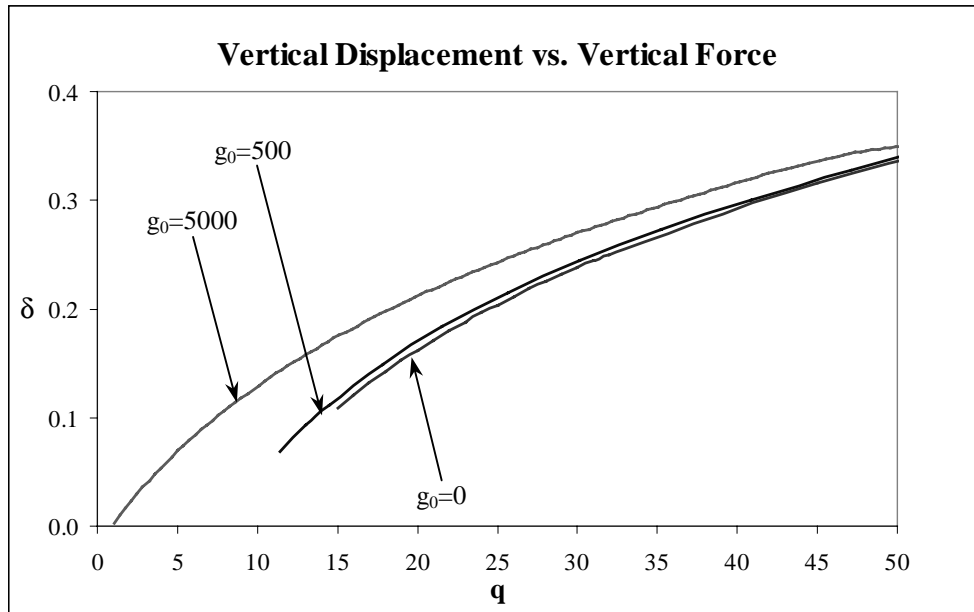


Figure 5.85: Vertical Displacement vs. Vertical Force for $c=0.4$, $\eta=-2$, and $\alpha=0.001$ (Dugdale Force)

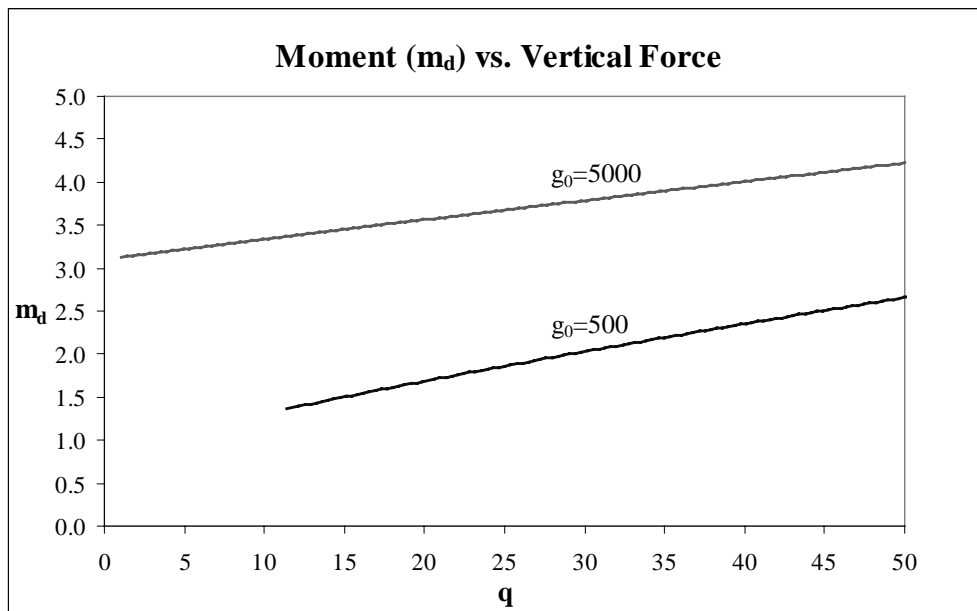


Figure 5.86: Moment (m_d) vs. Vertical Force for $c=0.4$, $\eta=-2$, and $\alpha=0.001$ (Dugdale Force)

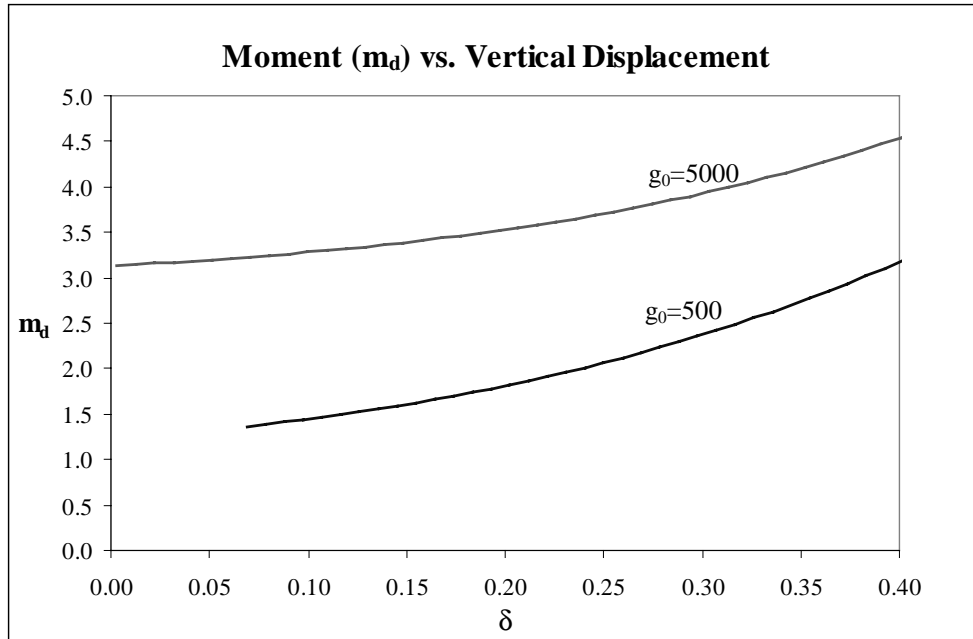


Figure 5.87: Moment (m_d) vs. Vertical Displacement for $c=0.4$, $\eta=-2$, and $\alpha=0.001$ (Dugdale Force)

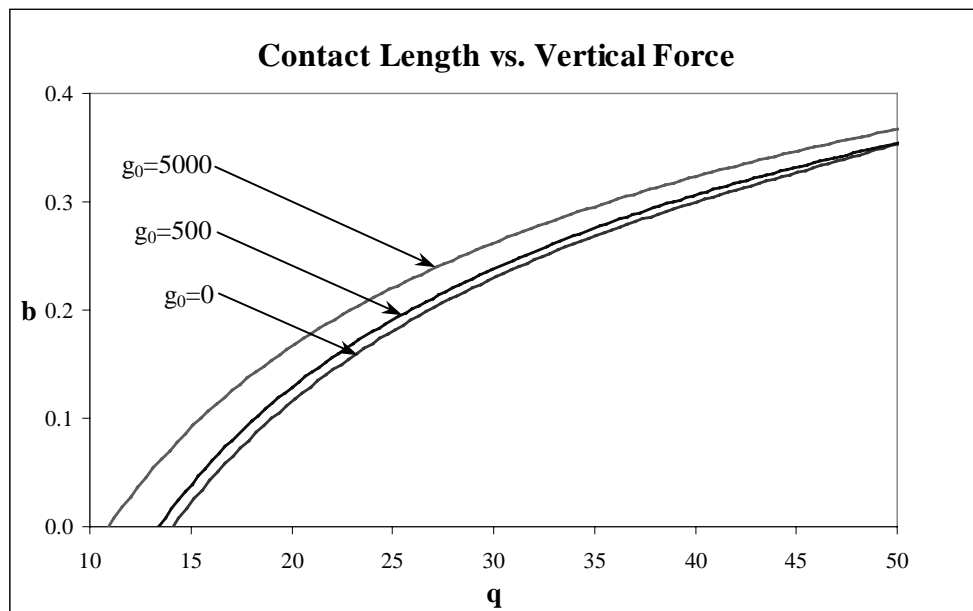


Figure 5.88: Contact Length vs. Vertical Force for $c=0.4$, $\eta=-2$, and $\alpha=0.0001$ (Dugdale Force)

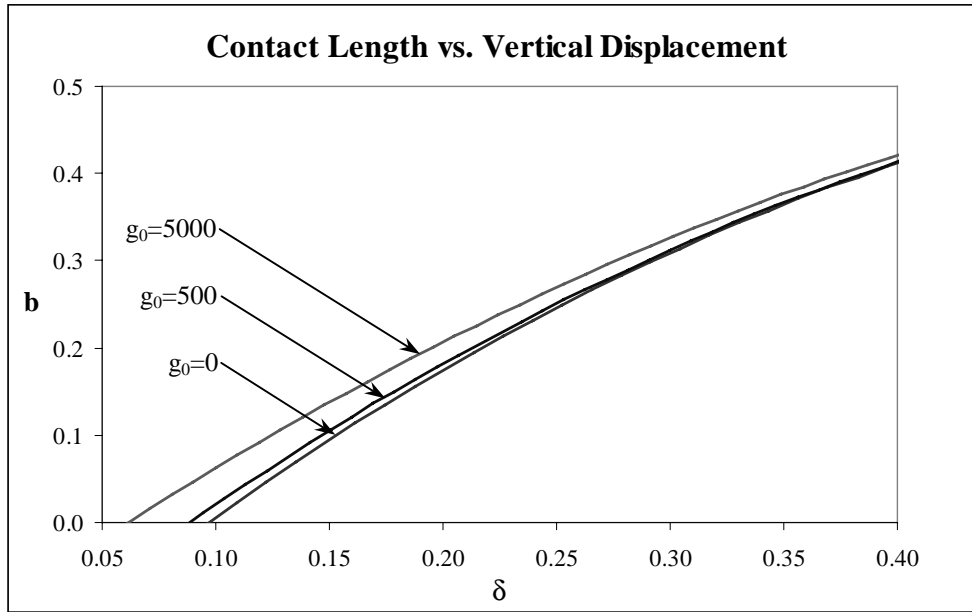


Figure 5.89: Contact Length vs. Vertical Displacement for $c=0.4$, $\eta=-2$, and $\alpha=0.0001$ (Dugdale Force)

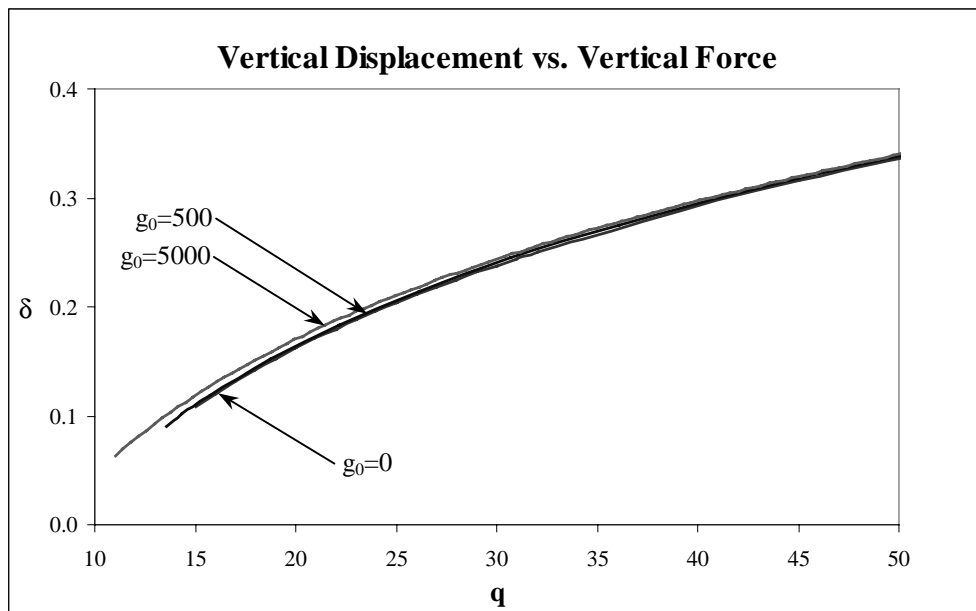


Figure 5.90: Vertical Displacement vs. Vertical Force for $c=0.4$, $\eta=-2$, and $\alpha=0.0001$ (Dugdale Force)

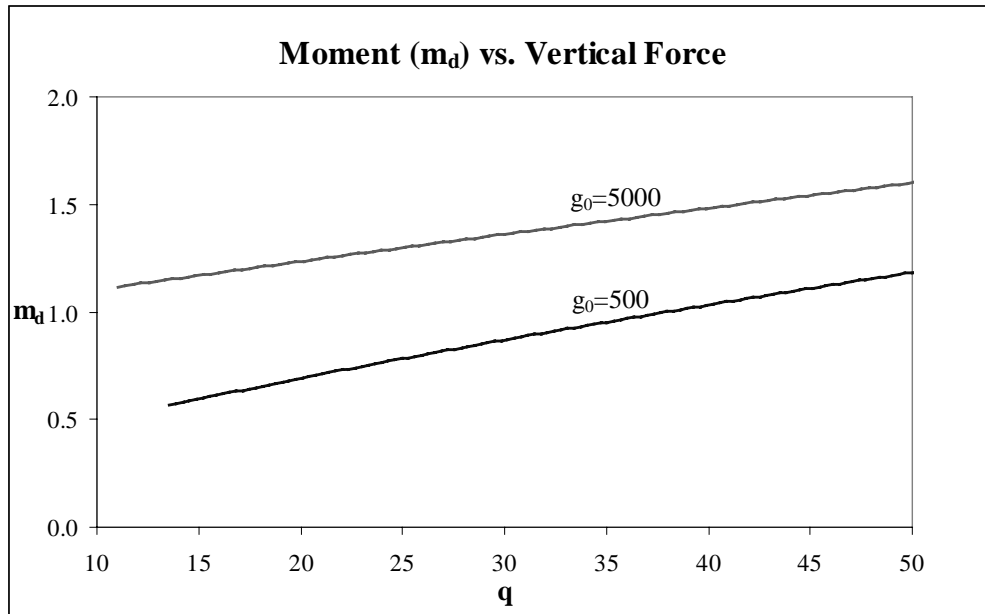


Figure 5.91: Moment (m_d) vs. Vertical Force for $c=0.4$, $\eta=-2$, and $\alpha=0.0001$ (Dugdale Force)

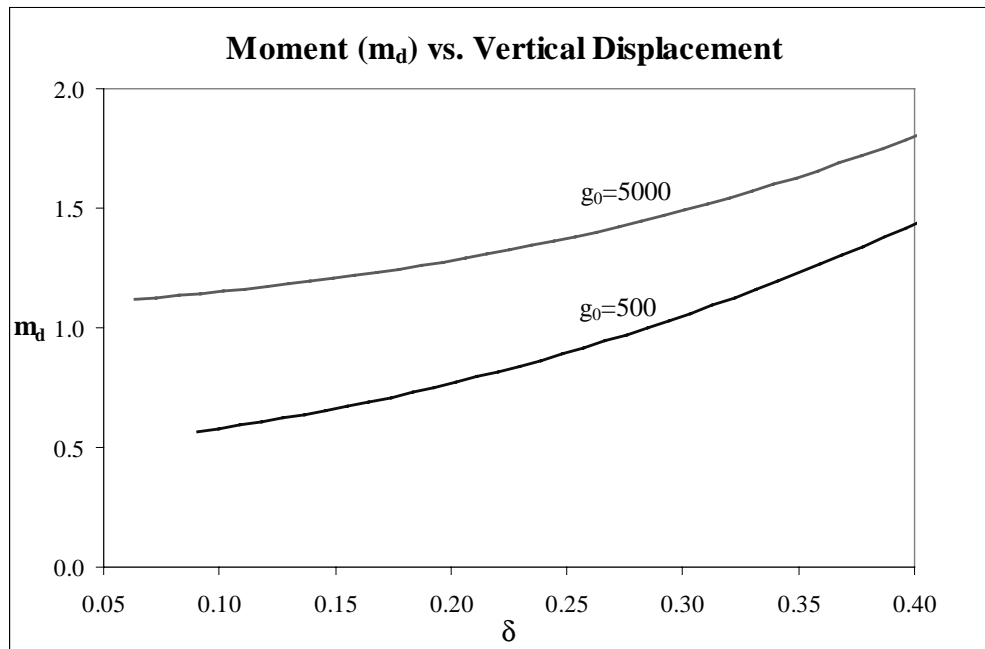


Figure 5.92: Moment (m_d) vs. Vertical Displacement for $c=0.4$, $\eta=-2$, and $\alpha=0.0001$ (Dugdale Force)

5.4 RESULTS FOR THE NO CONTACT AND POINT CONTACT CASES

The vertical displacement vs. vertical force graphs contained in Sections 5.2 and 5.3 show only the line contact solutions and neglect the curves obtained when the point contact and no contact cases were considered. Figure 5.93, however, displays a typical plot (when there is no self-weight η) of the vertical displacement vs. the vertical force including the point contact and no contact solutions. The solid blue line in Figure 5.93 between Points A and B represents the point contact solution. The solid curves are associated with stable equilibrium states (at which the total energy has a local minimum with respect to admissible changes in displacement). Point contact ($b=0$) begins where the line contact ($b>0$) ends. The transition point which separates the line contact and the point contact regions is denoted Point A, while the transition point between the point contact and no contact curves is denoted Point B. Point B was calculated using Equations 3.1-3.3 and Equation 4.6 as the governing equations. At $s=1$, the end conditions were defined as $x=c$ and $\theta=\pi/2$. The clear vertical distance between the center of the elastica and the rigid surface, denoted as y_0 in Section 5.1 for the no contact case, was set equal to zero. Values for c , η , f_0 (or g_0 for the Dugdale force analysis), and α were specified and values were guessed for p and d . The FindRoot command in Mathematica was used to obtain values for p and d at the transition point B. Values for d , q , p , δ , and m_d at this transition point are given in Tables 5.15-5.17.

The no contact curve, when $0 < y_0 < \alpha$, is denoted by the dashed line from Points B to C in Figure 5.93. On this curve, the central region of the elastica feels the adhesion force even though no contact is present between the two surfaces. The no contact curve intersects the point contact curve at the transition point B described above and ends when $\delta = -\alpha$ and $q = -\eta$ (Point C, Figure 5.93). When the self-weight is excluded from the analysis ($\eta=0$), Point C will occur at $\delta = -\alpha$, $q=0$. Because the no contact curve from B to C represents unstable equilibrium states, the elastica will jump through the region where $0 < y_0 < \alpha$.

Figures 5.94 and 5.95 illustrate the path followed by the elastica through the point contact and no contact regions when $\eta=0$. The behavior of the elastica was dependent on two factors: whether the elastica was pushed onto or pulled off the rigid surface, and whether the vertical displacement or the vertical force was controlled. Note that “pulling” here refers to reducing the downward force q until the elastica loses contact with the substrate, which may occur when $q=0$ or may require $q<0$, i.e., an upward force. When $q > 0$ at Point B, no upward force is required to separate the elastica from the substrate. The elastica will simply separate itself from the substrate when the force reaches the specified value of q . The upward vertical force ($q < 0$) required to pull the elastica apart from the substrate is the “pull-off force” $f_p=-q$ (although $-2q$ is the total upward force).

Figure 5.94 illustrates the case in which the vertical displacement was controlled. When the elastica was pushed onto the rigid substrate (blue arrows), it first experienced a period of no contact with no adhesion forces acting. Once Point C was reached, a horizontal jump from the point $\delta = -\alpha$, $q=0$ to the point contact curve occurred. That is, as soon as the center of the elastica felt the adhesion force, it jumped onto the substrate. As the elastica continued to experience pushing against the rigid surface, values for q and δ were obtained from the point contact and then line contact curves. When the elastica experienced line contact and was gradually pulled off of the rigid surface (black arrows), values for q and δ were obtained initially from the line contact curve. As the pulling action continued, the contact length approached zero and the point contact curve was encountered. Values for q and δ were obtained from the point contact curve until Point B was reached. At Point B, a horizontal jump occurred from the point contact curve to the no contact region with no adhesion forces acting ($y_0 > \alpha$). Therefore, the center of the elastica jumped off the substrate and past the region in which the adhesion forces were active ($0 < y_0 < \alpha$). Following the horizontal jump, the value for q was zero and $\delta < -\alpha$.

The vertical displacement experienced by the elastica when the vertical force was controlled can be seen in Figure 5.95. When the elastica was pushed onto the rigid

substrate (blue arrows), it initially experienced a period of no contact with no adhesion forces acting. Once Point C was reached, a vertical jump from the point $\delta = -\alpha$, $q = -\eta$ to the point contact curve occurred. As the elastica continued to experience pushing against the rigid surface, values for q and δ were obtained from the point contact and then line contact curves. When the elastica experienced line contact and was gradually pulled off of the rigid surface (black arrows), values for q and δ were obtained from the line contact curve. As the pulling action continued, the contact length approached zero and the point contact curve was encountered. Values for q and δ were obtained from the point contact curve until Point B was reached. At Point B, the center of the elastica jumps dynamically off the substrate and travels through and past the region of attraction created by the adhesive forces.

When the self-weight η was added to the analysis, Tables 5.15-5.17 indicate that the quantities d , δ , p , and m_d only change slightly, and that the pull-off force is approximately changed by η . This is expected, since the values of η used here do not significantly alter the overall shape of the elastica, and the weight of half of the strip is η .

By vertical equilibrium, at the instant of pull-off, the pull-off force f_p is given by the total attractive force of adhesion plus the self-weight η on one-half of the elastica. For the linear force, an approximate expression for this total force at the moment of pull-off is given in Appendix B. It utilizes the approximate function $y(x)$ for $0 \leq x \leq d$, and requires knowledge of the values of f_0 , α , and d . The values obtained for f_p when $c=0.4$ correspond to the first six rows of Table 5.15 and are 1.31, 13.48, 95.11, 0.43, 4.78, and 35.34. For Table 5.16, when $c=0.8$, they are 0.53, 3.07, 19.5, 0.19, 1.12, and 7.36. For the Dugdale force, the approximate pull-off force is $g_0 d + \eta$. The values corresponding to the pull-off force in the first four rows of Table 5.17 are $f_p=10.62$, 75.84, 3.68, and 27.95. Values for the approximate pull-off force f_a and the pull-off force f_p obtained by using the shooting method can be found in Appendices B and C.

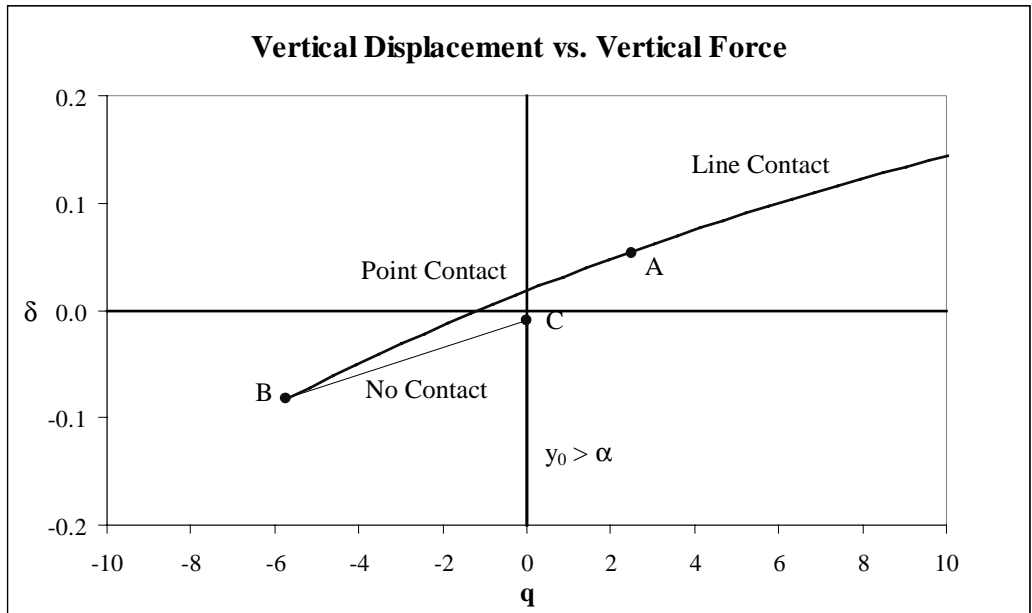


Figure 5.93: Typical Vertical Displacement vs. Vertical Force Plot for DMT-Type Analysis

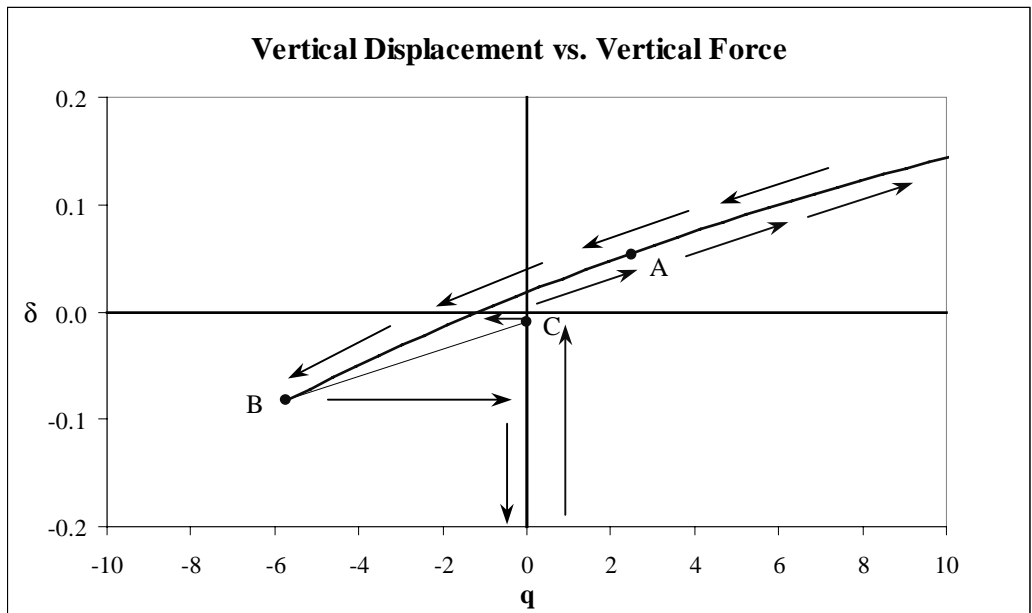


Figure 5.94: Vertical Force Experienced by the Elastica When it is Pushed Onto (Blue Arrows on Right Side) or Pulled Off (Black Arrows on Left Side) the Rigid Surface. Vertical Displacement is Controlled.

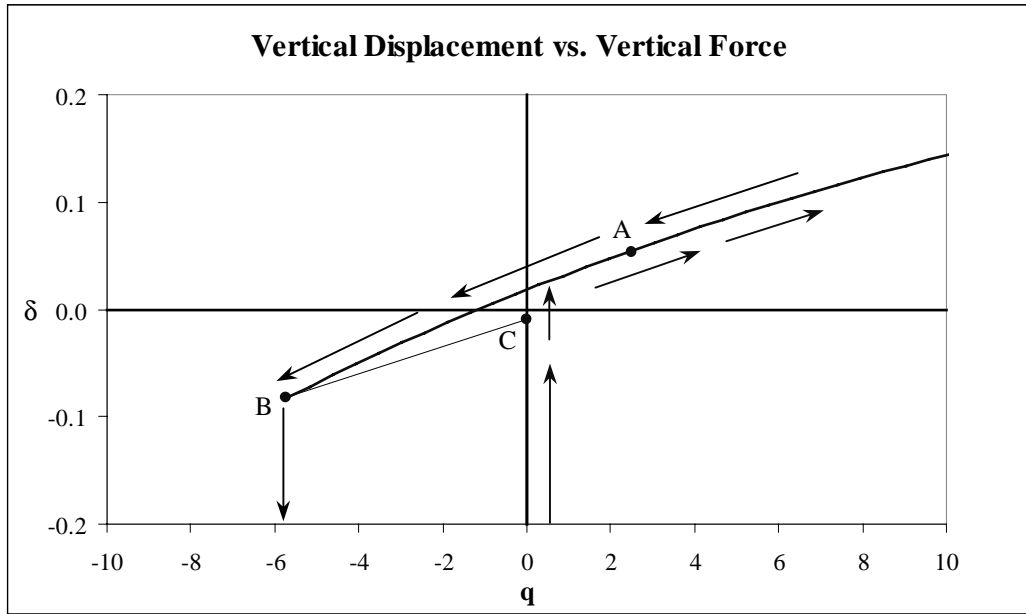


Figure 5.95: Vertical Displacement Experienced by the Elastica When it is Pushed Onto (Blue Arrows on Right Side) or Pulled Off (Black Arrows on Left Side) the Rigid Surface. Vertical Force is Controlled.

Table 5.15: Values corresponding to the transition point B between point contact and no contact for the linear force DMT-type analysis when $c=0.4$

		Curve	d	q	δ	p	m_d
$\eta=0$	$\alpha = 0.001$	$f_0 = 100$	0.0246	-1.31	-0.0153	4.097	3.2855
		$f_0 = 1000$	0.0201	-13.48	-0.0462	0.561	4.8349
		$f_0 = 10000$	0.0134	-95.11	-0.0930	-32.068	10.4607
	$\alpha = 0.0001$	$f_0 = 100$	0.0081	-0.43	-0.0052	4.194	3.0688
		$f_0 = 1000$	0.0073	-4.78	-0.0205	2.423	3.7617
		$f_0 = 10000$	0.0052	-35.34	-0.0667	-9.616	7.1747
$\eta=2$	$\alpha = 0.001$	$f_0 = 100$	0.0245	-3.32	-0.0150	3.853	3.3235
		$f_0 = 1000$	0.0200	-15.48	-0.0450	-0.829	4.8507
		$f_0 = 10000$	0.0134	-97.18	-0.0913	-32.434	10.4565
	$\alpha = 0.0001$	$f_0 = 100$	0.0080	-2.44	-0.0051	3.928	3.1079
		$f_0 = 1000$	0.0072	-6.77	-0.0198	2.155	3.7881
		$f_0 = 10000$	0.0052	-37.35	-0.0651	-9.936	7.1752
$\eta=-2$	$\alpha = 0.001$	$f_0 = 100$	0.0247	0.70	-0.0155	4.338	3.2461
		$f_0 = 1000$	0.0201	-11.47	-0.0458	-0.294	4.8186
		$f_0 = 10000$	0.0134	-93.04	-0.0948	-31.701	10.4650
	$\alpha = 0.0001$	$f_0 = 100$	0.0081	1.57	-0.0053	4.458	3.0280
		$f_0 = 1000$	0.0073	-2.79	-0.0212	2.689	3.7345
		$f_0 = 10000$	0.0052	-33.33	-0.0685	-9.296	7.1741

Table 5.16: Values corresponding to the transition point B between point contact and no contact for the linear force DMT-type analysis when $c=0.8$

		Curve	d	q	δ	p	m_d
$\eta=0$	$\alpha = 0.001$	$f_0 = 10$	0.0461	-0.53	-0.0726	-5.202	0.9333
		$f_0 = 100$	0.0391	-3.07	-0.0796	-9.091	1.2579
		$f_0 = 1000$	0.0255	-19.50	-0.1130	-32.484	2.8596
	$\alpha = 0.0001$	$f_0 = 10$	0.0169	-0.19	-0.0281	-6.745	0.6994
		$f_0 = 100$	0.0152	-1.12	-0.0331	-8.286	0.8555
		$f_0 = 1000$	0.0105	-7.36	-0.0606	-17.959	1.7604
$\eta=2$	$\alpha = 0.001$	$f_0 = 10$	0.0452	-2.60	-0.0706	-6.678	0.9709
		$f_0 = 100$	0.0387	-5.12	-0.0773	-10.537	1.2834
		$f_0 = 1000$	0.0255	-21.63	-0.1093	-34.005	2.8555
	$\alpha = 0.0001$	$f_0 = 10$	0.0164	-2.21	-0.0271	-8.347	0.7395
		$f_0 = 100$	0.0149	-3.13	-0.0317	-9.849	0.8876
		$f_0 = 1000$	0.0105	-9.38	-0.0577	-19.485	1.7670
$\eta=-2$	$\alpha = 0.001$	$f_0 = 10$	0.0472	1.53	-0.0749	-3.723	0.8928
		$f_0 = 100$	0.0395	-1.02	-0.0823	-7.644	1.2304
		$f_0 = 1000$	0.0255	-17.38	-0.1171	-30.959	2.8639
	$\alpha = 0.0001$	$f_0 = 10$	0.0175	1.82	-0.0295	-5.129	0.6553
		$f_0 = 100$	0.0155	0.88	-0.0347	-6.717	0.8206
		$f_0 = 1000$	0.0106	-5.35	-0.0639	-16.430	1.7532

Table 5.17: Values corresponding to the transition point B between point contact and no contact for the Dugdale force DMT-type analysis when $c=0.4$

		Curve	d	q	δ	p	m_d
$\eta=0$	$\alpha = 0.001$	$\xi_0 = 500$	0.0211	-10.62	-0.0327	-0.095	4.3872
		$\xi_0 = 5000$	0.0143	-75.84	-0.0830	-26.234	9.3586
	$\alpha = 0.0001$	$\xi_0 = 500$	0.0075	-3.68	-0.0140	2.724	3.5507
		$\xi_0 = 5000$	0.0055	-27.95	-0.0582	-7.014	6.4638
$\eta=2$	$\alpha = 0.001$	$\xi_0 = 500$	0.0211	-12.63	-0.0316	-0.389	4.4053
		$\xi_0 = 5000$	0.0143	-77.90	-0.0813	-26.612	9.3548
	$\alpha = 0.0001$	$\xi_0 = 500$	0.0075	-5.67	-0.0134	2.446	3.5793
		$\xi_0 = 5000$	0.0055	-29.95	-0.0567	-7.332	6.4666
$\eta=-2$	$\alpha = 0.001$	$\xi_0 = 500$	0.0212	-8.61	-0.0338	0.198	4.3685
		$\xi_0 = 5000$	0.0143	-73.77	-0.0848	-25.856	9.3625
	$\alpha = 0.0001$	$\xi_0 = 500$	0.0075	-1.68	-0.0146	3.000	3.5210
		$\xi_0 = 5000$	0.0055	-25.94	-0.0599	-6.697	6.4609

Chapter 6. Comparison of Experimental, Finite Element, and Analytical Results

6.1 INTRODUCTION

In conjunction with the analytical work that was conducted for this thesis, a finite element analysis and experimental work were also performed. Jia Qi, a Ph.D. student working with Dr. David Dillard of the Engineering Science and Mechanics Department at Virginia Polytechnic Institute and State University, has conducted a series of JKR-type tests involving thin, flexible strips of PDMS (polydimethylsiloxane). The commercial brand of PDMS used for these experiments was SYLGARD 184 manufactured by Dow Corning. The ends of the PDMS strips were lifted, bent, and fixed vertically at a known distance apart. The angle of the PDMS strip at the fixed end was $\theta=\pi/2$. The width, thickness, and length of the PDMS were measured and recorded. Samples of the PDMS were tested in tension to obtain a stress-strain curve, from which the modulus of elasticity (E) was calculated. The value of the moment of inertia was found using $I = bh^3/12$.

To conduct the experiments, it was necessary to orient the sample such that it was rotated 180 degrees from that shown in Figure 3.1. For tests 4 and 5, before the specimen was tested, it was blown with a volume static eliminator in an attempt to eliminate the effects of static electricity. The fixed ends of the sample were then moved upward and the strip made contact with the flat, rigid, horizontal substrate which was also coated with the PDMS. Since the two solids in contact were of the same material, the equation for the work of adhesion, $\Delta\gamma = \gamma_1 + \gamma_2 - \gamma_{12}$, was reduced to $\Delta\gamma = 2\gamma_1$. In order to measure the contact length using the microscope, it was necessary to use a clear substrate such as glass. The upward movement of the sample was controlled by a manual crank which measured the vertical position (and ultimately, the vertical displacement) of the sample.

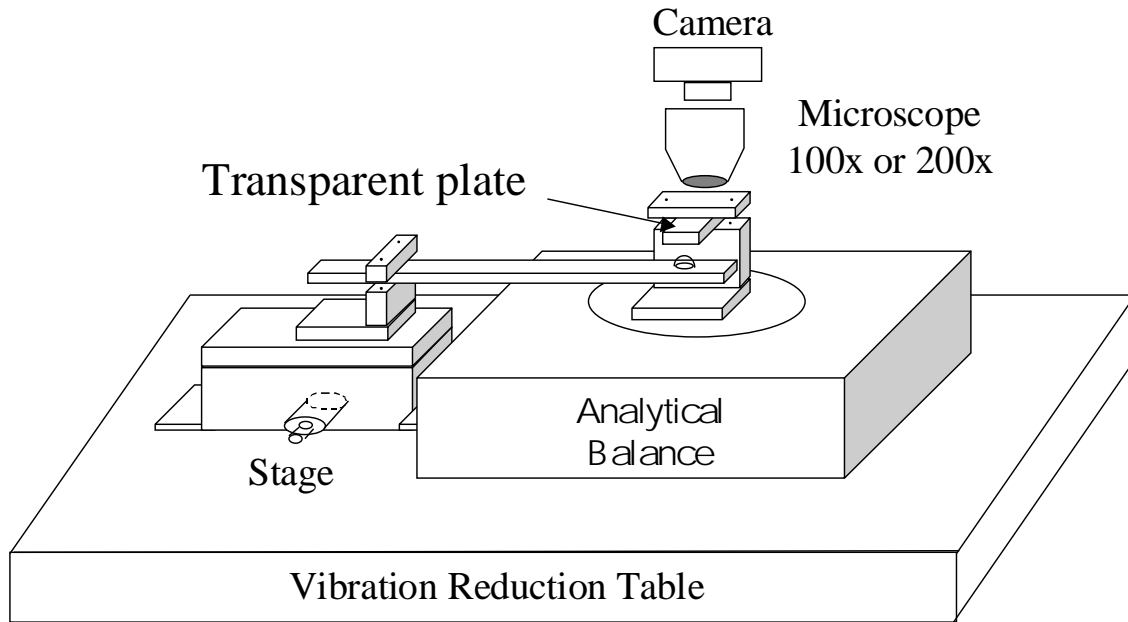


Figure 6.1 Set-Up Used for Experimental Tests (Courtesy of Jia Qi)

Values of the applied vertical force were measured using the balance. The test set-up can be seen in Figure 6.1.

In order to compare the experimental data with the analytical data, it was necessary to nondimensionalize the dimensions of the elastica, the work of adhesion, and the measured test parameters (i.e., the vertical force, contact length, and vertical displacement). This was accomplished by using the formulas in Table 3.1 and Equation 3.5. Once the values of the nondimensionalized separation distance between the clamped ends and the work of adhesion were calculated, the corresponding JKR-type analytical curve could be identified and compared to the experimental results. The self-weight of the test specimen was originally assumed to be zero ($\eta=0$); however, the self-weight term was later calculated and included in the JKR-type analysis for Test 4.

In addition to conducting experimental tests that could be compared to the JKR-type analysis performed for this thesis, Jia Qi also developed a finite element model. Dimensional values for the length, width, thickness, separation distance between the clamped ends, modulus of elasticity, and moment of inertia of the PDMS strip were specified. ABAQUS was then used to determine values for the applied vertical force and the contact area. The contact area was divided by the width of the strip to obtain a value for the contact length. This finite element model did not account for adhesion forces; therefore, the results obtained from the finite element analysis (FEA) were compared to those obtained analytically by Plaut et al. (1999) which also ignored the presence of adhesion forces. Additionally, the self-weight of the strip was assumed to be zero in the analytical solution.

In order to compare the results of the FEA to the analytical results obtained by Plaut et al. it was necessary to nondimensionalize the separation distance between the clamped ends, the contact length, and the vertical applied force using the equations supplied in Table 3.1. Once the nondimensionalized separation distance c was determined, the appropriate analytical curve was chosen and compared to the results of the FEA.

6.2 COMPARISON OF ANALYTICAL AND EXPERIMENTAL RESULTS

The experimental results obtained through the testing procedure described in Section 6.1 were compared to the analytical results obtained for the corresponding c and $\Delta\gamma$ values. The dimensions and material properties of the test specimens used in Tests 1-5 can be found in Tables 6.1-6.5. Additionally, the contact length vs. vertical force relationships for Tests 1-5 and the contact length vs. vertical displacement relationships for Tests 4 and 5 (a, b, and c) can be found in Figures 6.2-6.12. Figures 6.13-6.15 respectively plot the contact length vs. the vertical force, the contact length vs. the vertical displacement, and the vertical displacement vs. the vertical force for Test 4 when the self-weight of the

PDMS strip was included in the JKR-type analysis. The experimental data in these plots remained the same as that shown in Figures 6.5 and 6.6.

The dimensions and material properties of the test specimen used in Test 1 can be found in Table 6.1. The values obtained for the nondimensionalized work of adhesion $\Delta\gamma$ and separation distance c between the clamped ends were 0.0812 and 0.4001, respectively. The analytical curve of the contact length vs. vertical force for line contact when $c=0.4$ and $\Delta\gamma=0.0812$ was derived using the governing equations and end conditions described in Chapter 4, Section 1 for a JKR-type analysis when $\Delta\gamma>0$ and line contact was experienced. Additionally, the analytical curve for contact length vs. vertical force when $c=0.4$ and $\Delta\gamma=0$, which was originally obtained for the JKR-type analysis, was plotted along with the experimental and analytical curves for $c=0.4$ and $\Delta\gamma=0.0812$ (see Figure 6.2). The experimental data, which is represented by the individual data points on the plot of the contact length vs. the vertical force, shows both the loading and unloading curves. The loading curve starts at $q=6.60$ and $b=0.015$ (point A) and the vertical force is increased until $q=14.21$ and $b=0.105$. The loading is then steadily decreased until $q=0$. Note that the points on the unloading curve exhibit larger values for the contact length than the points on the loading curve (at a fixed value of q). Since the elastica was still in contact with the substrate when the vertical load equaled zero, a negative or upward force was applied to pull the elastica off of the surface of the substrate. The last vertical force and contact length measurements taken before the elastica separated from the substrate were $q=-2.43$ and $b=0.0032$. The self-weight η was assumed to be zero for both curves obtained analytically.

Table 6.1: Test Specimen Data for Test 1

TEST 1		
Modulus of Elasticity:	2.25 MPa	Work of Adhesion: 0.0812
Moment of Inertia:	$1.14 \times 10^{-15} \text{ m}^4$	
Work of Adhesion _{DIM} :	43.6 mJ/m^2	
Actual Dimensions (for Half of the Specimen)		Nondimensionalized Values
Width (W)	0.876 mm	0.1082
Length (L)	8.0934 mm	1.0000
Thickness (T)	0.25 mm	0.0309
Separation Distance (C)	3.238 mm	0.4001

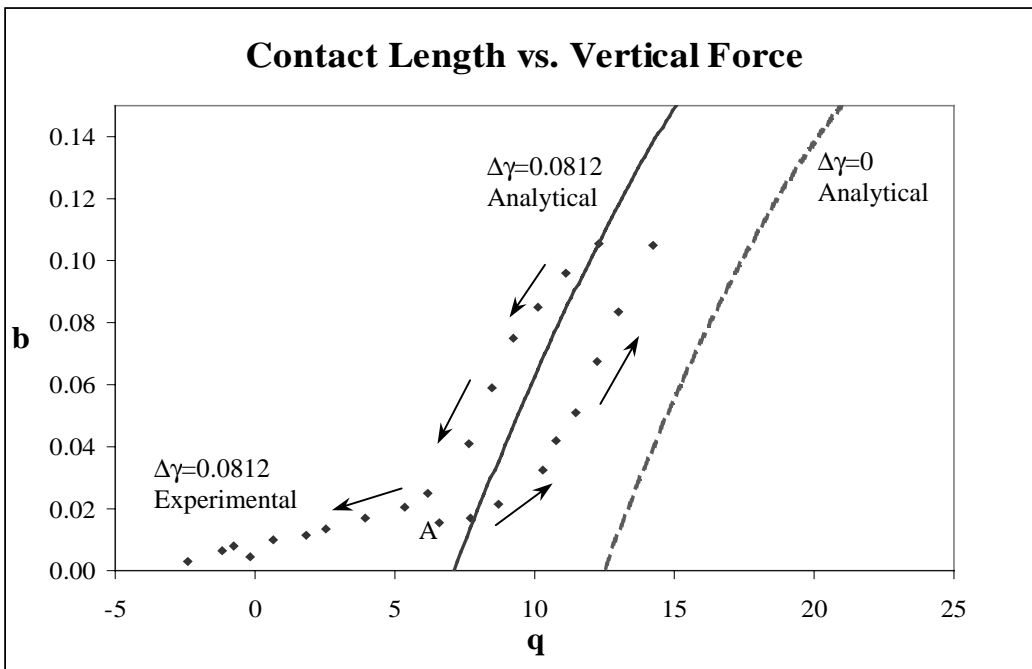


Figure 6.2: Contact Length vs. Vertical Force for c=0.4 (Test 1)

Table 6.2 contains the dimensions, material properties, and nondimensionalized parameters for the specimen used in Test 2. The calculated values of the nondimensionalized work of adhesion $\Delta\gamma$ and separation distance c between the clamped ends of the elastica were 0.2064 and 0.2509, respectively. Since the contact length and vertical force were the only two parameters that were measured during testing, the only relationship that could be plotted was the contact length vs. the vertical force (Figure 6.3). The analytical curve for line contact when $c=0.2509$ and $\Delta\gamma=0.2064$ was derived using the governing equations and end conditions described in Chapter 4, Section 1 for a JKR-type analysis when $\Delta\gamma>0$ and line contact was experienced. Additionally, the analytical curve for $c=0.2509$ and $\Delta\gamma=0$ was found by using the governing equations and end conditions described in Chapter 4, Section 1 for a JKR-type analysis when line contact was experienced and $\Delta\gamma=0$. The experimental data, which is represented by the individual data points on the plot of the contact length vs. the vertical force, shows both the loading and unloading curves and denotes them with arrows. The loading curve starts at $q=22.22$ and $b=0.013$ (point A) and the vertical force is increased until $q=39.39$ and $b=0.096$. The loading is then steadily decreased until $q=0$. Note that the points on the unloading curve exhibit larger values for the contact length b than the points on the loading curve (at a fixed value of q). Since the elastica was still in contact with the substrate when the vertical load equaled zero, a negative or upward force was applied to pull the elastica off of the surface of the substrate. The last vertical force and contact length measurements taken before the elastica separated from the substrate were $q=-4.49$ and $b=0.0032$. The self-weight η was assumed to be zero for both curves obtained analytically.

The dimensions, material properties, and nondimensionalized parameters of the test specimen used for Test 3 can be found in Table 6.3. Additionally, Figure 6.4 plots the contact length vs. the vertical force relationship for the analytical and experimental data when $c=0.3515$ and $\Delta\gamma=0.1052$, and for the analytical data when $c=0.3515$ and $\Delta\gamma=0$. The values for the analytical curve when $c=0.3515$ and $\Delta\gamma=0.1052$ were obtained using the

governing equations and end conditions described in Chapter 4, Section 1 for a JKR-type analysis when $\Delta\gamma > 0$ and line contact was experienced. The values for the analytical curve when $c=0.2509$ and $\Delta\gamma=0$ were found by using the governing equations and end conditions described in Chapter 4, Section 1 for a JKR-type analysis when line contact was experienced and $\Delta\gamma=0$. As in Tests 1 and 2, the experimental data seen in Figure 6.4 shows both a loading and an unloading curve. The loading curve begins when $q=13.55$ and $b=0.017$ (point A) and continues until $q=25.22$ and $b=0.113$. At this point, the loading is decreased. The unloading curve terminates when $q=1.34$ and $b=0.007$. Therefore, no pull-off force was required to separate the elastica from the rigid surface. The self-weight η was assumed to be zero for both curves obtained analytically.

Table 6.2: Test Specimen Data for Test 2

TEST 2		
Modulus of Elasticity:	2.25 MPa	Work of Adhesion: 0.2064
Moment of Inertia:	$1.75 \times 10^{-15} \text{ m}^4$	
Work of Adhesion _{DIM} :	43.6 mJ/m^2	
Actual Dimensions (for Half of the Specimen)		Nondimensionalized Values
Width (W)	1.341 mm	0.1039
Length (L)	12.903 mm	1.0000
Thickness (T)	0.25 mm	0.0194
Separation Distance (C)	3.238 mm	0.2509

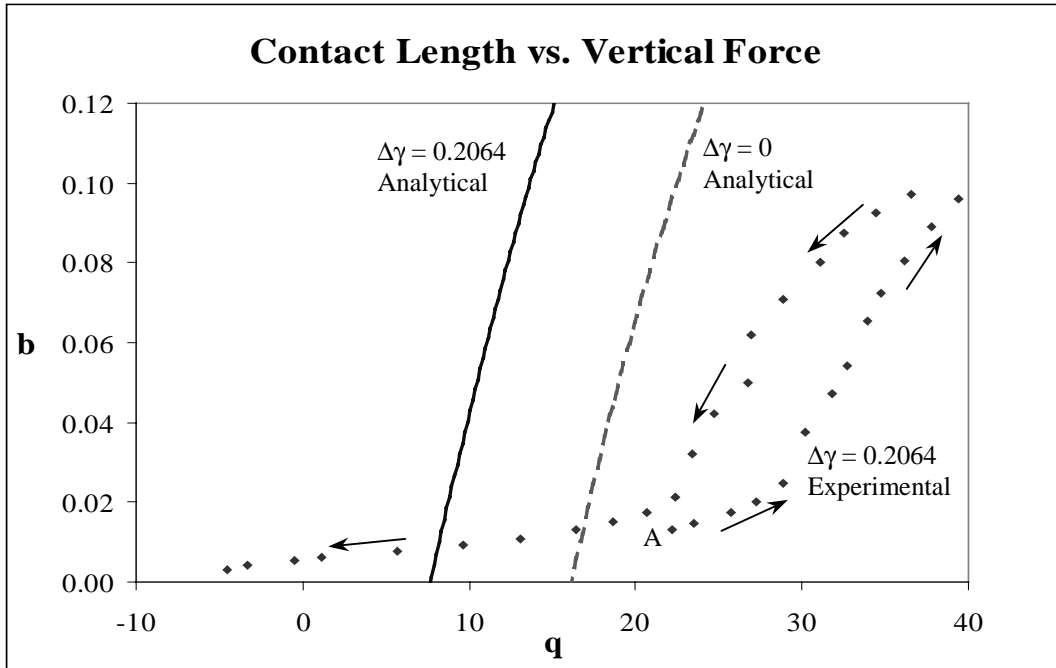


Figure 6.3: Contact Length vs. Vertical Force for $c=0.2509$ (Test 2)

Table 6.3: Test Specimen Data for Test 3

TEST 3		
Modulus of Elasticity:	2.25 MPa	Work of Adhesion: 0.1052
Moment of Inertia:	$1.39 \times 10^{-15} \text{ m}^4$	
Work of Adhesion _{DM} :	43.6 mJ/m^2	
Actual Dimensions (for Half of the Specimen)		Nondimensionalized Values
Width (W)	1.066 mm	0.1157
Length (L)	9.212 mm	1.0000
Thickness (T)	0.25 mm	0.0271
Separation Distance (C)	3.238 mm	0.3515

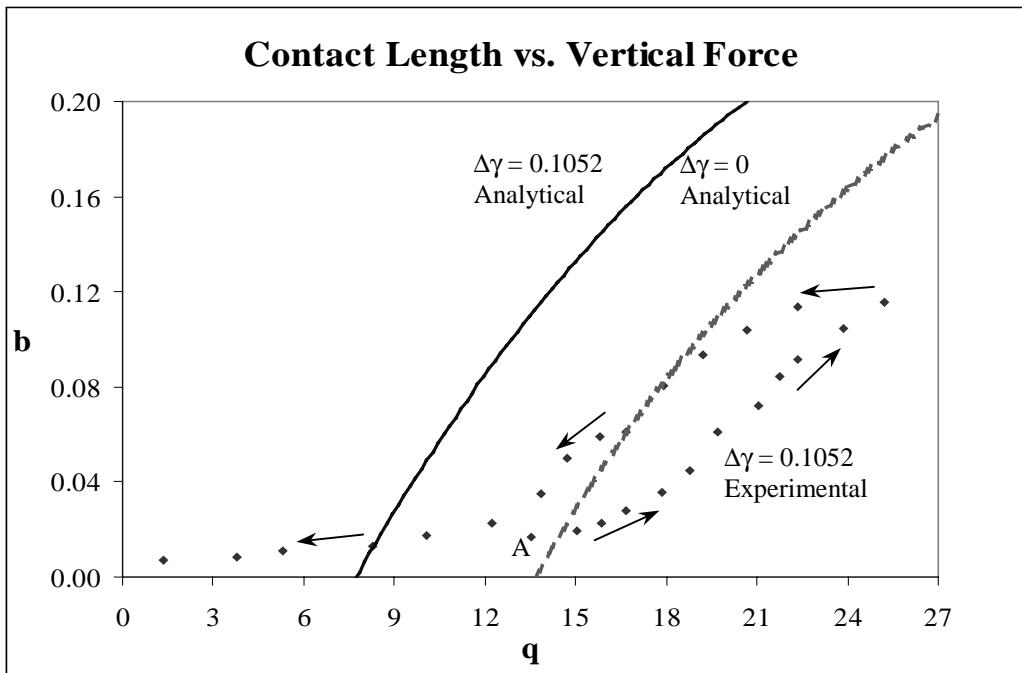


Figure 6.4: Contact Length vs. Vertical Force for $c=0.3515$ (Test 3)

Table 6.4 contains the dimensions, material properties, and nondimensionalized parameters for the specimen used in Test 4. The calculated values of the nondimensionalized work of adhesion $\Delta\gamma$ and separation distance c between the clamped ends of the elastica were 0.4186 and 0.5348, respectively. For Test 4, the contact length, vertical force, and vertical displacement were measured. The contact length vs. vertical force relationship can be found in Figure 6.5, while the contact length vs. vertical displacement relationship is located in Figure 6.6. The values for the analytical curve when $c=0.5348$ and $\Delta\gamma=0.4186$ were obtained using the governing equations and end conditions described in Chapter 4, Section 1 for a JKR-type analysis when $\Delta\gamma>0$ and line contact was experienced. The values for the analytical curve when $c=0.5348$ and $\Delta\gamma=0$ were found by using the governing equations and end conditions described in Chapter 4,

Section 1 for a JKR-type analysis when line contact was experienced and $\Delta\gamma=0$. The raw data from the experimental tests was converted to a nondimensional form using the formulas $b=B/L$, $q=QL^2/(EI)$, and $\delta=\Delta/L$. The experimental data is shown as individual data points on the contact length vs. vertical force plot. Both the loading and unloading curves are shown in Figures 6.5 and 6.6. The loading curve begins when $q=10.72$, $\delta=0$, and $b=0.049$ (point A). The vertical loading and vertical displacement increased until $q=27.78$, $\delta=0.137$, and $b=0.167$. At this point, the vertical displacement (and therefore the vertical force q) was decreased. The last vertical force, vertical displacement, and contact length measurements taken before the elastica separated from the substrate were $q = -13.36$, $\delta= -0.130$, and $b=0.010$. Note that the loading and unloading curves in the contact length vs. vertical force plot for Test 4 cross at approximately $q=15$. Therefore, when $q<15$, the loading curve exhibits larger values for the contact length than the unloading curve (for a fixed value of q). When $q>15$, the unloading curve exhibits larger values for the contact length than the loading curve (for a fixed value of q). The loading and unloading curves in the contact length vs. vertical displacement plot do not cross and the unloading curve always produces larger values for the contact length (at a fixed value of δ). The self-weight η was assumed to be zero for both curves obtained analytically.

Table 6.4: Test Specimen Data for Test 4

TEST 4		
Modulus of Elasticity:	2.25 MPa	Work of Adhesion: 0.4186
Moment of Inertia:	$1.39 \times 10^{-15} \text{ m}^4$	
Work of Adhesion _{DIM} :	43.6 mJ/m^2	
Actual Dimensions (for Half of the Specimen)		Nondimensionalized Values
Width (W)	0.579 mm	0.0945
Length (L)	6.124 mm	1.0000
Thickness (T)	0.25 mm	0.0408
Separation Distance (C)	3.275 mm	0.5348

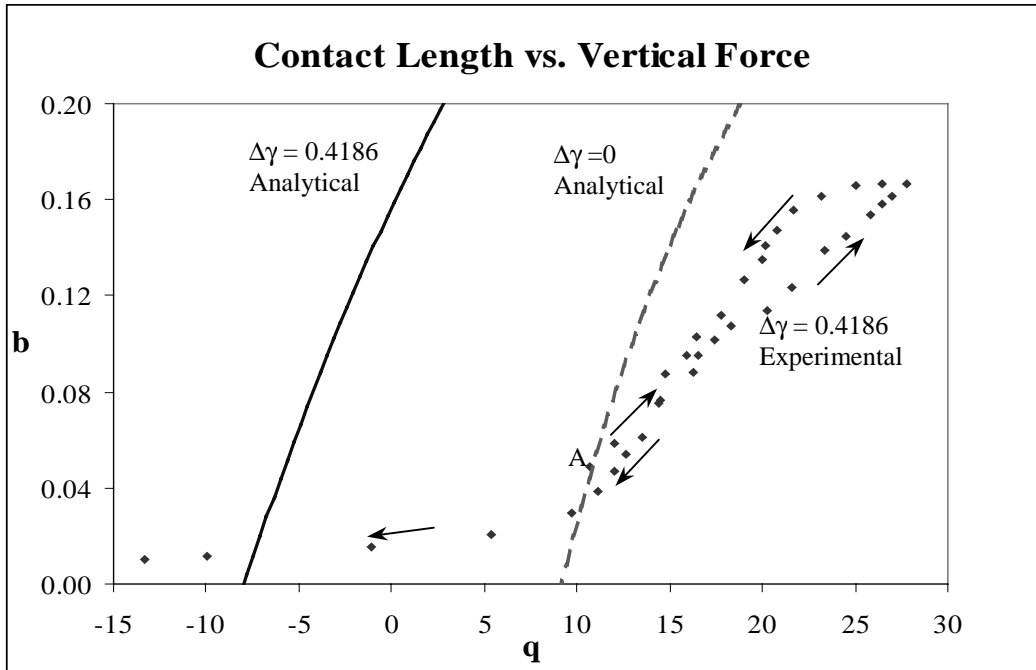


Figure 6.5: Contact Length vs. Vertical Force for $c=0.5348$ (Test 4)

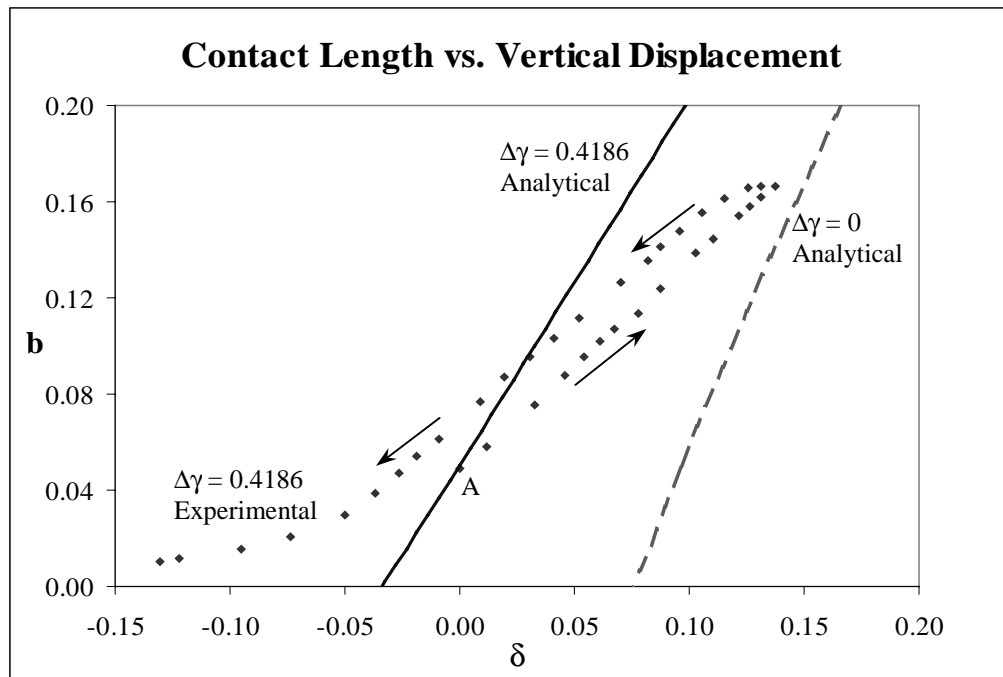


Figure 6.6: Contact Length vs. Vertical Displacement for $c=0.5348$ (Test 4)

The dimensions, material properties, and nondimensionalized parameters of the test specimen used for Tests 5 a, b, and c can be found in Table 6.5. The values for the work of adhesion $\Delta\gamma$ and separation distance c between the clamped ends of the elastica for this test were $\Delta\gamma=1.223$ and $c=0.4305$. For Test 5, a slightly different approach was taken. The specimen used in Test 5 was first tested using a 5 minutes/step loading protocol with a total of 15 steps and a 10 minutes/step unloading protocol with a total of 22 steps. This allowed for the measurement of the contact length, vertical force, and vertical displacement of the elastica after it had achieved a static, stable state for each step. After approximately 24 hours had passed, the same test specimen was loaded and unloaded again (Test 5b). The same loading and unloading protocols and number of steps were used as in Test 5a. Values were obtained for the contact length, vertical force, and vertical displacement. Finally, approximately 24 hours after Test 5b was completed, Test 5c was conducted. This time, a 5 minutes/step loading procedure with a total of 8 steps was used and a 10 minute/step unloading procedure with a total of 11 steps was used. Values for the vertical force, vertical displacement, and contact length at the beginning of each loading curve (point A), at the point of largest vertical displacement, and at the conclusion of each test can be found in Table 6.6. Note that the loading and unloading curves cross in the contact length vs. vertical force plot for Test 5a. The loading and unloading curves in the contact length vs. vertical displacement plot for Tests 5a, b, and c do not cross and the unloading curve produces a larger value for the contact length (at a fixed value of δ). Figures 6.7-6.12 show the contact length vs. vertical force and contact length vs. vertical displacement relationships for the experimental results obtained from Tests 5 a, b, and c. These experimental results were plotted in conjunction with the analytical results for $c=0.4305$ and $\Delta\gamma=1.223$, and $c=0.4305$ and $\Delta\gamma=0$. The values of b , q , and δ used in the analytical curves were obtained by using the shooting method along with the appropriate governing equations and boundary conditions described in Chapter 4. The self-weight η was assumed to be zero for this test.

Table 6.5: Test Specimen Data for Test 5 (a, b, and c)

TEST 5 (a, b, c)		
Modulus of Elasticity:	2.25 MPa	Work of Adhesion: 1.223
Moment of Inertia:	$1.39 \times 10^{-15} \text{ m}^4$	
Work of Adhesion _{DIM} :	43.6 mJ/m ²	
Actual Dimensions (for Half of the Specimen)		Nondimensionalized Values
Width (W)	0.921 mm	0.1229
Length (L)	7.491 mm	1.0000
Thickness (T)	0.100 mm	0.0133
Separation Distance (C)	3.225 mm	0.4305

Table 6.6: Experimental Values for b, q, and δ

Test	Time	b	q	δ
Test 5a	Start of Test	0.028	25.44	0
	Point of Largest δ	0.108	60.19	0.126
	Conclusion of Test	0.009	-40.49	-0.134
Test 5b	Start of Test	0.028	28.30	0.000
	Point of Largest δ	0.109	62.17	0.126
	Conclusion of Test	0.009	*	-0.134
Test 5c	Start of Test	0.030	22.02	0.000
	Point of Largest δ	0.113	60.37	0.126
	Conclusion of Test	0.010	-50.70	-0.134
* Due to an error which occurred during testing, the value of q at this point is not available				

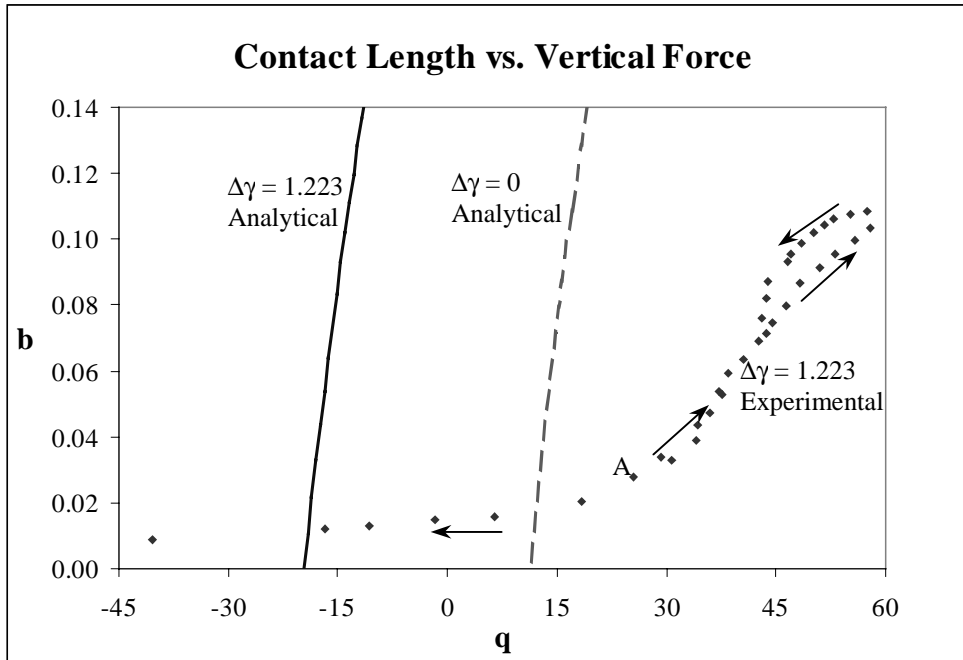


Figure 6.7: Contact Length vs. Vertical Force for $c=0.4305$ (Test 5a, Day 1)

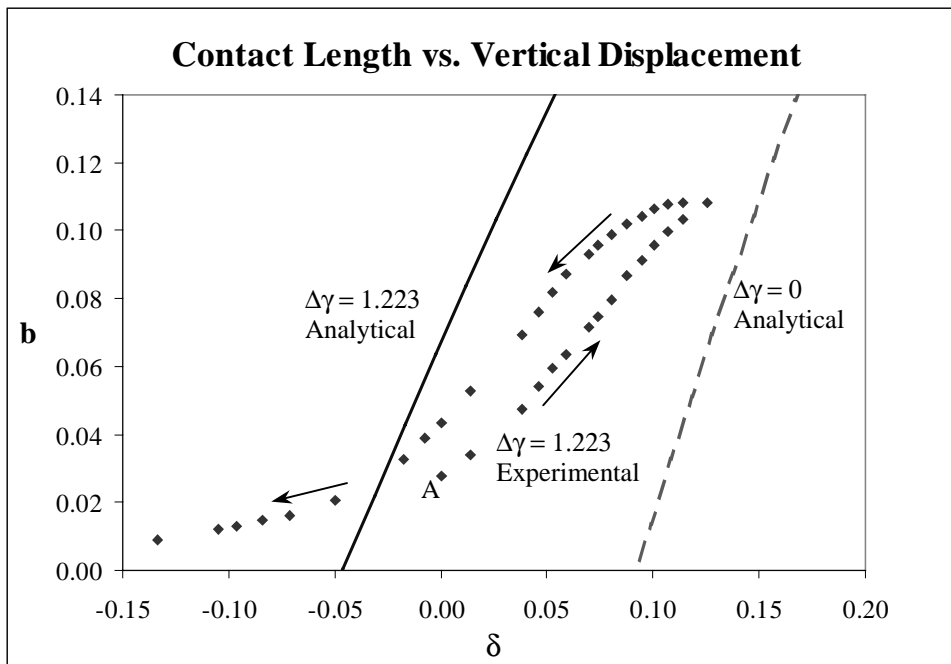


Figure 6.8: Contact Length vs. Vertical Displacement for $c=0.4305$ (Test 5a, Day 1)

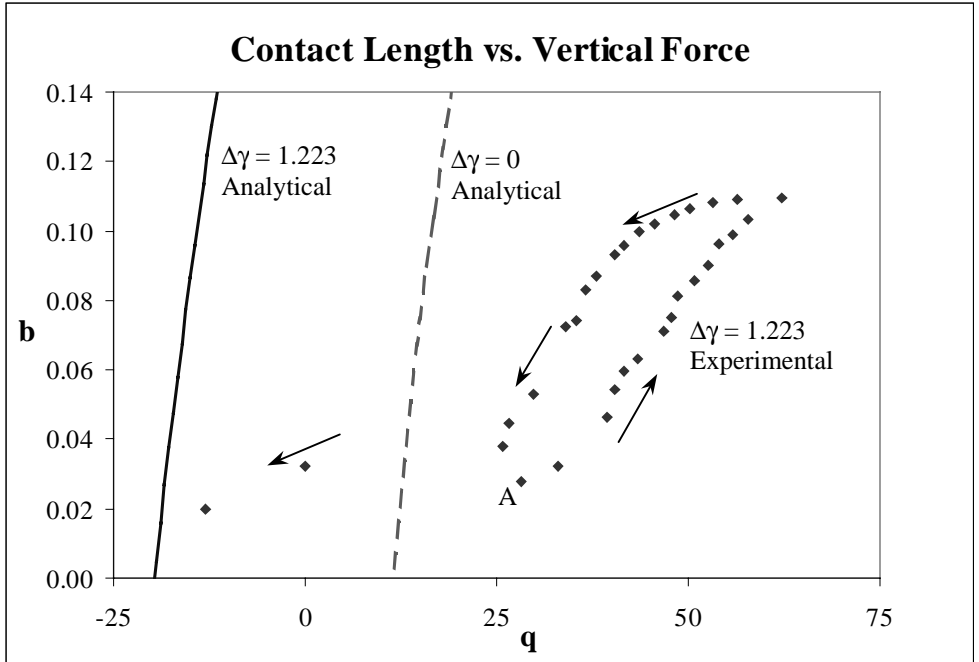


Figure 6.9: Contact Length vs. Vertical Force for $c=0.4305$ (Test 5b, Day 2)

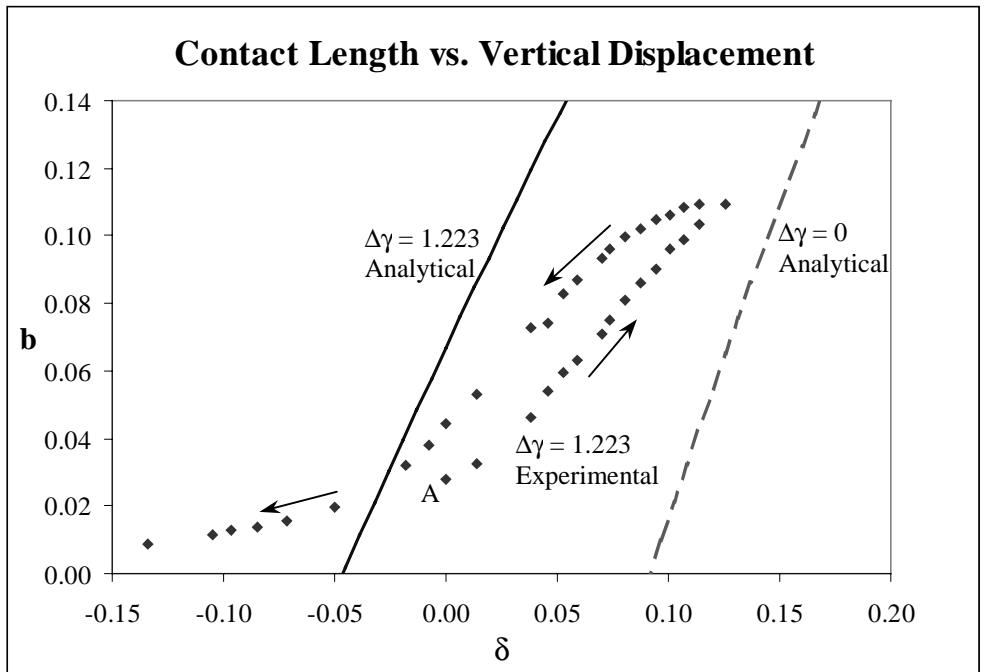


Figure 6.10: Contact Length vs. Vertical Displacement for $c=0.4305$ (Test 5b, Day 2)

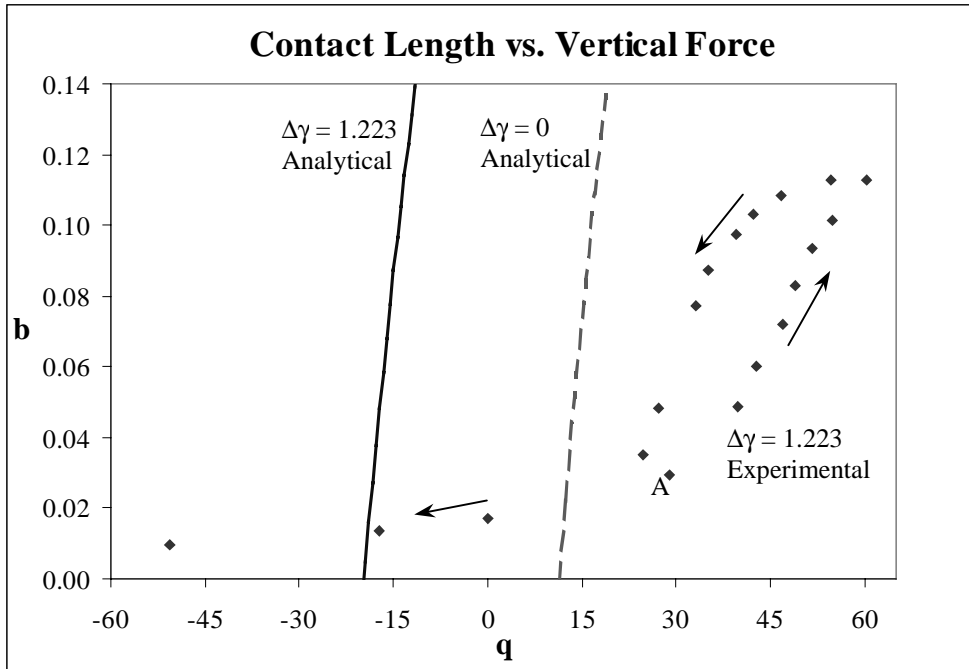


Figure 6.11: Contact Length vs. Vertical Force for $c=0.4305$ (Test 5c, Day 3)

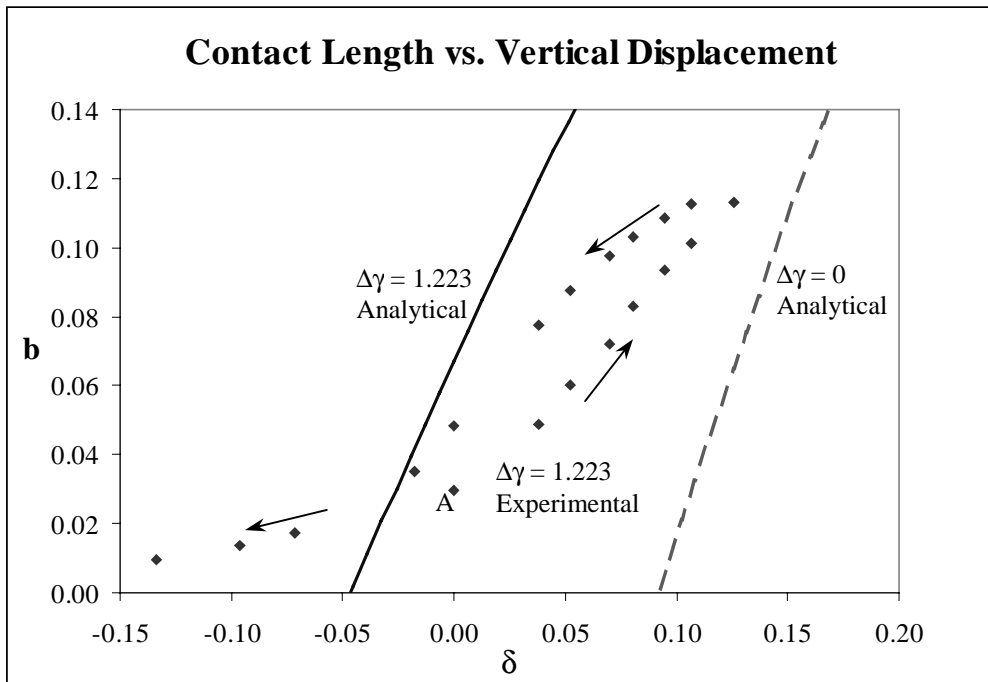


Figure 6.12: Contact Length vs. Vertical Displacement for $c=0.4305$ (Test 5c, Day 3)

To examine the effect of the self-weight on the JKR-type analysis, and to investigate whether better agreement between the experimental and analytical results could be attained by considering the self-weight of the elastica, the specific gravity of the PDMS was obtained from the product information guide (s.g.=1.05 at 25 degrees C). The specific gravity was used to calculate the density of the material. The density was then nondimensionalized to obtain a value for η . For a specific gravity of 1.05, the self-weight of the elastica was -0.91 . The analytical values for b , q , and δ when $c=0.5348$, $\eta= -0.91$, and $\Delta\gamma=0.4186$ were obtained using the governing equations and end conditions described in Chapter 4, Section 1 for a JKR-type analysis when $\Delta\gamma>0$, line contact was experienced, and the self-weight of the elastica was included. Similarly, the analytical values for b , q , and δ when $c=0.5348$, $\eta= -0.91$, and $\Delta\gamma=0$ were obtained using the governing equations and end conditions described in Chapter 4 Section 1 for a JKR-type analysis when $\Delta\gamma=0$, line contact was experienced, and the self-weight of the elastica was included. The experimental data plotted in the contact length vs. vertical force, contact length vs. vertical displacement, and vertical displacement vs. vertical force plots was the same as the experimental data seen in Figures 6.5 and 6.6. Both analytical curves in Figure 6.15 represented line contact solutions only ($b>0$) and terminated when $b=0$.

The experimental testing conducted by Jia Qi is ongoing. New testing equipment is being used in the hopes of increasing the accuracy of the data obtained. A more detailed account of testing procedures and results will be included in Jia Qi's M.S. thesis.

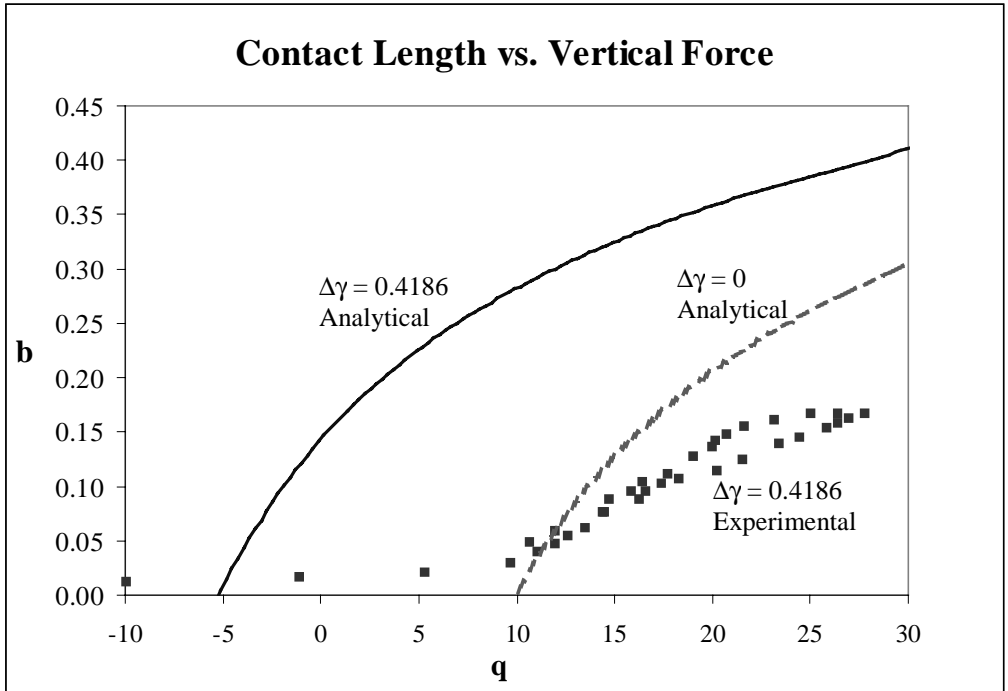


Figure 6.13: Contact Length vs. Vertical Force for $c=0.5348$, $\eta=-0.91$ (Test 4)

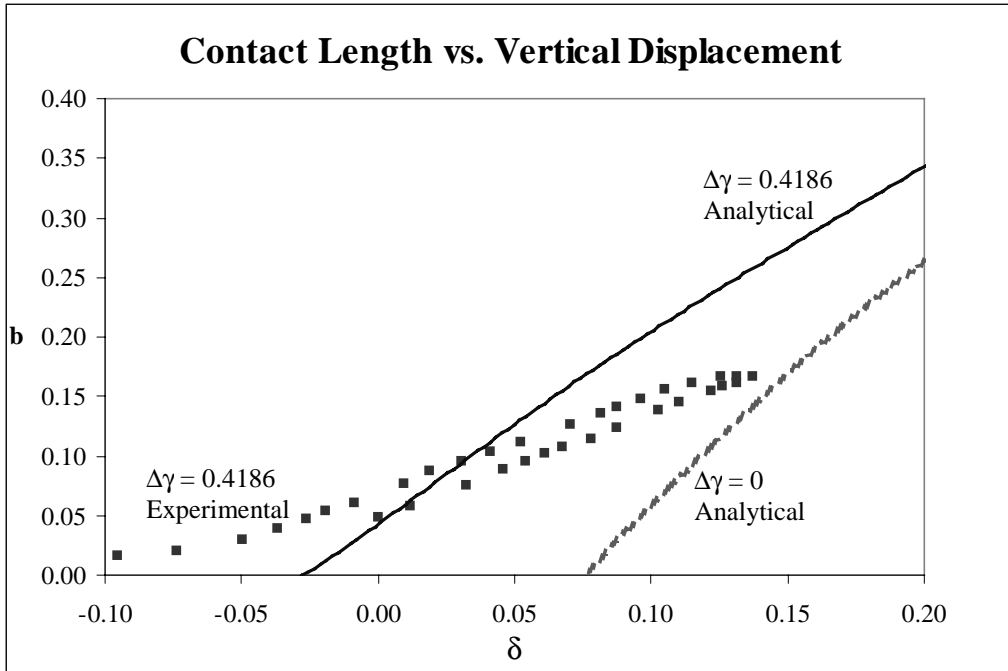


Figure 6.14: Contact Length vs. Vertical Displacement for $c=0.5348$, $\eta=-0.91$ (Test 4)

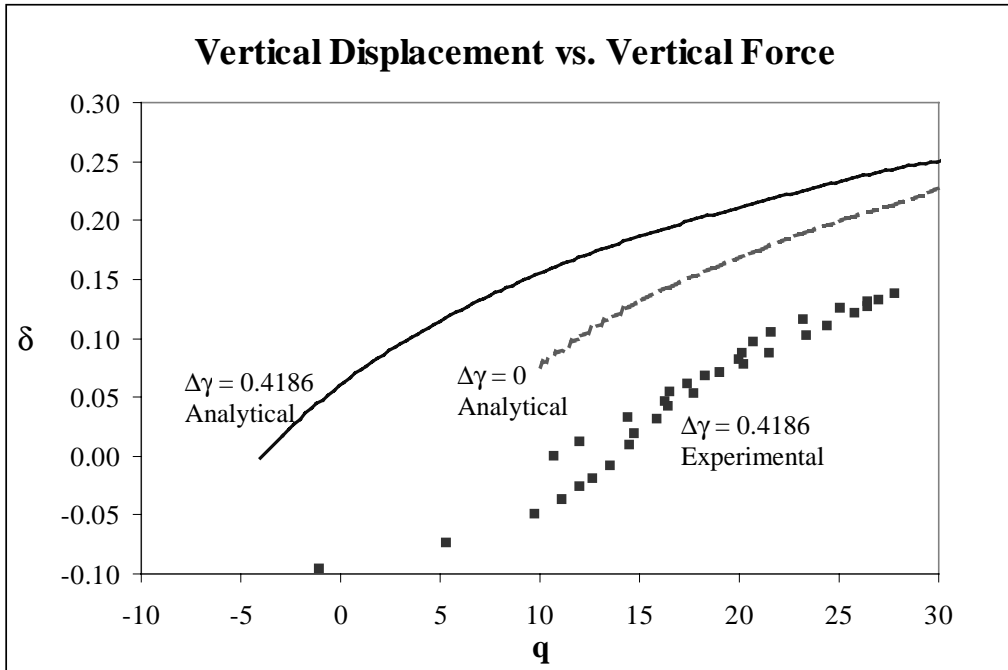


Figure 6.15: Vertical Displacement vs. Vertical Force for $c=0.5348$, $\eta=-0.91$ (Test 4)

6.3 COMPARISON OF THE FINITE ELEMENT AND ANALYTICAL RESULTS

In addition to conducting a series of JKR-type experiments, Jia Qi also developed a finite element model. Values for the dimensional width, length, thickness, and modulus of elasticity of the test strip were specified and ABAQUS was used to solve for the contact length at various values of the vertical force. The values obtained through the finite element analysis (FEA) were then nondimensionalized using the equations in Table 3.1 in order to compare the FEA results to the analytical results. Since the FEA did not include adhesion forces, the values obtained from the FEA were compared to the values calculated by Plaut et al. (1999) for the contact length. Note also that the self-weight of the elastica was ignored. Once the nondimensionalized separation distance c between the clamped ends of the elastica was determined for the FEA, the analytical curve for the corresponding c value could be identified and compared to the curve obtained by the FEA. The dimensions and material properties of the test strips can be found in Tables

6.7-6.9. Additionally, plots of the contact length vs. vertical force for FEA 1-3 can be found in Figures 6.16-6.18.

Although the finite element model did not include the effect of adhesion forces, it did take into account the anticlastic bending of the strip. As the strip is pushed down onto the surface, initial contact occurs at the edges of the strip (at midlength between its ends) due to anticlastic curvature. Then the contact zone spreads across the width of the strip and propagates towards its ends, with curved fronts. The values obtained for the contact length in tests FEA 1-3 were obtained by determining the last node in the FEA mesh that experienced contact pressure. This node was then considered to be the edge of the contact zone and the distance from the center of the elastica to the node was calculated and denoted as the contact length.

The separation distance c between the clamped ends of the elastica was $c=0.4$ for FEA 1. Values specified for the vertical force and obtained for the contact length through the FEA were nondimensionalized and plotted against the analytical data. To obtain the value for the nondimensional vertical force q , the equation $q=17.45Q$ was used. This equation was derived from Table 3.1. Figure 6.16 shows the comparison of the analytical and FEA results. In Figure 6.16, the analytical curve began at $b=0, q=0$ (before which there was no applied vertical force and the strip was not in contact with the substrate). At $b=0, q=0$, point contact between the elastica and the substrate was established. Point contact continued for the analytical curve until approximately $q=12.5$. When $q>12.5$, the elastica spread, causing the contact length b to become greater than zero. The finite element results have the same form as the analytical results but predict a larger contact length at a given value of the force.

Figures 6.17 and 6.18 yielded results similar to those obtained in Figure 6.16. Figure 6.17 shows the finite element and analytical results when $c=0.6$. The analytical curve began at $b=0, q=0$ (before which there was no applied vertical force and the strip was not

in contact with the substrate). At $b=0$, $q=0$, point contact between the elastica and the substrate was established. Point contact continued for the analytical curve until approximately $q=7.6$. When $q>7.6$, the elastica spread, causing the contact length b to become greater than zero. Values obtained analytically and through the finite element analysis had good agreement, although the finite element results yielded slightly higher values for the contact length at a specified value for the vertical force.

Figure 6.18 shows the finite element and analytical results when $c=0.8$. The analytical curve began at $b=0$, $q=0$ (before which there was no applied vertical force and the strip was not in contact with the substrate). At $b=0$, $q=0$, point contact between the elastica and the substrate was established. Point contact continued for the analytical curve until approximately $q=2.5$. When $q>2.5$, the elastica spread, causing the contact length b to become greater than zero. Values obtained analytically and through the finite element analysis for the contact length and the vertical force had fair agreement, although the finite element curve produced slightly larger values for the contact length at specified values of q .

The values obtained for the contact length in tests FEA 1-3 were obtained by determining the last node in the FEA mesh that experienced contact pressure. This node was then considered to be the edge of the contact zone and the distance from the center of the elastica to the node was calculated and denoted as the contact length.

Table 6.7: Test Specimen Data for FEA 1

FEA 1		
Modulus of Elasticity:	2.20 MPa	Work of Adhesion: 0
Moment of Inertia:	$1.30 \times 10^{-3} \text{ mm}^4$	
Work of Adhesion _{DIM} :	0 mJ/m ²	
Actual Dimensions (for Half of the Specimen)		Nondimensionalized Values
Width (W)	1.000 mm	0.100
Length (L)	10.000 mm	1.000
Thickness (T)	0.250 mm	0.025
Separation Distance (C)	4.000 mm	0.400

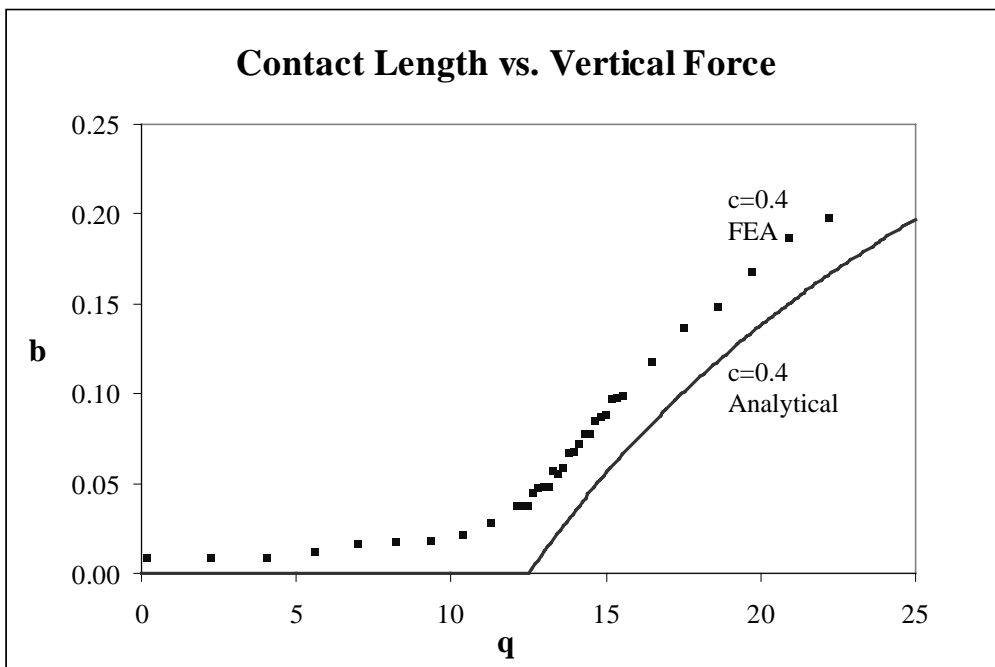


Figure 6.16: Contact Length vs. Vertical Force for c=0.4 (FEA 1)

Table 6.8: Test Specimen Data for FEA 2

FEA 2		
Modulus of Elasticity:	2.20 MPa	Work of Adhesion: 0
Moment of Inertia:	$1.30 \times 10^{-3} \text{ mm}^4$	
Work of Adhesion _{DM} :	0 mJ/m ²	
Actual Dimensions (for Half of the Specimen)		Nondimensionalized Values
Width (W)	1.000 mm	0.100
Length (L)	10.000 mm	1.000
Thickness (T)	0.250 mm	0.025
Separation Distance (C)	6.000 mm	0.600

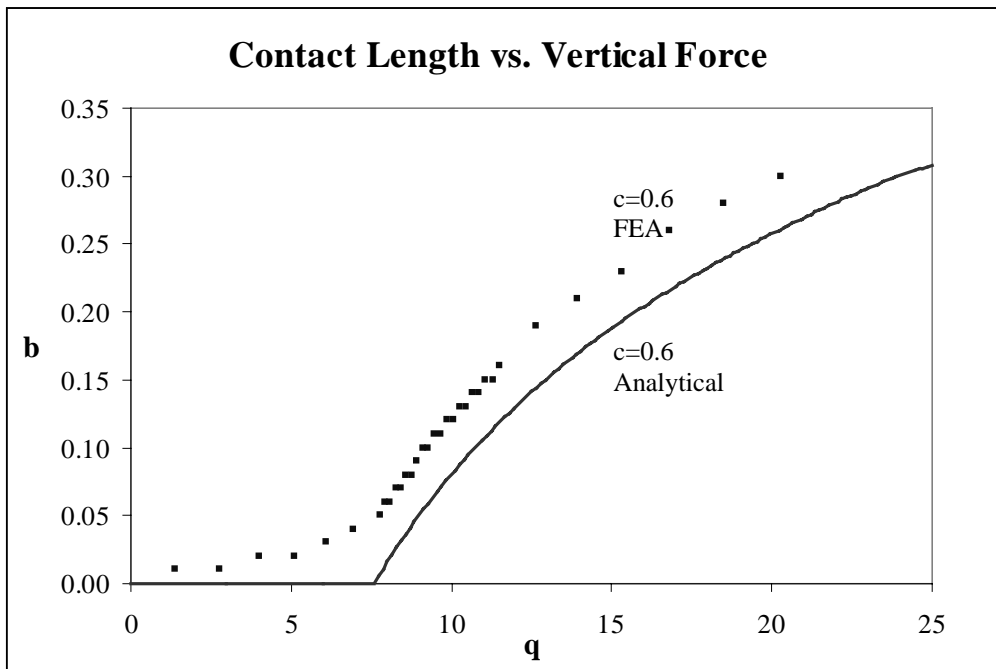


Figure 6.17: Contact Length vs. Vertical Force for c=0.6 (FEA 2)

Table 6.9: Test Specimen Data for FEA 3

FEA 3		
Modulus of Elasticity:	2.20 MPa	Work of Adhesion: 0
Moment of Inertia:	$1.30 \times 10^{-3} \text{ mm}^4$	
Work of Adhesion _{DM} :	0 mJ/m ²	
Actual Dimensions (for Half of the Specimen)		Nondimensionalized Values
Width (W)	1.000 mm	0.100
Length (L)	10.000 mm	1.000
Thickness (T)	0.250 mm	0.025
Separation Distance (C)	8.000 mm	0.800

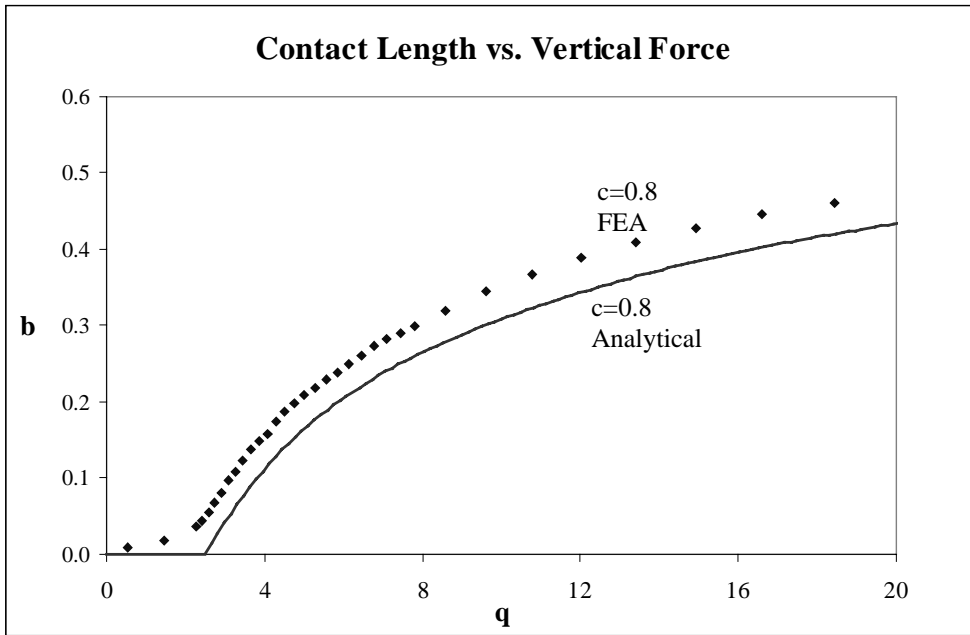


Figure 6.18: Contact Length vs. Vertical Force for $c=0.8$ (FEA 3)

Chapter 7: Conclusions and Recommendations for Future Research

7.1 INTRODUCTION

For this thesis, two different adhesion models were used to investigate the effects of adhesion on the contact of an elastica with a rigid surface. This analysis was carried out in terms of nondimensional quantities. First a JKR-type model was considered. Separation distances of $c=0.4$ and $c=0.8$ between the clamped ends of the elastica were examined and values of $\Delta\gamma=0.16, 0.32, 0.48,$ and 0.64 were used for each c value. The self-weight η of the elastica was also included in the analysis for $c=0.4, \Delta\gamma=0$ and $0.64,$ and $\eta=2, 1, 0, -1,$ and -2 . Next a DMT-type model was considered. Within the DMT-type analysis, two types of force were examined: a linear DMT force and a Dugdale DMT force. For the linear force DMT-type analysis, separation distances of $c=0.4$ and $c=0.8$ were considered, while for the Dugdale force DMT-type analysis, only $c=0.4$ was considered. These DMT forces model an attraction between the elastica and the substrate, which is active from the lift-off point $s=0$ until $s=d$ when the vertical distance y between the solids reaches a specified value of α . Both DMT-type analyses used a variety of values for the distance α and for the maximum DMT force (f_0 or g_0). Additionally, the self-weight of the elastica, $\eta=2, 0,$ and $-2,$ was included in the DMT-type analysis. The following sections contain conclusions drawn from these JKR- and DMT-type analyses. Recommendations for future research are included in the final section.

7.2 JKR-TYPE ANALYSIS

The results from the JKR-type analysis for both $c=0.4$ and $c=0.8$ indicated that as the work of adhesion was increased, the contact length (for fixed values of the vertical force q or the vertical displacement δ) also increased. Therefore, the existence of adhesion forces within the contact area further distorted the shape of the elastica and caused an

elongation of the contact length. Additionally, the results from the JKR-type analysis indicated that the moment at the lift-off point from the substrate was independent of the separation distance c between the clamped ends of the elastica and was independent of the vertical force q . The moment at $s=b$ was solely dependent on the value for the work of adhesion.

The vertical forces and vertical displacements experienced by the elastica as it traveled through the no contact, point contact, and line contact regions were dependent upon two factors: whether the elastica was being pushed onto or pulled off of the substrate, and whether the vertical displacement or the vertical force was being controlled. Figures 4.6-4.10 illustrate the paths experienced by the elastica from no contact to line contact or vice versa. When the vertical force was controlled, the vertical displacement experienced a sudden jump in value. When the vertical displacement was controlled, the vertical force experienced a sudden jump in value. Tables 4.1 and 4.2 supply the values for the contact length, vertical force, vertical displacement, horizontal force, and moment at $s=d$ at points A-M labeled in plots 4.6 through 4.10 for $c=0.4$ and $c=0.8$, respectively. When the value for q was negative at the transition point between point contact and no contact (i.e., Points A and D in Figure 4.6, and Points A, D, G, and J in Figure 4.20), it represented the pull-off force f_p necessary to separate the elastica from the substrate. The pull-off force is equal to $-q$ and is designated as f_p .

Next, the self-weight of the elastica was added to the JKR-type analysis for $c=0.4$ and $\Delta\gamma=0$ and 0.64 . The addition of the self-weight caused the curves in the contact length vs. vertical force and contact length vs. vertical displacement plots to shift toward larger values of b when $\eta>0$ and caused them to shift to lower values of b for $\eta<0$. The addition of the self-weight values considered here, for a specified value of $\Delta\gamma$ and c , created a noticeable change in the contact length.

7.3 DMT-TYPE ANALYSIS

7.3.1 Linear Force DMT-Type Analysis

The results obtained from the linear force DMT-type analysis for both $c=0.4$ and $c=0.8$ when $\eta=2, 0,$ and -2 showed that as the value of the maximum linear adhesion force, f_0 , was increased, the contact length also increased (for fixed values of α and q or δ). Additionally, the contact length increased with increasing values for the area under the adhesion force vs. y curve (in other words, for increasing values of the product $0.5f_0\alpha$). Therefore, the existence of adhesion forces in the region just outside of the contact area further distorted the shape of the elastica and caused an elongation of the contact length. As the value of the vertical distance α between the elastica and the substrate at $s=d$ was increased to $\alpha=0.01$, the value for the angle at $s=d$ was too large for the small-angle theory (used here for $0<s<d$) to be valid. Therefore, in the DMT-type analysis, results obtained for $\alpha=0.01$ were considered invalid. Unlike the moment at lift-off, m_b , calculated in the JKR-type analysis, the moment m_d at $s=d$ is not independent of the separation distance c between the clamped ends of the elastica, nor is it independent of the vertical applied force q . The moment at $s=d$ increases with increasing values of q and with increasing values of the vertical displacement δ .

Again, the vertical forces and vertical displacements experienced by the elastica as it traveled through the no contact, point contact, and line contact regions were dependent upon two factors: whether the elastica was being pushed onto or pulled off of the substrate, and whether the vertical displacement or the vertical force was being controlled. Figures 5.93-5.95 illustrate this idea and show that sudden jumps in the values of the vertical force or vertical displacement curves may occur. Tables 5.15 and 5.16 for the linear force DMT-type analysis supply the values for the contact length, vertical force, vertical displacement, horizontal force, and moment at $s=d$ at the transition point between point contact and no contact when $c=0.4$ and $c=0.8$, respectively. The negative value for q at the transition point between point contact and no contact

represents the pull-off f_p force necessary to separate the elastica from the substrate. Positive values for q at the transition from point contact to no contact indicate that no pull-off force was required to separate the elastica from the substrate. Positive values for q at the transition point only existed when $\eta \neq 0$. The equilibrium states for which the center of the elastica is less than the distance α from the substrate are unstable, and hence the center jumps through this region (whether the elastica is being pushed onto the substrate or pulled off of it).

7.3.2 Dugdale Force DMT-Type Analysis

The results obtained from the Dugdale force DMT-type analysis for $c=0.4$ when $\eta=2, 0,$ and -2 showed that as the value of the constant Dugdale adhesion force g_0 was increased, the contact length also increased (for fixed values of α and q or δ). Additionally, the contact length increased with increasing values for the area under the adhesion force vs. y curve (in other words, for increasing values of the product $g_0\alpha$). Therefore, the existence of adhesion forces in the region just outside of the contact area further distorted the shape of the elastica and caused an elongation of the contact length. The moment m_d at $s=d$ is not independent of the separation distance c between the clamped ends of the elastica nor is it independent of the vertical applied force q . The moment at $s=d$ increases with increasing values of q and with increasing values of δ .

Again, the vertical forces and vertical displacements experienced by the elastica as it traveled through the no contact, point contact, and line contact regions were dependent upon two factors: whether the elastica was being pushed onto or pulled off of the substrate, and whether the vertical displacement or the vertical force was being controlled. Figures 5.93-5.95 illustrate this idea and show that sudden jumps from one curve to another are possible. Table 5.17 for the Dugdale force DMT-type analysis supplies the values for the contact length, vertical force, vertical displacement, horizontal force, and moment at $s=d$ at the transition point between point contact and no contact

when $c=0.4$. The negative value for q at the transition point between point contact and no contact represents the pull-off force f_p necessary to separate the elastica from the substrate. The same jump of the center of the elastica through the region $0 < y < \alpha$ occurs, as for the linear force.

7.3.3 Comparison on the Linear Force and Dugdale Force DMT-Type Analyses

Values were specifically chosen for the maximum DMT forces and the separation distances α between the elastica and the substrate at $s=d$ to allow for direct comparison of the linear force and Dugdale force DMT-type analyses when $c=0.4$. Linear force and Dugdale force DMT-type analyses can be compared directly when the areas under the adhesion force vs. y plots are equal (see Figures 3.6 and 3.7). Additionally, the results from different combinations of the maximum adhesion force and the separation distance α , within either the linear force or the Dugdale force analysis, that yield the same value for the area under the adhesion force vs. y plot can be compared. For instance, Figure 7.1 is a plot of the contact length vs. the vertical force for a linear force DMT-type analysis when $c=0.4$ and $\eta=0$. The curve generated by the linear force analysis when $f_0=100$ and $\alpha=0.001$ (area under curve = 0.05) is virtually identical to the curve generated by the linear force analysis when $f_0=1000$ and $\alpha=0.0001$ (area under curve = 0.05). The contact length vs. the vertical displacement plot (Figure 7.2) for the identical linear force analyses yields the same conclusions.

Figure 7.3 is a plot of the contact length vs. the vertical force for $c=0.4$ and $\eta=0$. One curve was obtained by a linear force DMT-type analysis using $f_0=10,000$ and $\alpha=0.001$. The other curve was generated by a Dugdale force DMT-type analysis using $g_0=5000$ and $\alpha=0.001$. The area under both adhesion force vs. y plots is equal to 5 ($g_0\alpha = 5$ and $0.5f_0\alpha = 5$). The curves obtained from the Dugdale force and linear force analyses produce virtually the same values for the contact length at a fixed value of q . Figure 7.4

is a plot of the contact length vs. the vertical displacement for these same cases. The curves obtained from the Dugdale force and linear force analyses produce virtually the same values for the contact length at a fixed value of δ .

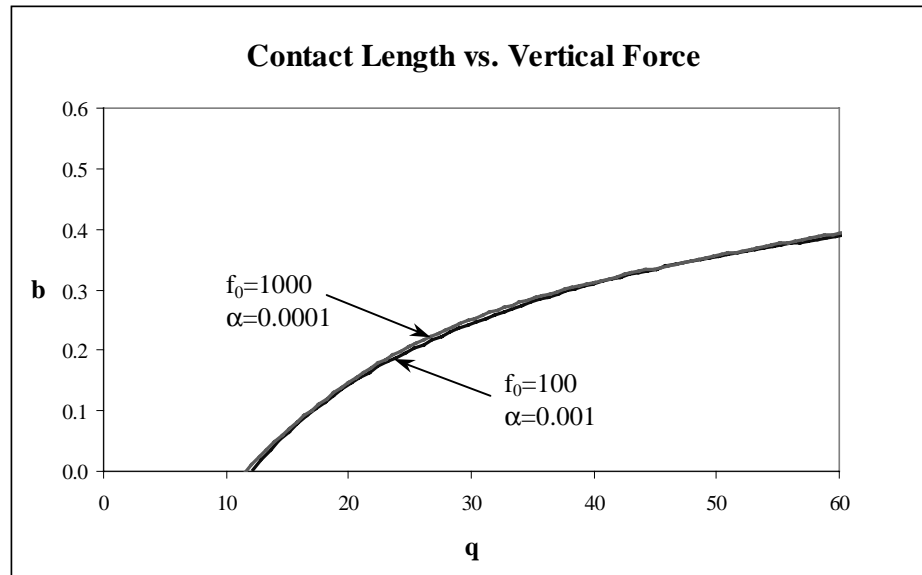


Figure 7.1: Contact Length vs. Vertical Force for $c=0.4$ and $\eta=0$ (Linear Force DMT-Type Analysis)

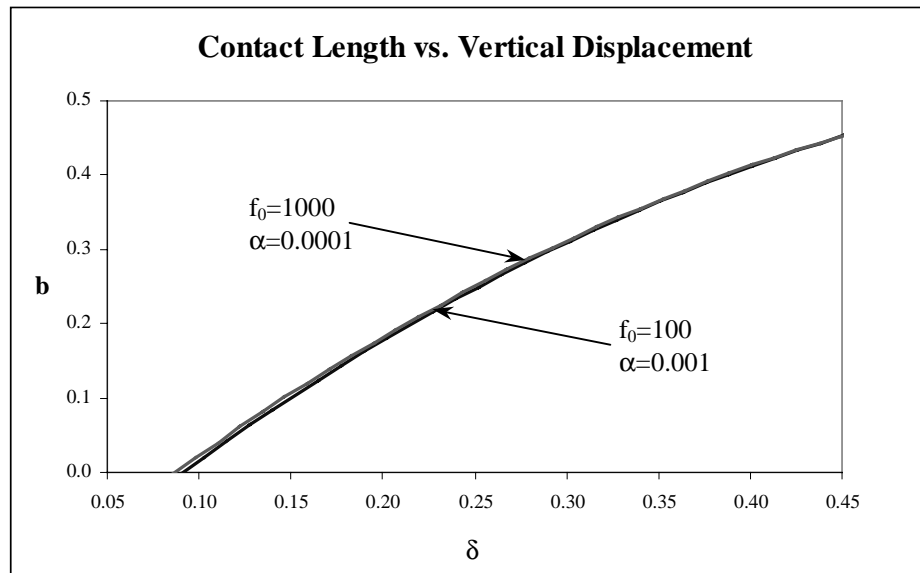


Figure 7.2: Contact Length vs. Vertical Displacement for $c=0.4$ and $\eta=0$ (Linear Force DMT-Type Analysis)

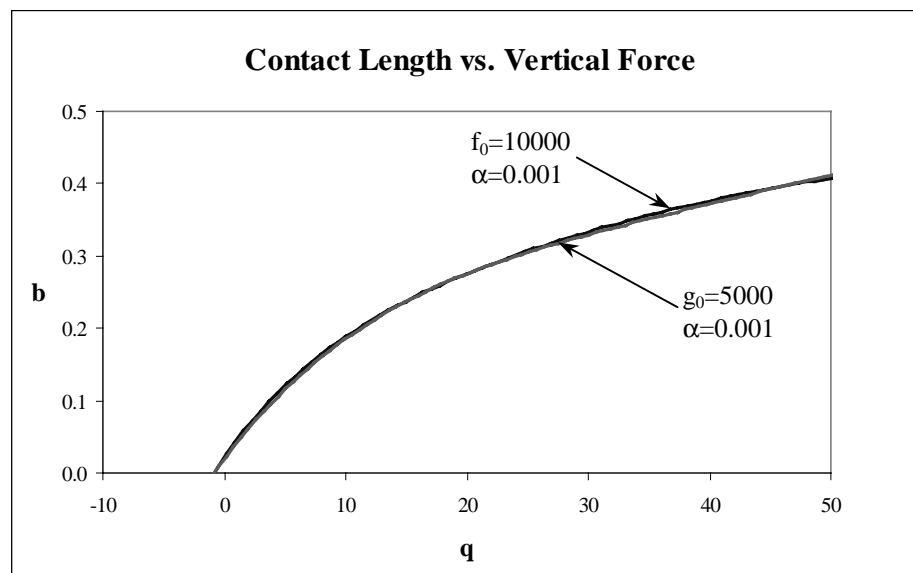


Figure 7.3: Contact Length vs. Vertical Force for $c=0.4$ and $\eta=0$ (Linear and Dugdale Force DMT-Type Analyses)

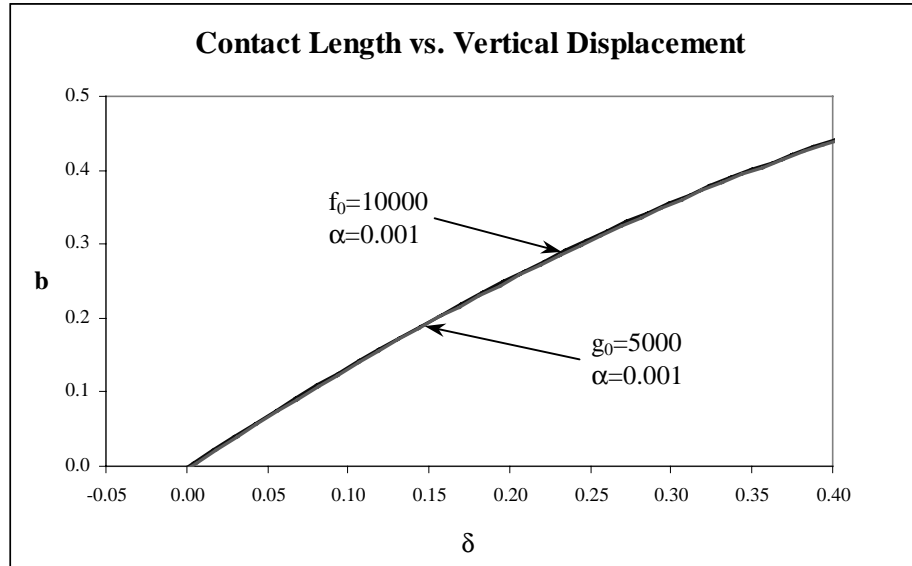


Figure 7.4: Contact Length vs. Vertical Displacement for $c=0.4$ and $\eta=0$ (Linear and Dugdale Force DMT-Type Analyses)

7.4 COMPARISON OF THE JKR- AND DMT-TYPE ANALYSIS RESULTS

By examining the pull-off forces obtained for similar adhesion forces, a comparison of the results obtained through the JKR-type analysis and the DMT-type analysis is possible. The work of adhesion $\Delta\gamma$, acting in the region of contact in the JKR-type analysis was nondimensionalized using Equation 3.5. The work of adhesion can also be nondimensionalized using the formula $\Delta\gamma = (\Delta\gamma)_{DIM}L^2/EI$ where $I=bh^3/12$. The nondimensionalization process used in Equation 3.5 eliminated the factor of 12 generated by the substitution $I = b h^3 / 12$. This factor of 12 could be ignored in the JKR-type analysis because the value of the work of adhesion was only used in determining the relative total energy of a particular equilibrium configuration of the elastica. Therefore, all the u_γ terms did not include a factor of 12 and its deletion had no bearing on the minimum total energy. However, in order to compare the JKR-type analysis with the

DMT-type analysis, it was necessary to include the factor of 12. Therefore, the values for the contact length, vertical force, vertical displacement, horizontal force, the moment at $s=d$, and the pull-off forces for $\Delta\gamma$ can be compared to those values obtained when the area under the adhesion force vs. y plot for the DMT-type analysis ($0.5f_0\alpha$ or $g_0\alpha$) is divided by 12 and is equal to $\Delta\gamma$.

Figure 7.5 is a plot of the vertical force q vs. the work of adhesion $\Delta\gamma$ for $c=0.4$ and $\eta=0$ at the transition between line contact and point contact. Using the vertical forces obtained for $\Delta\gamma=0, 0.16, 0.32, 0.48,$ and 0.64 at the transition point from line contact to point contact, a curve was fitted to the data to create a continuous plot for the JKR-type analysis. Values for q at $\Delta\gamma=0, 0.16, 0.32, 0.48,$ and 0.64 were $q=12.52, 4.86, 0.96, -2.58,$ and $-5.85,$ respectively. Also included in Figure 7.5 are Points 1 and 2 from the DMT-type analysis. Point 1 marks the vertical force for the DMT-type analysis when $\alpha=0.001$ and $f_0=10,000$ or when $\alpha=0.001$ and $g_0=5,000$ (both combinations have an area of 5 under the adhesion force vs. y curve and have almost identical values for the force: -0.83 in Table 5.5 and -0.73 in Table 5.12). Similarly, Point 2 marks the vertical force for the DMT-type analysis when $\alpha=0.0001$ and $f_0=10,000$ or when $\alpha=0.0001$ and $g_0=5,000$ (both combinations have an area of 0.5 under the adhesion force vs. y curve and have almost identical values for the force: 9.23 in Table 5.5 and 9.27 in Table 5.12). Good agreement exists between the values obtained by the DMT-type analysis and the curve generated for the JKR-type analysis. Note that the negative values obtained for q in the JKR-type analysis for the transition point from point contact to line contact also correspond to the pull-off force f_p for those particular values of $\Delta\gamma$.

Figure 7.6 is a plot of the vertical force vs. the work of adhesion for $c=0.8$ and $\eta=0$. Using the vertical forces obtained for $\Delta\gamma=0, 0.16, 0.32, 0.48,$ and 0.64 at the transition point from line contact to point contact, a curve was fitted to the data to create a continuous plot for the JKR-type analysis. Values for q at $\Delta\gamma=0, 0.16, 0.32, 0.48,$ and 0.64 were $q=2.49, -8.83, -15.90, -22.60,$ and $-28.90,$ respectively. Also included in

Figure 7.6 is a data point from the DMT-type analysis. This point marks the vertical force when $\alpha=0.001$ and $f_0=1000$ (which yields an area of 5 under the adhesion force vs. y curve). The vertical force $q=-2.27$ at this point (see Table 5.9). Good agreement exists between the value obtained by the DMT-type analysis and the curve generated for the JKR-type analysis for the values of q and $\Delta\gamma$ at the transition point between point contact and line contact. Note that the negative values obtained for q in the JKR-type analysis for the transition point from point contact to line contact also correspond to the pull-off force f_p for those particular values of $\Delta\gamma$.

The relationship between the pull-off forces f_p and the work of adhesion $\Delta\gamma$ for the JKR- and DMT-type analyses when $c=0.4$ and $\eta=0$ can be seen in Figure 7.7. Using the pull-off forces obtained for $\Delta\gamma=0, 0.16, 0.32, 0.48,$ and $0.64,$ a curve was fitted to the data to create a continuous plot for the JKR-type analysis. Note that when $\Delta\gamma$ is less than approximately 0.36, the pull-off force $f_p=0$. When $\Delta\gamma<0.36$ and $f_p=0$, the JKR curves are comparable to those shown in Figures 4.7 and 4.9. Also plotted in Figure 7.7 are Points 1, 2, and 3 obtained from the linear force DMT-type analysis. Point 1 represents the pull-off force for $f_0=10,000$ and $\alpha=0.0001$ (which yields an area of 0.5 under the adhesion force vs. y curve). The pull-off force obtained for Point 1 was 35.34. Point 2 represents the pull-off force for $f_0=1000$ and $\alpha=0.001$ (which also yields an area of 0.5 under the adhesion force vs. y curve). The pull-off force obtained for Point 2 was 13.48. Finally, Point 3 represents the pull-off force for $f_0=100$ and $\alpha=0.001$ (which yields an area of 0.05 under the adhesion force vs. y curve). The pull-off force obtained for Point 2 was 1.31. The pull-off forces obtained through the DMT-type analysis are significantly larger than those obtained through the JKR-type analysis. It is important to note, however, that once the elastica enters the point contact stage in the JKR-type analysis, the adhesion forces vanish and the values for the contact length, the vertical force, and the vertical displacement can be obtained from the $\Delta\gamma=0$ curve. Conversely, the adhesion forces act throughout the line contact, point contact, and no contact stages of the DMT-type

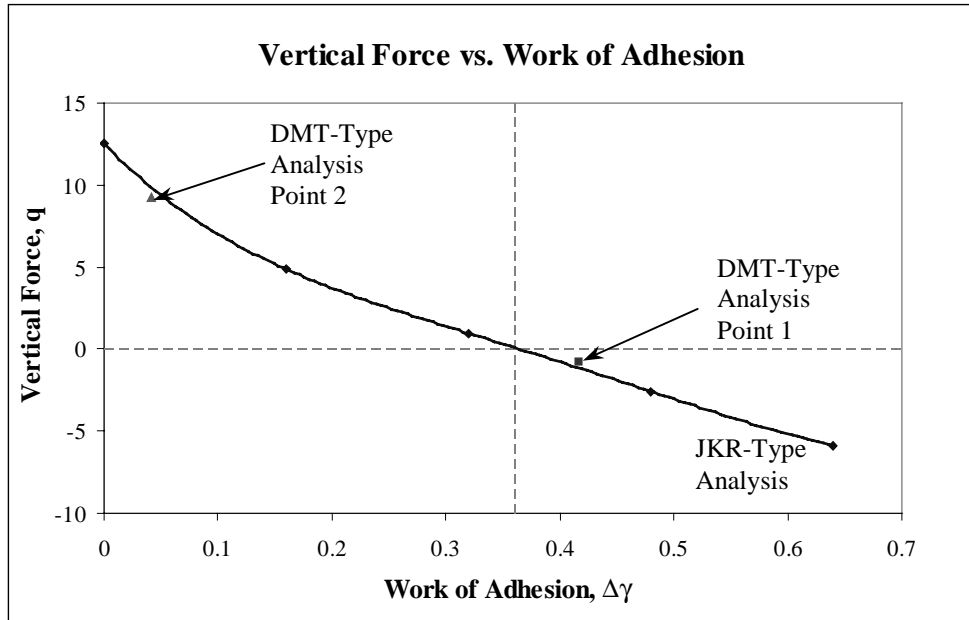


Figure 7.5: Vertical Force vs. Work of Adhesion for the Transition Point Between Point Contact and Line Contact when $c=0.4$ and $\eta=0$

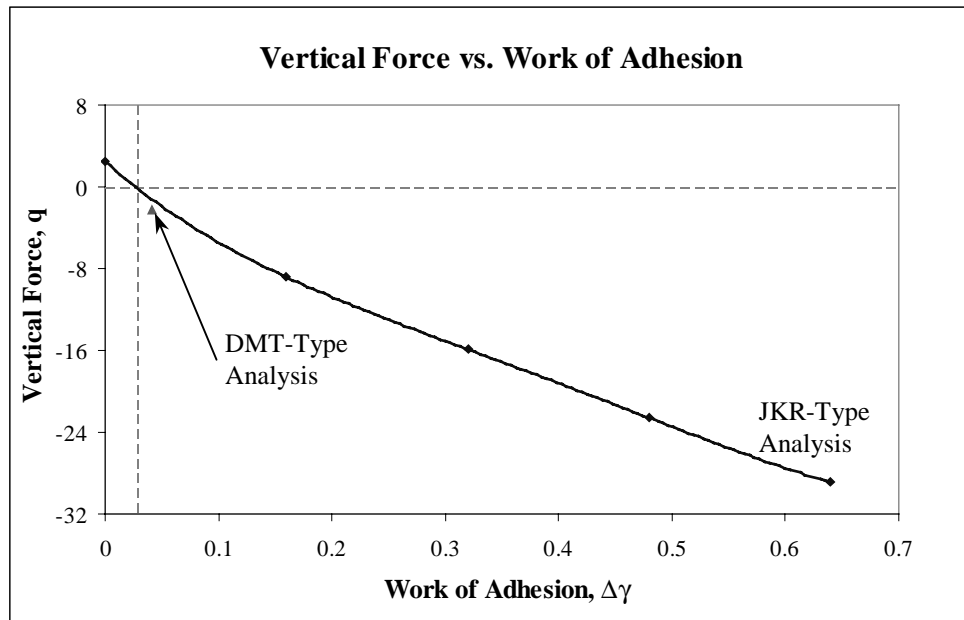


Figure 7.6: Vertical Force vs. Work of Adhesion for the Transition Point Between Point Contact and Line Contact when $c=0.8$ and $\eta=0$

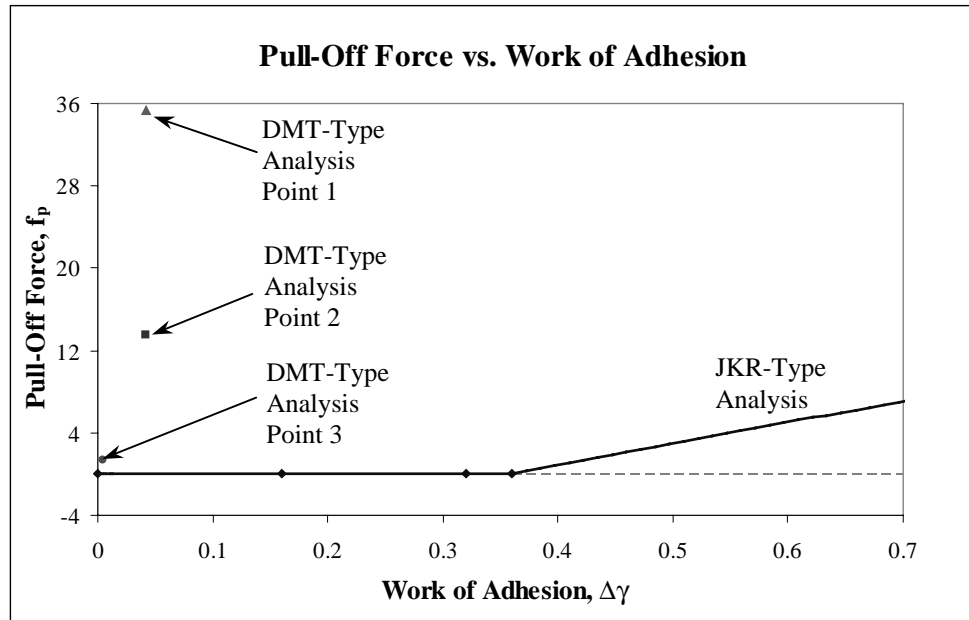


Figure 7.7: Pull-Off Force vs. Work of Adhesion for $c=0.4$ and $\eta=0$

analysis and cease to act only when the separation between the center of the elastica and the substrate is greater than α .

7.5 RECOMMENDATIONS FOR FUTURE RESEARCH

Although the results obtained from this thesis have provided insight into the effect of adhesion forces on the contact of a bent elastica with a rigid substrate, further research is necessary to obtain a more in-depth understanding of their effect and magnitude. First, an investigation of additional values for the separation distance c between the clamped ends of the elastica would be valuable. For instance, Plaut et al. (1999) examined values of $c=0, 0.2, 0.4, 0.6,$ and 0.8 for a bent elastica that experienced no adhesion forces. Future research should also consider a nonlinear relationship between the moment and the curvature and should incorporate this nonlinear relationship into the governing equations given in Chapter 3. Anticlastic curvature, which is observed in actual

experiments, should also be accounted for in future analyses. In terms of the DMT-type analysis, a nonlinear analysis in the region where the adhesion forces are active should be considered. Additionally, the effects of surface roughness on the analysis could be investigated. A broader range of f_0 , g_0 , α , and η values should also be used. Finally, additional experimental work should be performed to provide a mechanism for the evaluation of the accuracy of the analytical model.

References

- Adamson, A.W. (1967). Physical Chemistry of Surfaces, Interscience Publishers, New York.
- Barthel, E. (1999). "Modelling the Adhesion of Spheres: When the Form of the Interaction is Complex," *Colloids and Surfaces A*, Vol. 149, pp. 99-105.
- Bhushan, B. (1999). Principles and Applications of Tribology, John Wiley & Sons, Inc., New York, pp. 302-339.
- Chucheepsakul, S., Buncharoen, S., and Huan, T. (1995). "Elastica of Simple Variable-Arc Length Beam Subjected to End Moment," *Journal of Engineering Mechanics*, Vol. 121, No. 7, p.767-772.
- Derjaguin, B. V., Muller, V. M., and Toporov, Yu. P. (1975). "Effect of Contact Deformations on the Adhesion of Particles," *Journal of Colloid and Interface Science*, Vol. 53, No. 2, pp. 314-326.
- Evans, E. A. (1980). "Analysis of Adhesion of Large Vesicles to Surfaces," *Biophysical Journal*, Vol. 31, pp. 425-432.
- Faulkner, M. G., Lipsett, A. W. and Tam, V. (1993). "On the Use of a Segmental Shooting Technique for Multiple Solutions of Planar Elastica Problems," *Computer Methods in Applied Mechanics and Engineering*, Vol. 110, pp. 221-236.
- Griner, G. M. (1984). "A Parametric Solution to the Elastic Pole-Vaulting Pole Problem," *Journal of Applied Mechanics*, Vol. 51, pp. 409-414.

References, Continued

- Horn, R. G., Israelachvili, J. N., and Pribac, F. (1987). "Measurement of the Deformation and Adhesion of Solids in Contact," *Journal of Colloid and Interface Science*, Vol. 115, No. 2, pp. 480-492.
- Johnson, K. L., Kendall, K., and Roberts, A.D. (1971). "Surface Energy and the Contact of Elastic Solids," *Proceedings of the Royal Society of London A*, Vol. 324, pp. 301-313.
- Kendall, K. (1994). "Adhesion: Molecules and Mechanics," *Science*, Vol. 263, pp. 1720-1725.
- Kitching, R., Houlston, R., and Johnson, W. (1975). "A Theoretical and Experimental Study of Hemispherical Shells Subjected to Axial Loads Between Flat Plates," *International Journal of Mechanical Sciences*, Vol. 17, pp. 693-703.
- Mack, M. J., Jr., Gassman, P. M., and Baumgarten, J. R. (1983). "Analysis of a Thin-Walled Pressurized Torus in Contact with a Plane," *AAIA Journal*, Vol. 21, pp. 1162-1167.
- Mangipudi, V. S., Huang, E., Tirrell, M., and Pocius, A. V. (1996). "Measurement of Interfacial Adhesion Between Glassy Polymers Using the JKR Method," *Macromolecular Symposia*, Vol. 102, pp. 131-143.
- Maugis, D. (1992). "Adhesion of Spheres: The JKR-DMT Transition Using the Dugdale Model," *Journal of Colloid and Interface Science*, Vol. 150, No. 1, pp. 243-269.

References, Continued

- Muller, V. M., Derjaguin, B. V., and Toporov, Yu. P. (1983). "On Two Methods of Calculation of the Force of Sticking of an Elastic Sphere to a Rigid Plane," *Colloids and Surfaces*, Vol. 7, pp. 251-259.
- Muller, V. M., Yushchenko, V. S., and Derjaguin, B. V. (1980). "On the Influence of Molecular Forces on the Deformation of an Elastic Sphere and Its Sticking to a Rigid Plane," *Journal of Colloid and Interface Science*, Vol. 77, No. 1, pp. 91-101.
- Pashley, M. D. (1984). "Further Consideration of the DMT Model for Elastic Contact," *Colloids and Surfaces*, Vol. 12, pp. 69-77.
- Pashley, M. D. and Tabor, D. (1981). "Adhesion and Deformation Properties of Clean and Characterized Metal Micro-Contacts," *Vacuum*, Vol. 31, Nos. 10-12, pp. 619-623.
- Plaut, R. H., Suherman, S., Dillard, D. A., Williams, B. E., and Watson, L. T. (1998). "Deflections and Buckling of a Bent Elastica in Contact with a Flat Surface," *International Journal of Solids and Structures*, Vol. 36, pp. 1209-1229.
- Shanahan, M. E. R. (1997). "A Novel Test for the Appraisal of Solid / Solid Interfacial Interactions," *Journal of Adhesion*, Vol. 63, pp. 15-29.
- Stoker, J. J. (1950). Nonlinear Vibrations, Interscience Publishers, New York.

References, Continued

- Tabor, D. (1977). "Surface Forces and Surface Interactions," *Journal of Colloid and Interface Science*, Vol. 58, No. 1, p 2-13.
- Thacker, W. I., Wang, C. Y. and Watson, L. T. (1997). "Global Stability of a Thick Solid Supported by Elastica Columns," *Journal of Engineering Mechanics*, Vol. 123, No. 3, pp. 287-289.
- Timoshenko, S. P. and Gere, J. M. (1961). Theory of Elastic Stability, 2nd ed., McGraw-Hill Book Company, Inc., New York, pp. 76-82.
- Urdike, D. P. and Kalnins, A. (1972). "Contact Pressure Between an Elastic Spherical Shell and a Rigid Plate," *Journal of Applied Mechanics*, Vol. 39, pp. 1110-1114.
- Vaillette, D. P. (1982). "Stability of a Beam in a Rigid Channel," M.S. Thesis, Northeastern University, Boston, Mass.
- Vaillette, D. P. and Adams, G. G. (1983). "An Elastic Beam Contained in a Frictionless Channel," *Journal of Applied Mechanics*, Vol. 50, pp. 693-694.
- Wang, C. Y. (1981). "Folding of Elastica - Similarity Solutions," *Journal of Applied Mechanics*, Vol. 48, pp. 199-200.

Appendix A

Mathematica Files

Shooting Method to determine variables p (horizontal force) and m_b (moment at $s=b$).

This file can be used to determine values for p , m_b , u_E , and h for a JKR-type analysis when point contact exists. The values used for c , q , b , gP , and gMB below are for illustrative purposes only.

Definition of variables:

c = separation distance between ends of elastica

q = vertical force applied at fixed end of elastica (one side only)

gP = initial guess for parameter P , horizontal force applied at fixed end of elastica

gMB = initial guess for parameter MB , moment existing at center of bent elastica

b = contact length (one half of elastica)

Shooting Method

Variables:

$$c = 0.4$$

$$q = 3$$

$$b = 0$$

$$pi = N[\pi]$$

Unknown Variables:

$$gP = 5$$

$$gMB = 1.97$$

Derivatives of the 5 Characteristic Equations:

$$de[y3_, y4_, P_] := \{y1'[t] == \text{Cos}[y3[t]], y2'[t] == \text{Sin}[y3[t]],$$

$$y3'[t] == y4[t], y4'[t] == -P \text{Sin}[y3[t]] + q \text{Cos}[y3[t]]\}$$

$$v[y3_, P_] := q \text{Cos}[y3[t]] - P \text{Sin}[y3[t]]$$

$$n[y3_, P_] := -q \text{Sin}[y3[t]] - P \text{Cos}[y3[t]]$$

Left Boundary Conditions:

$$\text{leftBC}[MB_] := \{y1[0] == 0, y2[0] == 0, y3[0] == 0, y4[0] == MB\}$$

Solving for y1-y5

```

soln := NDSolve[Flatten[Append[de[y3, y4, P], leftBC[MB]]],
  {y1, y2, y3, y4}, {t, 0, 1 - b}, MaxSteps -> 2200]
endpt[P_, MB_] := {y1[t], y2[t], y3[t], y4[t]} /.
  First[NDSolve[Flatten[Append[de[y3, y4, P], leftBC[MB]]],
    {y1[t], y2[t], y3[t], y4[t]}, {t, 0, 1 - b},
    MaxSteps -> 2200]} /. t -> 1 - b;
endpt[
  gP,
  gMB]
Clear[P, MB]
rts := FindRoot[{endpt[P, MB][[3]] ==  $\frac{\pi}{2}$ , endpt[P, MB][[1]] == c - b},
  {P, {gP, 0.99 gP}}, {MB, {gMB, 0.99 gMB}},
  AccuracyGoal -> 4, MaxIterations -> 200]

rts
endpt[P /. rts, MB /. rts]

P = P /. rts
  MB = MB /. rts

P /. soln /. rts
Print[P /. soln /. rts]
Print[MB /. soln /. rts]
Clear[yy]
yy[t_] := {y1[t], y2[t], y3[t], y4[t]} /. First[soln]
Clear[UE]
UE[P_, MB_] :=
  NIntegrate[Evaluate[(yy[t][[4]])^2], {t, 0, 1 - b}]
UE[P /. rts, MB /. rts]
List[y1[1 - b], y2[1 - b], y3[.777], y4[1 - b]] /. soln /. rts
numbers = TableForm[Table[{b, P = P /. rts, MB = MB /. rts,
  UE[P, MB], Part[endpt[P, MB], 2]}, {b, 0.55, .5, .005}],
  TableHeadings -> {None, {"b", "P", "MB", "UE", "h"}}]

```

Shooting Method used to Determine variables p,d, and ε.

A linear force DMT-type analysis was used, with the maximum force being f_0 . Values for q , ϵ , b , p , and h are for line contact only.

Definition of variables:

c = separation distance between ends of the elastica

d = distance from lift-off point to end of DMT force zone (along s)

η = term used to account for the weight of the elastica

f_0 = the initial DMT force experienced at the lift-off point ($s=0$)

α = the height when $f_0=0$ ($s=d$)

gP = the initial guess for parameter p , horizontal force applied at fixed end of elastica

$g\epsilon$ = the initial guess for parameter ϵ , the value for u ($u=1-b-d$) at $t=0$

Shooting Method

Variables:

$$c = 0.4$$

$$d = .005$$

$$\eta = (0)$$

$$f_0 = 100$$

$$\alpha = 0.0001$$

$$pi = N[\pi]$$

$$B = (f_0 / \alpha)^{1/4}$$

$$Y_{ps} = \alpha (1 + \eta / f_0)$$

$$D_1 = \frac{(\alpha + 0.5 * Y_{ps} (\cosh[B * d] + \cos[B * d] - 2))}{\sinh[B * d] - \sin[B * d]}$$

$$\$RecursionLimit = 2000$$

Unknown Variables:

$$gP = (-25)$$

$$g\epsilon = .9$$

Derivatives of the 5 Characteristic Equations

```

de[y3_, y4_, y5_, p_] :=
  {y1'[t] == y5[t] Cos[y3[t]],
    y2'[t] == y5[t] Sin[y3[t]],
    y3'[t] == y5[t] y4[t],
    y4'[t] == -y5[t] p Sin[y3[t]] +
  y5[t]
  ((1/Cos[B D1 (Cosh[B*d] - Cos[B*d]) -
    0.5*B*yps (Sinh[B*d] - Sin[B*d])]) *
  (B3 D1 (Cosh[B*d] + Cos[B*d]) -
    0.5*B3 yps (Sinh[B*d] + Sin[B*d]) +
    p*Sin[B D1 (Cosh[B*d] - Cos[B*d]) -
    0.5*B*yps (Sinh[B*d] - Sin[B*d])]) - y5[t] η(t))
  Cos[y3[t]],
  y5'[t] == 0}

```

Left Boundary Conditions

```

leftBC[ε_] :=
  {y1[0] == d,
    y2[0] == α,
    y3[0] == B D1 (Cosh[B*d] - Cos[B*d]) -
  0.5*B*yps (Sinh[B*d] - Sin[B*d]),
    y4[0] == B2 D1 (Sinh[B*d] + Sin[B*d]) -
  0.5*B2 yps (Cosh[B*d] - Cos[B*d]),
    y5[0] == ε}

```

Solving for y1-y5

```

soln := NDSolve[Flatten[Append[de[y3, y4, y5, p], leftBC[ε]]],
  {y1, y2, y3, y4, y5}, {t, 0, 1}, MaxSteps -> 3000]

endpt[p_, ε_] :=
  {y1[t], y2[t], y3[t], y4[t], y5[t]} /.
  First[NDSolve[Flatten[Append[de[y3, y4, y5, p], leftBC[ε]]],
  {y1[t], y2[t], y3[t], y4[t], y5[t]}, {t, 0, 1},
  MaxSteps -> 3000]] /. t -> 1;

endpt[gp, gε]

```

```
Clear[p, ε]
```

```
rts := FindRoot[{endpt[p, ε][[3]] ==  $\frac{\pi}{2}$ ,  
                endpt[p, ε][[1]] == c - 1 + d + ε}, {p, {gp, 0.99 gp}},  
                {ε, {gε, 0.99 gε}}, AccuracyGoal → 7, MaxIterations → 500]  
rts
```

```
endpt[p /. rts, ε /. rts]
```

```
p = p /. rts
```

```
ε = ε /. rts
```

```
Clear[yy]
```

```
yy[t_] := {y1[t], y2[t], y3[t], y4[t], y5[t]} /. First[soln]
```

Values for yy[t], b, and q

```
yy[1][[1]]
```

```
yy[1][[2]]
```

```
yy[1][[3]]
```

```
yy[0][[3]]
```

```
yy[0][[4]]
```

```
yy[1][[5]]
```

```
yy[0][[5]]
```

```
b = 1 - d - ε
```

```
q =
```

$$\begin{aligned} & 1 / \cos[B D_1 (\cosh[B * d] - \cos[B * d]) - \\ & \quad 0.5 * B * y_{ps} (\sinh[B * d] - \sin[B * d])] * \\ & (B^3 D_1 (\cosh[B * d] + \cos[B * d]) - 0.5 * B^3 y_{ps} (\sinh[B * d] + \sin[B * d]) + \\ & \quad p * \sin[B D_1 (\cosh[B * d] - \cos[B * d]) - \\ & \quad \quad 0.5 * B * y_{ps} (\sinh[B * d] - \sin[B * d])]) - \eta * \epsilon \end{aligned}$$

Plotting the Shape of the Elastica

```
ParametricPlot[Evaluate[{y1[t], y2[t]} /. soln /. rts], {t, 0, 1},  
                PlotRange → All, AspectRatio → Automatic]
```

Shooting Method used to Determine variables p,d, and ε.

A Dugdale force DMT-type analysis was used, with the constant adhesion force being g_0 . Values for q , ϵ , b , p , and h are for line contact only.

Definition of variables:

c = separation distance between the clamped ends of the elastica

d = distance from the lift-off point to end of DMT force zone (along s)

η = eta; term used to account for the weight of the elastica

g_0 = the initial DMT force experienced at the lift-off point ($s=0$)

α = the height when $g_0=0$ ($s=d$)

gP = the initial guess for parameter p , horizontal force applied at fixed end of elastica

$g\epsilon$ = the initial guess for parameter ϵ , the value for u ($u=1-b-d$) at $t=0$

Shooting Method

Variables:

$$c = 0.4$$

$$d = .0193$$

$$\eta = (0)$$

$$g_0 = 5000$$

$$\alpha = 0.0001$$

$$pi = N[\pi]$$

$$A_4 = \frac{\alpha}{d^3} + \frac{(\eta + g_0) * d}{24}$$

$$\$RecursionLimit = 2000$$

Unknown Variables:

$$gp = (15)$$

$$g\epsilon = .8$$

Derivatives of the 5 Characteristic Equations

```

de[y3_, y4_, y5_, p_] :=
  {y1'[t] == y5[t] Cos[y3[t]],
    y2'[t] == y5[t] Sin[y3[t]],
    y3'[t] == y5[t] y4[t],
    y4'[t] ==
- y5[t] p Sin[y3[t]] +
  y5[t]
  \left( \frac{6 * A_4 - (\eta + g_0) * d + p * \text{Sin}\left[3 * A_4 * d^2 - \frac{(\eta + g_0) * d^3}{6}\right]}{\text{Cos}\left[3 * A_4 * d^2 - \frac{(\eta + g_0) * d^3}{6}\right]} -
    \eta * y5[t] \right) + y5[t] \eta (1 - t) \left. \text{Cos}[y3[t]],
    y5'[t] == 0}

```

Left Boundary Conditions

```

leftBC[ε_] :=
  {y1[0] == d,
    y2[0] == α,
    y3[0] == 3 * A_4 * d^2 - \frac{(\eta + g_0) * d^3}{6},
    y4[0] == 6 * A_4 * d - \frac{(\eta + g_0) * d^2}{2},
    y5[0] == ε}

```

Solving for y1-y5

```

soln :=
  NDSolve[Flatten[Append[de[y3, y4, y5, p], leftBC[ε]]],
    {y1, y2, y3, y4, y5}, {t, 0, 1}, MaxSteps -> 3000]

```

```

endpt[p_, ε_] :=
  {y1[t], y2[t], y3[t], y4[t], y5[t]} /.
  First[
    NDSolve[Flatten[Append[de[y3, y4, y5, p],
      leftBC[ε]]], {y1[t], y2[t], y3[t], y4[t],
      y5[t]}, {t, 0, 1}, MaxSteps -> 3000] /. t -> 1;

```

```

endpt[gp, gε]

```

```
Clear[p, ε]
```

```
rts := FindRoot[{endpt[p, ε][[3]] ==  $\frac{\pi}{2}$ ,  
endpt[p, ε][[1]] == c - 1 + d + ε},  
{p, {gp, 0.99 gp}}, {ε, {ge, 0.99 ge}},  
AccuracyGoal → 7, MaxIterations → 500]
```

```
rts
```

```
endpt[p /. rts, ε /. rts]
```

```
p = p /. rts
```

```
ε = ε /. rts
```

```
Clear[yy]
```

```
yy[t_] := {y1[t], y2[t], y3[t], y4[t], y5[t]} /.  
First[soln]
```

Values for yy[t], b, and q

```
yy[1][[1]]
```

```
yy[1][[2]]
```

```
yy[1][[3]]
```

```
yy[0][[3]]
```

```
yy[0][[4]]
```

```
yy[1][[5]]
```

```
yy[0][[5]]
```

```
b = 1 - d - ε
```

$$q = \frac{6 * A_4 - (\eta + g_0) * d + p * \sin\left[3 * A_4 * d^2 - \frac{(\eta + g_0) * d^3}{6}\right]}{\cos\left[3 * A_4 * d^2 - \frac{(\eta + g_0) * d^3}{6}\right]}$$

```
η * y5[t]
```

Plotting the Shape of the Elastica

```
ParametricPlot[Evaluate[{y1[t], y2[t]} /. soln /. rts],  
{t, 0, 1}, PlotRange → All, AspectRatio → Automatic]
```

Appendix B

Linear Analysis for Linear Force DMT-Type Analysis

The linear formulation in Appendices B and C was derived by Professor R. H. Plaut and verified by the author. It applies from $x=0$ to $x=d$, the region where the DMT-type adhesion forces act on the right side of the elastica.

For the linear force $f = f_0 - (f_0/\alpha)y$ and self-weight η , the equilibrium equation for $y(x)$ is

$$y'''' - (f_0/\alpha) y = -\eta - f_0$$

The general solution has the form

$$y(x) = A_1 \cos \beta x + A_2 \sin \beta x + A_3 \cosh \beta x + A_4 \sinh \beta x + y_p$$

where $\beta = (f_0/\alpha)^{1/4}$ and $y_p = \alpha + (\alpha\eta/f_0)$.

The rotation $\theta(x)$, bending moment $m(x)$, and shear force $v(x)$ can be approximated by

$$\theta = y' \quad m = y'' \quad v = y'''$$

The initial conditions at $s=d$ for the subsequent elastica equations are obtained from continuity of x , y , θ , and m . Continuity of shear at $s=d$ furnishes a condition in which $v(d)$ is set equal to the formula dm/ds at $s=d$ obtained from the elastica equations, and this condition is solved for the vertical force q at the clamped ends.

I. No Contact

The elastica is assumed to be above the substrate with its central region within a vertical distance α from the rigid surface. The value of $y(0)$ is denoted y_0 , with $0 < y_0 < \alpha$. Coefficients A_1 , A_2 , A_3 , and A_4 are obtained using the conditions

$$\begin{aligned}y(0) &= y_0 \\y'(0) &= 0 \\y''(0) &= 0 \\y(d) &= \alpha\end{aligned}$$

This gives:

$$y(x) = A_1(\cos \beta x - \cosh \beta x) + (y_0 - y_p) \cosh \beta x + y_p$$

$$\text{where: } A_1 = \frac{\alpha + (y_p - y_0) \cosh \beta d - y_p}{(\cos \beta d - \cosh \beta d)}$$

$$\theta(x) = -A_1\beta (\sin \beta x + \sinh \beta x) + \beta (y_0 - y_p) \sinh \beta x$$

$$m(x) = -A_1\beta^2(\cos \beta x + \cosh \beta x) + \beta^2 (y_0 - y_p) \cosh \beta x$$

From the condition of continuous shear force at $x=d$:

$$q = \frac{A_1\beta^3 (\sin \beta d - \sinh \beta d) + \beta^3 (y_0 - y_p) \sinh \beta d + p \sin \theta(d) + \eta (d-1)}{\cos \theta(d)}$$

II. Point Contact

If the elastica only contacts the substrate at $x=0$, the boundary conditions are

$$\begin{aligned}y(0) &= 0 \\y'(0) &= 0 \\y(d) &= \alpha\end{aligned}$$

This gives:

$$y(x) = A_4 (\sinh \beta x - \sin \beta x) + y_p (1 - \cosh \beta x) + A_1 (\cos \beta x - \cosh \beta x)$$

where:
$$A_4 = \frac{\alpha + A_1(\cosh \beta d - \cos \beta d) + y_p(\cosh \beta d - 1)}{(\sinh \beta d - \sin \beta d)}$$

$A_1 =$ constant representing magnitude of $y(x)$

$$\theta(x) = A_4\beta (\cosh \beta x - \cos \beta x) - A_1\beta (\sin \beta x + \sinh \beta x) - y_p\beta \sinh \beta x$$

$$m(x) = A_4\beta^2 (\sinh \beta x + \sin \beta x) - A_1\beta^2 (\cos \beta x + \cosh \beta x) - y_p\beta^2 \cosh \beta x$$

$$q = \frac{A_4\beta^3 (\cosh \beta d + \cos \beta d) - A_1\beta^3 (-\sin \beta d + \sinh \beta d) - y_p\beta^3 \sinh \beta d + p \sin \theta(d)}{\cos \theta(d)} + \eta (d - 1)$$

III. Line Contact

When the elastica contacts the substrate for length b on the right of the center, the boundary conditions for $y(x)$ are

$$y(0) = 0$$

$$y'(0) = 0$$

$$y''(0) = 0$$

$$y(d) = \alpha$$

where $x=0$ at the end of the contact region. This gives

$$y(x) = A_4(\sinh \beta x - \sin \beta x) - 0.5 y_p (\cosh \beta x + \cos \beta x - 2)$$

where:
$$A_4 = \frac{\alpha + 0.5 y_p (\cosh \beta d + \cos \beta d - 2)}{(\sinh \beta d - \sin \beta d)}$$

$$\theta(x) = A_4\beta (\cosh \beta x - \cos \beta x) - 0.5 y_p \beta (\sinh \beta x - \sin \beta x)$$

$$m(x) = A_4\beta^2 (\sinh \beta x + \sin \beta x) - 0.5 y_p \beta^2 (\cosh \beta x - \cos \beta x)$$

$$q = \frac{A_4\beta^3 (\cosh \beta d + \cos \beta d) - 0.5 y_p \beta^3 (\sinh \beta d + \sin \beta d) + p \sin \theta(d) - \eta (1-b-d)}{\cos \theta(d)}$$

IV. Pull-Off

Conditions at the instant of pull-off of the elastica can be obtained by putting $y_0=0$ in the no contact solution, or putting $y'''(0) = 0$ in the point contact solution (i.e. no shear force at the center of the elastica) which leads to $A_4 = 0$.

For the case $\eta=0$, one obtains

$$y(x) = \alpha - \frac{\alpha (\cos \beta d \cosh \beta x - \cosh \beta d \cos \beta x)}{(\cos \beta d - \cosh \beta d)}$$

An approximate value f_a for the pull-off force $f_p = -q$ at one support is given by

$$|f_a| = \int f \, dx$$

With the above deflection, integration yields

$$|f_a| = \frac{f_0 (\cos \beta d \sinh \beta d - \cosh \beta d \sin \beta d)}{\beta (\cos \beta d - \cosh \beta d)}$$

If $\eta \neq 0$, one gets

$$f_a = (1-d)\eta + f_0 [\xi (\sin \beta d - \sinh \beta d) + \phi (\cos \beta d \sinh \beta d - \sin \beta d \cosh \beta d) + \xi \beta d (\cosh \beta d - \cos \beta d)] / [\beta (\cos \beta d - \cosh \beta d)]$$

$$\begin{aligned} \text{where:} \quad \xi &= \eta/f_0 \\ \phi &= 1 + \xi \end{aligned}$$

Comparison of the Approximate Pull-off Force f_a and the Pull-off Force f_p Calculated by the Shooting Method for a Linear Force DMT-Type Analysis when $c=0.4$

η	α	f_0	d	β	ϕ	ξ	f_a	f_p
0	0.001	100	0.0246	17.78	1.0000	0.0000	1.6395	1.31
		1000	0.0201	31.62	1.0000	0.0000	13.3835	13.48
		10000	0.0134	56.23	1.0000	0.0000	89.1164	95.11
	0.0001	100	0.0081	31.62	1.0000	0.0000	0.5400	0.43
		1000	0.0073	56.23	1.0000	0.0000	4.8656	4.78
		10000	0.0052	100.00	1.0000	0.0000	34.6476	35.34
2	0.001	100	0.0245	17.78	1.0200	0.0200	3.5839	3.32
		1000	0.0200	31.62	1.0020	0.0020	15.2772	15.48
		10000	0.0134	56.23	1.0002	0.0002	91.0895	97.18
	0.0001	100	0.0080	31.62	1.0200	0.0200	2.5173	2.44
		1000	0.0072	56.23	1.0020	0.0020	6.7846	6.77
		10000	0.0052	100.00	1.0002	0.0002	36.6372	37.35
-2	0.001	100	0.0247	17.78	0.9800	-0.0200	-0.3044	-0.70
		1000	0.0201	31.62	0.9980	-0.0020	11.4238	11.47
		10000	0.0134	56.23	0.9998	-0.0002	87.1432	93.04
	0.0001	100	0.0081	31.62	0.9800	-0.0200	-1.4438	-1.57
		1000	0.0073	56.23	0.9980	-0.0020	2.8802	2.79
		10000	0.0052	100.00	0.9998	-0.0002	32.6580	33.33

Comparison of the Approximate Pull-off Force f_a and the Pull-off Force f_p Calculated by the Shooting Method for a Linear Force DMT-Type Analysis when $c=0.8$

η	α	f_0	d	β	ϕ	ξ	f_a	f_p
0	0.001	10	0.0461	10.00	1.0000	0.0000	0.3072	0.53
		100	0.0391	17.78	1.0000	0.0000	2.6021	3.07
		1000	0.0255	31.62	1.0000	0.0000	16.9459	19.50
	0.0001	10	0.0169	17.78	1.0000	0.0000	0.1127	0.19
		100	0.0152	31.62	1.0000	0.0000	1.0129	1.12
		1000	0.0105	56.23	1.0000	0.0000	6.9936	7.36
2	0.001	10	0.0452	10.00	1.2000	0.2000	2.2108	2.60
		100	0.0378	17.78	1.0200	0.0200	4.4404	5.12
		1000	0.0255	31.62	1.0020	0.0020	18.8948	21.63
	0.0001	10	0.0164	17.78	1.2000	0.2000	2.0765	2.21
		100	0.0149	31.62	1.0200	0.0200	2.9632	3.13
		1000	0.0105	56.23	1.0020	0.0020	8.9726	9.38
-2	0.001	10	0.0472	10.00	0.8000	-0.2000	-1.5910	-1.53
		100	0.0395	17.78	0.9800	-0.0200	0.7076	1.02
		1000	0.0255	31.62	0.9980	-0.0020	14.9970	17.38
	0.0001	10	0.0175	17.78	0.8000	-0.2000	-1.8483	-1.82
		100	0.0155	31.62	0.9800	-0.0200	-0.9361	-0.88
		1000	0.0106	56.23	0.9980	-0.0020	5.0812	5.35

Appendix C

Linear Analysis for Dugdale Force DMT-Type Analysis

For the constant force $f=g_0$ and self-weight η , the equilibrium equation is

$$y'''' = -j$$

where $j = \eta + g_0$.

The general solution has the form

$$y(x) = A_1 + A_2x + A_3x^2 + A_4x^3 - (jx^4/24)$$

I. No Contact

The solution is

$$y(x) = y_0 + x^2A_3 - (jx^4 / 24)$$

$$\text{where: } A_3 = \frac{(\alpha - y_0)}{d^2} + \frac{j d^2}{24}$$

$$j = \eta + g_0$$

y_0 = vertical distance between elastica and substrate
 $0 < y_0 < \alpha$

$$\theta(x) = 2xA_3 - (jx^3 / 6)$$

$$m(x) = 2A_3 - (jx^2 / 2)$$

$$q = \frac{p \sin \theta(d) - jd - \eta (1-d)}{\cos \theta(d)}$$

II. Point Contact

The solution is

$$y(x) = A_3x^2 + A_4x^3 - (jx^4 / 24)$$

$$\text{where: } A_3 = \frac{\alpha + (jd^4 / 24) - A_4d^3}{d^2}$$

A_4 = constant representing magnitude of $y(x)$

$$\theta(x) = 2A_3x + 3A_4x^2 - (jx^3 / 6)$$

$$m(x) = 2A_3 + 6A_4x - (jx^2 / 2)$$

$$q = \frac{6A_4 - jd + p \sin \theta(d) + \eta (d-1)}{\cos \theta(d)}$$

III. Line Contact

The solution is

$$y(x) = A_4x^3 - (jx^4/24)$$

$$\text{where: } A_4 = \frac{\alpha + jd}{d^3 - 24}$$

$$\theta(x) = 3A_4x^2 - (jx^3/6)$$

$$m(x) = 6A_4x - (jx^2/2)$$

$$q = \frac{6A_4 - jd + p \sin \theta(d) - \eta(1 - b - d)}{\cos \theta(d)}$$

IV. Pull-Off

At the instant of pull-off, $y_0 = 0$ and the no contact solution gives

$$y(x) = \left[\frac{a}{d^2} + \frac{jd^2}{24} \right] x^2 - \frac{jx^4}{24}$$

By equilibrium of vertical forces, an approximate value of the pull-off force is

$$|f_a| = g_0 d + \eta$$

Comparison of the Approximate Pull-off Force f_a and the Pull-off Force f_p Calculated by the Shooting Method for a Dugdale Force DMT-Type Analysis when $c=0.4$

η	α	g_0	d	f_a	f_p
0	0.001	500	0.0211	10.56	10.62
		5000	0.0143	71.49	75.84
	0.0001	500	0.0075	3.75	3.68
		5000	0.0055	27.68	27.95
2	0.001	500	0.0211	12.54	12.63
		5000	0.0143	71.50	77.90
	0.0001	500	0.0075	3.73	5.67
		5000	0.0055	27.67	29.95
-2	0.001	500	0.0212	8.59	8.61
		5000	0.0143	71.47	73.77
	0.0001	500	0.0075	3.76	1.68
		5000	0.0055	27.68	25.94

Vita

Amy Janel Dalrymple was born March 12, 1976 in Plainwell, Michigan. She graduated from Plainwell High School in May of 1994 and began her undergraduate work at Michigan Technological University in Houghton, Michigan the following fall. In August of 1998 she completed her Bachelor of Science degree in Civil Engineering. Following graduation, the author moved to Blacksburg, Virginia to pursue her Master of Science degree in Civil Engineering at Virginia Tech, which was completed in December of 1999.